Membrane type I metalloproteinase (MT1-MMP) as a target in cancer: a study of two inhibitors

by

DANIEL BOHNEN

BSc (Hons)

Submitted in fulfilment of the academic
requirements for the degree of
Master of Science in the Discipline of Biochemistry

School of Biological Sciences
College of Agriculture, Engineering and Science
University of KwaZulu-Natal
Pietermaritzburg

This dissertation is dedicated to those who do not accept mediocrity and strive to raise the standards in both their own lives and those of others.

Preface

The experimental work described in this dissertation was carried out in the School of Biochemistry, Genetics and Microbiology, University of KwaZulu-Natal, Pietermaritzburg, South Africa, from March 2010 to December 2012, under the supervision of Dr Edith Elliott.

These studies represent original work by the author (candidate) and have not otherwise been submitted in any form for any degree or diploma to any tertiary institution. Where use has been made of the work of others it was duly acknowledged in the text.

Supervisor signature: _____ Date: _____

Candidate signature:  Date: _____

Declaration – Plagiarism

I, Mr Daniel Bohmer ...declare that

(i) The research reported in this dissertation, except where otherwise indicated, is my original work.

(ii) This dissertation has not been submitted for any degree or examination at any other university.

(iii) This dissertation does not contain other persons' data, pictures, graphs or other information, unless specifically acknowledged as being sourced from other researchers.

(iv) This dissertation does not contain other persons' writing, unless specifically acknowledged as being sourced from other researchers. Where other written sources have been quoted, then:

a) their words have been re-written but the general information attributed to them has been referenced;

b) where their exact words have been used, their writing has been placed inside quotation marks, and referenced.

(v) Where I have reproduced a publication of which I am an author, co-author or editor, I have indicated in detail which part of the publication was actually written by myself alone and have fully referenced such publications.

(vi) This dissertation does not contain text, graphics or tables copied and pasted from the Internet, unless specifically acknowledged and the source being detailed in the dissertation and in the references sections.

Candidate Signed: 

Abstract

Several diseases, including cancer, have been associated with high membrane type-1 matrix metalloproteinase (MT1-MMP) expression levels. MT1-MMP together with a non-membrane-bound, soluble MMP, MMP-2, also associated with many other biological functions, have been implicated in breast cancer progression, invasion and metastasis, and poor prognosis. Researchers who ran early clinical trials that employed broad-spectrum MMP inhibitors (MMPIs) lacked understanding of the intricate physiological and patho-physiological roles that MMPs play in tissues. In addition, structural similarities between MMPs hamper selective inhibition. Selective inhibition of MT1-MMP is of particular interest as MT1-MMP is overexpressed in target cancer cells relative to normal cells and is key in signalling for invasion. The inhibition profiles of two structurally similar synthetic pyrimidine-class MMPIs, with increased bioavailability and stability compared to hydroxamates tested in earlier clinical trials, TF 17-2 and TF 22d, were assessed. TF 17-2 and TF 22d were applied to a normal MCF-10A breast epithelial cell line and its premalignant H-*ras*(V^{12})-transfected MCF-10AneoT derivative to assess their efficacy for inhibiting MT1-MMP-mediated normal and premalignant cell migration, and indirectly, invasion. Both inhibitors form a co-ordination complex with the zinc ion of the catalytic site of MT1-MMP and MMP-2 with greater affinity for MT1-MMP.

The computational molecular docking package, AutoDock Vina, was used for *in silico* predictions of binding affinities that could potentially substitute for *in vitro* kinetic assays when assessing inhibitor potential for inhibiting target MMPs. The binding of the two MMPIs was assessed using AutoDock Vina and compared to established kinetic data. The AutoDock Vina program was found to be an unreliable predictor for assessing relative efficacy of inhibition. During *in vitro* applications, analysis of the induction of apoptosis and metabolic effects were assessed using flow cytometry and the MTS assay, respectively. These showed no significant toxicity. Effects of inhibitors on collective and single cell migration in the normal and premalignant cell model, assessed using time lapse live cell imaging, cell morphology and labelling for vinculin and F-actin (for focal adhesions, FAs) showed that the TF 17-2 and TF 22d inhibitors reduced the collective cell migration of MCF-10A cells in scratch assays. Live-cell analysis of single cell migration, however, showed that TF 22d increased cell migration rates, and reduced the size of FAs and actin stability in MCF-10AneoT cells, resulting in a predominently rounded cell morphology in the premalignant cell line. TF 17-2, on the other hand was seen to be a relatively selective inhibitor of premalignant cell migration and resulted in MCF-10AneoT cells re-establishing larger focal

adhesions due to more stable F-actin networks resembling those of the non-transfected MCF-10A cell line, but reduced MCF-10AneoT cell migration most markedly. FA size and velocity of movement seemed inversely related in the normal and premalignant cells. The results of the current study suggest that, TF 17-2 seemed to have the greater therapeutic potential than TF 22d for inducing phenotype reversion, inhibition of dissemination, invasion and metastasis. Three promising selective pharmacological actions of TF 17-2 on the premalignant MCF10AneoT cell line include the suppression of proliferation, induction of increased in metabolic activity (possibly indicating cell stress) and a decrease in premalignant cell migration. A lack of cytotoxicity, however, suggests that TF 17-2 would need to be administered with an ancillary chemotherapeutic agent. This study showed that MMPIs directed against MT1-MMP, may still represent an effective strategy for inhibiting the migration of premalignant cells expressing high levels of MT1-MMP, and suggests further studies on this topic may be profitable.

Acknowledgments

During the course of my studies I have been fortunate to interact with outstanding scientists that offered their help and expertise so freely. For sharing their thoughts and expertise I would like to thank the following people:

Dr Edith Elliott for allowing me the opportunity to extend my academic horizons and test my abilities; for a style of supervision and energy that always motivated me to work harder; for always checking that I had the correct controls, something I seemed to repeatedly initially omit, and for constructive criticisms, proof reading and edits.

Dr Celia Snyman for seeing potential in me and showing me that altruistic people really do exist, by assisting me financially to do this MSc, for scientific guidance, technical skills, proof reading, compassion, encouragement, humour and friendship.

Professor Harald Tschesche and Dr Tim Fisher for synthesising and providing the MMPIs, TF 17-2 and TF 22d.

The ladies of the EM unit for making the dull windowless premises of the EM unit the happiest, most hospitable and accommodating place to be and a place where I always enjoyed time spent; Mrs Shirley McKellar for technical skills, humour and devotion to assisting students; Mrs Patricia Joubert for some great recipes, jokes and assistance whenever needed; Miss Tutuzwa Xuma and Mrs Nelisha Murugan, for their overall assistance and support with SEM.

Dr Mahmoud Soliman, Discipline of Pharmaceutical Sciences, School of Health Sciences, UKZN, Westville, for invaluable assistance with molecular modelling using AutoDock Vina.

Dr Chrisna Durandt, of Beckman Coulter, for teaching me the basics of flow cytometry and helping me with the setup of my protocol.

Mr Yegan Pillay for limitless dedication to helping me with Linux software and a rare brand of kindness, for which he is wished much success in all his endeavours.

Mrs Jessica Moodley for always being understanding and generous to Lab 43; she deserves the award of Lab. Tech. of the year!

Mr Oliver Bodhlyera for his assistance with statistical issues and being a great teacher.

Robert Krause, Laurelle Jackson (my fellow die-hards of Honours 2009), Melissa Govender and Nick Walker for some really fun and memorable times and keeping me sane!
Kyle and Dayne Goetsch, special thanks for their friendship, making every day an interesting and enjoyable one and allowing me to live with them for a year, an achievement worthy of an award for putting up with me for that long.

Dr Carola Niesler for being a model scientist and allowing me to tag along to a conference and exposing me to the fascinating world of stem cells.

Mrs Charmaine Ahrens and Mrs Robyn Hillebrand for being wonderful, efficient and helpful people at all times.

Mayuri Jagmohan for her guidance, support and friendship in the lab on good and bad days.

The NRF for funding the confocal microscope and for awarding me a bursary in 2011.

My amazing mother, for casting doubt exactly when needed and being a great motivator causing me to stick with the program like a barnacle; for sacrificing so much to give me this opportunity and for being there for me through it all and for giving me a better future at the expense of her own.

Table of Contents

CHAPTER 2.

Materials and Methods

CHAPTER 3.

Comparative docking of two MMP inhibitors

List of Figures

List of Tables

List of abbreviations

ΔG	free energy (kcal/mol)
2D	two dimensions
3D	three dimensions
aa	amino acid
Ab	antibody
ADAM	a disintegrin and metalloproteinase
ADP	adenosine diphosphate
ADT	Auto Dock Tools
AIF	apoptosis inducing factor
AKT	serine/threonine protein kinase, also protein kinase B (PKB)
AMBER	Assisted Model Building with Energy Refinement
AP-2	adaptor protein 2
Asp^{12}	aspartate in position 12
ATP	adenosine triphosphate
BAD	Bcl-2 associated death promoter
BAK	Bcl-2 homologous antagonist killer
BAX	Bcl-2-associated X protein
Bcl-2	B-cell lymphoma 2
BH3	Bcl-2 homology
BID	BH3 interacting-domain death agonist
BIM	Bcl-2 like protein 11
BM	basement membrane
BMF	Bcl-2 modifying factor
Ca^{2+}	calcium ion
CAD	caspase-activated DNase
cal	calories
CAM	chicken chorioallantoic membrane
CANNTG	cytosine-adenine-nucleotide-nucleotide-thymine-guanine
CD147	cluster of differentiation 147, also known as EMMPRIN
CD44	cluster of differentiation 44, hyaluronic acid receptor
Cdc42	cell division control protein 42 homolog
CDK4	cyclin dependent kinase 4
c-Ha-*ras*(V^{12})	constitutively active Harvey *ras* oncogene with Gly^{12} mutated to Val^{12}
CHX	cycloheximide

conc.	concentration
Da	Dalton
ddH_2O	deionised water
dH_2O	distilled water
dil.	dilution
DISC	death-inducing signalling complex
DMEM	Dulbecco's minimal essential medium
DMSO	dimethyl sulfoxide
DNA	deoxyribonucleic acid
DNA	deoxyribose nucleic acid
DP	dimerisation partner
E2F	family of transcription factors
ECL	enhanced chemiluminescence
ECM	extracellular matrix
EDTA	ethylenediaminetetra-acetic acid
EGF	epidermal growth factor
EMMPRIN	extracellular matrix metalloproteinase inducer (CD147)
EMT	epithelial to mesenchymal transition
ERK	extracellular signal related kinase
Ext/Em	excitation/emission
FA	focal adhesion
FADD	Fas-associated death domain
FASTA	Pearson protein sequence file format
FITC	fluorescein isothiocynate
FS	forward scatter
FSC	forward scatter channel
g	relative centrifugal G-force
G1-phase	post-mitotic phase of cell cycle, before S-phase
GA	Genetic Algorithm
GAP	GTPase activating protein
GAPDH	glyceraldehyde 3-phosphate dehydrogenase
GDP	guanosine diphosphate
GEFs	guanine nucleotide exchange factors
GHz	giga Hertz
GPI	glycosylphosphoinositol
GSK-3β	glycogen synthase kinase-3β
GTP	guanosine triphosphate

GUI	Graphical User Interface
h	hour
HBSS	Hanks' balanced salts
HExHxxGxxH	histidine-glutamate-aa-histidine-aa-aa-glycine-aa-histidine
HMW	high molecular weight
H-Ras	Harvey-Ras
HRP	horseradish peroxidase
ICAD	inhibitor of caspase-activated DNase
K	Kelvin
Ka	association constant
kcal	kilocalories
kDa	kiloDalton
K*i*	affinity constant
K-Ras	Kirsten-Ras
l	litre
LGA	Lamarckian Genetic Algorithm
M	molar concentration
MAP	mitogen activated protein
MAPK	mitogen activated protein kinase (ERK)
MAPKK	mitogen activated protein kinase kinase (MEK)
MAPKKK	mitogen activated protein kinase kinase kinase (Raf)
MCF	Michigan Cancer Foundation
MCF-10A	immortal beast epithelial cells (attached)
MCF-10AneoT	c-Ha-*ras* transfected MCF-10A cells
MD	Molecular Dynamics
MDM2	murine double minute 2
Mg^{2+}	magnesium ion
mm	millimetre
MMP	matrix metalloproteinase
MMPI	matrix metalloproteinase inhibitor
mol	Mole
MPIs	metalloproteinase inhibitors
Mr	molecular weight
mRNA	messenger ribonucleic acid
ms	milliseconds
MT1-MMP	membrane-type 1 matrix metalloproteinase

MTS	3-(4,5-dimethylthiazol-2-yl)-5-(3-carboxymethoxyphenyl)-2-(4-sulfophenyl)-2H-tetrazolium
MTT	3-(4,5-dimethylthiazol-2-yl)-2,5-diphenyltetrazolium bromide
NAD^+	nicotinamide adenine dinucleotide
NADH	nicotinamide adenine dinucleotide reduced form
NF-κB	nuclear factor kappa-light-chain-enhancer of activated B cells
N-ras	human neuroblastoma-*ras*
Nε2	Nitrogen epsilon two of the histidine imadazoyl
p14ARF	p14 alternative reading frame
$p16^{INK4}$	cyclin-dependent kinase inhibitor 2A (tumour suppressor protein)
p53	tumour suppressor gene and transcription factor
PAGE	polyacrylamide gel electrophoresis
PDK1	phophoinositide-dependent kinase 1
PEX	haemopexin domain
PI	propidium iodide
PI3K	phosphatidylinositol-3 kinase
PIP2	phosphatidylinositol 4,5-biphosphate
PIP3	phosphatidylinositol 3,4,5-triphosphate
PKC	protein kinase C
PM	plasma membrane
PMS	phenzinemethosulfate
pRb	phophorylated retinoblastoma
PRO	prodomain
proMMP	precursor/immature MMP
PS	phosphatidyl serine
R	gas constant (1.98719 cal)
Rac	Ras-related C3 botulinum toxin substrate (GTPase protein)
Raf	serine/threonine kinase
Ras	GTP-signal transduction molecule
Rb	retinoblastoma
Rho	Ras homologue
RNA	ribonucleic acid
RT	room temperature (± 25°C)
SDS	sodium dodecylsulfate
Slug	transcription factor of Snail family
Smac	second mitochondria-derived activator of caspase
Snail	transcription factor, also known as Snai1

S-phase	synthesis/DNA replication
SS	side scatter
SS	signal sequence
SSC	side scatter channel
T	temperature
TGF-β	transforming growth factor-β
TIMP	tissue inhibitor of matrix metalloproteinase
TNF	tumour necrosis factor
TRAIL	TNF-related apoptosis-inducing ligand
TRITC	tetramethyl rhodamine iso-thiocyanate
TTBS	tween 20 Tris buffered saline
Val^{12}	valine in position 12
vol.	volume
XTT	2,3-bis(2-methoxy-4-nitro-5-sulphophenyl)-2H-tetrazolium-5-carboxanilide
ZBG	zinc binding group
Zn^{2+} or Zn(II)	zinc ion

CHAPTER 1.

Introduction

1.1. Breast cancer: a global and local burden

The last decade has seen a shift from cervical cancer to breast cancer becoming the leading cause of death among women in economically developing countries (Jemal et al., 2011). Cancer survival tends to be worse in developing countries (Jemal et al., 2011), most likely due to late stage initial diagnosis (Jemal et al., 2011; Vorobiof et al., 2001). In South Africa, black African women have historically shown a low incidence of breast cancer, 15.1 per 100 000 (age adjusted annual incidence rate), when compared to the high incidences of developed Westernised countries which range from 40-89 per 100 000 individuals (Walker et al., 2004). The gradual influence of Westernised culture on developing countries, however, has brought with it socioeconomic improvements, but also less desirable habits like dietary changes and decreased exercise. This has dramatically increased breast cancer incidence, especially among black African women (Porter, 2008). Although risk factors are usually similar between racial groups, with urbanisation, breast cancer occurrences rise steeply (Walker et al., 2004).

South Africa, however, faces two problems, late stage initial diagnosis and a future of increasing breast cancer incidence. In first world countries, patients with breast cancer are diagnosed in the early stages (I and II), before lymph node metastasis. In developing countries such as South Africa, women present on initial diagnosis with late stage invasive cancers; III, IV and V (Vorobiof et al., 2001), usually associated with a poor prognosis and high mortality (Jemal et al., 2010; Vorobiof et al., 2001). This late diagnosis may be due to a geographical lack of accessibility to public health systems or cultural practices which encourage holistic approaches. It is, therefore, important to explore new therapeutic targets of cancer cell invasion and metastasis to reduce mortality both globally and locally.

1.2. Cancer cell origins: the conventional cancer model

In normal tissues, cells respond to biological cues that regulate cell division, death and other cellular activities. This “sense of community” maintains tissue homeostasis through limiting proliferation and is the reason tissues and organs do not grow out of proportion. Genetic mutations in cancer cells disrupt this balance allowing uncontrolled proliferation and enhanced cell survival (Bertram, 2001). Progression to malignancy is thus marked by a loss of

responsiveness to growth regulatory signals (Velcich et al., 2006). A limitless replicative potential (immortality) and the ability to avoid programmed cell death (apoptosis) are both hallmarks of neoplasia (abnormal new growth) (Velcich et al., 2006). These acquired mutations have sparked a new controversy in cancer biology involving two theories that describe the successive acquisition of mutations and the origin of the first oncogenic insult.

The conventional clonal evolution model for cancer progression proposes that early neoplastic cells harbour an initial mutation that causes cells to hyper-proliferate and form large tissue masses called tumours (Bertram, 2001). Hyper-proliferation results in the stochastic acquisition of multiple mutations that may equip the tumour with a phenotypic advantage such as enhanced survival, tumour aggressiveness or therapy resistance. Such advantages would drive tumour progression through natural selection pressures that would tend to select for faster growing, more aggressive tumours (Al-Ejeh et al., 2011). Mutated tumour suppressor genes, such as *p53* or retinoblastoma (Rb) or the transcription factor c-Myc, would confer such advantages. The p53 protein, for example, not only controls cell cycle progression but ensures DNA integrity during replication (Dang et al., 2009; Soussi and Lozano, 2005).

1.2.1. Cancer cell origins: cancer stem cell model

The origin of cancer, immortality and plasticity of differentiation has been linked to a subpopulation of cancer cells that possess stem cell characteristics (Prat and Perou, 2011). Such stem cell characteristics include, immutability, the ability to colonise other parts of the body and the ability to remain quiescent for long periods of time rendering these cells resilient to electromagnetic and chemical insults (Clevers, 2011). The cancer stem cell (CSC) model is a hierarchical model proposing that only a subset of cells can propagate the tumour by acting as multipotent progenitors resulting in cellular heterogeneity within the tumour (Al-Ejeh et al., 2011). Unlike normal stem-cells that terminate replication after the stem cell niche has been replenished, CSCs and stem cell-derived cancer progenitor cells overpopulate the niche and infiltrate the surrounding tissue (Strewler, 2006). Following conventional therapy and tumour remission, a small number of quiescent CSCs may have been resistant to therapy causing relapse and regeneration of the entire recurrent tumour (Federici et al., 2011). CSCs are, therefore, an attractive therapeutic target to increase the efficacy of current therapies and improve the outcome of therapy in cancer patients by reducing recurrence (Prat and Perou, 2011).

1.2.2. Bidirectional conversions between CSCs and non-CSCs

Normal epithelial cells form layers held together by a lateral belt of a variety of junction proteins forming cell-cell contacts, such as tight junctions, adherens junctions, desmosomes and gap junctions (Berx et al., 2007). Adhesion molecules such as cadherins (cell-cell contacts) and integrins (cell-matrix or cell-cell contacts) interact with the actin cytoskeleton polarising the cell layer, forming the characteristic apical and basal polarity in epithelial cells. Epithelial cells that acquire a transient motile phenotype undergo an epithelial-to-mesenchymal transition (EMT) from a non-motile, polarised phenotype to become non-polarised and more like a mesenchymal flattened and extended, migratory cell like a fibroblast (Figure 5.2)(Berx et al., 2007).

EMT is characterised by a loss of these interactions between cells, and as a result, loss of apicobasal polarisation of organelles and the cytoskeleton. During this process, cell-cell contacts of epithelial cells are down regulated, growth becomes anchorage-independent, and motility-stimulating signalling proteins are activated (Larue and Bellacosa, 2005). EMT is a transient process involved in normal wound healing, but may have pathophysiological consequences if sustained, such as in invasive cancers (Berx et al., 2007). Invasion into the vascular system allows transport of malignant cells to distant sites where they may extravasate and form secondary tumours (metastasis). Examples of tissues to which metastasising breast cancer cells relocate include the bone (Kang et al., 2003), central nervous system (Weil et al., 2005) and the lung (Minn et al., 2005).

EMT has been widely studied in the context of embryonic morphogenesis. During embryogenesis signals from the microenvironment, such as transforming growth factor-β (TGF-β) and Wnt ligands, induce EMT. Such plasticity is reminiscent of EMT induced during wound healing and cancer metastasis. Once EMT stimuli are removed, cells may revert to their original epithelial morphology in a process known as, mesenchymal to epithelial transition (MET). Pathways associated with CSCs, EMT and embryogenesis include the Hedgehog, Notch, Wnt and PTEN pathways which also control self-renewal, proliferation and survival. Mutations that activate these pathways may support the "stemness" characteristics of CSCs (Liu et al., 2006; Liu et al., 2005; Sansone et al., 2007; Woodward et al., 2007).

The CSC model is still a controversial theory. Many postulate that CSCs are transformed normal stem cells, however, it is also possible that they may arise from lineage-restricted progenitor or differentiated cells by acquiring stem cell-like properties (Lindeman and Visvader, 2010;

Shackleton et al., 2009). In addition, CSC and non-CSC may interconvert between phenotypes (Gupta et al., 2009). Experimental evidence that supports "bidirectional conversion" was presented by Bhat-Nakshatri et al. (2010) after studies on a phenotypically "normal" breast epithelial cell line containing CSCs (the MCF-10A cell line of a basal stem cell breast epithelial origin) used in the current study, Section 1.4. A surface marker profile of $CD44^{+}/CD24^{-}$, representing a subpopulation of tumourogenic and oligopotent breast CSCs, was found to be enriched upon the addition of tumour necrosis factor (TNF). The addition of this MAPK activating cytokine increased the number of stem cell-like $CD44^{+}/CD24^{-}$ cells in the MCF-10A basal breast epithelial cell line. Similar effects were observed with TGF-β1 (Morel et al., 2008), suggesting that microenvironments rich in proteins which trigger EMT may also confer a stem-like marker profile, $CD44^{+}/CD24^{-}$, in MCF-10A cells (Bhat-Nakshatri et al., 2010; Morel et al., 2008; Sheridan et al., 2006). Bidirectional conversion and the direct influence of the microenvironment may, therefore, play a role in producing tumours that are genetically identical but epigenetically distinct (Clevers, 2011). The CSC model and the clonal evolution model are not mutually exclusive in cancers that are hierarchically organised into epigenetically distinct populations of tumourogenic and non-tumourogenic invasive cancer cells, however. In these tumours, clonal evolution may still occur in the cancer stem cells (Clevers, 2011).

Nevertheless, the mesenchymal phenotype of either CSC or epithelial cells undergoing EMT, is associated with both normal cell migration and cancer cell invasion programs. Though the mechanistic differences in these programs are still unclear, such differences may constitute promising therapeutic targets that may enhance current therapies and improve the outcome of patient therapies. Key in signalling and promoting movement during EMT, is a membrane type matrix metalloprotease, MT1-MMP (Cao et al., 2008; Ota et al., 2009), the role of which forms the focus of this study and will be described in Section 1.6.

To adequately represent the heterogeneous populations observed in normal breast epithelial cells and tumours derived from epithelial origins, we used the MCF-10A cell line and its premalignant, stably-*ras* transformed mesenchymal derivative, the MCF-10AneoT cell line.

1.3. Establishment of immortality in the MCF-10A cell line

The Michigan Cancer Foundation (MCF) -10A (adherent) breast epithelial cell line was established from mastectomy tissue from a 36 year old, pre-menopausal, Caucasian patient with severe fibrocystic disease of the breast. This cell line, after extended cultivation in normal

calcium levels (1.05 mM), spontaneously immortalised without the use of viral or chemical carcinogens. The cell line possesses a near diploid karyotype and is non-invasive, exhibits normal epithelial characteristics [i.e. forms a single monolayer of cells and exhibits contact inhibition of growth upon becoming confluent, with well-established cell-cell adherence junctions, desmosomes, tight-and gap junctions and a polarised apical (top) and basolateral (basal) polarity] and control by hormone and growth factors. It also exhibits dome formation in confluent cultures and was initially thought to rely on anchorage-dependent growth (Soule et al., 1990; Tait et al., 1990). Characteristics of such epithelial cells include a non-tumourogenic phenotype in nude mice, the ability to form 3D structures such as acini when grown *in vitro* in 3D ECM-constituent overlay culture (Debnath et al., 2003) or in an anchorage-independent manner as hanging drops (Snyman and Elliott, 2011).

The MCF-10A cell line provides a model system for the study of non-malignant breast epithelia and the influence of mutationally activated oncogenes on morphogenesis (Soule et al., 1990) and progression towards malignancy (Kadota et al., 2010, explained further in Section 1.3.1). The system also allows differences in migration in normal and the invasive premalignant derivative to be assessed, as well as the possible differential effects of MT1-MMP inhibitors on a "normal" and premalignant breast epithelial cell, though the "normal" MCF-10A cell line is not entirely normal, due to spontaneous immortalisation (Debnath et al., 2003; Sharpless and DePinho, 2004).

In many cases, immortality is due to mutation of tumour suppressor proteins, p53 and Rb, and a resultant loss of control over cell cycle progression (Sharpless and DePinho, 2004). Immortality in the MCF-10A cell line arose due to a deletion at the *9p21* locus encoding the cyclin-dependent kinase inhibitor 2A (*CDNK2A*) gene, resulting in a lack of p16 (*p16INK4*) and p14 (*p14ARF*) tumour suppressor proteins (Debnath et al., 2003; Sharpless and DePinho, 2004). The p16 protein is an inhibitor of cyclin-dependent kinase 4 (CDK4) which is required in the G1 and S phases of the cell cycle (Figure 1.1-A). CDK4 phosphorylates retinoblastoma (pRb) which ultimately prevents cell progression through G1 into S phase (Weinberg, 1995). Hypo-phosphorylated Rb (Rb) binds to the E2F family of transcription factors, preventing the transcription of S phase promoting genes (Weinberg, 1995). In the absence of p16, Rb is hyper-phosphorylated by cyclin-dependent kinase-4 (CDK4) and loses its grip on E2F-dimerisation partners, allowing progression through to S-phase (Figure 1.1-B).

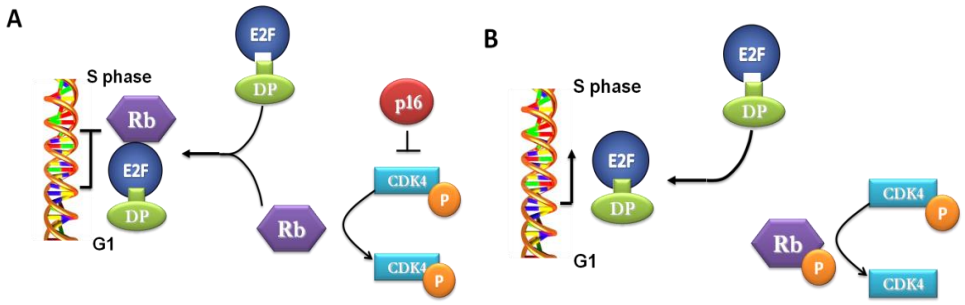

Figure 1.1. Cell cycle control in the absence and the presence of tumour suppressor protein p16.
(A) p16 inhibits phosphorylation of Rb. Hypo-phosphorylated retinoblastoma protein (Rb) binds the E2 promotor-binding-protein-dimerisation-partners (E2F-DP) in the presence of p16, causing the cell to remain in the G1 phase. **(B)** In the absence of p16, pRb is hyper-phosphorylated by cyclin dependent kinase-4 (CDK4) and releases E2F-DP, allowing progression through to S-phase. Lack of p16 may thus result in immortality [figure was compiled using information from references in the text].

In the presence of p14, p53 function is maintained (Figure 1.2-A). A lack of p14, however, allows binding of MDM2 to p53. In addition MDM2 also possesses E3 ubiquitin ligase activity specific for p53, and promotes export of p53 from the cell nucleus to the cytoplasm for degradation in the proteosome (Figure 1.2-B) (Sherr, 2006). Together, lack of p16 reduces control over CDK4, and lack of p14 results in low levels of free p53. These factors may account for the MCF-10A cell line's immortality (Imbalzano et al., 2009; Weinberg, 1995) and reduced control of progression through G1 and into S phase (Figure 1.2-B) (Thullberg et al., 2000). Thus, the MCF-10A cell line is permitted through the cell cycle with reduced DNA replication fidelity. This allows the progression of the cell line phenotype towards the malignant phenotype upon introduction of a promoting oncogene such as a mutationally activated H-Ras oncogene, which forms the focus of this study due to its association with an invasive phenotype.

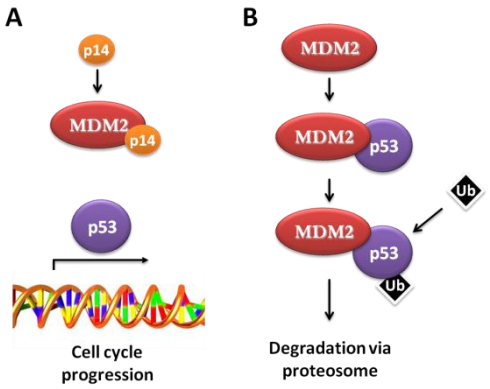

Figure 1.2. The effects of p14 tumour suppressor on p53 activity, and the inactivation and degradation of p53 when p14 is absent.
(A) In the presence of p14, MDM2 is bound by p14, allowing free p53 to act as a transcription factor co-ordinating cell cycle arrest, apoptosis or p53 transcription. **(B)** In the absence of p14, MDM2 binds p53 allowing ubiquitination and subsequent degradation of p53. This in turn, may facilitate immortalisation and proliferation [figure was compiled using information from references in the text].

1.3.1. The MCF-10AneoT cell line and the H-Ras proto-oncogene

To study one of the H-Ras mutations associated with the invasive phenotype and progression to malignancy, the MCF-10A cell line was initially transfected with a plasmid containing a neomycin resistance gene and the constitutively active c-H-*ras*(V^{12}) oncogene, cloned from the human T24 bladder carcinoma (Basolo et al., 1991). This gave rise to the MCF-10AneoT cell line that contains a H-Ras(V^{12}) mutation in which the twelfth amino acid, glycine, is replaced with valine. This mutated oncoprotein induced characteristics of the malignant phenotype, including an increase in motility and invasion, and a mesenchymal morphology [a cell without apical or basolateral polarity that does not show contact inhibition but tends to grow over neighbouring cells when grown in a monolayer format (2D), has reduced levels cell-cell adherence junctions, desmosomes, tight-and gap junctions and no apical (top) and basolateral (basal) polarity so, but instead adopts an elongated cell migratory structure, with lamellipodia-like protrusions at the front and a trailing tail resembling a migrating cell, as depicted in Figure 5.2 as described in Section 5.1] (Basolo et al., 1991; Ochieng et al., 1991). This cell line, therefore, constitutes a model of a premalignant invasive cell.

1.3.2. H-Ras in cell migration.

Ras proteins belong to a small family of GTPases that regulate proliferation, survival, differentiation and apoptosis in normal cells (Castellano and Downward, 2011). Three mammalian *ras* genes encode four Ras proteins, H-Ras, K-RasA, K-RasB and N-Ras, that have tissue specific functions (Olson and Marais, 2000). The effective differences between these proteins has been reviewed by Bar-Sagi (2001) and for the purpose of this study, only H-Ras will be described as mutations of this oncoprotein have been shown to be involved in cancer cell invasion and migration (Moon et al., 2000), the focus of this study.

Due to post translational addition of hydrophobic lipids (farnesyl and palmitoyl groups) to the C-terminus (Willumsen et al., 1984), H-Ras proteins are localised to the inner face of cholesterol-rich lipid rafts in the plasma membrane (Roy et al., 1999). Caveolin-1, a protein component of caveolae, binds cholesterol, sphingolipids and signalling-molecules into organised, flask-shaped, microdomain structures. Within caveolae, H-Ras links upstream activators and downstream effectors. Guanine nucleotide exchange factors (GEFs) regulate the strength of H-Ras signalling by promoting exchange of GDP for GTP, while GTPase-activating proteins (GAPs) stimulate hydrolysis of active GTP to inactive GDP (Figure 1.3) (Bos, 1989). Molecules which collect in caveolae may interact with H-Ras (Olson and Marais, 2000), resulting in the stimulation of

certain effector pathways. Active H-Ras proteins are known to stimulate the lipid kinase, phosphatidylinositol 3' kinase (PI3K) (Voice et al., 1999), and a cascade including mitogen activated protein (MAP) kinase kinase kinases (the Raf proteins), MAP kinase kinases (the MEKs) and MAP kinases (the ERKs) (Robinson and Cobb, 1997). The MAP, MEK and ERK pathways, in turn, have many downstream effector molecules, but ultimately regulate proliferation, survival and differentiation.

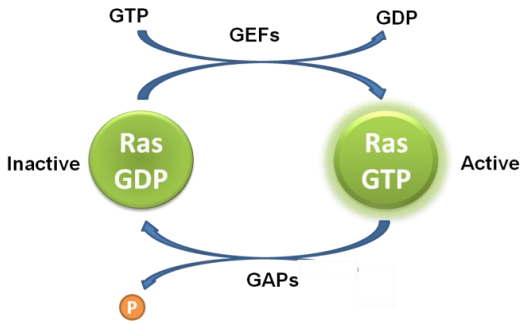

Figure 1.3. The H-Ras activation cycle.
Ras cycles between an active GTP bound state and an inactive GDP bound state facilitated by guanine nucleotide exchange factors (GEFs) and GTPase activating proteins (GAPs) [redrawn from Olson and Marais (2000)].

In addition, H-Ras regulates the cytoskeleton elements Rho, Rac and Cdc42 to facilitate migration and is of particular importance in an invasive phenotype, though the differences in the normal and abnormal processes are not clear. These GTPases are responsible for stress fibre, lamellipodia and filopodia formation, respectively (these cell structures are further described in Chapter 5). Normally activated Ras (activated e.g. by G protein-linked growth factor receptors) can briefly and reversibly activate Rac via PI3K, stimulating membrane ruffling and promoting stress-fibre and focal adhesion formation under the influence of RhoA (Yamazaki et al., 2005). In the MCF-10AneoT, however, where H-Ras(V^{12}) is irreversibly activated, Ras induces sustained cytoskeleton reorganisations and more sustained characteristics associated with EMT, and hence increased motility (Ochieng et al., 1991).

PI3K/AKT axis in H-Ras signalling

Constitutive signalling of H-Ras(V^{12}) and subsequent preferential activation of PI3K (Voice et al., 1999) in the abnormal, premalignant MCF-10AneoT cell line gives rise to a suitable model of a premaligant cell progressing towards the malignant phenotype. PI3K signalling is involved in processes critical to cancer progression, including increased metabolic activity, proliferation,

survival, and motility. Research has shown that such mutational activation of PI3K is present in 25% of human breast cancers (Bachman et al., 2004).

Activation of PI3K and subsequent phosphorylation of phosphatidylinositol 4,5-biphosphate (PIP_2) to phosphatidylinositol 3,4,5-triphosphate (PIP_3), results in PIP_3 binding to phosphoinositide-dependent kinase 1 (PDK1) and a serine/threonine protein kinase (AKT) (Cantley, 2002). PIP_3-PDK1 and AKT are brought to the plasma membrane where PKD1 activates AKT, promoting cell survival by three mechanisms. First, AKT inhibits pro-apoptotic Bcl-2 family members Bad and BAX, inhibiting the release of cytochrome-c from the mitochondria preventing the induction of programmed cell death or intrinsic apoptosis, further discussed in Section 4.1. Second, AKT negatively regulates transcription factor NF-κB, resulting in increased transcription of anti-apoptotic and pro-survival genes. Third, AKT phosphorylates MDM2 allowing translocation into the nucleus, where MDM2 sequesters tumour suppressor p53, antagonising p53-mediated apoptosis and monitoring of DNA replication fidelity (Castellano and Downward, 2011). H-Ras signalling along the PI3K/AKT pathway, therefore, promotes cell survival. PI3K/AKT signalling is also a central feature of EMT where MT1-MMP is a key protease in this process (Larue and Bellacosa, 2005).

1.4. Molecular determinants of EMT

H-Ras related signalling via AKT has been shown to regulate down-regulate mRNA and protein levels of cell-cell adhesion molecules, such as E-cadherin (Grille et al., 2003). Loss of E-cadherin functionality as levels drop is a hallmark of EMT and the progression towards malignancy (Yilmaz and Christofori, 2009). Studies show that suppression of the E-cadherin gene occurs through activation and expression of the *Snail/Slug* gene (Batlle et al., 2000; Cano et al., 2000). Snail and Slug proteins belong to a family of transcription factors which are involved in the progression of epithelial malignancies, mediating EMT, migration, invasion and survival.

In a study using breast carcinomas, E-cadherin mRNA expression was found to be lower when Snail expression was elevated, suggesting an inverse relationship between the two (Elloul et al., 2005). Three consensus sequences on the E-cadherin gene have been identified as Snail and Slug binding sites and appear to be involved in the induction of EMT in breast carcinomas (Westermarck and Kahari, 1999). In addition to induction of EMT and repression of E-cadherin, Snail binding to E-cadherin gene consensus sequences up-regulates expression of matrix metalloproteinases (MMPs) (Gilles et al., 1997a).

MMPs are able to degrade extracellular matrix (ECM) and basement membrane (BM) components underlying epithelial cells (Folgueras et al., 2004). A key MMP is MT1-MMP which facilitates cell migration and invasion through cleavage of cell-cell contacts such as E-cadherin, and processing of adhesion components such as integrins. Integrins bind ECM components and signal through adaptor proteins, such as vinculin, linked to the actin cytoskeleton (Section 5.1) (Lock et al., 2008; Moissoglu and Schwartz, 2006). In some instances, such as those in which mutational activation of *ras* occurs, sustained activation causes sustained upregulation of MT1-MMP increasing integrin signalling by negatively affecting cell adhesion, thereby giving rise to signals that induce and sustain EMT. Studies have shown that H-Ras up-regulates MMP-2 in MCF-10A H-Ras(Asp^{12}) transient transfected cells (Kim et al., 2007; Kim et al., 2003; Shin and Moon, 2002). MMP up-regulation and possible redistribution in cancer cells may sustained EMT by two mechanisms, shedding of cell surface molecules through cleavage of cell-cell contacts, and release of the anchored cell by processing/degradation of ECM components (Cao et al., 2008). MT1-MMP and MT2-MMP, in particular, may co-operate to facilitate and promote migration and invasion through ECM turnover (Ota et al., 2009). Therefore, MMPs appear to be major contributors to migration, invasion and EMT.

Depending on the surrounding extracellular microenvironment, cleavage of cell-cell contacts and changes in integrin repertoire may result in the dissemination of cells from the collective mass or tumour to other parts of the body, usually the brain or bone in the case of breast cancer. MT1-MMP in particular, has been implicated in tumour dissemination and metastasis of gastric (Yoshikawa et al., 2006), prostate (Cao et al., 2008), ovarian (Moss et al., 2009a) and breast cancers (Perentes et al., 2011; Szabova et al., 2007).

1.4.1. Migration and invasion programs.

Migration and invasion programs use similar molecular tools for cellular movement (described in Chapter 5) (Friedl and Wolf, 2003b). Briefly, during migration of a cancer or a normal cell, the cell establishes localised contacts with the ECM or substratum at the leading front through integrins (described in Chapter 5) (Friedl and Wolf, 2003a) and the hyaluronan receptor, CD44 (Marrero-Diaz et al., 2009). Integrin clustering at the leading front results in the formation of focal adhesions that mature into larger structures capable of supporting tensile forces during migration (Puklin-Faucher and Sheetz, 2009). MT1-MMP plays multiple roles in integrin functioning. MT1-MMP cleavage of the ECM component fibronectin, encourages β1 integrin clustering and subsequent focal adhesion formation (Takino et al., 2006). In addition, MT1-

MMP-processing of pro-α_v integrin to $\alpha_v\beta_3$ (Ratnikov et al., 2002) facilitates $\alpha_v\beta_3$-dependent adhesion (Deryugina et al., 2000) and enhanced $\alpha_2\beta_1$ integrin adhesion to collagen type-I in normal breast epithelial cells (Baciu, 2003). Therefore, during a controlled migration program MT1-MMP-mediated migration is required for cell-matrix adherence and cell-matrix release through ECM proteolysis. Due to the up-regulation of MT1-MMP in MCF-10A cells stimulated to migrate on collagen (Gilles et al., 2001) and the observed increase in migration and invasion programs in the presence of collagen type-I (Barkan et al., 2010), collagen type-I will be used in 2D migration assays (Section 5.4).

In non-malignant and malignant migratory cells, CD44 facilitates MT1-MMP trafficking to the leading front, an area of focussed proteolysis of ECM components (Mori et al., 2002). Here, MT1-MMP and other collagenases cleave native collagens and other structural proteins allowing further degradation by gelatinases and serine proteases (Friedl and Wolf, 2003b), thereby exposing binding sites for further integrin adherence (Hangai et al., 2002; Schenk and Quaranta, 2003; Xu et al., 2001). In addition, ECM-associated growth factors (epidermal growth factor, lysophosphatidic acid and insulin-like growth factor-1) or migratory-stimulating factors (autocrine motility factors and mitogens) are released triggering migration/invasion programs (Friedl and Wolf, 2003b). At the rear or trailing end of the cell, MT1-MMP cleaves CD44 (Marrero-Diaz et al., 2009) and ECM components releasing integrins (Takino et al., 2006). The fundamental difference between 2D migration and 3D invasion is that 2D migration or movement requires protease-mediated processing of integrins and cleavage of CD44 for adherence and release from the substratum. This facilitates single-plane cellular adherence and movement along a matrix substratum. Invasion (3 D), on the other hand, may be achieved either by a similar mechanism accompanied by additional proteolytic breakdown of the matrix, or by non-proteolytic amoeboid movement through available spaces in protein barriers (Friedl and Wolf, 2003a) (Figure 1.4). A 2D model system, where only proteolytic movement is assessed, and not a 3D system, where both proteolytic and non-proteolytic movement may occur, was, therefore, required in the current study to assure the testing of the role of MT1-MMP in migration and not amoeboid movement was being assessed.

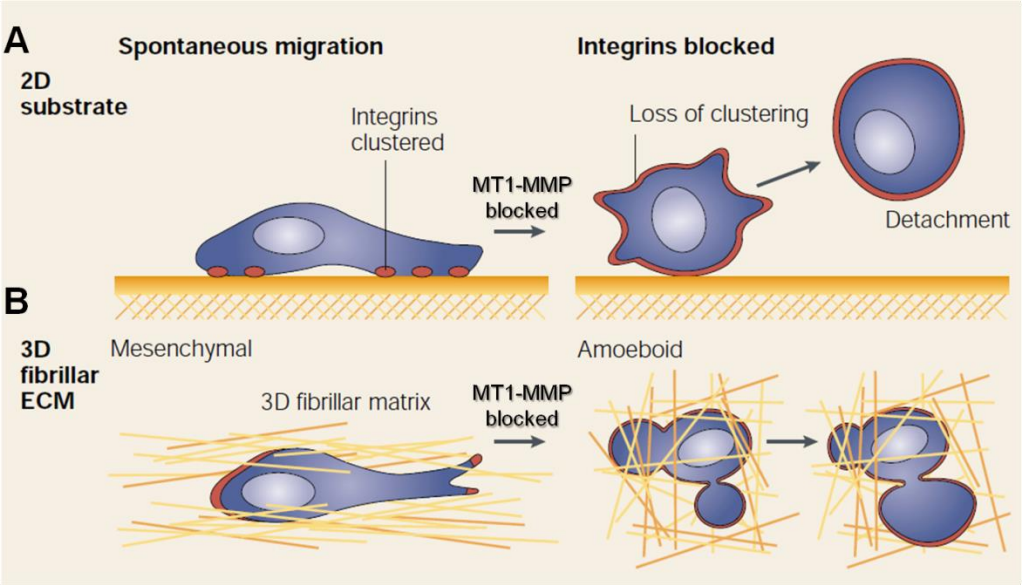

Figure 1.4. Methodologies for assessing cell migration.
In 2D models (**A**), migration is dependent on cell adhesion to the substratum and processing of integrins and CD44 by MT1-MMP, without which, cells would detach or become only partially adherent and migration inhibited. In 3D (**B**), cells are embedded in a scaffold and may utilise adhesion independent mechanisms of cell migration if MT1-MMP is blocked [reproduced with minor modifications from Friedl and Wolf, (2003b)].

The assessment of integrin-associated focal adhesions that form in a single plane offers a more directly viewed perspective and evidence of proteolytic activity. Visualisation and interpretation of cytoskeletal partners and focal adhesions or other molecular interactions is also simpler as targets of immunolabelling for revealing the workings of the machinery involved in migration are fewer. The 3D protein barrier in which non-proteolytic amoeboid movement may substitute for proteolytic invasion is also removed and hence targets for immunolabelling are more exposed (Figure 1.4-A vs. B).

For all the above reasons, though a 3D model is more representative of the *in vivo* situation, since MT1-MMP is a membrane-tethered protein involved in both 2D migration and 3D invasion (Itoh, 2006), we assessed MT1-MMP inhibition in cells stimulated to migrate on type-I collagen in 2D using a scratch assay (Section 5.4). This was done to ensure the assessment of only protease-mediated migration. The MMP family and the role of some of the MMPs that may also be relevant in migration and invasion will now be described.

1.5. Overview of the metallopeptidase family

There are over 30 different zinc-dependent metallopeptidase families, which can be divided into 5 groups according to their mode of zinc binding. Those with the ligand zinc in the active site and

three histidine residues in a sequence motif HExHxxGxxH, are all endopeptidases and have been termed metzincins. The MMPs are one of a group four metzincins (Rawlings and Barrett, 1995). Currently, there are 26 MMPs, 6 of which are tethered to the membrane and the remaining are secreted into the pericellular space (Folgueras et al., 2004).

MMPs are a family of ECM degrading enzymes that play roles in physiological development, tissue remodelling and repair. However, MMPs also contribute to pathopysiological processes like invasion and metastasis (Shapiro, 1998). Most MMPs contain a conserved catalytic domain with a propeptide to ensure enzyme latency, a signal peptide that directs their secretion from the cell, and a hemopexin domain which contributes to substrate specificity and interactions with endogenous inhibitors (Figure 1.5) (Folgueras et al., 2004; Piccard et al., 2007). MMPs were initially classified according to their substrate specificities, collagenases, stromelysins, elastases and matrilysins became identifiers of enzyme classes. Given their overlapping substrate specificities, MMPs are now classified according to their genetic and structural properties. However, the previous "trivial" enzyme classes are still used if they reflect enzyme function, location or a structural feature of the enzyme (Figure 1.5) (Somerville et al., 2003). MMPs can be divided into true collagenases i.e. that cut triple-helical collagen at a site across the three chains, giving rise to products ¾ and ¼ of the length of the original molecule; or gelatinases, which target denatured collagens; or gelatins and stromelysins, which have a broad specificity and may degrade proteoglycans. Whereas most MMPs are secreted and occupy the extracellular milieu, some are tethered to the cell plasma membrane by a transmembrane domain and are referred to as membrane type (MT)-MMPs, or are tethered via a glycosylphosphoinositol (GPI) anchor (Figure 1.5) (Folgueras et al., 2004; Somerville et al., 2003). Secreted MMPs may be located on the cell surface via interaction with membrane-bound molecules or complexes with, integrin αvβ3 (Brooks et al., 1996), the extracellular matrix metalloproteinase inducer EMMPRIN/CD147 (Guo et al., 2000), the hyaluronan receptor CD44 (Yu et al., 2002), cell-surface heparan-sulfate proteoglycans (Li et al., 2002), or MT-MMPs (Sato et al., 1994).

Structural Domains	Nomenclature	Schematic representation
Minimal domain	**Matrilysin (MMP-7)** **Matrilysin-2 (MMP-26)**	
Standard domain	**Collagenase-1 (MMP-1), Collagenase-2 (MMP-8), Collagenase-3 (MMP-13).** **Stromeolysin-1 (MMP-3), Stromeolysin-2 (MMP-10). Metalloelastase (MMP-12)** **MMP-19, Enamelysin (MMP-20)**	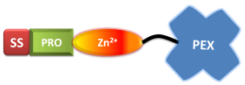
Gelatin binding	**Gelatinase A (MMP-2)**	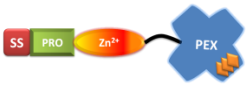
	Gelatinase B (MMP-9)	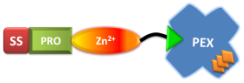
Furin activated		
Secreted	**Stromelysin-3 (MMP-11)** **MMP-21 (X-MMP)** **Epilysin (MMP-28)**	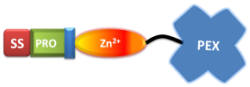
Membrane bound		
Transmembrane (Type i)	**MT1-MMP (MMP-14), MT2-MMP (MMP-15), MT3-MMP (MMP-16), MT5-MMP (MMP-24)**	
GPI-anchored	**MT4-MMP (MMP-17)** **MT6-MMP (MMP-25)**	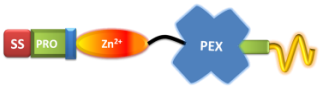
Transmembrane (Type ii)	**MMP-23A** **MMP-23B**	

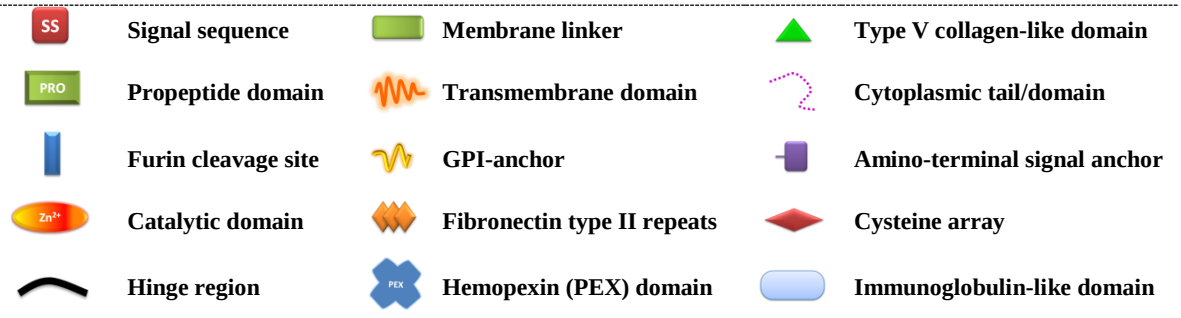

Figure 1.5. The MMP family.
Structural characteristics, "trivial" nomenclature and schematic representation of the MMP family in humans [reproduced from Sommerville et al. (2003) and Folgueras et al. (2004)].

MT1-MMP has been implicated in cellular migration (Kajita et al., 2001; Ueda et al., 2003) and is a major contributor to proteolysis and subsequent tumour invasion (Sato et al., 2005; Seiki, 2003).

The focus in this study is the inhibition of MT1-MMP. The structure, trafficking, regulation and roles of MT1-MMP will now be discussed in more detail.

1.6. MT1-MMP: domain structure and function

The inactive precursor of MT1-MMP consists of a signal sequence (SS), prodomain (PRO), catalytic domain (Zn^{2+}), hinge region, hemopexin domain (PEX), transmembrane domain and a cytoplasmic tail, with a cumulative molecular weight of 64 kDa (Figure 1.5 & 1.6-B) (Fernandez-Catalan et al., 1998; Lehti et al., 2002). The SS (M^{1}-T^{20}) and PRO (A^{21}-R^{111}) ensure enzyme latency through a cysteine-switch (C^{93}), by chelating the zinc active site with the thiol group of C^{93} with high affinity (K_i = 200 nM). Upon PRO cleavage, water molecules enter and hydrolyse the coordination of the cysteine to the $zinc^{2+}$ ion. This system is referred to as the "cysteine-switch", which is conserved among MMP family members and activated by proprotein convertases (Morgunova et al., 1999). Golgi-associated furin-like serine endoproteinases and other proprotein convertases cleave off the PRO (Sato et al., 1996) in a two-step mechanism (Golubkov et al., 2007). First, bait regions are cleaved at either $P^{47}GD{\downarrow}L^{50}$ or $P^{58}QS{\downarrow}L^{61}$, or both, and finally the dibasic sequence $R^{108}RKR^{111}{\downarrow}Y^{112}$ is cleaved off (Figure 1.6-A), releasing the active 57 kDa enzyme (Golubkov et al., 2010). Cleavage at the dibasic sequence alone releases an auto-inhibitory prodomain, thus, bait region cleavage is necessary to render the prodomain non-functional (Golubkov et al., 2010).

The catalytic domain (Y^{112}-G^{285}) contains two structural calcium ions and two zinc ions, one structural and one catalytic (Fernandez-Catalan et al., 1998). The catalytic zinc ion is ligated by the imidazoyl nitrogens of three histidine residues making up MT1-MMP's catalytic site, $H^{239}ELGH^{243}ALGLEH^{249}$ (Figure 1.6-A) (Fernandez-Catalan et al., 1998). When molecular modelling experiments are conducted, it is these residues that dictate binding efficiency (further described in Chapter 3).

The hinge region (E^{286}-I^{318}), between the catalytic domain and the hemopexin (PEX) domain, is the most variable region among the MMPs and is a site for multiple posttranslational modifications. O-glycosylation of residues T^{291}, T^{299}, T^{300}, and S^{301} in the hinge region (Figure 1.6-A) are essential for the role that MT1-MMP plays in recruitment of tissue inhibitor of metalloproteinases-2 (TIMP-2) to the cell surface for the maturation of proMMP-2 (Section 1.7.5) (Wu et al., 2004). The hemopexin domain (PEX, C^{319}-C^{508}) is a common structure in many proteins outside the MMP family and is responsible for substrate binding, attachment and

localisation of MMPs at the cell surface and homodimerisation/multidimerisation (Piccard et al., 2007). The PEX domain forms a propeller with four blades (Figure 1.6-B), arranged around a central axis, of which the first blade is linked to the fourth by means of a disulfide bridge (Paoli et al., 1999). MT1-MMP's PEX domain has been shown to associate with the membrane bound glycoprotein CD44 through its stem region. CD44 is associated with actin via its cytoplasmic tail, resulting in CD44-MT1-MMP-complex localisation to lamellipodia as CD44 is relevant in migration and invasion (Mori et al., 2002; Suenaga et al., 2005).

A stem region, known as the membrane linker (P^{509}-S^{538}), links the PEX domain to the transmembrane domain of MT1-MMP (Figure 1.6). The membrane linker has been shown to undergo catalysis, releasing a soluble 50 kDa fragment of active MT1-MMP. This form of ectodomain shedding is thought to be a physiological response to broaden activity to the pericellular space (Toth et al., 2002). The transmembrane domain (A^{539}-F^{562}) which tethers MT1-MMP to the plasma membrane is involved in surface associations and regulation of active MT1-MMP on the plasma membrane. Protein kinase C (PKC) mediated phosphorylation at T^{567} has been reported to enhance cell invasion and proliferation (Moss et al., 2009b). Sequences on the cytoplasmic tail are relevant in the trafficking of MT1-MMP to and from the plasma membrane. When C^{574} is palmitoylated (Anilkumar et al., 2005), the LLY^{573} sequence of the cytoplasmic tail (R^{563}-V^{582}) interacts with the µ2 subunit of adaptor protein 2 (AP-2) which mediates incorporation of MT1-MMP into clathrin coated pits for endocytosis (Uekita et al., 2001). The sequence $YCQR^{575}$, but particularly Y^{573} in its phosphorylated form, appears to aid cell cycle progression (Nyalendo et al., 2008). Accumulation or phosphorylation of $YCQR^{575}$ by kinases results in the acvtivation of the Ras-MEK-ERK pathway involved in migration (Gingras et al., 2001). DKV^{582} sequence within the cytoplasmic tail has been shown to be critical for recycling of active MT1-MMP back to the plasma membrane and maintaining levels of proteolytic activity (Wang et al., 2004). Finally, Src-dependent phosphorylation of Y^{573} results in the mono-ubiquitination of K^{581} and the subsequent increase in MT1-MMP's ability to invade through collagen type-I (Eisenach et al., 2012).

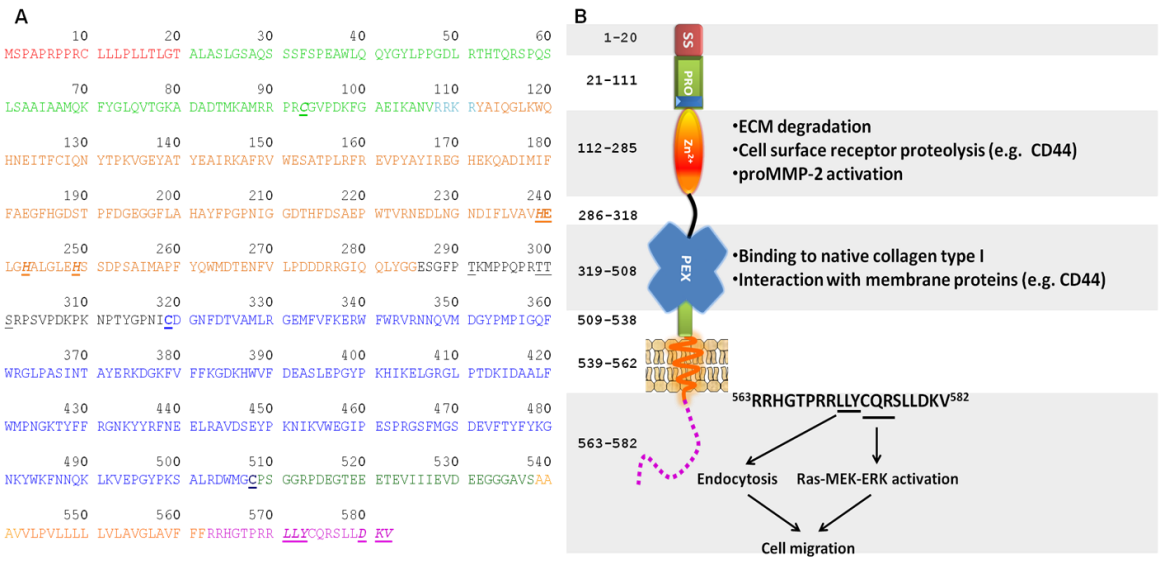

Figure 1.6. FASTA sequence with colour co-ordinated domains of MT1-MMP.
(**A**) Full length FASTA sequence of MT1-MMP. Underlined amino acids are mentioned in the text. (**B**) Schematic annotated diagram of MT1-MMP. Numbering to the left of the schematic diagram and domain colours correspond with the FASTA sequence. MT1-MMP domains are represented indicating some functional information. Underlined residues of the cytoplasmic domain thought to be involved in endocytosis and ERK activation [reconstructed with minor modifications from Gingras and Béliveau, (2010)].

1.6.1. Trafficking and regulation of MT1-MMP

Since MT1-MMP is a membrane tethered protein, it is subject to regulation via vesicle trafficking of the two major cellular pathways, the secretory/biosynthetic pathway and the endo/exocytic pathway (Frittoli et al., 2011). MT1-MMP polypeptides synthesised in the cytoplasm dock to ribosomes which translocate them into the lumen of the ER (Lee et al., 2004). ProMT1-MMP leaves the ER as a folded 64 kDa structure and enters the Golgi (Frittoli et al., 2011) where glycosyltransferase adds O-linked carbohydrate moieties to glycosylation residues of the hinge region (Wu et al., 2004). In the trans-Golgi network (TGN), proprotein convertases and furin-mediated cleavage of the prodomain of MT1-MMP occurs (Golubkov et al., 2007; Sato et al., 1996). From here, MT1-MMP is transported to the plasma membrane as an active 57 kDa transmembrane fragment (Frittoli et al., 2011). Localisation of MT1-MMP to the plasma membrane is restricted in normal cells, as evident by low surface level activity which may be due to recycling (Jiang et al., 2001a; Remacle et al., 2003; Zucker et al., 2002). During directed cell migration and invasion on the other hand, MT1-MMP is prominently located in lamellipodia and invadopodia (Clark et al., 2007; Poincloux et al., 2009).

Regulation of plasma membrane localised MT1-MMP is achieved through endocytosis and subsequent degradation or recycling. As mentioned, endocytosis of MT1-MMP may occur

through two mechanisms, clathrin-dependent endocytosis (Figure 1.6-B) or clathrin-independent internalisation via lipid rafts and caveolae (Remacle et al., 2003). Involved in both pathways is the tetraspanin, CD63, expressed on the cell surface and associated with the endosomal system. A major pool of CD63 is found in the late endosome/multivesicular body and lysosomes (Pols and Klumperman, 2009). Thus, direct association of MT1-MMP's PEX domain with the N-terminus of CD63 may direct MT1-MMP towards endosomal-lysosomal degradation (Takino et al., 2003). MT1-MMP, however, may be recycled back to the leading edge during migration (Remacle et al., 2003). Recycling of active 57 kDa MT1-MMP to the PM is thought to be a rapid response mechanism to repopulate invasive structures with active enzyme. Rab8 GTPase is a major regulator of the polarised exocytic pathway, suggested to facilitate the recycling process of MT1-MMP to membrane protrusions (Bravo-Cordero et al., 2007). Recycling of MT1-MMP is also achieved in caveolae (Remacle et al., 2003). Gálvez et al. (2003) showed that caveolae-mediated internalisation of MT1-MMP plays an important role for migrating endothelial cells cultured on collagen type I. In addition, this substratum induced RhoA signalling and localised MT1-MMP to cell-cell contacts in confluent cells. Anilkumar et al. (2005), however, showed that various cancer cells cultured on collagen type I, internalise MT1-MMP through clathrin-dependent endocytosis, as C^{574} on the cytoplasmic tail is palmitoylated and orientates the LLY^{573} phosphorylation site for binding to µ2 adaptor proteins (Figure 1.6-B). MT1-MMP missing C^{574}, was internalised through caveolae only, and was unable to stimulate cell migration due to the less rapid rate of internalisation via caveolae, compared to clathrin. Whether caveolae are able to facilitate migration independently may be cell type and matrix dependent (Anilkumar et al., 2005), leaving the matter of caveolae's capacity to facilitate MT1-MMP-dependent migration unanswered for epithelial cells. The cytoplasmic domain of MT1-MMP, therefore, plays an important role in the regulation of recycling at the plasma membrane. Studies have shown that cytoplasmic tail deleted mutants of MT1-MMP results in the accumulation of active MT1-MMP enzyme on the cell's surface, reflected by enhanced MMP-2 activation (Jiang et al., 2001a; Lehti, 2000).

CD44, a transmembrane cell surface receptor of hyluronan, associates with MT1-MMP while attached to ezrin/radixin/moesin (ERM) proteins associated with the actin cytoskeleton, thereby indirectly facilitating the linkage of MT1-MMP to the actin cytoskeleton and subsequent localisation to the cell migratory front (Itoh, 2006; Mori et al., 2002) (further described in Section 1.7.3). As a result of this actin interaction, CD44 has been shown to play a role in breast cancer basal motility (Hamilton et al., 2007), migration and invasion (Bourguignon et al., 1998; Kajita et

al., 2001; Marrero-Diaz et al., 2009; Wanga et al., 2005). Such interactions have also been shown to promote Rho/Ras activation (Bourguignon et al., 2006), and up-regulate MMPs including MT1-MMP (Miletti et al., 2004). When localised to lamellipodia or invadopodia, MT1-MMP-CD44 complexes are suggested to act in concert to promote migration or invasion (described further in Section 1.7.3) (Kuo et al., 2009; Miletti et al., 2004).

MT1-MMP activity is regulated by the degree of association with endogenous reversible inhibitors known as the tissue inhibitors of metalloproteinases (TIMPs). Active 57 kDa MT1-MMP is inhibited in a 1:1 stoichiometric manner by TIMP-2, -3 and -4, but not TIMP-1 (Bigg et al., 2001; Will et al., 1996). TIMP-1, -2 and -4 are secreted proteins whereas TIMP-3 is anchored in the ECM (Folgueras et al., 2004). TIMP-2 appears to have a concentration-dependent role in MT1-MMP inhibition and MMP-2 activation. In studies using non-physiological concentrations of TIMP-2 (1-5 µg/ml or 50–250 nM), MT1-MMP is inhibited (Albini et al., 1991; Lu et al., 2010). This is confirmed in retroviral-delivery-over-expression studies where excess TIMP-2 inhibited MT1-MMP (Ahn et al., 2004). When physiological concentrations (10-100 ng/ml or 0.5-5 nM) (Kasahara et al., 1997; Murawaki et al., 1999; Ulrich et al., 2004) are used, MT1-MMP/TIMP-2 may induce Ras-Raf-ERK signalling through an unknown indirect signalling/proteolytic mechanism (D'Alessio et al., 2008). As previously mentioned, ERK or MAPK signalling regulates proliferation, survival and differentiation, and hence, MT1-MMP has a role in such signalling pathways in addition to facilitating invasion. D'Alessio et al. (2008) also highlighted a potential side effect of ERK activation, induced by low systemic concentrations of TIMP-2, resulting in TIMP-2-MT1-MMP mediated cell proliferation and non-MT1-MMP mediated migration *in vivo*.

MT1-MMP is endowed with the ability to change and degrade the cellular microenvironment, release growth factors bound to ECM, activate other MMPs, and indirectly stimulate migratory signals. The regulation of MT1-MMP activity at the cell surface is of utmost importance in the prevention of invasion and remains a promising drug target in malignancy (Remacle et al., 2012), as will now be explained.

1.7. Substrates of MT1-MMP

MT1-MMP previously classified as a collagenase by the "trivial" classification system, implies a narrow range of substrates for proteolysis by MT1-MMP. In recent years, the substrate list has grown considerably from ECM components (Gilles et al., 2001; Lee et al., 2006) to cell surface

receptors (Suenaga et al., 2005) and molecules localised in the nucleus (Golubkov et al., 2006) (Table 1.1). Given this variety of substrates, up-regulation of MT1-MMP may have a long lasting effect on the cell through processing of these cell-surface receptors and the release of the cell from the ECM/BM (Strongin, 2010). Due to the long list of substrates (Table 1.1), only those considered relevant to breast cancer and this study will be further described and discussed in the sections that follow.

Table 1.1. Substrates of MT1-MMP and MMP-2.

Only bolded substrates will be described in the text.

Protein	Collagenous substrates	Non-collagenous ECM substrates	Non-structural ECM component substrates
MT1-MMP	**Collagen types I**[1], II, III and gelatin	Aggrecan, dermatan sulphate proteoglycan, fibrin, fibronectin, laminin 1 & 5, nidogen, perlecan, **lumican**[2], tenascin and vitronectin	$\alpha_v\beta_3$ integrin, **CD44**[3], gC1qR, **Syndecan-1**[4], **pro-MMP-2**[5], pro-MMP-13, pro-TNFα, KiSS-1, interleukin-8, secretory leukocyte protease inhibitor, connective tissue growth factor, amyloid precursor protein, tissue transglutaminase and pericentrin-2.
MMP-2	Collagen types I, IV, V, VII, X, XI, XIV and gelatin	Aggrecan, elastin, fibronectin, laminin, nidogen, proteoglycan link protein and versican	Active MMP-9, active MMP-13, FGF R1, IGF-BP3, IGF-BP5, IL-1β, recombinant TNF-α peptide, and TGF-β.

Reconstruced from Sato et al. (2005) and Sommerville et al. (2003) with minor additions from Golubkov et al. (2006) and Ohuchi et al. (1997). [1]Section 1.7.1. [2]Section 1.7.2. [3]Section 1.7.3. [4]Section 1.7.4. [5]Section 1.7.5.

1.7.1. Collagen type-I

Collagen is a major ECM component and biomechanical scaffold for cell attachment and anchorage of macromolecules, maintaining tissue architecture. Collagen fibrils self-assemble and consist of three alpha chains forming a triple helical structure (Kadler et al., 1996). Collagen is resistant to most proteinases at neutral pH, with the exception of collagenolytic MMPs including MT1-MMP (Tam et al., 2004). MT1-MMP binds native collagen through its PEX domain in the vicinity of collagen's cleavage site and induces localised helix unwinding (Tam et al., 2004).

Collagen fibrils are subsequently cleaved at a specific site, 3/4 distant from the N-terminus, initialising denaturation of triple helical collagen into gelatin. This renders collagen susceptible to further degradation by gelatinases such as MMP-2 (Visse and Nagase, 2003).

An interesting relationship exists in the interstitial tissue between MT1-MMP and collagen type-I in which the collagen environment may initiate its own clearance (Tam et al., 2004). Clustering of β1 integrin due to binding collagen type-I, stimulates MT1-MMP gene expression and stabilisation of MT1-MMP mRNA (Ellerbroek and Stack, 1999; Gilles et al., 1997b). MT1-MMP's PEX domain binds to collagen abrogating internalisation (Lafleur et al., 2006) resulting in cell surface accumulation and clustering of MT1-MMP. Such clustering promotes dimerisation between PEX domains and subsequent proMMP-2 activation (Strongin et al., 1995; Tam et al., 2002). Thus, triple helical collagen is cleaved by MT1-MMP generating gelatin, a substrate of MMP-2. However, MT1-MMP clustering also induces autocatalysis (Toth et al., 2002) generating a membrane tethered 44 kDa form, starting at Gly^{285}, lacking the catalytic domain (Hernandez-Barrantes et al., 2000). This 44 kDa form in turn binds with collagen to competitively inhibit further collagenolysis by MT1-MMP but not by MMP-1 or MMP-8 (Tam et al., 2002). Thus, collagen type I may induce localised MT1-MMP pericellular collagenolysis, but also regulates the extent of degradation by inducing autocatalysis through a negative feedback loop mechanism.

In an alternative situation where the afore mentioned negative feedback loop fails, MT1-MMP can function in a positive feedback loop to induce sustained ERK activation and subsequent MT1-MMP accumulation, collectively promoting cell migration on collagen type-I (Takino et al., 2004). This positive feedback loop provides compelling evidence to motivate for the use of collagen type-I as a substratum in this study. In addition, collagen type-I has been shown to increase the steady-state mRNA levels of MT1-MMP in human breast carcinoma cells (Gilles et al., 1997b).

1.7.2. Lumican

Lumican, is a keratin sulphate proteoglycan that plays an important role in determining the structural phenotype of the mature collagen fibril in tissues such as skin, muscle and cartilage (Iozzo, 1999). Leygue et al. (2000) have shown that lumican mRNA levels are up-regulated in breast cancer. Lumican protein is not immunolocalised within the tumour, but rather the collagenous stroma. MT1-MMP degrades lumican on the tumour cell surface, therefore, further

promoting tumorigenicity in breast cancer, where non-degraded lumican may act as a tumour suppressor (Li et al., 2004).

1.7.3. CD44

CD44, on the other hand, is a major receptor for hyaluronan that mediates cell adherence and migration (Bourguignon et al., 1998) via ezrin/radixin/moesin (ERM)-actin cytoskeleton associations through its cytoplasmic tail. CD44 is cleaved by MT1-MMP at the stem region releasing a soluble fragment (ectodomian), and a cytoplasmic tail fraction (Kuo et al., 2009; Suenaga et al., 2005) that acts as a transcription factor to promote migration (Cichy and Puré, 2003; Okamoto et al., 2001). Through its activity on CD44, MT1-MMP may also influence cell adherence to the underlying matrix thereby reducing adherence during migration (Marrero-Diaz et al., 2009).

1.7.4. Syndecan 1

Syndecan1 appears to be an important regulator of migration and invasion (Inki and Jalkanen, 1996). This is a transmembrane heparin sulphate proteoglycan expressed on all adherent cells including normal epithelial cells (Sato et al., 2005) and binds to a variety of ECM molecules through a covalently attached glycosaminoglycan chain. Shedding of syndecan-1's ectodomain by MT1-MMP leads to EMT transition via an undefined pathway, and in cultured cells has also been shown to stimulate migration (Endo et al., 2003), a process once again underpinning the key role of MT1-MMP in EMT and hence migration.

1.7.5. ProMMP-2

ProMMP-2 activation is also a key facilitator of migration by degrading many components of the ECM. The propeptide domain of MMP-2 is a substrate of MT1-MMP and cleavage of this region results in MMP-2 activation (Strongin et al., 1995). Activation of MMP-2 requires complex formation with TIMP-2 (Wang et al., 2000). The C-terminal domain of TIMP-2 binds the PEX domain of pro-MMP-2 permitting the N-terminal inhibitory domain of TIMP-2 to bind to MT1-MMP. A nearby MT1-MMP, free of TIMP-2, dimerises with the MT1-MMP-TIMP-2-proMMP-2 complex and cleaves the propeptide domain of MMP-2 in its bait region. Subsequent dissociation of MMP-2 from the complex and the membrane allows for intermolecular processing and complete activation of MMP-2 (Itoh et al., 2008; Lehti, 2000). Cao et al. (1995) have shown that the PEX domain of MT1-MMP is not required for MMP-2 activation, but rather this process is dependent on the proximal association/dimerisation of two MT1-MMP molecules via their

transmembrane domains, later confirmed by Itoh et al. (2008). Interestingly, proMMP-2 activation by MT2-MMP is direct and independent of TIMP-2 (Morrison et al., 2001). The combined substrate range of MT1-MMP and MMP-2 confer a cell with the ability to traverse almost any membrane barrier while sustaining EMT (Table 1.1) (Sato and Takino, 2010). This is why these two proteases are often targeted by inhibitors to limit invasion (Hashimoto et al., 2011; Remacle et al., 2012; Suojanen et al., 2009).

1.8. MT1-MMP as a target for synthetic inhibition.

Proteases that degrade the underlying epithelial matrix during metastasis have often been proposed as therapeutic targets. Before the discovery of MT1-MMP by Sato et al. (1994), matrix metalloproteinase inhibitors (MMPIs) had already gone into clinical trials as anti-metastatic agents. Clinical trials proved to be disappointing, with unforeseen side effects. In early phase I clinical trials (dose escalation to evaluate safety), prolonged treatment with MMPIs caused musculoskeletal pain and inflammation, known as tendinitis (Coussens et al., 2002). Tendinitis symptoms were reversible after MMPI removal, however, dosages were reduced in subsequent trials. Due to these side-effects, the question was raised as to which MMPs were valid targets in cancer when given the degree of homology between MMP catalytic domains, the role of MMPs in many molecular processes, and the broad-spectrum (non-selectivity) of MMPIs administered. Phase II trials (drug efficacy) were also problematic because MPIs were cytostatic (cells are growth arrested but viable) rather than cytotoxic. Therefore, measuring reduction in tumour size as a conventional method was not possible. Rather, tumour markers in serum were evaluated as indicators of drug efficacy (Nemunaitis et al., 1998; Primrose et al., 1999; Rosemurgy et al., 1999). This was criticised as changes in biomarkers do not necessarily reflect tumour regression (Coussens et al., 2002). Phase III trials were conducted in the mid-1990s when MMP studies were escalating in number. With new information emerging, ongoing trials tended to evolve. Initially, MPI efficacy was compared against cytotoxic drugs. Later, MMPIs were tested and compared in combination with cytotoxic drugs, or compared after the administration of cytotoxic drugs (Nelson et al., 2000). As a consequence of inconsistencies, the conclusion drawn from phase III clinical trials was that MMPIs have no therapeutic benefit in human cancer (Coussens et al., 2002). The broad targets of these MMPI included both soluble and membrane tethered MMPs, however.

New and accumulating evidence for the major role of cancer cell associated MT1-MMP in cancer progression, dissemination and malignancy is emerging, prompting discovery and synthesis of

new MMPIs. MT1-MMP has also been shown to associate with adenine nucleotide transporter proteins, suggesting a possible influence on cellular metabolism (Chevrollier et al., 2005; Radichev et al., 2009). Gingras et al. (2001) have further reported that phosphorylated MT1-MMP acts as a signal transducing molecule activating ERK, promoting cell locomotion. Moreover, there is evidence of MT1-MMP's involvement in pericentrin processing in the centrosome during mitotic spindle formation affecting chromosomal stability contributing to aneupolidy in malignancies (Golubkov et al., 2005). MT1-MMP has also been shown to contribute to neovascularisation through gene modulation of vascular endothelial growth factor (VEGF) underlying a crucial role of this enzyme in tumour progression (Gingras and Béliveau, 2010). Inhibitors of MT1-MMP have been reported upon previously and show promising results. Immune inhibition of active-MT1-MMP only, was shown to be effective in slowing tumour progression and metastasis, and inhibited angiogenesis in mice with xenogenic human cancer implants (Devy et al., 2009). Inhibition of MT1-MMP by retroviral delivery of TIMP-2 was shown to decrease migration and metastasis in MCF-10AneoT cells (Ahn et al., 2004). Combined synthetic inhibition of MMP-2 and MT1-MMP showed a reduction in tumour weight using pancreatic ductal adenocarcinoma mouse xenographs (Kapischke et al., 2008). Transcriptional silencing of MT1-MMP reduced migration and invasion in the HT1080 human fibrosarcoma cell line (Ueda et al., 2003). The cyclic peptide inhibitor of MT1-MMP designated peptide-G, administered at high concentrations (IC50 of 150-500 μM) inhibited cell migration and invasion (Suojanen et al., 2009). These studies provide evidence for the motivation behind the use of synthetic inhibitors of MT1-MMP in our study.

In this study, we focus on two novel synthetic MT1-MMP inhibitors synthesised by our collaborators. These are small cyclic compounds, stabilised by a sulphonamide group, that inhibit MT1-MMP, namely TF 17-2 and TF 22d (Fischer, 2004). TF 17-2 was successfully applied to an orthotopic pancreatic ductal adenocarcinoma xenograft model in immune deficient mice and showed a reduction in tumour weight and inhibition of metastasis (Kapischke et al., 2008). With this new class of triazine inhibitors synthesised to target MT1-MMP with greater affinity than other MMPs, it is hoped that the specificity of these inhibitors will deliver even more favourable results using a breast cancer cell model. In this study we assessed TF 17-2 and TF 22d levels of toxicity, structural basis for binding, activity and effect on cellular migration in 2D.

The first aim of this study was to establish whether computational modelling, using a freeware package, AutoDock Vina, can be used as a reliable *in silico* substitute for K*i* values for MMPIs

when *in vitro* kinetic assay materials are not available. The second aim of this study was to establish the minimal level of DMSO solvent required to solvate the TF 17-2 or TF 22d without toxicity to the test MCF-10A or MCF-10AneoT cells lines and the level toxicity of the TF 17-2 or TF 22d over a test range (50-300 µM). This was to be determined by assessing deviations in metabolic activity, detecting markers of cell death and determining whether any selective effect on the premalignant cell line was evident. Finally, we hypothesised that the synthetic inhibition of MT1-MMP would decrease normal and premalignant epithelial migration *in vitro* allowing predictions to be made on the potential use of these inhibitors as anti-metastatic or anti-invasion agents.

This dissertation contains six chapters and is structured as follows. In Chapter 1 the background information required for this study has been provided. In Chapter 2 common laboratory methods used in this study are listed. In Chapter 3, the focus is the comparative computational modelling of two MMP inhibitors in the active site of MT1-MMP and MMP-2, and the reliability of these *in silico* K*i* studies compared to *in vitro* K*i* values. In Chapter 4, the influence of TF 17-2 and TF 22d on metabolic activity and cellular toxicity is assessed in MCF-10A and MCF-10AneoT cells. In Chapter 5 the application of inhibitors is explored in 2D cell migration assays as this assay allows the assessment of protease-mediated migration. Finally, Chapter 6 will conclude our findings in the context of MT1-MMP inhibition and cell migration.

Before the *in silico* studies are presented (Chapter 3), however, a brief chapter outlining recurring methods is given in the following chapter (Chapter 2).

CHAPTER 2.

Materials and Methods

2.1. Materials

All chemical reagents were of analytical grade unless otherwise specified. Glycerol was from AR–Associated Chem. Enterprises (Glenvista, South Africa). Acrylamide, N,N`-bismethylenebisacrylamide, ammonium persulfate, Triton X-100, calcium chloride, glycine, hydrochloric acid, glacial acetic acid, Na_2HPO_4, $Na_2HPO_4.H_2O$, paraformaldehyde (PFA), potassium chloride, sodium chloride and sodium hydroxide were from Merck (Poole, England). Sodium dodecyl sulfate (SDS) was from Boehringer Mannheim (Mannheim, Germany). Horse serum, penicillin streptomycin, and fungizone were from Gibco (Paisley, United Kingdom). Ponceau S was from Searle (High Wycombe, Bucks, United Kingdom). Elite fat free milk powder was from Clover SA (Pty) Ltd (Roodepoort, South Africa). 2-Mercaptoethanol and glacial acetic acid was from Merck Schuchardt OHG (Munich, Germany). Magnesium chloride and potassium dihydrogen orthophosphate were from Saarchem (Wadeville, South Africa). Dimethyl sulphoxide (tissue culture grade), bovine serum albumin (BSA) (Mr 68 kDa), carbonic anhydrase (Mr 30 kDa), Coomassie brilliant blue R-250, Dulbecco's minimal essential medium (DMEM): Ham's F-12 medium, Hanks' balanced salts (HBSS), horseradish peroxidase (HRP), hydrocortisone, insulin, lysozyme (Mr 14 kDa), ovalbumin (OVA, Grade V) (Mr 45 kDa), phosphorylase B (Mr 97.4 kDa), saponin, Ponceau S, dialysis tubing (25 mm x 16 mm), sodium bicarbonate, ethylenediaminetetra-acetic acid (EDTA), trypsin-EDTA solution (x 10), RIPA buffer and inhibitor cocktail were from Sigma (St. Louis, Mo). Annexin-V-FITC was from BD Pharminogen (United States). Epidermal growth factor was from Upstate Biotechnology. 2-Amino-2-(hydroxymethyl)-1,3-propandiol (Tris) and PEG-20 000 were from Merck (Darmstadt, Germany). Methanol and ethanol were purchased from Saarchem (Gauteng, South Africa) and were of chemically pure grade. Carbon dioxide was from Air Products (Pietermaritzburg, South Africa). The novel TF 22d and TF 17-2 triazine type MMP inhibitors were supplied collaboratively by Prof. H. Tschesche (University of Bielefeld, Germany). Cell culture flasks (T_i 75 and 25 cm^3), sterile freezing vials (2.0 ml) and 24 well Terasaki plates were from Nunc (Roskilde, Denmark). Glass bottomed 30 cm culture plates for confocal imaging were obtained from MaTek Corporation, Ashland, MA, USA). Sterile 15 ml and 50 ml plastic screw top tubes used in cell culture were purchased from Sterilin Bibby Sterilin (Staffordshire, UK) and Nunc (Roskilde, Denmark), respectively. Distilled water (dH_2O) was obtained from a Milli-RO® water

purification system (Millipore, Marlboro, USA). Deionised water (ddH_2O) was produced by a Milli-Q plus ultra-pure water system (Millipore, Marlboro, USA) and had a minimum resistance of 18 $M\Omega.cm^{-1}$.

2.2. MCF-10A and MCF-10AneoT cell culture

MCF-10A and MCF-10AneoT cell lines were collaboratively obtained from Prof. Bonnie F. Sloane (Wayne State University, Detroit, MI) and were described in Section 1.3.

2.2.1. Reagents

Base medium: DMEM:Ham's F-12 incomplete medium.

Dulbecco's modified Eagle medium Ham's F-12 nutrient medium was prepared according to manufacturer's instructions. Briefly, media was dissolved in Milli-Q ddH_2O (900 ml) using a magnetic stirrer. Sodium bicarbonate (1.2 g) was added and allowed to dissolve. The pH was corrected to 6.9 ± 0.3 with 1 M HCl or NaOH if necessary, and made up to 1 l. Base medium was filter sterilised into five 200 ml volumes and incubated (37°C) overnight to ensure no contamination had occurred. Solutions were subsequently stored at 4°C.

Hank's balanced salt solution (HBSS).

HBSS powder was prepared according to manufacturer's instructions. Briefly, HBSS powder was dissolved in Milli-Q ddH_2O (900 ml) using a magnetic stirrer. Sodium bicarbonate (0.35 g) was added and allowed to dissolve. The pH was corrected to 7.3 ± 0.3 with 1 M HCl or NaOH if necessary, and made up to 1 l. The HBSS solution was filter-sterilised into five 200 ml volumes and incubated (37°C) overnight to ensure no contamination had occurred. Solutions were subsequently stored at 4°C.

Epidermal growth factor (EGF) [100 µg/ml].

EGF (100 µg) was aseptically dissolved in sterile dH_2O (1 ml) and stored at 4°C.

Equine serum.

Equine serum (Gibco, Grand Island, NY) was aseptically dispensed into 10 ml volumes and decomplemented using heat inactivation (56°C, 30 min) of complement proteins. Once decomplemented, aliquots were stored at -20°C.

Sodium hydroxide [0.1 M NaOH].

NaOH (0.2 g) was dissolved in dH_2O (50 ml) using a magnetic stirrer. Solution was kept for 1 month before replacement, at RT.

Insulin [0.6 mg/ml insulin, (0.1 M NaOH) in HBSS].

Bovine pancreas insulin (6 mg) was mixed into HBSS (300 µl) and dissolved after NaOH (0.1 M, 300 µl) was added to correct the pH. The solution was diluted in HBSS (9.4 ml) and filter-sterilised. The sterile insulin solution was stored at -20°C.

Hydrocortisone stock [3.33 mg/ml hydrocortisone in absolute ethanol].

Hydrocortisone (10 mg) was dissolved in absolute ethanol (3 ml) and stored at -20°C.

Fungizone anti-mycotic [250 µg/ml amphotericin B, 250 µg/ml sodium deoxycholate in dH_2O].

Fungizone required no additional preparation.

Penicillin-Streptomycin (PenStrep).

PenStrep required no additional preparation.

Complete medium [DMEM:Ham's F-12, hydrocortisone (0.5 µg/ml), insulin (10 µg/ml), epidermal growth factor (20 ng/ml), equine serum (5% (v/v)), fungizone (0.25 µg/ml), pH 7.3].

Base medium (200 ml) was aseptically supplemented with decomplemented equine serum (10 ml), hydrocortisone (30 µl), insulin (3 ml), epidermal growth factor (40 µl), and fungizone or PenStrep (2 ml). Completed medium was incubated overnight (37°C) to ensure no contamination occurred during supplementation.

Trypsin-EDTA (1x working solution).

Trypsin-EDTA (10x stock) was aliquoted (1 ml) into 15 ml centrifuge tubes and diluted with sterile HBSS (9 ml), when required. Solutions were stored at 4°C.

Cryo-medium.

Complete medium (700 µl), equine serum (200 µl) and dimethyl sulfoxide (100 µl, tissue culture grade) were mixed into a 2 ml cryotube. Solution was made up just before use.

2.2.2. Procedure

Passaging

MCF-10A and MCF-10AneoT cell lines were cultured in Ham's F12 complete medium at 37°C in a 5% CO_2 jacketed incubator (Nuaire, US autoflow). Cells were cultured in either 75 or 25 cm^3 culture flasks and passaged at 80% confluency. Media was aspirated off and cells were washed with sterile HBSS. Trypsin-EDTA (1 ml/75 cm^3 flask, 500 µl/25 cm^3 flask) was added to lift cells and incubated (37°C, <10 min). Once cells were dislodged, the trypsin-EDTA was neutralised with fresh complete medium (~15 ml/75 cm^3 flask, ~5 ml/25 cm^3 flask). Equal amounts of the suspensions were poured into two new culture flasks.

Freezing and thawing

MCF-10A and MCF-10AneoT cell lines were cultured in a 75 cm^3 culture flask to 80% confluency. Cells were washed with HBSS and trypinsed as described above. Trypsin was neutralised with 2 ml complete medium and the cell suspension was poured into a 15 ml centrifuge tube. Cells were pelleted by centrifugation (240 x*g*, 5 min) and the supernatant was aspirated off. Cells were re-suspended in cryo-medium and frozen overnight at -80°C before storing in liquid nitrogen.

Frozen cells in cryotubes were thawed slowly in warm water (~40°C). The 1 ml contents were split into two 25 cm^3 flasks containing 5 ml of pre-warmed complete medium.

2.3. Cell counts

Cells were counted manually using a haemocytometer. This method is prone to experimental sampling and human error, therefore, three counts per sample were performed and averaged. Cell counts were used before seeding to achieve equal seeding numbers or after seeding in proliferation assays to determine cell numbers relative to a control.

2.3.1. Reagents

Cell culture reagents as described in Section 2.2.1.

2.3.2. Procedure

Cells were cultured and trypsinised as described in Section 2.2. Cells were resuspended in 1-5 ml of medium, and a sample (20 µl) was taken for counting. The haemocytometer was prepared by

pressing the coverslip onto the smooth etched side of the haemocytometer. Once Newton's rings could be seen, sample (10 µl) was loaded into each side of the haemocytometer. A total of 10 squares (10 mm^2) were counted and averaged before multiplying this number by 10^4 to return a cell number in cells/ml as the depth of the counting chamber is only $1/10^{th}$ of a mm. Three counts were performed and averaged. The equation used is as described by Freshney (2005). Briefly, "*c*" represents concentration (cells/ml), "*n*" represents the average number of cells counted per square, "*v*" represents the volume of a single square (10^{-4} cm^3 = 1 ml) and "*d*" represents the dilution factor.

$$c = \frac{n \times v}{d} \quad \rightarrow \quad c = \frac{n \times 10^4}{10} \quad \rightarrow \quad c = n \times 10^3$$

2.4. Lysate sample preparation

For protein analysis, cells were harvested and cell homogenates prepared. Cells were lifted with EDTA, as EDTA chelates the zinc ion of MT1-MMP blocking enzymatic activity. Trypsin-EDTA was not used because MMP pro-domains may be cleaved by trypsin into their mature forms distorting the perceived cellular forms (Okada et al., 1990). As MT1-MMP is a membrane tethered protein, the lipid content of the cell was not removed by alcohol clearing. To ensure stringy DNA did not interfere with protein loading, cell homogenates were sonicated to disrupt membranes and break up the DNA. Inhibitor-cocktail was added to inhibit serine, cysteine, aspartic proteases, and amidopeptidases present in the homogenate, preventing proteolytic degradation.

2.4.1. Reagents

Hank's balanced salt solution (HBSS).

Described in Section 2.2.1.

EDTA stock solution (10 x EDTA, 0.53 mM).

EDTA (7.75 g) was dissolved in HBSS (30 ml). The pH was adjusted to 7.3 using 1 M NaOH and made up to 50 ml using HBSS. The solution was sterile filtered through 0.2 µm pore-size syringe filter. Stocks were stored at -20°C.

EDTA working solution (1 x EDTA) [0.053 mM].

10 x EDTA solution (1 ml) was diluted to a 1 x EDTA working solution with sterile HBSS (9 ml), and stored at 4°C.

Lysis buffer (RIPA buffer) [50 mM Tris-HCl, pH 8.0, 150 mM sodium chloride, 1.0% Igepal CA-630 (NP-40), 0.5% sodium deoxycholate, and 0.1% sodium dodecyl sulfate].

RIPA buffer required no further preparation and was stored at 2-8°C.

Protease inhibitor cocktail.

Inhibitor cocktail was aliquoted out (250 µl) and stored at -20°C.

2.4.2. Procedure

Protein samples were prepared as described by Coon et al. (2003). MCF-10A and MCF-10AneoT cell lines were cultured in a 75 cm^3 culture flask to 80% confluency. Cells were washed with HBSS and lifted with 1x EDTA (2 ml, ≤ 15 min) or a cell scraper when necessary. Cells were re-suspended in cold HBSS three times after centrifugation (240 x*g*, 5 min) to remove serum proteins. Excess HBSS was aspirated off and the cell pellet was resuspended in RIPA buffer (90 µl), inhibitor cocktail (10 µl), HBSS (100 µl) and incubated (4°C, 30 min) before sonicating (3 sec). Protein concentrations of samples were quantified (Section 2.5) and aliquots were stored at -20°C.

2.5. Bradford protein quantification assay

The Bradford method is a rapid spectrophotometric protein quantification technique (Bradford, 1976). Coomassie brilliant blue G-250 (CBBG) dye used in this assay binds to basic amino acid residues such as arginine, and to a lesser extent histidine, lysine, tyrosine, tryptophan and phenylalanine (Comptom and Jones, 1985). The assay is carried out under acidic conditions, with the cationic red form of CBBG exhibiting an absorption of 365 nm, which shifts to the anionic blue form with an absorption of 595 nm upon protein binding (Bradford, 1976).

Unlike the Lowry (1951) procedure for the quantification of protein concentrations, the binding specificity of Bradford reagent is generally not altered by potassium ions, magnesium ions, EDTA, Tris, thiol reagents or carbohydrates (Bradford, 1976). Exceptions, however, do exist. Relatively high concentrations (1%) of detergents such as SDS and Triton X-100, reducing

reagents, phenols and basic buffers can produce anomalous readings (Comptom and Jones, 1985). Biological components, such as lipids in cell homogenates for example, result in the formation of blue particles which may skew results. This problem may be overcome by solvent precipitation of the protein using ethanol (Zuo and Lundahl, 2000). In addition, the amino acid binding specificity of the dye can lead to inaccurate quantification if the measured protein is disproportionally devoid of basic amino acids to the calibration protein. As a protein standard, ovalbumin was found to be comparable to the average of three other commonly used laboratory proteins: lysozyme, BSA and γ-globulin (Pike, 1990), and has, therefore, been used as a calibration protein in this study. A disadvantage of the Bradford assay is that the protein-dye complex tends to bind to cuvettes, resulting in blue coloured opaque cuvettes (Bradford, 1976). This problem is easily overcome by soaking the cuvettes in SDS solution and rinsing well before use (Dennison, 2003).

This study made use of the macro-assay (detection limits of 10-100 µg/ml) (Bradford, 1976), and perchloric acid (2% (v/v)) which improved stability of the Bradford reagent (Bearden, 1978).

2.5.1. Reagents

Perchloric acid [2% (v/v)].

Perchloric acid (5 ml) was made up to 250 ml with dH_2O.

Bradford assay dye [Coomassie Brilliant blue G-250].

CBBG (0.15 g) was dissolved in dH_2O containing perchloric acid (2% (v/v), 250 ml). The solution was stirred for 1 h, filtered through Whatman No. 1 filter paper and stored at room temperature in an amber glass bottle.

Ovalbumin macro-assay protein standards [10-100 µg/ml ovalbumin].

Ovalbumin protein standards were dissolved in dH_2O (1 mg/ml).

2.5.2. Procedure

The macro-assay protein samples (10-100 µg) were mixed with Bradford assay dye (900 µl) in 1.5 ml eppendorf tubes, and made up to 1 ml with HBBS. Blank solutions contained HBSS (100 µl) and Bradford assay dye (900 µl). The solutions were vortexed briefly and coloured product allowed to develop (2 min). Absorbance values were read at A_{595} nm in plastic cuvettes. Sample readings were normalised against the A_{595} nm values of blank solution. The procedure was

conducted in sextuplicate at 10 successive concentrations of ovalbumin (10 – 100 µg/ml) (Figure 2.1). Mean absorbance readings were calculated and plotted against the ovalbumin concentration. A trend line was inserted over the linear graph to determine the correlation co-efficient (R^2-value), which was $R^2 \geq 0.9$ for this study, indicating linear correlation.

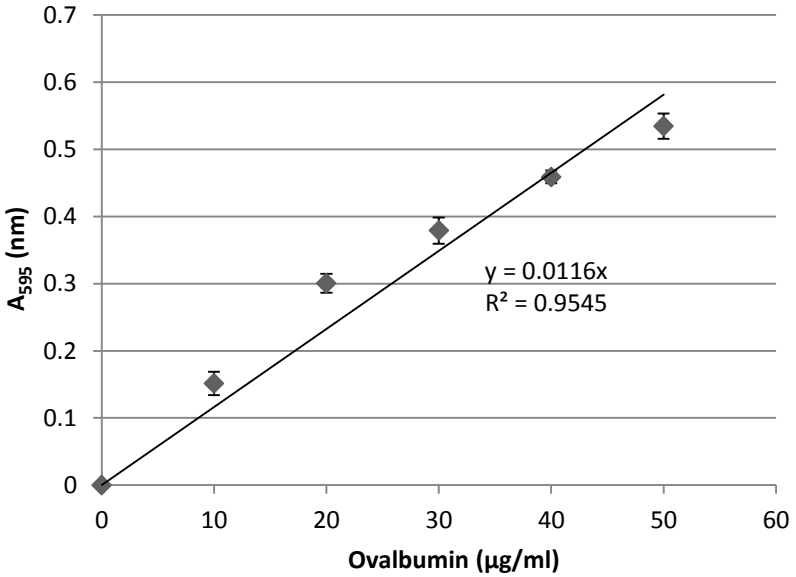

Figure 2.1. Bradford macro protein assay standard curve.
Mean values were plotted of each protein concentration performed six times. Bars represent standard deviation. The trend line equation was calculated to be: y = 0.0116x.

2.6. Protein molecular weight estimation using SDS-PAGE

Sodium dodecyl-sulfate-polyacrylamide gel electrophoresis (SDS-PAGE) has been used as a standard method in biochemistry since the method was first described in its infant form by Raymond and Weintraub (1959). The synthetic monomers, acrylamide and N,N'-methylene bisacrylamide, polymerise in the presence of free radicals producing a transparent gel-like medium containing a lattice of pores. The pores oppose protein migration when an electric current is applied to the gel without the gel depolymerising under the generation of heat (Raymond and Weintraub, 1959). The method was later adapted by Ornstein (1964) to include a discontinuous gel that made use of two different pH systems to improve protein band resolution. Shapiro et al (1967) subsequently applied this technique to estimate the molecular weight of proteins broken into their polypeptide chains in the presence of the detergent, SDS. SDS is an anionic surfactant which masks the charge of proteins, consequently creating the same charge to mass ratio and causing proteins to form linear rod-like structures (Weber and Osborn, 1969). SDS molecules bind to proteins in the ratio of 1.4 mg SDS per 1 mg of protein (Reynolds and Tanford, 1970). Thus, the overall charge of all proteins boiled in the presence of SDS becomes

negative (Kapadia et al., 1974). Upon subjection to an electric field, SDS treated proteins migrate through the cross-linked acrylamide at a rate determined by their size/molecular weight, only.

The current method used in this study is primarily that of Laemmli (1970), which was later reformulated and improved by Read and Northcote (1981) to detect smaller quantities of protein. Treatment with the reducing agent, 2-mercaptoethanol breaks disulfide bonds opening up protein structures to further promote SDS binding. Using proteins of known molecular weight, a standard curve can be generated to size unknown proteins (Weber and Osborn, 1969). When protein mobility from an SDS-PAGE gel is plotted against the logarithm of its molecular weight, a straight line graph is obtained irrespective of the tertiary or quaternary protein structure (Kresge et al., 2006; Laemmli, 1970). SDS-PAGE was carried out using the discontinuous Tris glycine buffer and gel system described by Laemmli (1970) using the Mighty Small II vertical slab electrophoresis unit.

2.6.1. Reagents

Solution A: 30% (m/v) acrylamide, 2.7% (m/v) bis-acrylamide.

Acrylamide (73 g) and bis-acrylamide (2 g) were dissolved in 200 ml dH_2O using a magnetic stirrer. The solution was made up to 250 ml with dH_2O. The solution was stored in an amber coloured glass bottle at 4°C.

Solution B: 4 x running gel buffer [1.5 M Tris-HCl, pH 8.8].

Tris (45.37 g) was dissolved in dH_2O (200 ml), adjusted to pH 8.8 with HCl and made up to 250 ml. The buffer solution was stored in a plastic reagent bottle at 4°C.

Solution C: 4 x stacking gel buffer [500 mM Tris-HCl, pH 6.8].

Tris (3 g) was dissolved in dH_2O (40 ml), adjusted to pH 6.8 with HCl, and made up to 50 ml with dH_2O. The buffer was stored at 4°C.

Solution D: 10% (m/v) SDS.

SDS (10 g) was dissolved in dH_2O (90 ml) using a magnetic stirrer and gentle heating. The final volume was adjusted to 100 ml. The solution was stored at room temperature.

Solution E: Initiator [10% (m/v) ammonium persulfate].

Ammonium persulfate (1 g) was dissolved in dH_2O (1 ml) in a 1.5 ml plastic eppendorf tube made up just before use.

Solution F: Tank buffer [250 mM Tris-HCl, 192 mM glycine, 0.1% (m/v) SDS, pH 8.3].

Tris (15 g) and glycine (72 g) were dissolved and made up to 5 l with dH_2O. The buffer was stored at 4°C. Prior to use 2.5 ml of the 10% (m/v) SDS stock solution (solution D) was added to 250 ml of buffer for use in the Mighty Small-II PAGE apparatus.

Solution G: Reducing treatment buffer [125 mM Tris-HCl, 4% (m/v) SDS, 20% (v/v) glycerol, 10% (v/v) 2-mercaptoethanol, pH 6.8].

Buffer C (2.5 ml), 10% SDS (solution D; 4 ml), glycerol (2 ml) and 2-mercaptoethanol (1 ml) were made up to 10 ml with dH_2O. The buffer was stored at 4°C in a sealed container.

Staining stock solution [1% (m/v) Coomassie blue R-250].

Coomassie blue R-250 (1 g) was dissolved in dH_2O (100 ml) by magnetic stirrer (1 h, RT) and filtered through Whatman No. 1 filter paper.

Staining solution [0.125% (m/v) Coomassie blue R-250, 50% (v/v) methanol, 10% (v/v) acetic acid].

Stain stock (62.5 ml) was mixed with methanol (250 ml), acetic acid (50 ml) and made up to 500 ml with dH_2O.

Destaining solution I [50% (v/v) methanol, 10% (v/v) acetic acid].

Methanol (500 ml) was mixed with acetic acid (100 ml) and made up to 1 l with dH_2O.

Destaining solution II [7% (v/v) acetic acid, 5% (v/v) methanol].

Acetic acid (70 ml) was mixed with methanol (50 ml) and made up to 1 l with dH_2O.

Molecular weight standards [MW: 97.2, 68, 45, 30 and 14 kDa].

Common laboratory proteins of known molecular weight were used as standards for molecular mass determination. phosphorylase B (97.2 kDa), bovine serum albumin (68 kDa), ovalbumin (45 kDa), carbonic anhydrase (30 kDa) and lysozyme (14 kDa) proteins were used. Each protein was separately weighted out (1 mg) and dissolved in reducing treatment buffer (Solution G, 1 ml) to

yield a final concentration of 1 mg/ml. The separate protein samples were boiled for 2 minutes and vortexed. Aliquots (30 µl) of each sample were separated into multiple PCR tubes and stored at -20°C until needed. Aliquots were added together (10 µl each) to form a complete molecular weight standard. This standard was stored at 4°C.

Table 2.1. SDS-PAGE reagent volumes to cast 12.5% running and 4% stacking gels of 1.5 mm thickness.

Solution	Running gel (ml)	Stacking gel (ml)
A	6.25	0.94
B	3.75	-
C	-	1.75
D	0.15	0.07
E	0.075	0.035
dH_2O	4.75	4.3
TEMED	0.0075	0.015
Final vol.	15	7

2.6.2. Procedure

Hoefer Scientific Instruments SE 250 Mighty Small II vertical slab electrophoresis units were assembled as described by the manufacturer. Briefly, aluminium and glass plates were washed with ethanol and dH_2O and allowed to air-dry. The glass and aluminium plates were separated using 1.5 mm plastic spacers and clamped into the vertical gel setting apparatus. The apparatus rubber block was pre-coated with GelSeal (Hoefer Inc.) to prevent leakage.

Running-gel was prepared according to Table 2.1. In both the running and stacking gels, solution E and TEMED were added last, to prevent premature gel polymerisation (Richards and Lecanidou, 1974). The running gel solution was dispensed into the prepared plate sandwich using a 1 ml pipette, leaving a 3 cm space from the top of the glass plate. Distilled water was overlaid for even polymerisation. After gel polymerisation (1 h) the dH_2O was poured off and replaced with prepared stacking gel solution (Table 2.1). Spacer combs (15 well) were inserted and stacking gels were allowed to set (1 h, RT). The complete sandwich was removed from the

gel-setting apparatus and clamped into the gel apparatus. Cold tank buffer (solution F) containing SDS was used to fill both the cathodic and anodic compartments.

Protein samples were combined with reducing treatment buffer (solution G) in a 1:1 ratio and boiled (2 min). Bromophenol blue, 10% (m/v) was added to a final concentration of 0.005% (v/v) after boiling, to track the buffer front. Protein preparations were loaded at approximately 5 µg/well and molecular weight markers were loaded at 1 µl/well using fine-tipped 50 µl loading pipette tips.

The electrophoresis unit was connected to a 4°C circulating water bath to remove latent heat. The electrophoresis unit lid was attached and connected to a power supply at a constant 25 mA per gel. Electrophoresis was carried out for approximately 1.5 h or until the bromophenol blue tracking dye had reached the bottom of the gel. The gel was removed using gloves and placed into staining solution overnight. The gel was placed into destain I solution (4 h) and finally destain II (4 h). Gels were photographed using the VersaDoc 4000 Image capturing system (BioRad, California, USA).

2.7. Semi-dry western blotting and probing with ECL

To probe and characterise specific proteins, the qualitative technique known as Western blotting was utilised with enhanced chemi-luminesence (ECL). Proteins separated by SDS-PAGE are electrophoretically transferred to a matrix with high binding affinity i.e. nitrocellulose, as described by Towbin et al. (1979) with minor reagent modifications. Antigens present on the nitrocellulose are probed with primary antibodies (see Table A.1 of appendix for a detailed list of antibodies) and detected by a complementary secondary antibody and ECL (Renart et al., 1979). The secondary antibody detection system is coupled with horseradish peroxidise (HRPO) which catalyses luminol and results in a luminescent signal. X-ray film is exposed to the chemi-luminescent signal and the signal is recorded by developing and fixing the x-ray film.

2.7.1. Reagents

Blotting and transfer buffer [34 mM Tris-HCl, 173 mM glycine, 20% (v/v) methanol, 0.01% (m/v) SDS, pH 8.3].

Tris (27.23 g), glycine (64.8 g) and methanol (900 ml) were dissolved in 4.5 l of dH_2O. SDS [4.5 ml of 10% (m/v) stock solution D, Section 2.6.1] was added to the buffer prior to use. Buffer was stored at 4°C.

Ponceau-S stain solution [0.1% (m/v) Ponceau-S, 1% (v/v) acetic acid].

Ponceau-S (0.1 g) was dissolved in acetic acid (1 ml) and made up to 100 ml with dH_2O. The staining solution was stored at RT in a sealed container to prevent acetic acid evaporation.

Tween-20 Tris bluffered saline (TTBS) [150 mM NaCl, 3 mM KCl, 20 mM Tris-HCl, 0.05% Tween-20, pH 7.5].

NaCl (8 g), KCl (0.2 g), Tris-HCl (3 g) and Tween-20 (0.5 ml) were dissolved in dH_2O. The pH was adjusted to 7.5 with HCl (30% (v/v)) and made up to 1 l with dH_2O. TTBS was stored at 4°C until use.

Blocking solution [10% (m/v) non-fat milk powder in TTBS].

Non-fat milk powder (10 g) was dissolved in TTBS (100 ml) using a magnetic stirrer bar.

Developer and fixative.

Kodak processing chemicals for autoradiography were made up freshly before use. Developer was mixed 1:3 with dH_2O and fixative was mixed 1:4 with dH_2O.

Enhancer and substrate.

Pierce® ECL western blotting substrate, luminol and peroxide solutions were mixed 1:1 in an 1.5 ml eppendorf microfuge tube just before use.

2.7.2. Procedure

Immediately after SDS-PAGE electrophoresis (Section 2.6), using gloves, gels were removed from the apparatus and submerged in transfer buffer to equilibrate the gel (5 min). Whatman filter paper (6 filters per gel) and nitrocellulose were cut to size (7.5 x 5.5 cm) and submerged in transfer buffer. Three filter papers were laid onto the semi-dry blotting apparatus-grid. Nitrocellulose was carefully laid over the filter paper to avoid trapping air bubbles. Next, the gel was laid on top of the nitrocellulose and finally three more pieces of filter paper. Using a 1 ml pipette, air bubbles were removed from between the pieces by rolling the pipette over the layers. A SemiPhore transfer unit (TE 70) was connected to the power pack (constant 50 mA/gel, 50 V limit, 90 min) and the bands were electrophoretically transferred to the nitro cellulose.

Following transfer, the nitrocellulose was stained with Ponceau-S and allowed to air dry before marking the position of transfer of the molecular weight markers (MWM) with a pencil. The

nitrocellulose was placed in blocking solution (1 h) to prevent non-specific absorption of antibodies onto the membranes. Blocking solution was washed off twice with TTBS before adding primary antibody diluted in TTBS (2 ml, 2 h, RT). The specific primary antibody was washed off (3 x 5 min, RT) with TTBS. Secondary HRPO-tagged antibody (2 ml) was subsequently incubated (1 h, RT). Nitrocellulose was washed (8 x 5 min, RT) with TTBS and gentle rocking to remove unbound secondary antibody.

The probed nitrocellulose was laid onto the smooth side of a transparency sheet. A 1:1, luminol to substrate solution, was pipetted over the nitrocellulose. A separate sheet of an overhead transparency sheet was placed over the nitrocellulose to spread the luminol:substrate mix. The transparency edges were sealed with masking tape and MW pencil marks were traced with green fountain pen. X-ray film was cut to size and laid over the nitrocellulose in a red-light lit dark room. The film was exposed for a short period and submerged in developer and then fixed before rinsing with water and air drying. Densitometry was assessed using the VersaDoc 4000 Image capturing system (BioRad, California, USA).

2.8. Preparation of inhibitors

Dimethyl sulphoxide (DMSO) is a widely used solvent in bioassays and in high-throughput screening (HTS) environments (Waybright et al., 2009). It was recommended as a suitable solvent for dissolving TF 17-2 and TF 22d in this study. DMSO is a dipolar aprotic solvent, since it accepts protons, in contrast to protic solvents such as water and alcohols which donate protons. In polarised form, the oxygen and sulphur have unshared electron pairs allowing DMSO to form either stable solvates by dipole-dipole interactions or solvent-solute associations by hydrophobic interactions (Rammler and Zaffaroni, 1967). DMSO is also hygroscopic, forming a strong 1:2 association complex with water. During water uptake, compound solubility steadily decreases. Long term compound storage in DMSO can lead to structural changes and precipitation by some compounds, affecting initial molar concentrations (Waybright et al., 2009). Therefore, DMSO was stored in small aliquots, in air tight, DMSO resistant, polypropylene containers in the freezer. Final concentrations of DMSO (1-3% (v/v)) have been shown to perturb enzyme structure and function by disrupting hydrophobic substrate interactions (Overall, 2002; Xu et al., 2004) and reduce MMP-2 gelatinolytic activity by 64-79% (Murphy et al., 1994). Therefore, the final volume of DMSO applied to cells in solution with inhibitors was kept to a minimum (0.05% (v/v)) to reduce possible background effects on cells and MMPs.

2.8.1. Reagents

TF 17-2 [Mr 334.4 g.mol^{-1}] and TF 22d [Mr 352.5 g.mol^{-1}].

MMP inhibitors were acquired collaboratively through Prof. Harald Tschesche (Institute for Biochemistry, University of Bielefeld, Germany).

DMSO.

Culture grade DMSO was aliquoted (50 µl) into sterile 0.2 ml thin wall PCR tubes (Porex Bio Products Group) and stored at -20°C to reduce water absorption.

Cycloheximide (CHX) [10 mg/ml].

CHX (50 mg) was dissolved in culture grade DMSO (250 µl). Working stock solution (10 mg/ml) was made by mixing CHX/DMSO (2.5 µl) with sterile dH_2O (47.5 µl).

2.8.2. Procedure

TF 17-2 (28.6 mg) and TF 22d (20 mg) were dissolved in DMSO (100% (v/v), 100 µl) to give a stock solution of 855 mM and 562 mM, respectively. Stock solutions were aliquoted (50 µl) into PCR tubes and stored at -20°C. Working stocks (5 mM) were made up with complete medium when required in order to preserve drug efficacy. A range of final concentrations (50, 100, 150 and 300 µM) were made up in complete medium containing a final background DMSO concentration of 0.05% (v/v). The following example shows how the DMSO background was equalised across samples.

Example: Making TF 22d working solutions from stock solutions.

TF 22d was diluted from 562 mM in 100% (v/v) DMSO to 5 mM with complete medium,

C: concentration, V: volume.

$C_1V_1 = C_2V_2$

562 mM x V_1 = 5 mM x 300 µl

$562x10^{-3}$ g/l x V_1 = $5x10^{-3}$ g/l x $300x10^{-6}$ l

$562x10^{-3}$ x V_1 = $1.5x10^{-6}$ g

V_1 = $2.7x10^{-6}$ l

V_1 = 2.7 µl transferred to 297.3 µl complete medium.

Since 2.7 µl of the stock solution contains nearly 100% DMSO, the background DMSO percentage is estimated as,

$$\frac{2.7\ \mu l}{300\ \mu l} \times 100 = 0.9\%$$

When the final volume required per sample is 1ml.

$C_1V_1 = C_2V_2$

5 mM x V_1 = 300 µM x 1 ml

$5x10^{-3}$ g/l x V_1 = $3x10^{-6}$ g/l x $1x10^{-3}$ l

$5x10^{-3}$ g/l x V_1 = $3x10^{-4}$ g

V_1 = $6x10^{-5}$ l

V_1 = 60 µl transferred to 940 µl of complete medium.

Therefore, the final DMSO background concentration was calculated as,

$$\frac{60\ \mu l \times 0.009}{1000\ \mu l} \times 100 = \ 0.05\%$$

Table 2.2 shows equalisation to a final DMSO background of 0.05% (v/v) using 100% DMSO volumes.

Table 2.2. DMSO background equalisation.

Example of TF 22d containing solutions made up to a final volume of 1 ml.

$[TF\ 22d]_{Final}$ (µM)	Sample volume (µl)	DMSO equalising volume (µl)
300	60	0
150	30	30
100	20	40
50	10	50

CHX served as a positive control for induction of apoptosis. Media containing only 0.05% (v/v) DMSO was used as the negative control.

2.9. Coating of plates with collagen type I

Collagen type I is the most abundant protein in the human body and acts as a growth stimulatory protein when cells are cultured in 2D (Takino et al., 2010). Collagen type-I coating of culture plates and glass coverslips was performed in this study to improve cell adherence to glass and cell directional persistence (Haga et al., 2005), enhance MT1-MMP redistribution to the cell periphery (Lafleur et al., 2006), as well as accumulation at the leading front and subsequent migration

promoting effect (Takino et al., 2004). The protocol used in this study was described by Gharaibeh et al.(2008).

2.9.1. Reagents

Glacial acetic acid 100%.

Required no additional preparation.

Rat tail collagen type-I [1 mg/ml].

Collagen type-I (100 mg) was dissolved in glacial acetic acid (570 µl) and ddH_2O (99.43 ml) using a stirrer bar (4°C, 2 h or o/n).

Chloroform.

Required no additional preparation.

Base medium: DMEM:Ham's F-12 incomplete medium.

As described in Section 2.2.1

2.9.2. Procedure

Chloroform was used to disinfect the collagen solution. Chloroform (1:10 parts collagen solution) was carefully layered at the bottom of the cold collagen solution and left undisturbed (4°C, o/n). The cold collagen solution (top layer) was removed using a 5 ml pipette being careful not to disturb the chloroform layer or incorporate collagen precipitates into the disinfected soluble collagen solution. This working solution (1 mg/ml) was stored at 4°C until use. The working solution was diluted with cold base medium to a final working concentration (25 µg/ml). MaTek live cell imaging glass bottomed plates (MaTek Corporation, Ashland, MA, USA) and plastic Nunc 24-well plates were coated with collagen (500 µl). Culture flasks, 75 cm^3 and 25 cm^3 were coated with 15 ml and 5 ml, respectively. Coated flasks were incubated (37°C, 4 h) to allow collagen fibril formation. Excess collagen solution was removed and plates were allowed to air dry under ultraviolet light overnight. Plates were stored at room temperature until use. Prior to use, plates were rinsed once with base medium (37°C, 1 h) to remove collagen crystals.

CHAPTER 3.

Comparative docking of two MMP inhibitors

3.1. Introduction: predictive docking

Computational molecular docking is a method which predicts the preferred orientation or "pose" of one molecule with respect to another and their affinity for binding to form a stable complex (Kitchen et al., 2004). Predictive docking is frequently used for 'rational drug design' to predict binding orientation and affinity of drug candidates for target proteins. In some instances, the amino acid sequence (primary protein structure) is modeled against a known 3D depiction of a folded protein (tertiary structure) from the same family. Such advancements have rendered protein crystallisation unnecessary when crystal structures of protein families are well documented, saving time and money. Predictive computational modeling has thus become an integral part of the pharmaceutical industry and allows screening of compound libraries against potential target proteins. When a 3D target and details of its binding site are available, high-throughput docking using compound libraries is used as an initial hit-identification tool (Kitchen et al., 2004). This provides a means for narrowing down potential drug candidates in compound libraries, prior to expensive compound synthesis or experimental applications. In addition, active/successful compounds may be digitally re-configured or changed to improve drug-target interactions before compound synthesis (Kitchen et al., 2004). Thus, predictive computational docking is an inexpensive tool that provides theoretical data of molecular interactions.

Docking relies on two experimental approaches: first, the establishment of a theoretical force field to estimate the free energy of binding of the complex, and second, the exploration of the conformational space available to the ligand (inhibitor) and target (protein) (Cosconati et al., 2010). Algorithms that calculate such parameters use quantum mechanics and molecular mechanics to estimate configurations, the specifics of which fall outside the scope of this study. These calculations require more time and computational power with increased molecular complexity. As a result, approximations are included into algorithms. These may include simplified force field parameters, restriction of the search space, and limitations to the conformational flexibility of inhibitor and protein (Cosconati et al., 2010). These approximations reduce calculation time allowing current desktop computers to undertake preliminary small-molecule-protein docking procedures such as those performed in this study.

One of the original problems with synthetic MMP inhibitors is their lack of specificity (Jacobsen et al., 2010). Specificity of inhibitors for their target is defined by the affinity of association (Ka), whereas potency of inhibition is the inverse of Ka and is defined by the concentration required to produce half maximum inhibition (K*i*) (Voet and Voet, 2004). Unfortunately, MMP catalytic domains are structurally similar (Folgueras et al., 2004) resulting in "incidental" inhibition of non-target MMPs in a concentration-dependent manner. Due to the extensive experimental procedures (vector cloning, expression, isolation and purification) involved with *in vitro* kinetic studies, inhibitors may not have been tested against the full repertoire of structurally similar proteases, such as other MMPs, ADAMS and MT-MMPs. The question asked here is whether *in vitro* assayed inhibitor K*i* values reflect predicted docking K*i* values for MMPs for which 3D structures are known. If they do, can we use docking predictions to predict the extent of inhibition of these proteins when *in vitro* K*i* values are not available? Here we use the free ware program, AutoDock Vina as a tool to predict docking between inhibitor and its MMP target.

In this chapter we evaluate two recently developed MMP inhibitors and their affinity for MT1-MMP and MMP-2, two proteases involved in cancer migration (Deryugina et al., 2001) and invasion (Sato and Takino, 2010). In subsequent sections docking simulation is described in more detail, describing docking first, the receptor, and finally the ligand.

3.2. Docking: theoretical aspects and AutoDock4.2/Vina

AutoDock is a Linux-based molecular modeling freeware suite developed by the Scripps Research Institute (Morris et al., 2009). Previous ligand docking software packages employed a 'matching methodology' which created a model of the protein active site and included sites of hydrogen bonding and sterically accessible sites that docked a rigid ligand through geometric comparisons (Morris et al., 1998). A simplified analogy of this primitive docking protocol would be the common 'lock and key' concept, in which ligand and protein flexibility is ignored. AutoDock uses a class of docking techniques that are slower than geometric matching techniques, but allows flexibility within the ligand and utilises molecular mechanics to calculate the energy of the ligand in the context of the protein active site (Morris et al., 1998). AutoDock combines a semi-empirical free energy force field with a Lamarckian Genetic Algorithm (LGA), providing predictions of bound conformation and free energies of association (Morris et al., 1998). Free energies are so-called 'empirical' or 'knowledge-based' (statistical) scoring approaches, which are based on energy functions between atoms within a structure (Böhm, 1994; Eldridge et al., 1997) and consider intermolecular factors such as dispersion/repulsion, hydrogen bonding,

electrostatics, desolvation and entropy (Cosconati et al., 2010). AutoDock uses the Assisted Model Building with Energy Refinement (AMBER) software suite for its molecular dynamic (MD) simulations (Case et al., 2005; Kitchen et al., 2004). The LGA is best explained as "digital evolution", where solutions to conformational problems evolve towards more accurate conformations. As opposed to previous genetic algorithms (GAs) the LGA can tolerate ligands with more conformational degrees of freedom and with greater reliability (Morris et al., 1998). These algorithms and semi-empirical factors are not manipulated by the user, however, user guidance is required to identify the protein active site as another means to limit simulation time by including local conformational search restrictions.

Prior to ligand docking simulation, a box is centred on the binding site of the protein and assigned three dimensional co-ordinates. This method is known as a grid-based method used for energy evaluation and constitutes a method of approximation through restriction of the search space, and requires the target molecule to be treated as rigid (Cosconati et al., 2010). The grid-based method is necessary to eliminate redundant ligand interactions with non-active domains of the protein target. Thus, knowledge of the target protein is required before running a docking simulation (Huey and Morris, 2008). Free energy calculations measured in kcal/mol, are generally formulated in terms of estimating the relative free energy differences, ΔG, between two equilibrium states (Figure 3.1). Multiple enzyme-inhibitor poses are generated during a docking simulation. Poses are scored according to the measure of fit of the ligand. These poses are subsequently ranked according to the free energy of binding and parameters such as entropy or explicit solvation (Kitchen et al., 2004). Data generated is listed from the most energy efficient pose to the least efficient pose (Huey and Morris, 2008). Prediction of structural poses does not require an association constant (K_a), whereas biological activity predictions require K_a and use scoring terms such as steric (conformational space), electrostatic, hydrogen bonding, inhibitor and enzyme flexibility (Kitchen et al., 2004).

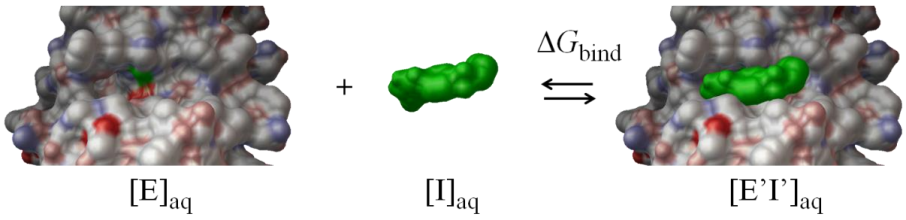

$$[E]_{aq} + [I]_{aq} \underset{K_i}{\overset{K_a}{\rightleftharpoons}} [E'I']_{aq} \qquad (1)$$

$$K_a = K_i^{-1} = \frac{[E'I']}{[E][I]} \qquad (2)$$

$$\Delta G = -RT\ln K_a \qquad (3)$$

Figure 3.1. Equilibrium states relating free energy of binding (Δ*G*) to binding affinity (K*i*).
Free enzyme (E) and inhibitor (I) are depicted in aqueous solution and exist in equilibrium with inhibitor bound to enzyme (E'I') (Eq. **1**). Binding affinity (K*i*) is inversely related to the association constant K_a (Eq. **2**). Changes in free energy are proportional to the logarithm of K_a (Eq. **3**) [depiction rendered using ADT, reconstructed from Kitchen et al. (2004)].

To compare the accuracy of predictions, a root mean square deviation (RMSD) value is assigned to a pose. The RMSD is a measure of distance between the experimental and predicted structures with a cutoff criterion of 2 Å representing the maximum tolerated deviation between the two (Trott and Olson, 2010). AutoDock will consistently dock small molecules with up to about 10 degrees of torsional freedom (Morris et al., 2009) and has an accuracy of free energy prediction of about 2-3 kcal/mol standard deviation (Huey et al., 2007). Visual inspection is also an important feature of molecular docking (Morris et al., 2009). The catalytic domains of the MMPs of interest will now be described in detail to clarify the relevant target structural characteristics.

3.3. Receptor site: structural features of the catalytic domain

The catalytic domain of MT1-MMP was briefly described in Chapter 1 (Section 1.6). In this section, the general structural features of MMP catalytic domains will be described followed by distinguishing features of MT1-MMP and MMP-2, the model enzyme focus of this study.

The active site, as described for all metzincins including MMPs, is comprised of a catalytic zinc binding site ligated by the imidazoyl Nε2 of three histidine residues (Figure 3.2-A&B) at a binding distance of ~2.1 Å (Fernandez-Catalan et al., 1998; Gomis-Rüth, 2009). This catalytic zinc is located on the "front" surface of the protein in a cleft which spans almost the entire ~40 Å diameter of the spherical MMP molecule (Figure 3.2-C), allowing binding of native substrates in an extended conformation (Tallant et al., 2010). The S1'-subsite (Figure 3.2-C) is a hydrophobic

cleft that becomes a tunnel and leads towards the solvent (Jacobsen et al., 2010). This pocket varies in size and depth among MMPs. The S1' specificity pockets of MT1-MMP and MMP-2 are generally characterised as being large and open channels (Jacobsen et al., 2010). This structural feature is important for inhibitor design, as larger molecules with hydrophobic lengths may selectively target these MMPs over MMPs such as MMP-1, which has a shallow specificity pocket (Jacobsen et al., 2010). The inhibitors used in this study, therefore, needed to be assessed for their ability to access the S1' pocket.

The typical secondary structural elements of MMPs are five beta sheets (βI to βV) and three alpha helices (αA to αC) linked by loop structures. Both MT1-MMP and MMP-2 exhibit these three conserved loops which distinguish them from other metzincins, respectively (Figure 3.2-D & E). These three loops (L) connect strands βII and βIII (L-βII-βIII), L-βIII-βIV, and L-βIV-βV (Fernandez-Catalan et al., 1998; Tallant et al., 2010). L-βIV-βV participates in binding a calcium ion, while L-βIII-βIV, known as the 'S-loop', meanders in the shape of the letter 'S' around two further ion-binding sites. The first site encountered by the S-loop is the structural zinc binding site co-ordinated by three histidines. The second half of the S-loop is involved in the second calcium binding site. The S-loop terminates upon entry into the lowermost part of βIV, which forms the boundary of the active site cleft (also visible in Figure 3.2-C) (Tallant et al., 2010). After the last strand, βV, the chain enters a large loop, L-βV-αB, which is highly variable among MMPs and contributes to substrate specificity. This loop leads to the active-site helix, αB, which contains the first of two active site histidines (His^{239} and His^{243}). The αB helix undergoes a sharp turn in the trajectory of the polypeptide to reach the third histidine (His^{294}) of the zinc-binding consensus sequence 'HExxHxxGxxH' (where 'x' is any amino acid) (Tallant et al., 2010). In this motif the Zn(II) is ligated by the these three histidine residues forming the active site (Figure 3.2-A & B) (Fernandez-Catalan et al., 1998). After the third histidine, the spiral of the loop terminates at the 1,4-tight "Met-turn" causing a perpendicular change in peptide trajectory. Between the Met-turn and the last helix, αC, is the "specificity loop", common to all MMPs and important for substrate specificity. Finally the peptide terminates after αC (Tallant et al., 2010) (Figure 3.2-D & E).

A structural element that distinguishes MT1-MMP from MMP-2 is the insertion of an extra 8 amino acids within L-βII-βIII (Lang et al., 2004). This 'MT-loop', is conserved among MT-MMPs and may have an exosite function during pro-MMP-2 activation (Figure 3.2-D) (English et al., 2001). In MMP-2, three fibronectin type-II repeats are found within L-βV-αB domain. These

are important for substrate interaction and influence inhibitor pose and hence, specificity (Figure 3.2-E.i) (Maskos, 2005).

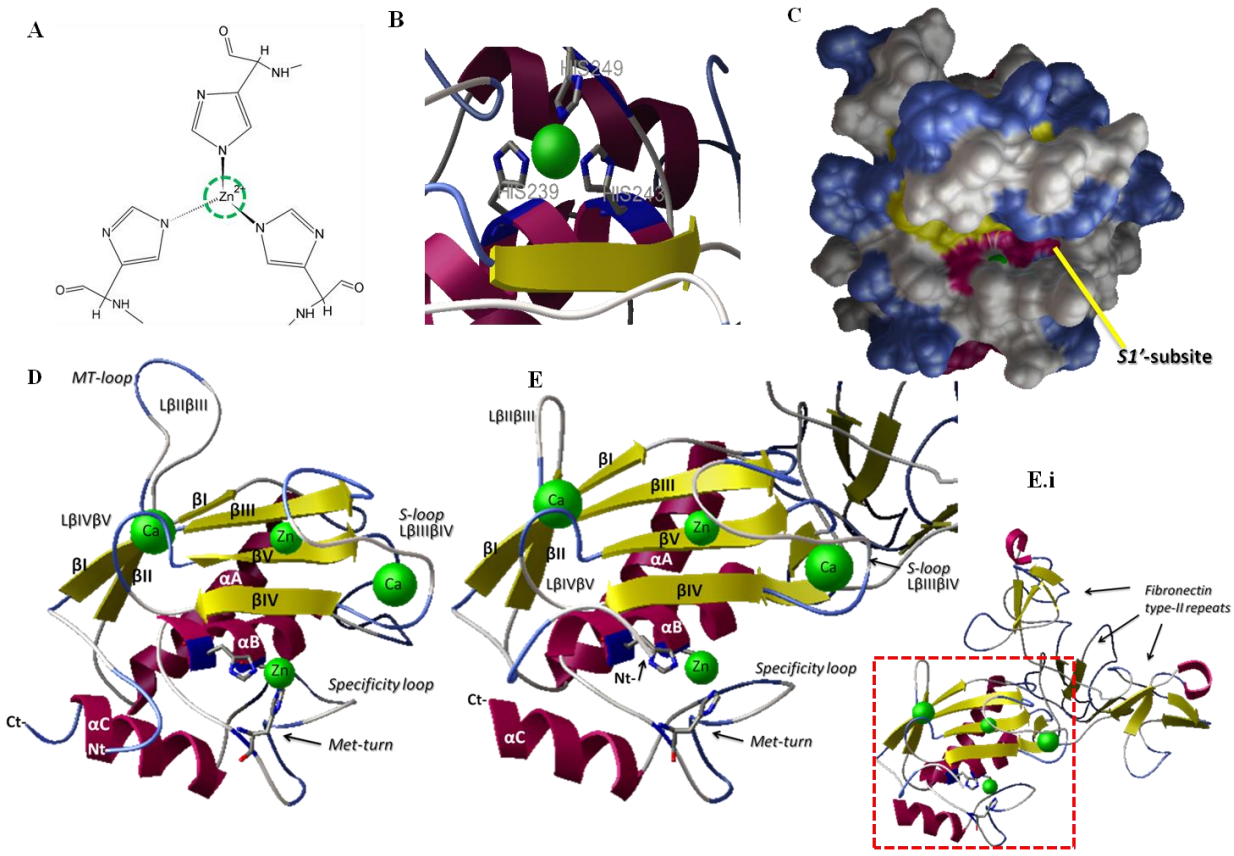

Figure 3.2. Structural features of MMP catalytic domains.
Fisher projection of the zinc ion ligated by the imidazoyl Nε2 of three histidine residues. (**A**) This tetrahedral coordination of zinc is conserved among metzincins. Ribbon representation of MT1-MMP catalytic domain showing secondary structures in tertiary conformation. (**B**) The catalytic zinc ion (green sphere) is depicted in a tetrahedral conformation with His^{239} and His^{243} of the purple alpha-helix (αB) and His^{249} of a coil forming the catalytic domain. Three dimensional surface plot of MT1-MMP coloured according to secondary structure where blue indicates a turn, grey indicates a coil, purple represents alpha-helices and yellow represents beta sheets. The zinc ion (green) protrudes from the surface of the alpha helix. (**C**) To the right of the zinc ion is the S1' subsite. (**D**) Ribbon structures of MT1-MMP and (**E**) MMP-2 depicting structural similarities as described in the text. (**E.i**) Fibronectin type-II repeats are substrate binding sites found in gelatinase A and B or MMP-2 and MMP-9 and are part of the catalytic domain [concept reproduced from Sela-Passwell et al. (2012) (for A-C) with additional information reconstructed from Tallant et al. (2010), including minor information from Fernandez-Catalan et al. (1998) and Morgunova et al. (1999) (for D-E). Images rendered using ChemSketch, ADT and Microsoft Power Point].

3.4. Ligand: MMPI designs

3.4.1. Previous MMPIs

Broad spectrum MMP inhibitors (MMPIs) employed in early clinical trials were used to explore a variety of zinc-binding pseudopeptide derivatives, called peptido-mimetics (Gialeli et al., 2011).

Hydroxamate functional groups incorporated into peptido-mimetic compounds were used in these trials, and chelated the zinc ion in a bidentate fashion via their hydroxyl and carbonyl oxygens (Figure 3.3, **a**) (Parkin, 2004). Although these hydroxamates exhibited effective anti-cancer activity in cell and animal models, it was later determined that hydroxamates are metabolically labile. In addition these early MMPIs also inhibited members of the 'a disintegrin and metalloproteinases' (ADAMs) protease family (Fisher and Mobashery, 2006) due to high catalytic domain homology between ADAMs and MMPs (Lopez-Otin and Matrisian, 2007). This possibly contributed to their failure in clinical trials.

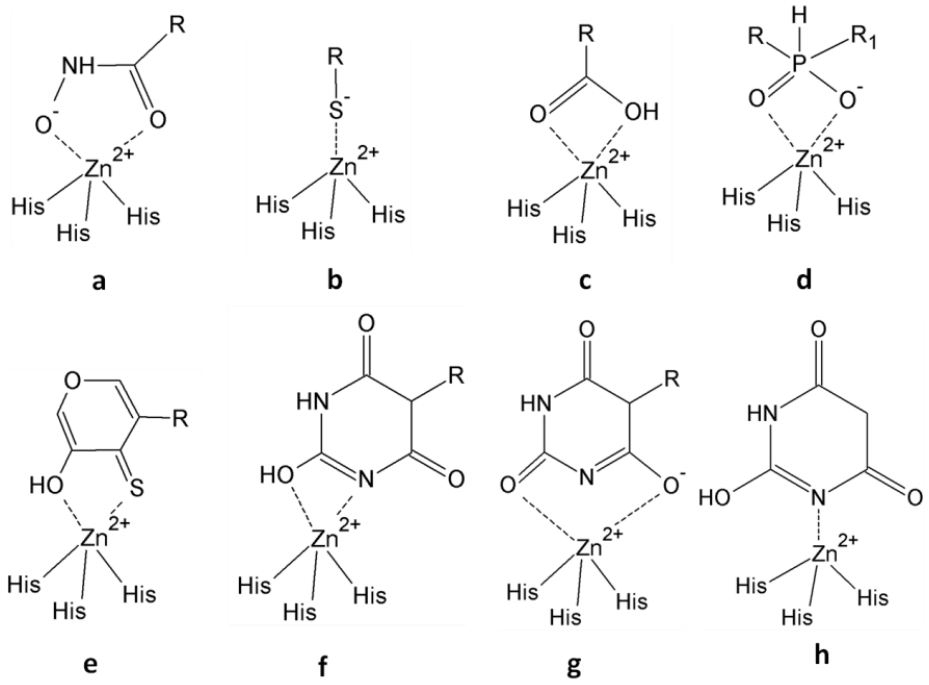

Figure 3.3. Schematic representation of zinc binding groups.
Dashed lines represent coordinating bonds that may form between functional groups of ligand structures with the catalytic zinc ion of MMPs. Hydroxamate (**a**), thiolate (**b**), carboxylate (**c**), phosphinate (**d**), hydroxythiopyrone (**e**), pyrimidinetrione (**f-h**) [reconstructed from Devel et al. (2010) with additions from Brandstetter et al. (2001) regarding 'f' and Jacobsen et al. (2010) regarding 'h'].

The use of hydroxamate MMPIs revealed the complex roles of MMPs in human physiology. MMPs have subsequently been shown to have roles in anti-tumour activity, apoptosis, metabolism, immune modulation as well as pathophysiological roles such as in metastasis, tumour growth, and angiogenesis (Table 3.1) (Fisher and Mobashery, 2006; Folgueras et al., 2004). These conflicting roles of MMPs complicate the selection of the target MMP and hence, the synthesis of selective MMPIs (Folgueras et al., 2004). MMPs, however, are mostly secreted proteases. In such a case, the best MMP target are those that are more associated with a specific

cell or tumour as opposed to normal tissue functions. The MMPs that are chosen as targets, however, should not be among the MMPs essential for anti-tumour activity (Table 3.1).

Non-hydroxamate zinc binding groups (ZGBs) were developed to overcome shortcomings of hydroxamates including solubility and metabolic lability. These contained thiolates, carboxylates, phosphinates, hydroxythiopyrones or pyrimidinetriones (Figure 3.3, **b-f**). In addition, non-peptidomimetic inhibitors were also developed incorporating the functional groups mentioned in Figure 3.3.

Table 3.1. MMPs that act as anti-tumour agents.

List of anti-tumourogenic MMPs that are undesirable MMPI targets [reconstructed from Lopez-Otin and Matrisian (2007)].

MMP	Anti-tumour mechanism	References
MMP-3	Stimulation of apoptosis	(McCawley et al., 2004; Witty et al., 1995)
MMP-8	Regulation of inflammation	(Balbín et al., 2003; McCawley et al., 2004)
MMP-9	Inhibition of angiogenesis	(Coussens et al., 2000; Pozzi et al., 2002; Takeha et al., 1997)
MMP-11	Suppression of metastasis	(Andarawewa et al., 2003)
MMP-12	Inhibition of angiogenesis	(Gorrin-Rivas et al., 2000a; Gorrin-Rivas et al., 2000b)
MMP-19	Inhibition of angiogenesis	(Jost et al., 2006)
MMP-26	Regulates oestrogen-signalling	(Savinov et al., 2006)

3.4.2. Current MMPIs

The two inhibitors, TF 17-2 and TF 22d, used in this study resemble the nucleotide head of uracil and are, therefore, grouped under pyrimidine-based inhibitors. This is an orally-available class of MMP inhibitors and is less likely to induce adverse muscular effects than earlier generations of MMPIs (Fisher and Mobashery, 2006). An MMPI named Ro 28-2653, with a similar MMP target repertoire to the TF inhibitors, achieved reduced tumour vascularisation, inhibited the tumour promoting effects of fibroblasts, and reduced tumour growth in breast adenocarcinoma cells (Maquoi et al., 2004). Ro 28-2653 structural analogues form co-ordinated interactions with Zn(II) as depicted by Figure 3.3-**f**. The phenyl group was shown to occupy the S1' binding pocket of the target MMP (Brandstetter et al., 2001). Such Zn(II) binding is anticipated for TF inhibitors as this would cause the hydrophobic R-group substituent of the TF inhibitors (Figure 3.4) to be projected into the hydrophobic pocket of the target MMP. Thus, the current docking study will, therefore, in essence, provide insight into the success with which the R-substitutes of

the TF inhibitors associate with MT1-MMP and MMP-2. Results will also be correlated with known K*i* values against MT1-MMP and MMP-2.

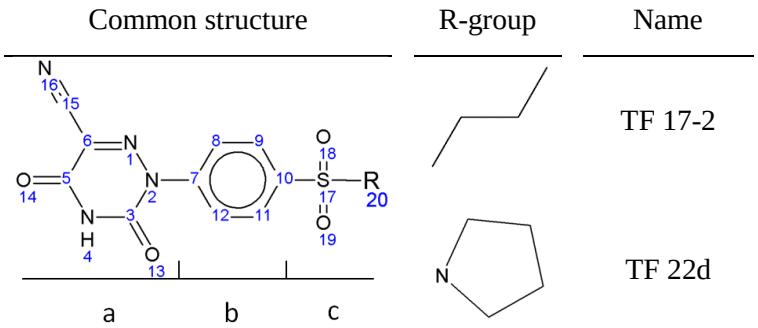

Figure 3.4. Chemical structure of inhibitors TF 17-2 and TF 22d.
The common structure comprises of 6-azauracil (**a**), phenyl (**b**) and a sulfoxide group (**c**). Substituted R-groups include butane making TF 17-2 (IUPAC name: 2-[4-(butylsulfonyl)phenyl]-3,5-dioxo-2,3,4,5-tetrahydro-1,2,4-triazine-6-carbonitrile) and pyrrolidine making TF 22d (IUPAC name: (5R)-5-hydroxy-3-oxo-2-[4-(pyrrolidin-1-ylsulfonyl)phenyl]-2,3,4,5-tetrahydro-1,2,4-triazine-6-carbonitrile). Atom numbers in blue are referred to in text [structures rendered using ChemSketch].

3.5. Considerations during modeling with MMPs

All experimental approaches have limitations, as is the case with the docking procedure used in this study. The quality of the crystal structure used in docking simulations is important. Fortunately the 1BUV.pdb file containing the catalytic domain of MT1-MMP was crystallised associated with TIMP-2, forcing the catalytic site to adopt a conformation that is more relevant to binding of a physiologically inhibitory molecule (Tallant et al., 2010).

In the search for a suitable MMP-2 crystal structure, multiple E403A mutant MMP-2 structures were found (Hashimoto et al., 2011; Morgunova et al., 1999; Morgunova et al., 2002). This E403A mutation means that glutamate^{403} in the catalytic domain was replaced by an alanine in order to render the enzyme catalytically inactive. As an alternative to these MMP-2 structures, the 1QIB.pdb file containing a MMP-2 structure in which the catalytic domain lacks the type-I fribronectin repeats, was available for use in the current study. This structure includes a hydroxamate inhibitor in the active site (Dhanaraj et al., 1999) providing an ideal conformation for use with inhibitor docking.

In the current study, computational docking was used to study the binding of two inhibitors (TF 17-2 and TF 22d) into the active site of two different MMPs, MT1-MMP and MMP-2. The *in*

silico binding energies and positioning of these inhibitors were compared to *in vitro* inhibition constants (K*i*) reported previously (Fischer, 2004; Kapischke et al., 2008).

3.6. Procedure

3.6.1. Software required

Chemsketch (ACD/ChemSketch, 2005).

The ACD/ChemSketch freeware allows the depiction of chemical structures, 2D and 3D conformation rendering, structure cleaning, and automated IUPAC naming of structures. The program was available from www.acdlabs.com.

VMware® Player.

The VMware® Player desktop application allows additional operating systems to run virtually and was downloaded from www.vmware.com. This program eliminates the requirement of dual boot sequences for running multiple operating systems and allows simultaneous operation of Windows 7 (by Microsoft) and Bio-Linux (freeware).

Bio-Linux 6.0.

Based on the Ubuntu Linux 10.04 base, Bio-Linux 6.0 was released by the Natural Environment Research Council (NERC) as a workstation for biologists and bioinformaticians. This software, available from http://nebc.nerc.ac.uk as freeware, and a Linux operating system was required in order to install and run AutoDockTools.

Swiss PDB viewer 4.0.1 (Guex et al., 1997).

Developed by the Swiss Insitute of Bioinformatics, Swiss PDB viewer supplies an application that provides a friendly graphical user interface (GUI) allowing the visualisation of protein data files with the file extension, pdb. Available from http://spdbv.vital-it.ch as freeware, this too was downloaded.

AutoDockTools 1.5.4 (ADT) (Morris et al., 1998).

ADT is the GUI for AutoDock Vina (Trott and Olson, 2010) developed by the Scripps Research Institute and available as a free package (MGLTools-1.5.4) from http://autodock.scripps.edu/downloads. This software includes third party programs, such as python molecule view 1.5.4 (PMV), Vision-1.5.4 for compiling ligand/protein libraries, AutoTors, AutoGrid and AMBER, and was also downloaded.

3.6.2. Co-ordinate file preparation

Inhibitors were "built" using ChemSketch and optimised using "Prepare ligands" in ADT. ADT was used to merge non-polar hydrogens, add Gasteiger charges (empirical atomic partial charges), and set up rotatable bonds through AutoTors, finally creating PDBQT files (a protein data bank text file with charges, 'Q', and torsions, 'T') from traditional PDB files. AutoTors detected 5 rotatable bonds in TF 17-2 and 3 rotatable bonds in TF 22d. The carbon of the carbonitrile was determined by ADT to be the root atom around which all other molecular torsions were calculated. For both protein and inhibitor, polar hydrogens were added, Gasteiger charges computed and non-polar hydrogens merged. Polar hydrogens are hydrogens bonded to electronegative atoms like oxygen and nitrogen. Non-polar hydrogens are hydrogens bonded to carbon atoms (Huey and Morris, 2008).

The X-ray 3D structures of the protein targets were downloaded from the Protein Data Bank (PDB) (http://www.rcsb.org) including MT1-MMP (1BUV.pdb) and MMP-2 (1CK7.pdb). MT1-MMP catalytic domain was co-crystallised with the endogenous TIMP-2, which was removed using Swiss-PDB-viewer prior to file preparation. Full length MMP-2, crystallised with its prodomain, linker region and hemopexin domain (Morgunova et al., 1999) were also removed using Swiss-PDB-viewer prior to file preparation leaving only catalytic domains for use in docking studies.

3.6.3. AutoGrid calculation parameters

AutoGrid was used to create affinity grid maps for all the atoms present between the active site residues of the protein and the inhibitors. Grid maps were centred on the catalytic zinc ion and co-ordinates were selected in order to encompass the entire active site for each protein. MT1-MMP grids enclosed an area of 40 Å (X) by 32 Å (Y) by 52 Å (Z) with 0.375 Å spacing centered on the co-ordinates x = 16.898, y = 8.002 and z = 19.516. MMP-2 grids enclosed an area of 40 Å (X) by 32 Å (Y) by 50 Å (Z) with 0.375 Å spacing centered on the co-ordinates x = 65.212, y = 26.102 and z= 24.994.

3.6.4. AutoDock calculation parameters

AutoDock Vina with the LGA was used to simulate inhibitor-protein docking and was run several times to generate various docked conformations. Docking parameters were set as follows: 4 docking runs, random starting position and conformation, with an output of 9 conformations. All other parameters provided by the default setting chosen according to Morris et al. (1998) who

established these LGA parameters. Docked conformations were ranked using a tolerance of 2.0 Å RMSD. The entire virtual experiment was performed on the Intel® Core™ i3-330M 4.26 GHz (combined processors) 63-bit computer running BioLinux 6 in WVM-player. Estimated K*i* values for both compounds were calculated by rearranging equation 3 of Figure 3.1:

$$Ki = e^{\frac{\Delta G \times 1000}{RT}}$$

where ΔG is the theoretical free energy calculated by AutoDock, R is the gas constant 1.98719 (cal) and T is the temperature at 298.15 (K) (Froufe et al., 2011).

3.6.5. In vitro affinity disclosure

The TF 17-2 (also known as TF 28d) and TF 22d compounds were obtained collaboratively through Prof. Harald Tschesche of the University of Bielefeld were synthesised by Dr. Tim Fischer (2004) during doctoral studies. Affinity constants were derived from kinetic assays and metabolic stability (Appendix Section C) determinations (Fischer, 2004) are as given below.

Table 3.2. Enzyme-inhibitor affinity results.

Butyl (TF 17-2) and pyrrolidin (TF 22d) R-substituent's show varied affinity constants when tested against similar MMPs [reproduced from Fischer (2004)].

Inhibitor	K*i*-for MMP- [µM]						
	2	7	8	9	12	13	MT1-
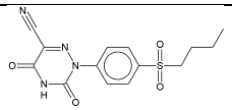 TF 17-2	28.0	0.05	4.0	10.8	14.9	2.50	0.22
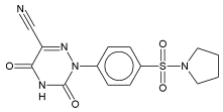 TF 22d	14.7	0.71	0.2	>50.0	N/A	0.091	0.2

Enzyme activity assays performed by Fischer (2004) show the affinity constant K*i* for each inhibitor to several MMPs (Table 3.2). According to these *in vitro* results, similar K*i* values were obtained with both inhibitors for MT1-MMP (200 nM). Both TF 17-2 and TF 22d achieved a ~100 fold decrease in affinity towards MMP-2 (28.0 µM and 14.7 µM, respectively) compared to MT1-MMP. To clarify, affinity of TF 17-2 for the range of MMPs tested is in order of greatest affinity to least: MMP-7, MT1-MMP, MMP-13, -8, -9, -12, and -2. Affinity of TF 22d for the range of MMPs tested is; MMP-13, MT1-MMP & MMP-8, -7, -2, and -9.

3.7. Results

Simulation of docking of inhibitors to MT1-MMP and MMP-2 performed using various software packages to assess docking efficiency and, hence, efficiency of inhibition of protease activity gave the following results:

3.7.1. Grid parameters

Grid boxes used to define the active site region surround the Zn(II) and S1' pocket using the co-ordinates mentioned (Section 3.6.3) to provide constraints producing the best free energy values for inhibitor docking to MT1-MMP and MMP-2 (Figure 3.5).

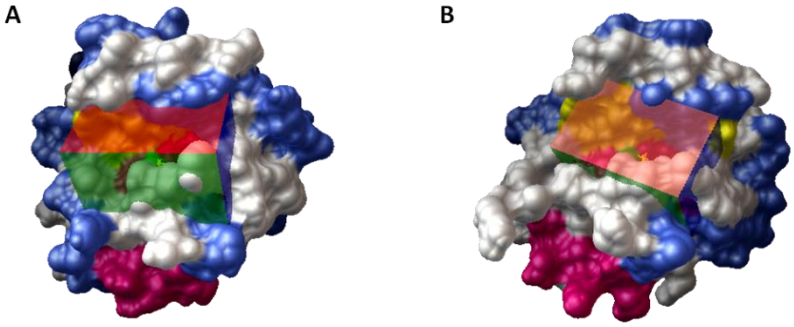

Figure 3.5. Grid Box positioning on the MMP catalytic site.
MMP catalytic sites embodied by grid boxes produced a grid map during simulation. Box co-ordinates are coloured red (X), green (Y) and blue (Z). (**A**) MT1-MMP grids enclosed an area of 40 Å (X) by 32 Å (Y) by 52 Å (Z) with 0.375 Å spacing centred on the co-ordinates x= 16.898, y= 8.002 and z= 19.516. (**B**) MMP-2 grids enclosed an area of 40 Å (X) by 32 Å (Y) by 50 Å (Z) with 0.375 Å spacing centred on the co-ordinates x = 65.212, y = 26.102 and z = 24.994. Proteins are coloured according to secondary structure where blue indicates a turn, grey indicates a coil, purple represents alpha-helices and yellow represents beta sheets.

3.7.2. Docking poses

The docking poses were ranked according to their docking scores and for theoretical legitimacy upon visual inspection, from best representative inhibitor-protein interactions to worst, as depicted in Figure 3.6 and Figure 3.7. Figure 3.6 shows details of enlarged MMP active sites with inhibitor orientations relative to protein structures, whereas Figure 3.7 shows the pose of inhibitors in proximity to the S1' pocket. In the schematic Figure 3.8-A&B of MT1-MMP's active site amino acids, the azauracil head of both inhibitors is co-ordinated with Zn(II) by atoms C_3=O_{13} (for atom numbering, see Figure 3.4). The Zn(II)-O_{13} coordination has a favourable distance of 2.4 Å (Figure 3.8-A & B). This interaction may be further strengthened by the partial negative charge of the adjacent glutamate (Glu^{240}) with a distance of 3.1 Å, indicating a hydrogen bond interaction. The phenyl ring of both inhibitors appears to interact with the carboxy group at the αC of $alanine^{200}$, stabilising molecule orientation (Figure 3.8-A & B). The hydrophobic

butanyl tail of TF 17-2 interacts with histidine[201] with a similar bond length as that achieved by the pyrrolidin ring of TF 22d (3.74 and 3.82 Å, respectively) (Figure 3.8-A & B). Both inhibitors adopt this similar pose, causing the phenyl ring to deny access to incoming substrates by sterically covering Zn(II) and projecting the sulfoxide group towards the solvent (Figure 3.6-A.i & B.i).

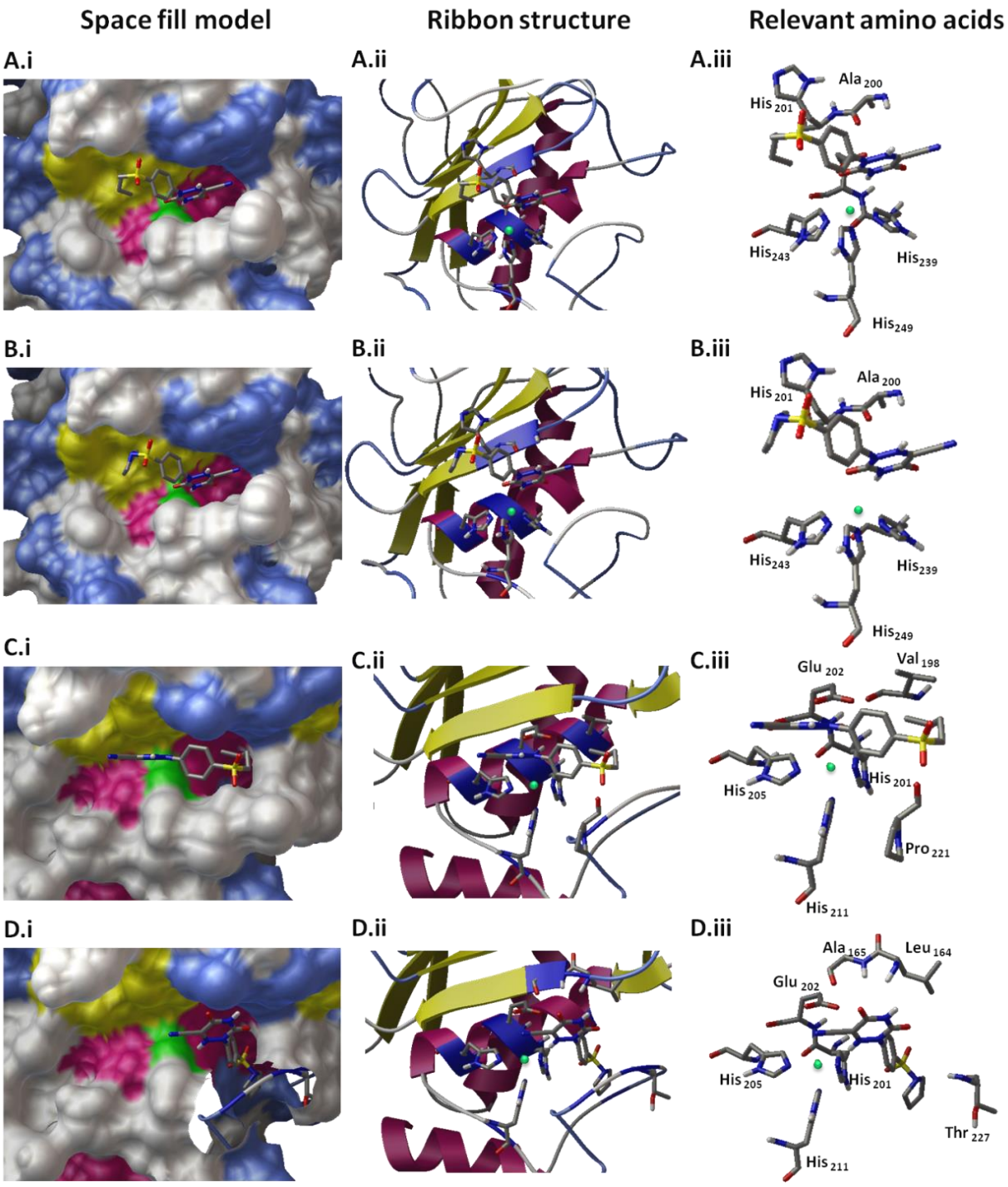

Figure 3.6. Docking conformations predicted for TF 17-2 & TF 22d in MT1-MMP & MMP-2.
All figures numbered 'i' are protein surface representations and are coloured according to secondary structure elements where blue indicates a turn, grey indicates a coil, purple represents alpha-helices and yellow represents beta sheets. Zinc is coloured green. Figures numbered 'ii' are ribbon structures showing only amino acids that contribute to ligand binding, coloured dark blue where the amino acids originates from the secondary structure. Figures numbered 'iii' omit the secondary structure and show only the relevant amino acids. (**A**) TF 17-2 in MT1-MMP, (**B**) TF 22d in MT1-MMP, (**C**) TF 17-2 in MMP-2 and (**D**) TF 22d in MMP-2 showing penetration of the S1'pocket by omitting the surface structures of isoleucine[222] and proline[221], numbered according to the truncated 1QIB.pdb file.

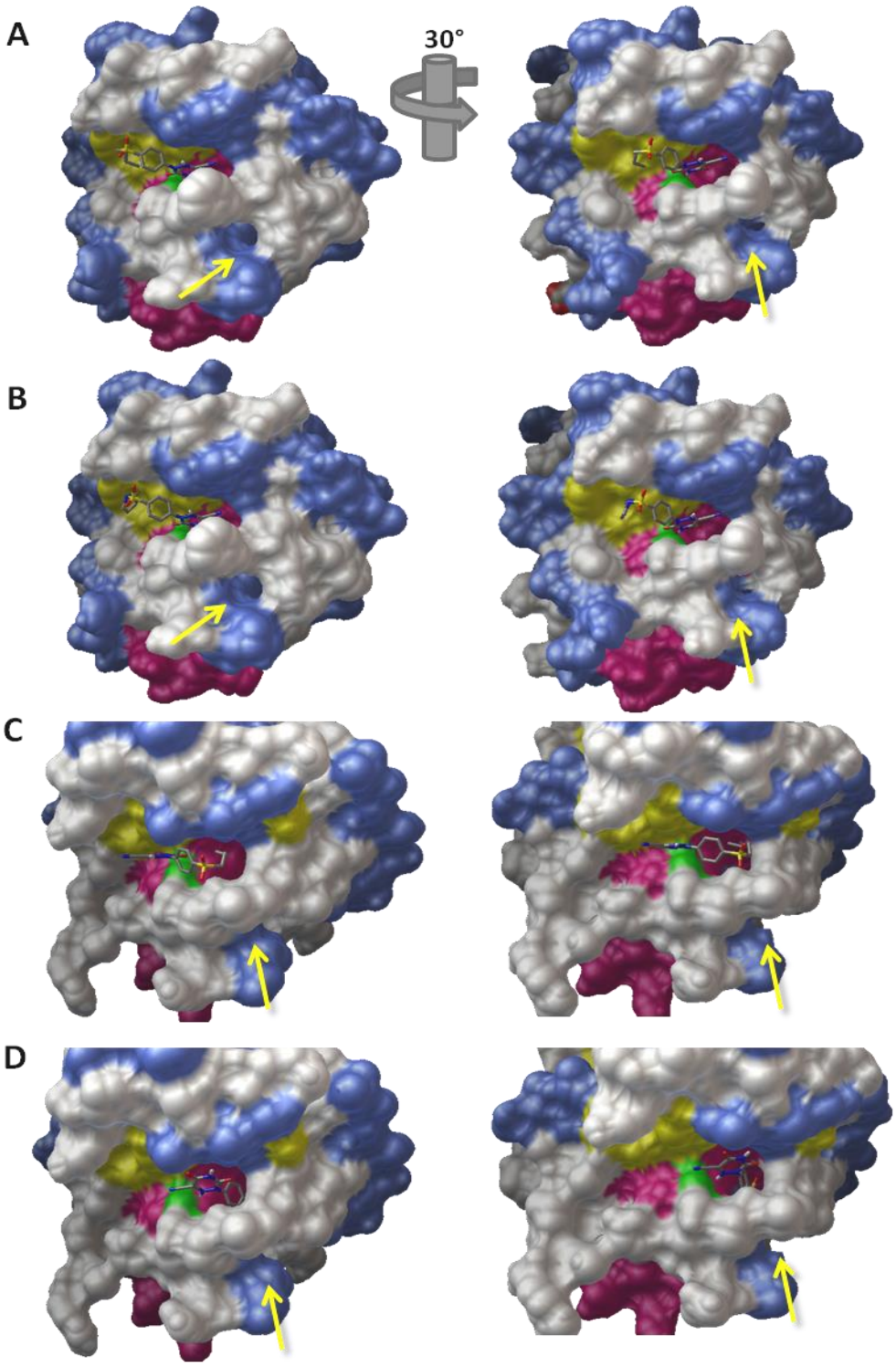

Figure 3.7. Catalytic domain view of inhibitor poses showing depth and proximity of S1' pocket. MMP surfaces coloured according to secondary structure elements where blue indicates a turn, grey indicates a coil, purple represents alpha-helices and yellow represents beta sheets. The zinc ion appears green. (**A**) MT1-MMP with TF 17-2 or (**B**) TF 22d and (**C**) MMP-2 with TF 17-2 or (**D**) TF 22d from the side showing the S1' pocket. When the MMPs are rotated by 30 degrees, the length of the active site is clearly visible. Yellow arrow points into the exit of the S1'pocket. The various poses are further described in the text [depictions rendered using AutoDock and Microsoft Power Point].

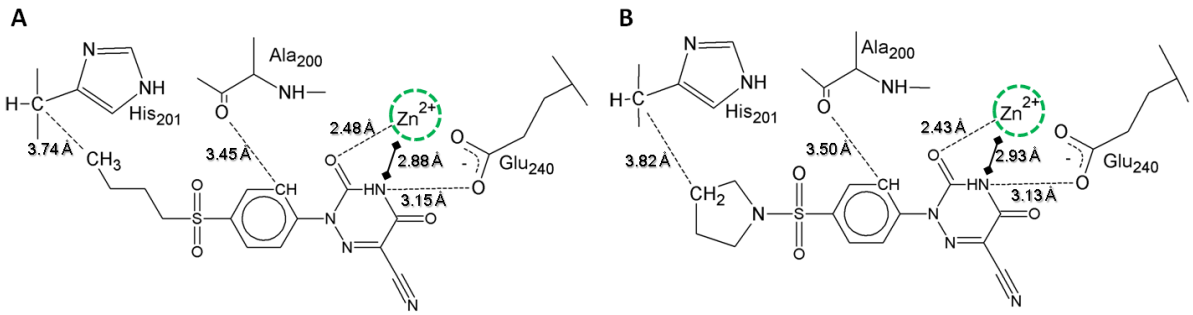

Figure 3.8. Schematic representation of inhibitor interactions with amino acids of MT1-MMP active site.
(**A**) TF 17-2 and (**B**) TF 22d show similar atomic interactions with amino acids residues of the catalytic active site (dashed lines). The 6-azauracil ring of both inhibitors forms a monodentate coordination complex with Zn(II) (green). The poses are stabilised by bonding to amino acid residues on the polypeptide backbone, further described in text [rendered using ChemSketch and Microsoft Power Point].

In MMP-2, TF 17-2 (Figure 3.7-C, arrow) appears to cover the entrance of S1'pocket with its butanyl group, a reversed pose to what was observed in MT1-MMP (Figure 3.7-A, arrow). TF 17-2 is co-ordinated with Zn(II) through atoms C_3=O_{13} (for atom numbering, see Figure 3.4). The monodentate Zn(II)-O_{13} coordination has a favourable distance of 2.56 Å (Figure 3.9-A). This orientation is strengthened by Zn(II)-NH_4 to achieve a distance of 3.06 Å. Such an association results in the tilting of the phenyl group towards the entrance of the S1' pocket and projection of the curved butanyl group into the S1' pocket, without entering the pocket (Figure 3.6-C). This butanyl group interacts with the carboxy backbone group of proline[221] (Figure 3.9-A). A secondary close proximity interaction is noted between the proline[221] and the inhibitor's sulfoxide group (Figure 3.9-A). This may contribute to repulsive forces and result in the observed inhibitor orientation (Figure 3.6-C). TF 22d does not share coordination similarities with TF 17-2 in its association with MMP-2. Instead, TF 22d forms a bidentate coordination complex (Figure 3.9-B) with Zn(II) through $C_{15}N_{16}$ and N_1 (for atom numbering, see Figure 3.4). The delta negative dipole of the carbon nitrile co-ordinates with Zn(II) with a favourable distance of 2.83 Å (Figure 3.9-B). This is further stabilized by a secondary, albeit weak, Zn(II)-N_1 coordination of 3.37 Å. The S1' pocket is completely occupied by the phenyl, sulfoxide and pyrrolidine groups of TF 22d. Figure 3.6-D.i, shows the inhibitor in the S1' pocket by removing isoleucine[222] and proline[221] from the surface view. The 6-azauracil head of TF 22d is further stabilised by the backbone of the hydrophobic amino acids alanine[165] and leucine[164]. C_5O_{14} forms a close interaction with the peptide bond between alanine[165] and leucine[164] with a distance of 3.02 Å, in the order of a hydrogen bond (Figure 3.9-B). In addition, a weak hydrophobic interaction between C_8 of the phenyl ring and leucine[165] with a distance of 4.55 Å is observed (Figure 3.9-B). Another, stronger interaction is observed between the backbone amide group of threonine[227] and

pyrrolidine with a distance of 2.7 Å (Figure 3.9-B). Overall, the inhibitors orientate themselves with their 6-azauracil heads facing into the S1'pocket in MT1-MMP, and in MMP-2 their R-groups block or access the S1' pocket (Figure 3.6-C.i & D.i).

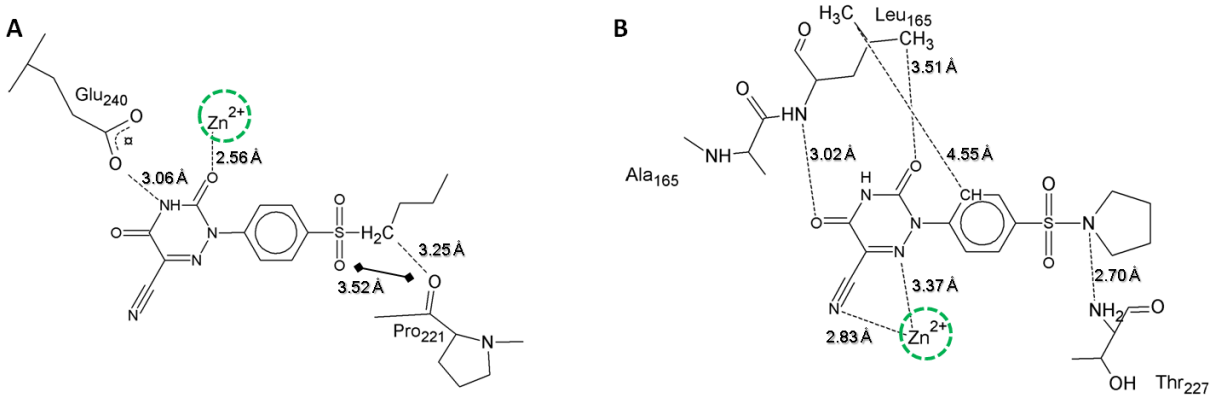

Figure 3.9. Schematic representation of inhibitor interactions with MMP-2 active site amino acids. (**A**) TF 17-2 forms a monodentate coordination complex with Zn(II), stabilised by glutamate[240] and proline[221]. (**B**) TF 22d forms a bidentate coordination complex with Zn(II), stabilised by hydrogen bonds to the backbone of alanine and leucine with further interaction between the pyrollidine ring and threonine[227]. Further described in text [rendered using ChemSketch and Microsoft Power Point].

3.7.3. *In silico* verses *in vitro* affinity values

The *in silico* ΔG values showed low free energy values indicating strong binding for both inhibitors (Table 3.3). These values were converted into K*i* values as previously described in Section 3.6.4. *In silico* free energies and inhibition constants generated are listed in Table 3.3 and were used to determine K*i* values in order to compare these with *in vitro* kinetic inhibition constants. In MT1-MMP, both inhibitors show similar *in vitro* catalytically determined K*i* values, and an *in silico* K*i* difference of 8.54 µM between inhibitors, suggesting similar molecular interactions which correlate well with the similar poses observed in Figure 3.6. The *in silico* K*i* values, however, do not correlate well with the *in vitro* results. In MMP-2, though, the *in vitro* and *in silico* K*i* values for TF 17-2 differ by 21.76 µM (4 times) suggesting a close correlation. In contrast, TF 22d in MMP-2 *in vitro* and *in silico* K*i* values differs by 245 times. The 0.06 µM affinity of TF 22d suggests an ideal inhibitor candidate for MMP-2. *In silico* results suggest TF 22d is 63 times more selective for MMP-2 than MT1-MMP, whereas the *in silico* results for TF 17-2 suggest a slightly lower potential (2 times) MMP-2 inhibition over MT1-MMP (Table 3.3). *In vitro* kinetic results, however, show that TF 17-2 and TF 22d are 127 and 74 times more selective for MT1-MMP over MMP-2, respectively. Since the *in silico* and *in vitro* results contradict one another, the credibility of K*i* values should be favoured by *in vitro* kinetic assays. Therefore, *in silico* docking to determine inhibition constants using AutoDock Vina do not

correlate with *in vitro* kinetic assays and therefore, cannot be used to reliably predict K*i* values for MMPs and their synthetic inhibitors.

Table 3.3. *In silico* free energy values and K*i* values compared to *in vitro* K*i* values. *In vitro* K*i* values were provided by Fischer (2004).

	Compound	*in silico* ΔG (kcal/mol)	*in silico* K*i* (μM)	*In vitro* K*i* (μM)
MT1-MMP	TF 17-2	-6.7	12.30	0.22
	TF 22d	-7.4	3.76	0.2
MMP-2	TF 17-2	-7.1	6.24	28.0
	TF 22d	-9.9	0.06	14.7

3.8. Discussion

A drug interacts with its receptors through bonding interactions such as hydrogen bonds, electrostatic attractions and hydrophobic (van der Waals) interactions. The most important factor for drug-receptor interaction is a snug fit. The greater the affinity of a drug for the binding site, the higher the drug's potential biological activity (Bruice, 2007). Computational docking was used to image structural information and co-ordinate interactions of inhibitors with the MMP catalytic zinc ion. In addition, computational docking elucidated the influence of substituted groups on binding affinity. Results for computational docking affinities, however, did not correlate with kinetically established K*i* values.

Since the synthesis of the MMPIs used in this study, in 2004, advances in MMPI design have moved towards gaining selectivity by targeting the S1'pocket of MMPs (Devel et al., 2010). Most of this work has been conducted on MMP-13 for the treatment of osteoarthritis (Blagg et al., 2005; Schnute et al., 2010). The structures of the MMPIs used in the current study were shown to possess hydrophobic substituents that could potentially interact with the hydrophobic S1'pocket.

In silico inhibitor docking studies using AutoDock Vina revealed conceptual differences in binding between MMPIs and MMPs tested. We have also shown that the flexible butanyl group of TF 17-2 could not enter the hydrophobic S1'-pocket and orientated the 6-azauracil head to cover the S1'-pocket in MT1-MMP rather than entering it. In MMP-2, however, predictive docking showed that the butanyl group of TF 17-2 sterically blocked access of substrates to the S1'-subsite. The pyrrolidine ring of TF 22d was predicted to fit into the S1'pocket of MMP-2 in a highly energy efficient pose (ΔG = -9.9 kcal/mol) revealing a high potency of inhibiton. In both

MT1-MMP and MMP-2, TF 17-2 was predicted to bind zinc through monodendate co-ordination. TF 17-2 exhibited, therefore, a consistent pattern of binding in both MMPs with monodentate coordination of zinc with bond lengths of about 2.5 Å, in the order of a hydrogen bond, and sterically restricted access of substrates to the S1'-pocket. These similarities in binding are consistent with the small difference in free energy of binding exhibited by TF 17-2 between MT1-MMP (ΔG = -6.7 kcal/mol) and MMP-2 (ΔG = -7.1 kcal/mol). In light of AutoDock's accuracy of free energy prediction of about 2-3 kcal/mol standard deviation (Huey et al., 2007), such free energy differences between these MMPs (-0.4 kcal/mol) appear negligible.

TF 22d did not show such consistencies, but rather exhibited different binding patterns reflected by greater differences in free energy of binding (-2.5 kcal/mol) between MMPs. The inflexible pyrrolidin group of TF 22d entered the hydrophobic S1'-pocket of MMP-2 suggesting that inflexible hydrophobic groups may better suite drug targets of MMP-2. Bidentate co-ordination with the zinc ion of MMP-2 was predicted indicating a strong affinity. Such co-ordination was not predicted for MT1-MMP by TF 22d, but rather formed monodentate co-ordiantion with zinc and sterically blocked the S1'-pockets with its 6-azauaracil head, much like TF 17-2. TF 22d, therefore, was predicted to possess selectivity for MMP-2, however, the difference in free energy of binding between the two MMPs tested did not exceed the standard deviation of AutoDock Vina's accuracy for free energy predictions.

Predicted conformations show that the butanyl (TF 17-2) and pyrrolidin (TF 22d) substituted groups assume similar orientations in targeting MT1-MMP but vary in MMP-2. As mentioned in Section 3.4.2 the anticipated pose for both inhibitors was that the R-group substituent would occupying the S1' pocket while the azauracil head would co-ordinate with Zn(II) through one of the three previously published methods of coordination listed in Figure 3.3, f-h. Only monodentate co-ordination was predicted with the exception of TF 22d in MMP-2 where bidentate coordination with Zn(II) was predicted. To our knowledge, such co-ordinations have not as yet been reported. These inconsistent Zn(II) co-ordination states may be indicative of a shortage of parameters relating to the zinc ion when using empirical force fields (Tuccinardi et al., 2006). Although, the zinc ion charge can be assigned in AutoDock Vina, the latest version (used in this study) did not include zinc parameters, such as bond-stretching and angle-bending, which have only recently been derived by Lin and Wang (2010) and further developed by Peters et al. (2010). Unfortunately the predicted *in silico* K*i* values did not correlate with the observed *in vitro* K*i* values, either. Thus, we are unable to confidently report the molecular interactions of

TF 17-2 and TF 22d with MT1-MMP and MMP-2, and the influences that the R-groups may have had on MMP affinity. Hence, using AutoDock Vina, we were unable to model these inhibitors into the active site of other MMPs with unknown kinetic K*i*'s, for example, other MT1-MMPs, soluble MMPs or ADAMs, to predict the efficacy of the test inhibitors on such targets.

The *in vitro* kinetic results, however, were shown to exhibit a favorable 100-fold increase in selectivity towards MT1-MMP over MMP-2 in the case of both inhibitors. The MMPIs used in this study have been shown to target anti-tumour MMPs such as MMP-8 and MMP-9 (Table 3.1), with K*i* values in the micro molar range (Table 3.2). The targeting of MMP-9 is, however, untested , but it is known that MMP-9 is not expressed in any significant quantity by the test cell lines (van Rooyen, 2009).

TF 17-2 has been shown to attenuate the growth of pancreatic tumours without affecting tumour eradication (Kapischke et al., 2008). This suggests that inhibitor testing is better performed in whole animal studies rather than *in vitro* and *in silico* simulations, a disappointing result. It remains important that the analogue of TF 17-2, TF 22d, is employed in *in vitro* or *in vivo* assays, similar to those previously performed by Kapischke et al. (2008) to elucidate their effects in breast cancer.

A simpler and cheaper system for measuring the effects of MT1-MMP inhibition than using animal models involves the use of cell migration assays in 2D. These studies more directly measure the effects of inhibiting MT1-MMP-mediated migration as MT1-MMP is intimately associated with migration, (Gilles et al., 2001) as already indicated. In the chapters to follow, we will first assess the toxicity of the inhibitors on epithelial cell lines before measuring their influence on cell migration.

CHAPTER 4.

Effects on metabolic activity and cellular toxicity by MMP inhibitors, TF 22d and TF 17-2 in MCF-10A and MCF-10AneoT cells

4.1. Introduction: cell death

MT1-MMP is a protease that is considered to play a primary role in invasion and the ability of cancer cells to disseminate from the primary tumour (Moss et al., 2009a; Szabova et al., 2007; Yoshikawa et al., 2006). Protease inhibitors designed for therapeutic applications should preferably affect the behaviour or metabolism of tumour cells selectively, while leaving normal surrounding cells and tissues relatively unaffected i.e. inhibitors should show selective toxicity (Choi et al., 2012). "Toxicity" in this context may be defined as the adverse effect on cellular functions and normal biological activity, induced by the exposure to a chemical inhibitor. In extreme cases such a toxic compound may induce cell death. Drug toxicity is, therefore, usually judged initially using a viability screening test, such as the 3-(4,5-dimethylthiazol-2-yl)-5-(3-carboxymethoxyphenyl)-2-(4-sulfophenyl)-2H-tetrazolium (MTS) assay, which gives indirect evidence of metabolic, pro-proliferative or anti-proliferative effects (Riss and Moravec, 1992). Of equal importance, is whether subsequent cell death is induced and whether this is via programmed cell death (apoptosis) or necrosis (Elmore, 2007). Necrosis has a pro-inflammatory effect and is therefore, undesirable. An ideal anti-cancer drug should induce apoptosis in cancer cells without affecting normal cells and their normal biological activity (Hsu et al., 2003).

Cell death may be assessed on induction of morphological changes as well by monitoring the up-regulation of cell-death associated markers [reviewed by Fulda and Debatin (2006) and Galluzzi et al.(2007)]. As the assessment method depends on the mechanisms by which cell death may occur, the catagories need to be defined. These are defined as, apoptosis (programmed cell death), necrosis (oncosis), autophagy and mitotic catastrophe. Autophagy and mitotic catastrophe will not be discussed further, as these modes of cell death are related to starvation (Hardie, 2011) and inability to undergo mitosis (Vitale et al., 2011), respectively, and thus fall outside the scope of this study. Induction of cell death via apoptotic pathways may trigger the removal of cellular debris such as cleaved DNA packaged into membrane-bound cell fragments. Membrane-bound particles for uptake are "labelled" with phosphatidyl serine (PS) present on the inner membrane that "flips" to the outer membrane allowing binding and phagocytosis by macrophages and parenchymal cells facilitating subsequent safely contained degradation within phagolysosomes

(Elmore, 2007). Phagolysosome destruction via apoptosis is the safer mode of inducing cell death as spillage of DNA, a process that is unfavourable, is avoided. In necrosis, the rupture and spillage of cellular constituents including DNA into the surrounding interstitial tissue can cause secondary necrosis of surrounding tissues and inflammation (Elmore, 2007).

Generally drugs have a level at which they are seen to be effective and a level at which they are toxic. When a drug is administered, during oral or subcutaneous administration, sites of administration may be exposed to non-physiological concentrations of compound, possibly exceeding tolerance levels leading to toxicity. All drugs must, therefore, be assessed to establish the highest concentration tolerated, and to ensure that this is not exceeded at any site of administration where drug concentration is initially high (Collins, 1984). Cell culture in monolayers affords a unique opportunity to establish ranges of toxicity. For the purpose of this study only apoptosis and necrosis need to be considered and distinguished, as explained above.

4.1.1. Necrosis

In necrosis, cell death results after destruction of the plasma membrane through external injuries such as frostbite or freezing, trauma or infections (Darzynkiewicz et al., 1997). Membrane lysis releases cytoplasmic components into the surrounding cellular spaces, causing an inflammatory response and subsequent tissue destruction or altered tissue structure (i.e. scarring) (Willingham, 1999). Apoptosis and necrosis are two processes that occur independently, sequentially, as well as simultaneously, which sometimes makes apoptosis indistinguishable from necrosis (Elmore, 2007). Necrosis is usually mediated by two mechanisms, energy supply and direct damage to cell membranes. Loss of energy will convert an ongoing apoptotic process into a necrotic process with a simultaneous decrease in caspases and ATP (Elmore, 2007). Morphological features that distinguish necrosis from apoptosis are summarised in Table 3.1, and relates mainly to the containment of cell debris within a membrane. Ultrastructural characteristics of necrosis include membrane swelling and lysis, swelling of organelles (i.e. mitochondria) and some condensation of nuclear chromatin (Table 4.1), all late indicators of cell death (Galluzzi et al., 2007).

Table 4.1. Distinguishing morphological features of apoptosis and necrosis.

Reproduced from Elmore (2007).

Apoptosis	Necrosis
Single cells or small clustering of cells.	Often contiguous cells
Cell shrinkage and convolution	Cell swelling
Pyknosis and karyorrhexis	Karyolysis, pyknosis, and karyorrhexis
Partially intact cell membrane	Disrupted cell membrane
Cytoplasm retained in apoptotic bodies	Cytoplasm released
No inflammation	Inflammation usually present

Due to the severe immune response induced by necrosis, apoptotic induced cell death is favoured over necrotic cell death, for any drug destined for human use (Elmore, 2007; Willingham, 1999).

4.1.2. Programmed cell death

In apoptosis or programmed cell death, while the plasma membrane remains intact and cytoplasmic organelles appear to have a normal morphology, other characteristic ultrastructural features of late apoptosis may include cytoplasmic and nuclear condensation (pyknosis), and nuclear fragmentation (karyorrhexis) which occurs in a final common execution pathway (Figure 4.1). After induction of apoptosis via one of the three pathways, the extrinsic, intrinsic or perforin/granzyme pathway, biochemical indicators of apoptosis include DNA breakdown, protein cleavage, protein cross-linking and phagocyte recognition (Elmore, 2007; Galluzzi et al., 2007; Kerr et al., 1972; Wyllie et al., 1980). Late indicators or tests for apoptosis include DNA laddering, for example, as opposed to DNA smearing seen in necrosis.

Besides the performin/granzyme pathway, two primary apoptotic pathways have been described. These are the extrinsic (receptor related) pathway (not related to drug trials), and the intrinsic (mitochondrial) pathway. Both pathways converge onto a caspase-dependent pathway of executioner cysteine proteases (Figure 4.1). The cysteine proteases cleave aspartic acid residues, and are divided into two groups, initiators and effectors. Initiator caspases are activated upon binding to adaptator molecules such as TNF and TRAIL, which activate effector caspases (Pommier et al., 2004). Initiator caspases include caspase-2, -8, -9, and -10. Effector caspases include caspase-3, -6, and -7 (Elmore, 2007). Once caspases are activated, their commitment towards cell death appears to be irreversible. Caspase aggregation and subsequent auto-activation, initiates a proteolytic cascade which results in the introduction of the final executioner

pathway of apoptosis (Elmore, 2007). Caspases also feed into the intrinsic, mitochondrial death pathway, which causes the release of cytochrome c from the mitochondria into the cytoplasm. Both pathways finally give rise to the morphological features of apoptotic cell death i.e. cellular blebbing, pyknosis, and karyorrhexis (Elmore, 2007; Fulda and Debatin, 2006; Taatjes et al., 2008). Cellular blebs or apoptotic bodies expose cell surface molecules that result in early phagocyte recognition and subsequent phagocytosis. An early event in apoptosis is the presentation of phosphatidylserine (PS) from the inner leaflet to the outer membrane, which act as ligands for phagocytes (Elmore, 2007; Vance, 2008). The flipping and increased level of PS to the outer membrane was used in this study as an early indicator of apoptosis. PS exposure and subsequent detection using annexin-V was a method of choice in this study as it constitutes an earlier indicator of apoptosis than DNA laddering or late morphological events. This method of detection is easier to perform than caspase enzyme assays or caspase probing which do have an advantage of distinguishing between intrinsic and extrinsic apoptotic pathways.

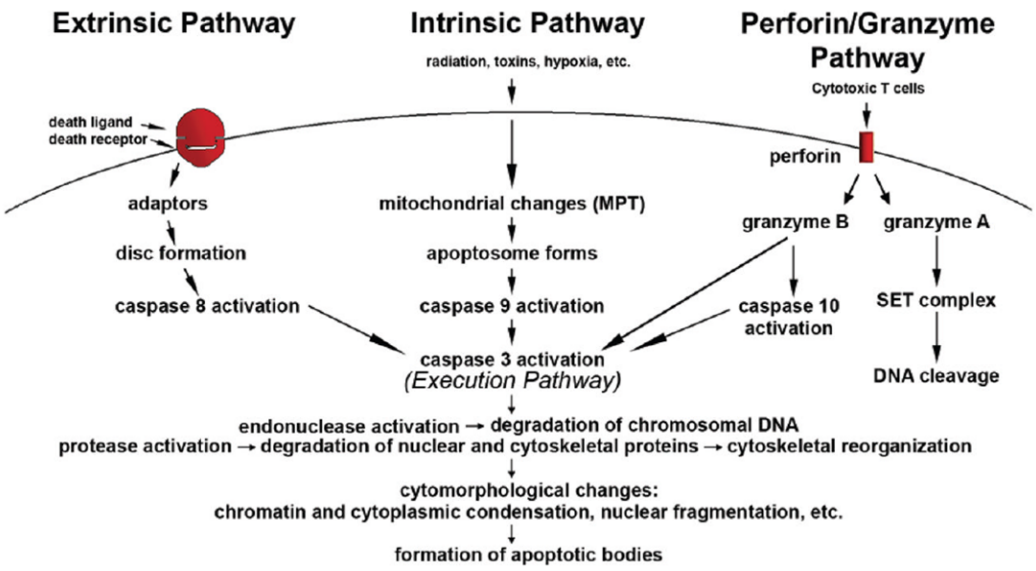

Figure 4.1. The three pathways of programmed cell death.
The extrinsic, intrinsic and the perforin pathways each require specific triggering events to activate their own initiator caspase. All pathways converge on caspase-3 which signifies the activation of the execution pathway. The execution pathway elicits the characteristic cytomorphological features including, cell shrinkage, chromatin condensation and blebbing [reproduced from Elmore, (2007)]

4.1.3. Extrinsic pathway

The extrinsic pathway is not usually related to drug testing as it involves death receptors of the tumour necrosis factor (TNF) receptor superfamily or the TNF-related apoptosis-inducing ligand (TRAIL) receptors. It is covered here as it activates different target caspases which can be

assessed to distinguish apoptosis induced via the intrinsic pathway. The extrinsic pathway is triggered at the plasma membrane, where TNF receptors such as CD95 (APO-1/Fas) or TRAIL receptors bind to their respective ligands. Binding results in receptor trimerization and death domain clustering (Fulda and Debatin, 2006). This death domain clustering recruits Fas-associated death domain (FADD, also known as MORT1) through homophilic interactions, which in turn recruits procaspase-8 to the CD95-trimer/FADD complex, forming the death-inducing signalling complex (DISC) (Figure 4.2-A) (Fulda and Debatin, 2006; Pommier et al., 2004; Youle and Strasser, 2008). Procaspase-8, involved only in the extrinsic pathway, subsequently auto-activates, releasing activated caspase-8. Caspase-8 propagates the apoptosis signal via two different signalling pathways, resulting in what has been classified as type I or type II cell death (Elmore, 2007). In type I cell death, large amounts of caspase-8 are formed at the DISC and induce direct cleavage of the downstream effecter, procaspase-3 (Elmore, 2007; Fulda and Debatin, 2006). In type II cells, little DISC formation and subsequent reduced procaspase-8 activation is insufficient to activate procaspase-3 directly. Instead, caspase-8 cleaves the 'BH3-only protein', Bid, generating an active fragment (tBid) that activates the intrinsic death pathway (Figure 4.2-B) (Elmore, 2007). In addition, caspases cleave a number of cytoplasmic substrates resulting in cascades giving rise to the activation of the common executioner pathway and the morphologic features associated with cell death such as DNA fragmentation (Elmore, 2007; Fulda and Debatin, 2006). Cleavage of an inhibitor of caspase-activated DNase (ICAD) and/or the inhibitor of the endonuclease CAD, produce characteristic oligomeric DNA fragments. Nuclear shrinkage occurs as a result of caspase-mediated proteolytic degradation of lamin, the major structural protein of the nuclear envelope (Cohen, 1997). Likewise, the loss of cell shape occurs due to actin or fodrin degradation (Fulda and Debatin, 2006). Fodrin is an abundant membrane-associated cytoskeletal protein (Cohen, 1997). Most drugs, however, activate the intrinsic pathway of apoptosis.

4.1.4. Intrinsic pathway

Under biologically stressful conditions, destabilization of the mitochondrion or the permeabilization of its membrane induces apoptosis (Figure 4.1-B). The mitochondrion is a cellular organelle responsible for chemical energy generation, in the form of ATP (Saelens et al., 2004). It is also the site of oxidative phosphorylation, the terminal reaction of respiration. Permeabilisation of the mitochondrion is regulated by proteins of the B-cell Lymphoma-2 (Bcl-2) family, which have either pro-survival or pro-apoptotic subfamilies (Youle and Strasser, 2008). In healthy cells pro-apoptotic proteins, BAD, BID, BIM and BMF, are localised at extra-

mitochondrial sites. Upon cellular damage, these proteins are post-translationally modified and relocate to the mitochondria where they induce mitochondrial destabilisation and inhibit Bcl-2 related anti-apoptotic proteins (Pommier et al., 2004; Yang et al., 1995). Disruption of the outer mitochondrial membrane releases apoptogenic factors usually found in the space between the inner and outer mitochondrial membranes. These factors include cytochrome-c (Cytc) (Liu et al., 1996), second mitochondria-derived activator of caspase (Smac), the serine protease Omi/HtrA2, apoptosis inducing factor (AIF) and endonuclease G (endo G) (Figure 4.2-B) (Saelens et al., 2004). Release of endonuclease G and AIF trigger cell death and contribute to nuclear DNA damage and caspase-independent paths (Fulda and Debatin, 2006; Saelens et al., 2004). The release of cytochrome-c causes the formation of the cytochrome-c/Apaf-1/caspase-9 apoptosome complex, which activates caspase-3 (Cain et al., 2000). Proteolytic release of caspase-activated DNase (CAD) from the inhibitor of CAD (ICAD), by caspase-3, is associated with other factors, such as AIF (caspase independent activation), which initiate high molecular weight (HMW) DNA fragmentation (1 Mb to 50 Kb) (Lecoeur, 2002). This forms one of the events induced in the common executioner pathway.

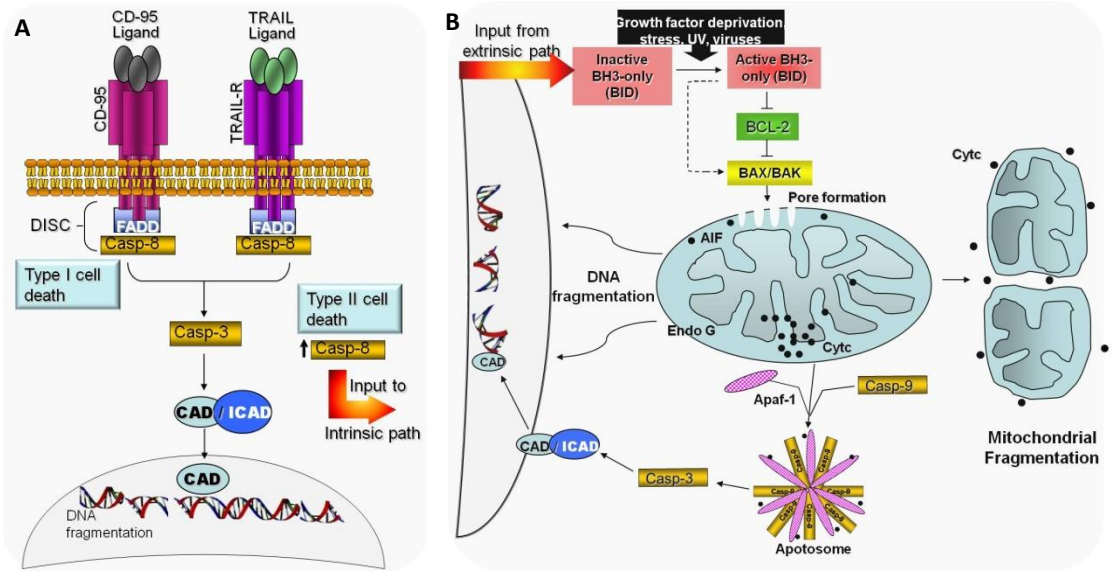

Figure 4.2. Pathways of Apoptosis
(A) Extrinsic pathway of apoptosis. Upon ligand binding to CD-95 or TRAIL-R receptors, subsequent trimerisation recruits FADD and procaspase-8 which oligomerise to form DISC. Subsequent auto-activation of procaspase-8 further activates procaspase-3 which cleaves ICAD releasing the endonuclease CAD, as described in text. Reconstructed from Fulda and Debatin (2006). **(B)** Intrinsic pathway. Described in Section 4.1.4. Redrawn from Fulda and Debatin (2006) and Saelens et al. (2004).

4.1.5. Execution pathway: Convergence of the extrinsic and intrinsic pathways

The executioner pathway is common to all apoptotic pathways (Figure 4.1). The pro-apoptotic BH3-only protein, BID, facilitates crosstalking between the intrinsic and extrinsic pathways

(Fulda and Debatin, 2006; Youle and Strasser, 2008). The BH3 domain binds and inhibits the anti-apoptotic Bcl-2 proteins to promote apoptosis (Youle and Strasser, 2008). Caspase-8 activation can cleave BID initiating BAX and BAK of the intrinsic pathway resulting in mitochondrial destabilisation (Youle and Strasser, 2008).

An important fact to consider is that the extent or type of DNA damage is dependent on the stimulus, the duration of the stimulus, cation dependence and local pH conditions. For example, CAD requires Mg^{2+} ions, DNase I and DNase γ require both Mg^{2+} and Ca^{2+} ions, DNase I and CAD have neutral pH optima, while DNase II and L-DNase II cleave DNA under acidic conditions. These factors will elicit different DNA cleavage products, either 3'OH/5'P or 3'P/5'OH termini (Lecoeur, 2002) products that may be detected using the terminal deoxyribonucleotidyl transferase mediated deoxyuridine triphosphate nick end labeling (TUNEL) assay (Kumari et al., 2008).

Drug concentration screening programs usually are conducted using nano- to milli-molar drug concentration ranges. However, since TF 17-2 has previously been described (Kapischke et al., 2008) and tested at a concentration range of 30 µM – 3 mM. Both TF 17-2 and TF 22d, a similarly structured novel counterpart, were tested at similar concentrations in the current study for comparative purposes.

4.2. Toxicity assays

In order to consider TF 22d and TF 17-2 as potential therapeutic agents, validation through toxicity assays is required. A number of toxicity assays exist for determining cellular viability or apoptosis (Fulda and Debatin, 2006; Galluzzi et al., 2007). These assays are based on the detection of the following aspects of apoptosis: cytomorphological alterations, DNA fragmentation, detection of caspases or caspase affected factors, membrane alterations, and mitochondrial alterations. However, apoptotic assays can detect either early or late stage events in apoptosis (Elmore, 2007). For this study chosen assays include those that reflect mitochondrial activity (MTS assay), and early changes in the plasma membrane (Annexin V-FITC binding &PI permeability assay). The reason for the choice of these methods follows (Section 4.3-4.4)

4.3. MTS assay

Mitochondrial activity assays are dependent on the presence or localisation of mitochondrial related factors and proteins. For example, mitochondrial integrity can be distinguished by

antibodies which target cytochrome-c. Cytoplasmic cytochrome-c localised to the mitochondria represents an intact mitochondria while cytosolic cytochrome-c represents a destabilised mitochondria (Elmore, 2007). However, antibody detection of cytochrome-c is not suitable for high through-put screening. Alternative assays that indicate the integrity of mitochondria are based on the metabolic conversion of a tetrazolium salt to a brightly coloured formazan product. These include 2,3-bis(2-methoxy-4-nitro-5-sulphophenyl)-2H-tetrazolium-5-carboxanilide (XTT), 3-(4,5-dimethylthiazol-2-yl)-5-(3-carboxymethoxyphenyl)-2-(4-sulfophenyl)-2H-tetrazolium (MTS) and the 3-(4,5-dimethylthiazol-2-yl)-2,5-diphenyltetrazolium bromide (MTT) assays (Goodwin et al., 1995). The MTS and XTT assays form soluble formazan products whereas MTT requires an extra solubilisation step. However, XTT, when combined with the required electron acceptor, phenazine methosulfate (PMS), becomes unstable causing assay data shifts (Goodwin et al., 1995). Therefore, the MTS assay was chosen for its general indications of mitochondrial function, its sensitivity and lack of requirement for a solubilisation step (Debnam and Shearer, 1997).

The CellTiter 96® AQueous Non-Radioactive Cell Proliferation Assay is one of the many commercially available kits that apply the colorimetric method for determining the number of viable cells in proliferation or chemo-sensitivity assays, e.g. MTT or XTT (Promega, 1996). The tetrazolium inner salt, MTS, reacts with the coupling reagent PMS, to form a soluble formazan product, with a measurable absorbance at 490 nm. PMS serves to shuttle electrons from reduced nicotinamide adenine dinucleotide (NADH), to MTS. Activity of cytosolic and mitochondrial dehydrogenase's that use NAD^+/NADH as a co-factor are exploited in this assay (Barltrop et al., 1991; Debnam and Shearer, 1997; Promega, 1996).

The MTS assay has been used in drug toxicity range-find experiments to determine IC_{50} (50% inhibitory concentration) and LD_{50} (50% lethal dose concentration) values (Hayes and Markovic, 2002; Lestari et al., 2005; Malich et al., 1997). Due to the spontaneous conversion of MTS over time, or reactions with culture media (Promega, 1996), the background absorbance of samples containing media only are subtracted from test samples (Lestari et al., 2005; Malich et al., 1997). Increases or decreases in metabolism due to cell stress also cannot be distinguished from an increase in cell number due to hyper-proliferation or cell death, respectively. Thus, the MTS proliferation assay should be performed in conjunction with a technique for assessing cell numbers i.e. cell counts or the crystal violet adherence assays in which dye uptake is directly proportional to cell number (Strongin, 2010).

The sensitivity of the MTS assay should also not be under-estimated and meticulous care should be taken during handling and incubation periods. Thermal gradients within 96-well plates may influence enzyme activity and, therefore, MTS conversion. In addition, small variations in the numbers of seeded cells may also skew absorbance readings. To compensate for these variations, which are a product of experimental technique, the experiment is performed several times. Experiments are ideally performed in triplicate, in 4 separate batches (n=4), to produce statistically acceptable results.

The level of absorbance measured at 490 nm is influenced not only by the incubation time but also the cell type, the cell number and the ratio of MTS detection reagents to culture media. Influence of incubation times on absorbance has been reported previously (Berg et al., 1994; Buttke et al., 1993; Cory et al., 1991). A linear relationship between incubation time and absorbance due to the conversion of MTS needs to be established for short incubation times, up to 5 hours in order to relate the absorbance levels of product with metabolic activity for a specific cell line and number. (Berg et al., 1994; Cory et al., 1991; Promega, 1996; Riss and Moravec, 1992). Cell numbers generating a linear graph for absorbance and cell number were selected for MTS assays.

4.3.1. Reagents

Dulbecco's phosphate buffered saline (DPBS) [0.2 g KCl, 8.0 g NaCl, 0.2 g KH_2PO_4, 1.15 g Na_2HPO_4, 100 mg $MgCl_2.6H_2O$, 133 mg $CaCl_2.2H_2O$].

Deionised water was added to KCl, NaCl, KH_2PO_4, and Na_2HPO_4 to a final volume of 900 ml. The pH was adjusted to 7.35 using 1 M HCl. The $MgCl_2.6H_2O$ and $CaCl_2.2H_2O$ was added and the volume made up to 1 L with deionised water.

3-(4,5-dimethylthiazol-2-yl)-5-(3-carboxymethoxyphenyl)-2-(4-sulfophenyl)-2H-tetrazolium (MTS) [2 mg/ml].

MTS (42 mg) was dissolved in 21 ml of DPBS, sterile filtered through a 2 µm pore size filter and decanted into an amber bottle, stored at -20°C.

Phenazine methosulfate (PMS) [0.92 mg/ml].

PMS (0.92 mg) was dissolved in 1 ml of DPBS, sterile filtered through a 0.2 µm pore size filter, and stored at -20°C

DMSO.

Stored in 50 µl aliquots at -20°C, keeping freeze thaw cycles to a maximum of 3 as a precaution.

Inhibitors.

Preparation described in Section 2.8.

4.3.2. Procedure

Cells were cultured as described in Section 2.2 and trypsinised into a cell suspension. For cell number optimisation, 96-well plates were pre-treated with medium for one hour before seeding. Approximately 500 to 7000 cells were seeded in triplicate, into a 96-well plate made up to a final volume of 100-200 µl with complete medium. After 24 hours the media was aspirated off, and cells were washed with HBSS to remove dead cells. The media was replaced with fresh media to a final volume of 100 µl per well and incubated for a further 24 hours (37°C, 5% CO_2, 95% humidity). Each experiment was performed in four separate batches in triplicate.

Inhibitors to be tested needed to be dissolved in a suitable vehicle solvent. Elimination of solvent-induced-effects required the optimisation of solvent levels. Plates (96-well) were pre-treated and each well seeded with 4500 cells/well as described above. After the 24 hour incubation, media was replaced with fresh media containing DMSO (0.0001 to 5% (v/v)) to a final volume of 100 µl per well and incubated for a further 24 hours (37°C, 5% CO_2, 95% humidity). Each experiment was performed in five separate batches (n=5) in triplicate.

For drug evaluations a 5 mM **working solution** of TF 22d or TF 17-2 was made up in complete medium from a **stock solution** of compound dissolved in 100% DMSO. Final concentrations of 50, 100, 150, 300 µM TF 22d or TF 17-2, topped up with the required volume of DMSO that yielded a background of 0.05% (v/v) (Table 2.2), were made up to a total volume of 100 µl with complete medium and were added to triplicate wells performed in five separate batches. Plates were incubated for 24 hours (37°C, 5% CO_2, 95% humidity).

To reduce thermal gradient effects in all 96-well plates, the spaces between wells were filled with sterile water before incubation. Plates were also rested upon an ELISA plate to eliminate direct contact with the stainless steel shelving of the incubator. Sterile filtered MTS and PMS dissolved in DPBS (2 mg/ml and 0.92 mg/ml in DPBS, respectively, stored at -20ºC in the dark before use) was prepared by adding MTS to PMS in the ratios of 2:1 and added to each well of cultured cells

in the ratio 1:5 (i.e. MTS/PMS working reagent : cell culture volume, 5 µl to cells in 100 µl final volume). After mixing and incubating (3 h, 37°C, 5% CO_2, 95% humidity), the plates were wiped clean prior to reading absorbance at 490 nm in a Versamax plate reader (BioRad), using the control that contained no cells as the blank. Results were subsequently expressed as the percentage of DMSO control or percentage untreated control for the DMSO concentration range.

Statistical analysis was performed using analysis of variance (ANOVA) from a split plot design where significance was $p < 0.05$. Posthoc comparison of the least significant difference (LSD) against the difference of means between controls and treatments was carried out. ANOVA assumes a normalised data distribution (Dukes and Sullivan, 2008), which was satisfied and confirmed with residuals plotted onto a histogram where results formed a bell shaped curve. In addition, a normal-plot was constructed of residuals plotted against the expected normal quantiles, which showed a linear distribution (data not shown). All concentrations of MMPIs were expressed as a percentage of the DMSO control.

4.3.3. Results

The calibration of MCF-10A and MCF-10AneoT for the MTS assay is shown in Figure 4.3, A and B, respectively. Cell numbers refer to the numbers seeded, and do not reflect the absolute number of cells before treatment or the subsequent 24 hour incubation. A linear range was observed between 1000 and 7000 cells/well for MCF-10A (Figure 4.3-A) and 1000 to 6000 cells/well for the MCF-10AneoT cells (Figure 4.3-B). The number of cells chosen for seeding assay dishes for both cell lines was 4500 cells (Figure 4.3-A & B).

The effect induced by various levels of DMSO solvent (0.0001% to 5% (v/v)) is shown in Figure 4.3, C. A significant difference in absorbance was observed for 5% (v/v) DMSO when compared against the untreated control, indicating cellular toxicity (Figure 4.3-C). Therefore, 0.05% (v/v) DMSO was chosen as an acceptable background vehicle solvent concentration which would not interfere with cytotoxic studies of TF 17-2 and TF 22d, as this concentration of DMSO fell well within non-toxic levels (Figure 4.3-C).

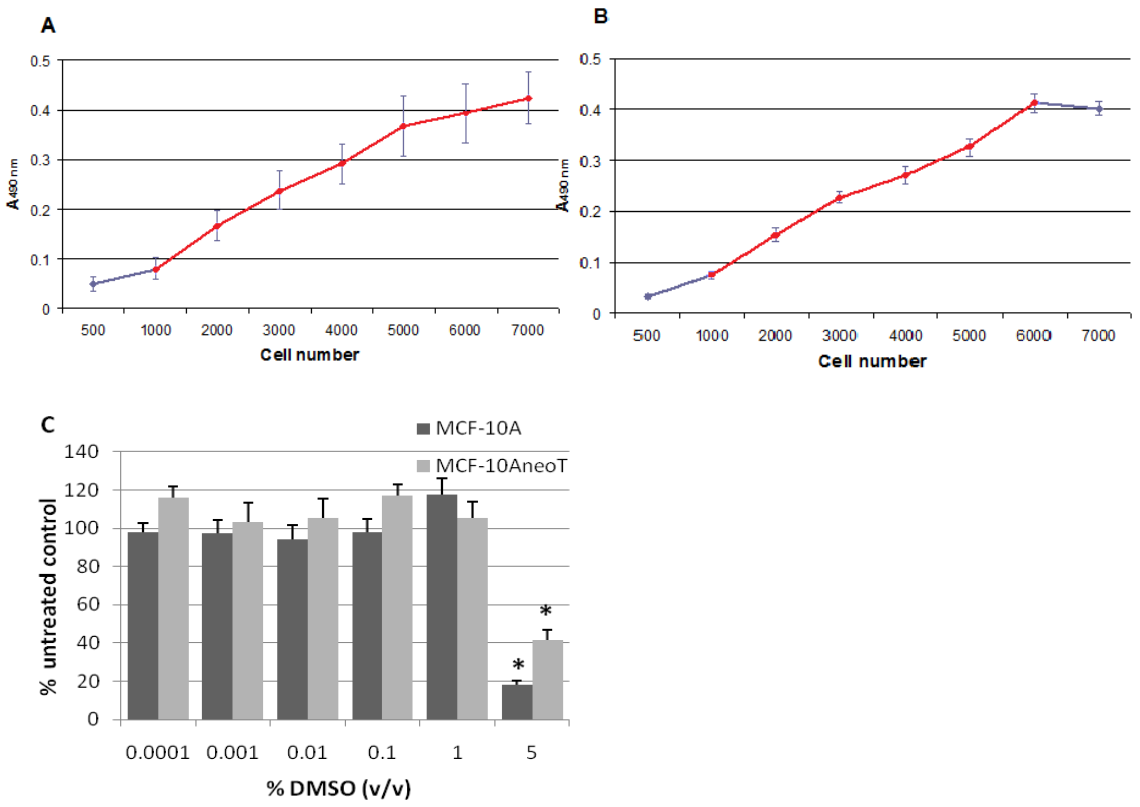

Figure 4.3. Optimisation of the MTS assay for the MCF-10A and MCF-10AneoT cell lines.
An increasing number of cells were seeded to determine the linear range of MTS conversion. **(A)** The MCF-10A showed a linear MTS conversion between 1000 and 7000 cells/well (red line). **(B)** The MCF-10AneoT showed a linear MTS conversion between 1000 and 6000 cells/well (red line). Cells were seeded into a 96-well plate in triplicate at the cell numbers indicated, and allowed to adhere (24 h). Medium was changed and the cells were incubated for a further 24 hours to mimic experimental treatment times. Error bars represent SEM with n=4. (**C**) Percentage DMSO toxicity of both cell lines measured against an untreated control. Cells were seeded (4500 cells/well) into a 96-well plate and allowed to adhere (24 h). Medium was changed with medium containing DMSO at the indicated concentrations and incubated further (24 h). The MTS assay was carried out as per manufacturer's instructions (Promega). Bars represent mean absorbance values, error bars represent the SEM of triplicate samples performed in quintuplicate (n=5), and 100% represents the untreated control value. *Significance vs. untreated control ($p < 0.05$).

A significant effect was observed at a concentration of 300 µM TF 17-2 in MCF-10A but not in the MCF-10AneoT cell line (Figure 4.4-A). The MTS assay shows no significant effect over the concentration range tested for TF 22d in both cell lines (Figure 4.4-B).

Upon visual inspection, MCF-10A cells treated with 300 µM TF 17-2 appeared as confluent as control MCF-10A cells; whereas, MCF-10AneoT cells treated with 300 µM TF 17-2 appeared less confluent than control MCF-10AneoT cells. Thus, cell counts of the 300 µM TF 17-2-treated cells were performed to distinguish between metabolic stress and hypo-proliferation or suppression of metabolism and proliferation (Figure 4.4-C). Cell counts showed that TF 17-2-treated MCF-10AneoT cell numbers decreased by 53% from the result given by the untreated control group, while MCF-10A cell numbers remained constant (Figure 4.4-C). This seemed to

contradict MTS results (Figure 4.4-A). These results may, however, indicate an anti-proliferative effect of TF 17-2 at a 300 µM level (Figures 4.4-C vs. 4.4-A) in the MCF-10AneoT cells and slight metabolic suppression of metabolic activity in MCF-10A cells. This seems to support findings of Kapischke et al. (2008) on pancreatic tumours where tumour sizes were decreased but no adverse effects were seen on normal cells.

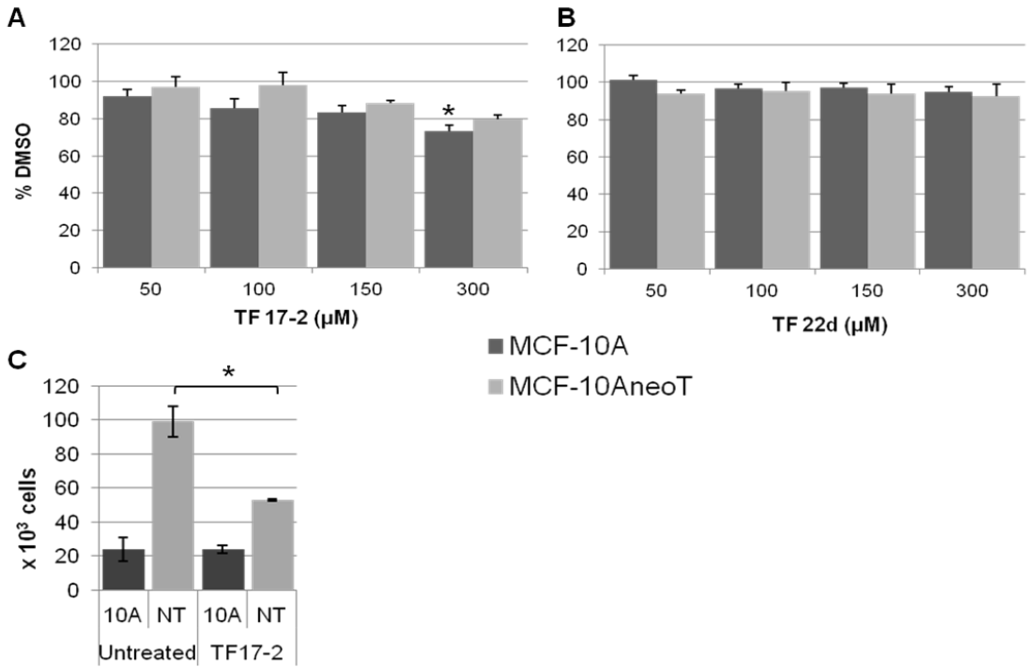

Figure 4.4. Percentage TF 17-2 and 22d toxicity measured against DMSO control in MCF-10A and MCF-10AneoT.
(**A**) TF 17-2 treated and (**B**) TF 22d treated cells were seeded (4500 cells/well) into a 96-well plate and allowed to adhere for 24 hours. The MTS assay was carried out as per manufacturer's instructions. Bars represent mean absorbance values, while error bars represent the SEM of triplicate samples performed in quintuplicate (n=5), 100% represents the DMSO control value and tests are expressed as a percentage of the DMSO control. *ANOVA tested significance at $p < 0.05$, DMSO control vs. treatment. (**C**) In order to investigate the influence of TF 17-2 on the proliferation of MCF-10AneoT cells, counts were performed to eliminate cell stress as a contributing factor to suppressed metabolic effects. Equal numbers of cells were seeded into 25 cm^3 tissue culture flasks. Cells were allowed to adhere (24 h) before treatment with TF 17-2 (300 µM). Cells were counted 24 hours after treatment. Bars represent mean cell counts. Error bars represent SEM of duplicate samples performed twice (n=2) with $p < 0.05$ using a paired Student's t-test.

This result shows the importance of performing cell counts in conjunction with the MTS assay. Interpretation of MTS assay results alone may have led to a false conclusion that TF 17-2 had no effect on metabolism or proliferation in the MCF-10AneoT cell line, whereas a significant reduction in metabolism was observed in the MCF-10A cell line. This effect, however, seems to be a suppression of metabolism of the MCF-10A cells confirmed by cell counts. The MTS assay did not reveal any metabolic effect induced by the TF 22d inhibitor in either cell line, and visual

inspection showed no differences between control and test samples, and hence cell counts were not performed. In retrospect cell counts should have been performed to unequivocally rule out an increase in metabolism accompanied by compensatory reduction in cell numbers. Cell counts are not usually performed in association with MTS assays, but from the evidence in Figure 4.4, C, relative to Figure 4.4, A, this is an unwise practice.

4.4. Annexin V/PI viability assay

To assess whether the decrease in metabolic activity observed in the MCF-10AneoT cells was due to apoptosis or anti-proliferative effects, a common assay for detecting cell membrane alterations that employs fluorescein isothiocyanate (FITC) conjugated annexin-V as the detection ligand for PS exposure, was used as an early detection event for apoptosis (Willingham, 1999). The advantage of this assay is its sensitivity. A single apoptotic cell in which caspases have been activated, may be detected (Elmore, 2007). The disadvantage, however, is that late stage apoptotic and necrotic cells are also labelled. This is overcome with the use of the membrane impermeable DNA binding dye, propidium iodide (PI) which only labels cell nuclear contents when the cell membrane is damaged during either necrosis or late stage apoptosis. Annexin V-FITC and PI labelling is referred to as the live-dead assay. When annexin V-FITC and PI labelling are used in conjunction with flow cytometry, one is able to distinguish four population groups ranging from, viable (no staining), apoptotic (annexin-V positive, PI negative), late apoptotic (annexin-V positive, PI positive) and necrotic (annexin-V negative, PI positive). These data distinguish apoptosis from necrosis providing quantitative data (van Engeland et al., 1997; Vermes et al., 1994).

The basic principles of flow cytometry are described in subsequent sections. Briefly, during flow cytometry single cells in suspension are illuminated as they flow individually past a focussed laser beam. A photomultiplier tube detects-, correlates and allows the plotting of the signals into histograms for analysis. When cells/particles (between approximately 1 µm and 30 µm in diameter) are detected and interpreted, an "event" is recorded and plotted onto a histogram (Givan, 2004). For cell suspensions, usually a single event equates to detection and interpretation of one cell. To achieve mostly single cell events, and not clumped cells, suspended cells should not exceed a concentration of $5x10^6$ cells/ml. The advantage of this single cell technique is that individual characteristics of a large number of cells can be interpreted at a rapid rate (500 to >5000 cells/second), known as the flow rate (Givan, 2004).

4.4.1. Flow rates and hydrodynamic focussing.

The flow rate is the velocity at which particles under pressure pass the interrogation point (Figure 4.5-A) (Givan, 2004). Rates are graded as low, medium or high with higher rates having a greater probability of coincidence events. An increased flow rate will have decreased detection sensitivity while a low flow rate will have increased detection sensitivity (Givan, 2004).

To achieve a stream of cells flowing in single file, the sample fluid is injected into a faster moving fluid forming a sheath around the sample fluid (Figure 4.5-A) (Rahman, 2006). The narrowing stream of cells flowing within a wider sheath stream is termed, hydrodynamic focussing (Givan, 2004; Hawley and Hawley, 2004; Rahman, 2006). The changes in diameter from injector tip to exit orifice are usually between 10- and 40-fold, bringing about an increase in flow velocity to 100- to 1600- fold (Pinkel and Stovel, 1985).

4.4.2. Light source, light scatter and fluorescence

After hydrodynamic focusing, each particle is illuminated as it passes through one or more beams of focused light at the interrogation point (Figure 4.5-A). Light that is scattered in the forward direction, no more than 20° offset to the laser beams axis, is detected by a forward scatter channel (FSC) lens (Figure 4.5-B). The FSC intensity approximates the particle size and can also be used to distinguish between cellular debris and living cells (Rahman, 2006). Cells with large cross-sectional areas refract a large amount of light onto the photodetector while an equally large cell, which is dead or has a permeable membrane, will have a lower refractive index. Forward scatter (FS) is commonly perceived as the "volume" of the cell, however, this can be misleading given that the refractive index of a live cell is different to that of a dead cell of the same size (Salzman et al., 1990). Therefore, alternative methods are employed to discern cells undergoing apoptosis and will be discussed later. The side scatter (SS) channel (SSC), at a 90° angle to the laser beams axis, provides information about the granularity (irregularities or texture in the surface or cytoplasm) of a particle. Both FSC and SSC are unique for every particle, and a combination of the two may be used to differentiate between cell types in a heterogeneous sample subsequently represented within a histogram (Figure 4.5-B) (Rahman, 2006).

In addition to FS and side scatter (SS), combinations of lasers with fluorescent probes are used to further distinguish cell populations. Different lasers (Light amplified by Stimulated Emission of Radiation) allow excitation wavelengths to be associated with particular fluorescent probes (Givan, 2004). Fluorescent probes such as fluorochrome-labelled antibodies or ligands, and

fluorescent dyes may target cellular organelles or cellular chemistry (e.g. Ca^{2+} concentration and pH). Probes provide quantitative and qualitative data about different particles or cells within larger populations (Rahman, 2006). Fluorochromes absorb light or energy at specific wavelengths resulting in their excitation from the stable ground state. This excited state is stable during excitation by a light source. Thereafter, the fluorochrome adopts its previous lower energy state, in the order of nanoseconds, releasing excess energy in the form of fluorescent light. These two processes are called excitation and emission, each having unique wavelengths. Optical filters and mirrors separate wavelengths allowing certain wavelengths to be detected by photo detectors (Figure 4.5-C) (Givan, 2004). The correct sequential placements of these mirrors will filter light for detection by photo detectors, known as photomultiplier tubes (PMTs). PMTs are light sensors which turn detected photons into an electrical signal (Rahman, 2006).

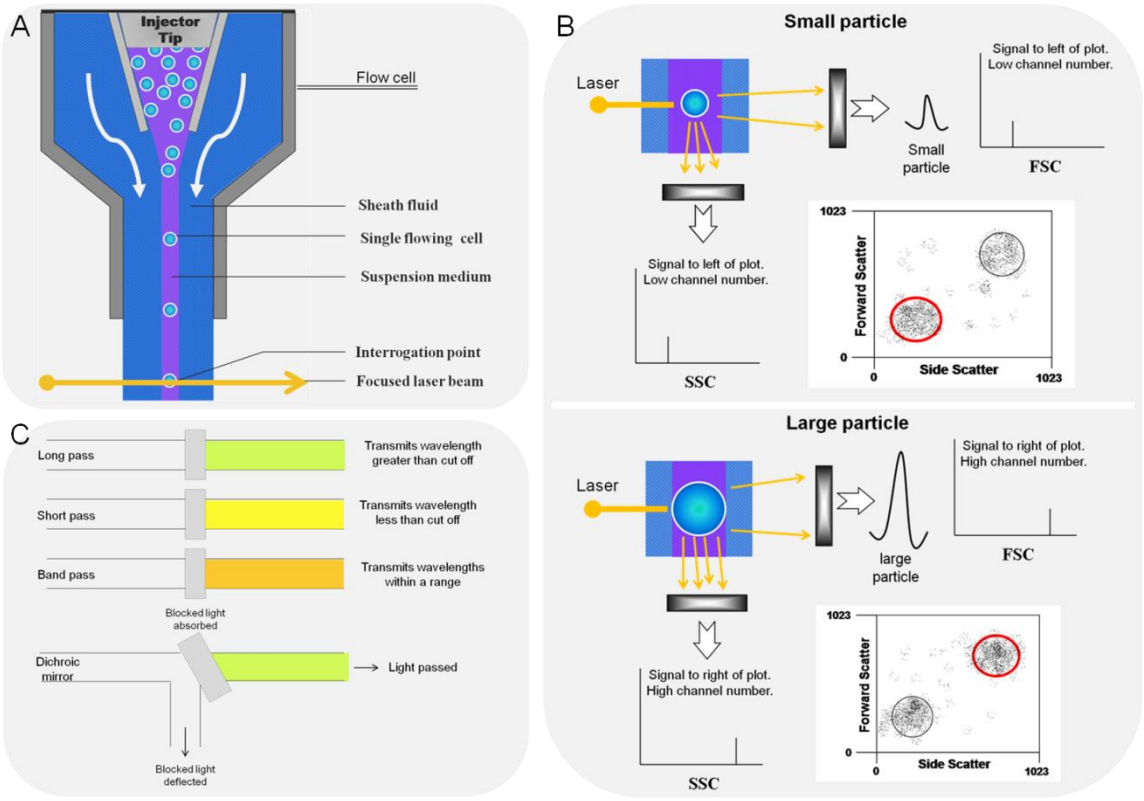

Figure 4.5. Principles of flow cytometry.
Flow cell schematic **(A)**. Sheath fluid flowing around the injector tip encompasses the suspension medium. The sheath fluid creates a drag effect at the narrowing central chamber, increasing the suspension medium's velocity. Particles are dispersed creating a greater distance between them as they pass by the focused laser beam/interrogation point. Detection of small and large particles using forward scatter verses side scatter, showing plotted positions within a linear scale **(B)**. Optical filters **(C)**. Long pass (LP) filters, permit light above a cut-off wavelength. Short pass (SP) filters, permit light below a cut-off wavelength, and band pass (BP) filters permit wavelengths within a narrow range i.e. 620-640 nm. Dichroic mirrors are filters placed 45° angle to the oncoming light. These can either be SP or LP filters, deflecting blocked light at a 90° angle. Reproduced from Rahman (2006).

When light is sensed by the PMT, the electrical output in volts is amplified proportionally to the number of photons colliding with the PMT. This voltage is then amplified by a series of linear or logarithmic amplifiers, and by analog to digital convertors (ADCs), that are plotted graphically (Rahman, 2006).

With linear amplification, light intensity is digitised and reported on a 10-bit or 1024-channel scale, referred to as "intensity". By contrast, logarithmic amplifier's voltage output is proportional to the logarithm of the original light intensity, referred to as "relative intensity units". Having a choice between a linear or a log scale is advantageous. Linear amplification displays a limited range of intensities whereas logarithmic scales display a larger range of

intensities. For example, cells undergoing mitosis will have twice the DNA content as non-proliferating cells, thus, DNA content analysis is better suited to a linear scale as DNA content will be double that of non-proliferating populations. By contrast, protein expression levels which can vary greatly are better suited to logarithmic amplification (Givan, 2004).

4.4.3. Reagents

Annexin-V-FITC.

Required no additional preparation, stored at 4°C.

Propidium Iodide stock solution (PI) [1 mg/ml].

PI (1mg) was dissolved in HBSS (1 ml) in a 1.5 ml eppendorf tube. The tube was covered with tin foil and stored at -20°C.

PI working solution [50 µg/ml].

PI stock solution (50 µl) was diluted in HBSS (950 µl) in a 1.5 ml eppendorf tube, covered with tin foil and stored at -20°C.

Cycloheximide.

Prepared as described in Section 2.8.

DMSO.

Prepared as described in Section 2.8.

Inhibitors.

Prepared as described in Section 2.8.

4.4.4. Procedure

According to the manufacturer's instructions for annexin-V-FITC binding (BD Pharmingen), treated cells required centrifugation to pellet live and dead cells. Samples required washing with PBS, containing 2 mM $CaCl_2$, re-suspension and centrifugation, repeated 3 times. Subsequently, sample (100 µl containing $1x10^3$ cells) required addition of PI (10 µl, 50 µg/ml) and annexin-V (5 µl), under non-sterile conditions, and 20 min for binding before the addition of PBS to a final volume of 500 µl. The manufacturer's instructions suggested a 2 mM $CaCl_2$ concentration for optimal annexin V-FITC binding to phosphatidylserine lipids. However, we found that 2 mM

calcium had an adverse effect on cell viability. In addition, centrifugation of cells treated with cycloheximide or hydrogen peroxide tended to clump and stick. For these reasons, the manufacturer's protocol was adjusted to follow a protocol described by Gatti et al. (1998), who added annexin V-FITC directly to cell culture medium.

Cells were cultured as described in Section 2.2, trypsinised, seeded into 25 cm^3 flasks and allowed to adhere (24 h). MCF-10A and MCF-10AneoT cells were treated with inhibitors at a range of concentration (50-300 µM), in a final volume of 3 ml and incubated (24 h). After treatment, spent medium containing apoptotic or dead non-adherent cells, was poured into 15 ml tubes. Adherent cells were washed with HBSS (500 µl) to remove serum proteins. This HBSS, also containing non-adherent cells, was decanted into the relevant 15 ml Falcon tubes containing spent medium. Cells were trypsinised into suspension, and the trypsin was neutralised using the spent medium containing dead or apoptotic cells. The final volume of live/dead samples did not exceed 5 mls to keep the cell concentration high. Live/dead sample (485 µl) was taken from the 15 ml tube and added to PI (10 µl, 50 µg/ml) and annexin-V-FITC (5 µl) under non-sterile conditions. Samples were briefly vortexed (1 s) and incubated (RT, 20 min) before analysis, to allow binding of Annexin-V and incorporation of PI. All samples were analysed within the hour using the Beckman Coulter Epics XL-MCL. Four histograms were generated per sample, which related to a gated region containing live and dead cells for FS verses SS (Appendix Figures B1-B2). The gated population within the scatter plot histogram represents the cellular constituents of the sample including dead, live and dying cells. Gate A is situated between SS Log10 and SS Log100 as this range generally represents the granularity of cell populations (Figure 4.6-A). Gate A spans almost the entire linear range of FS 0-128, because the volume of cells may change as apoptosis is induced either increasing or decreasing in size (e.g. nuclear condensation or cell blebbing). The PI vs. annexin-V-FITC is derived from the contents of Gate A, separating the fluorescently labelled and unlabelled cells into four distinctive quadrants; necrotic, late stage apoptotic, live cells and early apoptotic cells. Cell count verses annexin-V-FITC or PI staining represent the number of cells which possessed annexin-V or PI fluorescence. Any fluorescence below log10 is regarded as debris. Therefore, if cells were apoptotic or necrotic, their fluorescence would fall between log10 and log100. Cell count histograms were also derived from the contents of Gate A. Signal settings are shown in Table 4.2.

Table 4.2. Signal settings for Annexin-V-FITC/PI apoptosis assay.

Signal	Voltage	Gain
FS	258	1
SS	63	5
FL1 (FITC)	696	1
FL2 (PI)	737	1

4.4.5. Results

Results for the annexin V/PI assay for cell death using flow cytometry, are summarised in Table 4.3 which shows the mean results (n=3) of the percentage viability of both cell lines treated with inhibitors as well as positive (CHX) and negative (DMSO background) controls.

The "PI"-stained and "PI & Anx-V"-stained values represent the cell populations that have undergone necrosis or late stage apoptosis, respectively. Values for cells unstained for both PI and annexin-V (taken as viable) showed that CHX (200 µg/ml) treated MCF-10AneoT cells showed a viability of 83.87% and MCF-10A cells showed a viability of 48.33% (Table 4.3-unstained). According to annexin-V staining results, apoptosis induced by CHX was 13.9% for MCF-10AneoT and 21.53% for MCF-10A (Table 4.3-annexin-V). The fact that annexin-V staining for dead cells (13.9% and 21.53%) and the sum of the live cells adds to approximately 100% suggests that the assay was working correctly although differences between cell lines in tolerance to CHX treatment were apparent. This phenomenon of increased resistance to cell death in MCF-10AneoT cells has been observed before with high levels of hydrogen peroxide (van Rooyen, 2009). All ranges of inhibitor treatments (50-300 µM) were, therefore, non-toxic according to this asssay. For TF 22d and TF 17-2 treated MCF-10AneoT cells, apoptosis occurred in the range of 5.24-7.27% and 1.98-3.89%, respectively, showing comparative levels of apoptosis to the solvent control (3.84%) indicating the existence of a common background population undergoing apoptosis. In the same respect, similar percentages of apoptosis for MCF-10A treated with TF 22d and TF 17-2 (0.20-0.24% and 0.03-0.26%, respectively) were within the range of this background population of naturally apoptotic cells at 0.19% apoptosis (Table 4.3-annexin-V).

The flow cytometry scatter plots were interpreted using a four quadrant display as shown in Figure 4.6-A. When unstained cell data (Table 4.3-unstained) is plotted in a histogram format, Figure 4.6-B, both compounds do not appear to cause loss of viability when compared to the

DMSO and untreated control groups (Figure 4.6-B). Representative scatter plots showing treatment with 300 µM of each inhibitor, untreated, DMSO background and CHX positive controls, are depicted in Figure 4.6-C. In Figure 4.6-C, the CHX positive control shows dense scatter points in quadrant B4 indicating early apoptosis in both cell lines. Interestingly, less scatter points occupied quadrant B1 indicating necrosis was less in MCF-10AneoT than in the MCF-10A CHX-treated group. Table 4.3 shows that MCF-10A cells generally stain with higher levels of PI than the MCF-10AneoT, while the MCF-10AneoT stain with higher levels of Annexin-V than the MCF-10A cells. This trend was observed across both inhibitors including DMSO controls and is likely due to individual cell line characteristics.

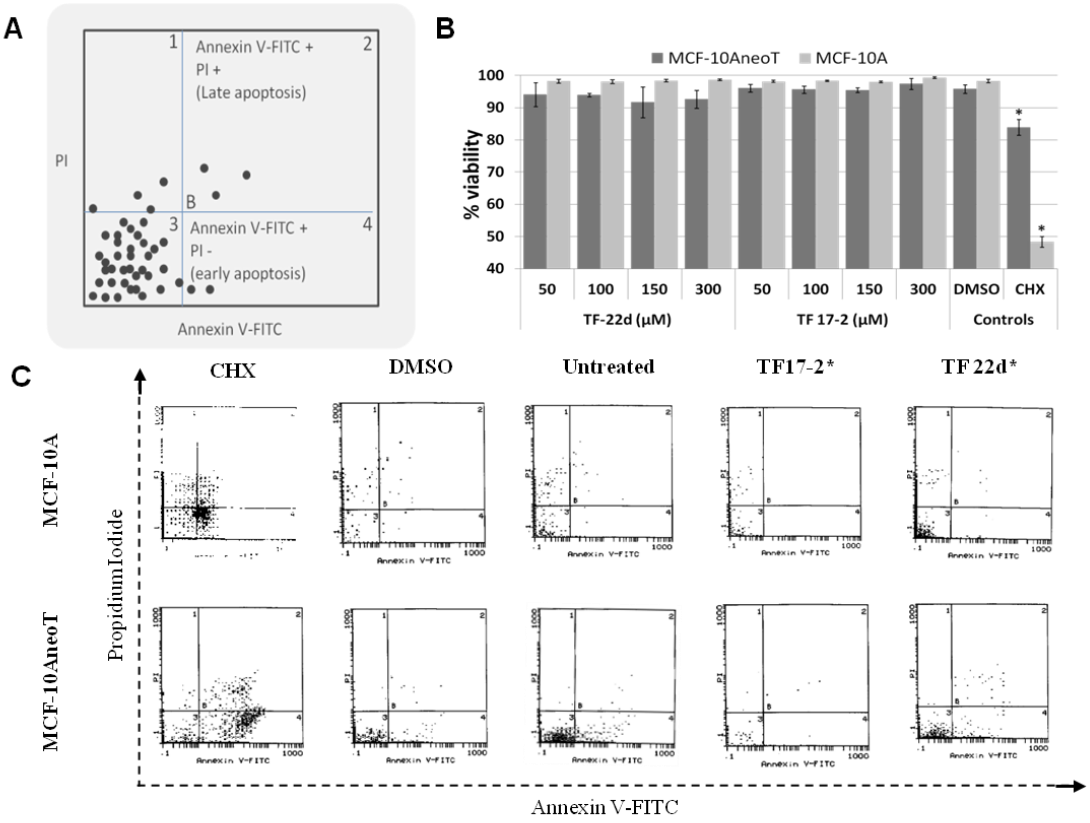

*Represents a concentration of 300 µM

Results of these representative figures may be viewed in the appendix.

Figure 4.6. Viability analysis using flow cytometry.
(**A**) Schematic interpretation of Annexin V-FITC vs PI scatter plot, the histogram is divided into quadrants, B1 (PI +, necrosis), B2 (annexin V-FITC and PI +, late stage apoptosis), B3 (unstained, live) and B4 (annexin V-FITC stained, apoptotic). **(B)** Mean percentage viability of MCF-10A and MCF-10AneoT cells treated with 50-300 µM of either TF 22d of TF 17-2, error bars represent standard deviation. *ANOVA tested significance at $p < 0.05$, DMSO control vs. CHX. **(C)** Representative figures for the annexin V-FITC/PI viability assay showing the scatter plots obtained for treatment and controls groups.

Table 4.3. Percentage viability of MCF-10A and MCF-10AneoT treated with TF 22d and TF 17-2 assessed using annexin-V-FITC/PI.

MCF-	Quadrant	TF 22d (µM)				TF 17-2 (µM)				Controls[a]	
		50	100	150	300	50	100	150	300	DMSO	CHX
10AneoT	[B1] PI	0.66 ± 0.69	0.34 ± 0.25	0.46 ± 0.35	0.46 ± 0.34	0.31 ± 0.28	0.31 ± 0.21	0.34 ± 0.14	0.42 ± 0.15	0.22 ± 0.19	0.39 ± 0.28
	[B2] PI & Anx-V	0.38 ± 0.33	0.51 ± 0.38	0.63 ± 0.66	0.73 ± 0.70	0.20 ± 0.06	0.24 ± 0.18	0.25 ± 0.15	0.29 ± 0.33	0.20 ± 0.06	1.84 ± 0.63
	[B3] Unstained	94.07 ± 3.72	93.90 ± 0.56	91.63 ± 4.73	92.60 ± 2.77	95.97 ± 1.18	95.57 ± 1.16	95.4 ± 0.75	97.3 ± 1.73	95.77 ± 1.33	83.87 ± 2.46
	[B4] Annexin-V	4.89 ± 2.82	5.24 ± 0.37	7.27 ± 3.80	6.22 ± 2.46	3.53 ± 1.40	3.89 ± 1.31	4.06 ± 0.68	1.98 ± 1.27	3.84 ± 1.49	13.90 ± 2.82
10A	[B1] PI	1.21 ± 0.32	1.33 ± 0.46	1.03 ± 0.33	0.90 ± 0.07	1.27 ± 0.28	1.00 ± 0.21	1.40 ± 0.14	0.58 ± 0.15	1.27 ± 0.54	14.70 ± 3.00
	[B2] PI & Anx-V	0.33 ± 0.16	0.39 ± 0.20	0.30 ± 0.18	0.29 ± 0.23	0.38 ± 0.12	0.41 ± 0.23	0.34 ± 0.19	0.02 ± 0.03	0.29 ± 0.14	15.47 ± 4.57
	[B3] Unstained	98.23 ± 0.58	98.10 ± 0.60	98.40 ± 0.40	98.60 ± 0.26	98.17 ± 0.32	98.33 ± 0.15	98.0 ± 0.30	99.4 ± 0.25	98.27 ± 0.5	48.33 ± 1.63
	[B4] Annexin-V	0.24 ± 0.10	0.20 ± 0.03	0.23 ± 0.10	0.20 ± 0.01	0.20 ± 0.06	0.26 ± 0.06	0.26 ± 0.07	0.03 ± 0.04	0.19 ± 0.02	21.53 ± 6.77

Mean values (n=3) and standard deviation are shown from the four quadrants of flow cytometry scatter plots.

[a]Dimethylsulfoxide final dilution (0.05%, v/v). Cycloheximide (CHX) final concentration of 200 µg/ml.

4.4.6. Discussion

Corwin Hansch postulated in the early 1960's that the biological activity of a drug depended on two processes. One was the successful distribution of the drug and the other was binding to its target. For instance, a drug must be able to travel from the point of entry in the body to the target where it exerts its effect. Once successfully distributed a drug must retain efficacy and interact with its target (Bruice, 2007). It is clear, therefore, that metabolic stability is an important attribute for any drug.

The metabolic stability of TF 17-2 was tested by our collaborators using human liver microsome preparations with known concentrations of cytochrome P450 (see Appendix Figure C.1 for detailed results). TF 17-2 was shown to be metabolically stable for over two hours, indicating a favourable pharmacokinetic profile for 6-azauracil containing analogues compared to the common hormone, testosterone (Fischer, 2004). Unfortunately, TF 22d has not been tested and its stability remains unknown.

Typically, drug screening concentrations range from the nano- to millimolar levels, and are subsequently narrowed down to optimal working concentrations. TF 17-2 was previously screened at 30 – 3000 µM showing significant toxicity at 3000 µM but not at 300 µM, and hence was applied at 300 µM to PancTu-1 (pancreatic adenocarcinoma) induced tumours (Kapischke et al., 2008). The study conducted by Kapischke et al. (2008), required the injection of TF 17-2 into SCID/bg mice to determine its effect on the reduction of orthotropic pancreatic ductal adenocarcinoma (PDAC) tumour size. For the purpose of this study, concentration ranges of both TF 17-2 and TF 22d inhibitors were kept to a narrow micromolar range of 50-300 µM for comparison with results from the Kapischke et al. (2008) study. From the Kapischke study, TF 17-2 is known to reduce tumour weight and inhibit metastasis. Therefore, TF 17-2 serves as a compound to which the effects of TF 22d, a novel MT1-MMP inhibitor, were compared.

The MTS assay is marketed as a cell proliferation/viability assay. These terms do not, however, adequately define this assay. MTS is converted from a tetrazolium salt to a soluble formazan product by the activity of dehydrogenase enzymes located primarily in the mitochondria, but may also be found within the cytoplasm. Given the direct association with the mitochondrion, one may also use the MTS assay to assess metabolic effects. The assay, therefore, may be termed a metabolic assay. For any MTS assay, a linear conversion of the tetrazolium salt to a formazan product within a range of cell densities is first established (Promega, 1996). These linear ranges are unique for every cell line, but fortunately similar in our two test cell lines which allowed direct comparison. The initial seeding density was expected to increase over a period of 24 hours, due to cell proliferation. Such

proliferation was taken into account by running the optimisation experiment for the same duration of time as the inhibitor screening experiments. This should validate results in instances when cell numbers, post-treatment, do not increase or decrease beyond those of untreated controls or optimised levels. MTS results should be checked with cell counts for further validation. This is a parameter almost never checked when the MTS assay is used to assess "toxicity" and is an essential control to allow accurate interpretation of the effect of the inhibitor or drug treatment.

DMSO was used to dissolve compounds before mixing the inhibitors into tissue culture medium. Levels of DMSO described in the literature reports final concentrations of DMSO should be less than 1% (v/v) for the commercially available MCF-10A cell line (Davis II et al., 2000; Richards and Smith, 2007). However, final DMSO concentrations had to be established for the MCF-10AneoT cell line, to determine the final concentration of DMSO which would not interfere with cell viability. Cell viability and metabolism became compromised at 1% (v/v) DMSO and both cell lines exhibited a significant reduction of viability in 5% (v/v). Variations in background DMSO concentrations can also lead to anomalous observations (data not shown). We decided, therefore, that DMSO backgrounds should be consistently maintained at 0.05% (v/v) for all experimental applications. The MCF-10AneoT cell line appears to be 20% more tolerant to similarly high concentrations of inhibitors than the MCF-10A cell line. Similar results were observed for hydrogen peroxide using the same cell lines (van Rooyen, 2009).

The results of the MTS assay showed that TF 22d appeared to have no effect on the metabolic activity of either cell line in the concentration range tested, though cell counts were not performed. The normal epithelial cell line (MCF-10A) treated with TF 17-2 showed less metabolic tolerance to the 300 µM concentrations than the pre-malignant cell line (MCF-10AneoT). To investigate the observed metabolic effects of TF 17-2, cell counts were performed to eliminate cell stress as a contributing factor. Interestingly, MCF-10A cells treated with TF 17-2 (300 µM) showed similar cell numbers to the DMSO control. Contrary to the MTS results, the MCF-10AneoT cell line appeared to decrease in cell number significantly by 53%, when treated with TF 17-2 (300 µM). These results suggest that the MTS assay, at times, is unable to distinguish between cell stress and anti-proliferative effects. The conclusion drawn from this data is that at 300 µM, TF 17-2 will reduce metabolic activity in the normal cell line and will suppress MCF-10AneoT growth while increasing metabolic activity possibly through cell stress effects or some other, as yet, indistinguishable pathway which induces dehydrogenase enzyme activity. Another possibility could be cell lysis (necrosis), where dehydrogenase enzymes and their co-factors are released into the medium where uncontrolled MTS conversion may take place.

Ideally, anti-cancer drugs target malignancies selectively, leaving normal tissues relatively unaffected. If TF 17-2 does indeed affect the metabolism of MCF-10A cell line, but reduces the population of MCF-10AneoT cells, then TF 17-2 meets the ideal requirements of an anti-cancer drug and may explain why TF 17-2 was seen to reduce the tumour size using an orthotopic pancreatic ductal adenocarcinoma xenograft model in SCID/bg mice (Kapischke et al., 2008).

To further validate MTS assay results, the Annexin-V/PI flow cytometry assay was performed to distinguish between apoptosis and necrosis (cell lysis). Across cell lines and inhibitor concentrations, PI entry and subsequent DNA staining occurred in less than 1% of the population. Having gated to include cell death debris, this data disproves cell lysis as a contributing factor for the observed increase in metabolic activity seen in TF 17-2 (300 µM) treated MCF-10AneoT cells as PI and annexin-V would have heavily labelled DNA and membrane debris that spilled into the medium. This data suggests that the MCF-10AneoT cells remained intact for the duration of exposure to inhibitor and that TF 17-2 imparts a proliferation suppression effect evidenced through cell counts.

The MCF-10AneoT cell line treated with 300 µl TF 17-2 inhibitor showed that there was significant depression of cell number. Flow cytometry seems to indicate that this was not due to an increased induction of cell death, but rather a depression of replication. This is a desirable selective inhibition of the metabolism of a cancer cell, with little effect on the normal cell line. We may conclude, therefore, that TF 17-2 (300 µM) causes anti-proliferative effects by blocking MT1-MMP activity and hence decreasing aerobic glycolysis and increasing cell stress by inducing energy deficiency (Sakamoto and Seiki, 2010).

In conclusion, TF 22d and TF 17-2 treated cells analysed using the annexin-V/PI flow cytometry viability assay do not show signs of necrosis or apoptosis which exceed those observed in the DMSO control, and shows high percentages of cell viability (>90%). Therefore, TF 22d and TF 17-2 are non-toxic at the concentrations tested on both cell lines, though at 300 µM TF 17-2 suppresses MCF-10AneoT growth while increasing its metabolic activity.

In order to assess the possible efficacy in selectively preventing migration of cancer cells by inhibiting MT1-MMP, a key enzyme in facilitating cell movement, inhibitors were tested on MCF-10A and MCF-10AneoT cells.

CHAPTER 5.

Application of MMP inhibitors in cell migration assays

5.1. Biochemistry of cell migration

Cell migration is a normal physiological process that plays a role in morphogenesis, development, injury repair, and immune defences (Ridley et al., 2003). Fundamental mechanisms of migration are similar to those adopted in pathophysiological processes such as cancer cell invasion. Motility can be divided into four sequential steps (Moissoglu and Schwartz, 2006). Cells (i) extend protrusions at the leading edge, (ii) make new adhesive contacts, (iii) contract to move the cell body forward, and (iv) detach the trailing end (Moissoglu and Schwartz, 2006) (Figure 5.1). As mentioned in Chapter 1 (Section 1.4.1), MT1-MMP is involved in both adhesion and detachment of the cell during migration (Marrero-Diaz et al., 2009; Ratnikov et al., 2002). In this chapter, the central dogma of cell migration and the classes of migration will be described and analysed in the context of MT1-MMP-mediated migration in both normal and premalignant breast epithelial cells.

As in the case where cancer cells metastasise to different organs, normal directional cell movement is stimulated by extracellular signals or chemotactic gradients (Yamazaki et al., 2005). During directional cell movement, the actin cytoskeleton undergoes rearrangements causing protrusions, such as those observed in lamellipodia. Protrusions can be large, sheet-like broad lamellipodia or spike-like filopodia, driven by actin polymerisation and stabilised by adhesion complexes that adhere to the ECM or adjacent cells (Ridley et al., 2003). These adhesions serve as sites for the establishment of myosin-contractile forces during forward movement and disassemble at the rear. PI3K has been suggested to contribute to cell polarity through chemo-attractant activation of PI3K and subsequent accumulation of PIP_3. PI3K is activated by heterotrimeric G-proteins (Brock et al., 2003), activated FAK (Chen et al., 1996) or non-receptor protein tyrosine kinases of the Src family (Stephens et al., 1993). PI3K phophorylates PIP_2 to PIP_3 that stimulates small GTPases of the Rho family, for example, Rac and Cdc42, inducing the formation of the leading edge through reorganisation of actin (Nobes and Hall, 1995; Small et al., 2002). Localised pools of globular actin (G-actin) polymerise into fibrillar actin (F-actin) at the leading edge, pushing the membrane forward (Figure 5.2).

Filopodia, are induced by Cdc42 and lamellipodia, are generated by Rac (Aplin et al., 1998; Yamazaki et al., 2005). Rac and Cdc42 bind and activate the PAK serine/threonine kinases (PAK1, PAK2, and PAK3) (Figure 5.1 and 5.2). In turn, PAK phosphorylates the myosin II regulatory light chain resulting in actin polymerisation, focal adhesion (FA) stability and contractile forces (Parsons et al., 2010). These structures participate in the generation of the locomotive force in migrating cells.

Unlike Rac and Cdc24, which are activated at the front of the cell (Kurokawa et al., 2005), Rho is prominently active at the rear and regulates myosin-mediated contractility promoting the locomotion of the cell body. Rho activates myosin through Rho-associated protein kinase 1 (ROCK1) and ROCK2 that indirectly lead to sustained phosphorylation of myosin II regulatory light chain (Figure 5.1). Succinctly, Rac and Cdc42 stimulate protrusions at the leading front while Rho induces retraction at the trailing edge (Yamazaki et al., 2005) (Figure 5.1).

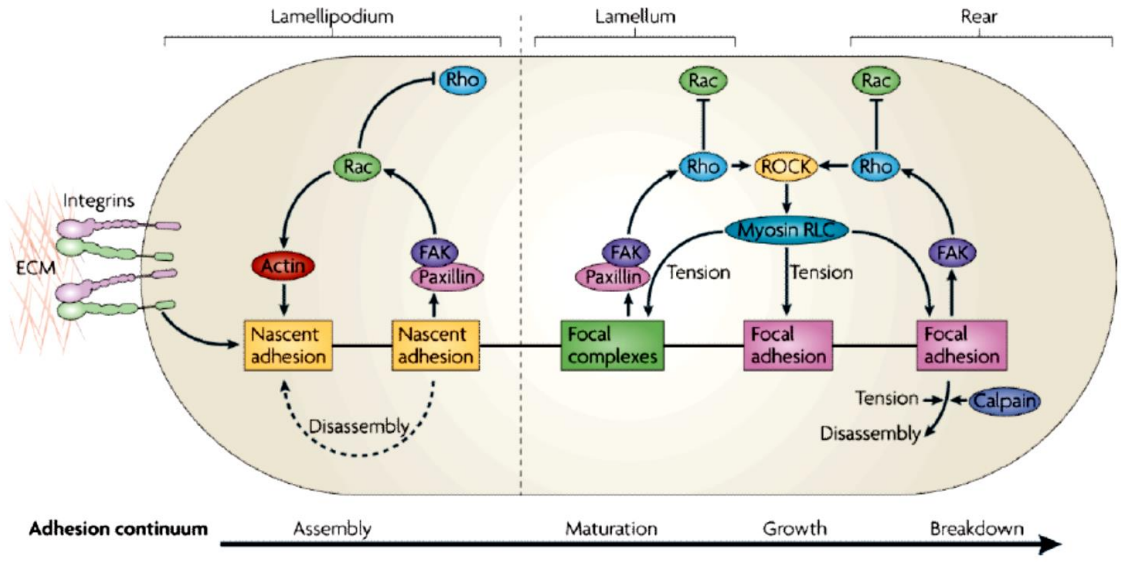

Figure 5.1. Adhesion maturation and Rho GTPase activation.
Polarisation during migration begins with the assembly of nascent adhesions at the lamellipodium. Assembly and disassembly of nascent adhesions in the lamellipodium is driven by Rac through phosphorlylation of paxillin and focal adhesion kinase (FAK). Localised suppression of Rho prevents premature maturation of focal complexes. In the lamellum, activated Rho sustains myosin II activation through Rho-associated protein kinase (ROCK), which controls kinase and phosphatase activity of the regulatory light chain (RLC) of myosin II facilitating maturation and growth of focal adhesions. Tension generated by myosin II activity induces calpain proteolysis of focal adhesions and subsequent disassembly at the rear [reproduced from Parsons et al. (2010)].

At the furthest tips of filopodia and lamellipodia, new cell adhesions to ECM components are mediated primarily by integrins (Lock et al., 2008). Integrins are a family of transmembrane receptors each containing an alpha (α) and a beta (β) subunit (Moissoglu and Schwartz, 2006). In mammals, combinations of 18 alpha and 8 beta subunits compose 24 distinct integrin alpha-beta heterodimers that bind in a specific, yet partially overlapping manner to various ECM components (Danen, 2003; Danen and Sonnenberg, 2003). Integrins function as both mechanical adhesion and signalling molecules, activating unique signalling networks depending on their expression repertoire (Lock et al., 2008). For example, human skin fibroblasts express the collagen type-I receptor $\alpha_2\beta_1$ integrin, which activated MMP-1 and MMP-13 genes induced by p38 MAPK signals generated after collagen-$\alpha_2\beta_1$ interaction (Ravanti et al., 1999). Integrins link to the actin cytoskeleton through a structural protein complex consisting of parvin, paxillin and vinculin. Integrins exist in low ligand-affinity conformations and high ligand-affinity conformations (Yilmaz and Christofori, 2009).

Activation to high ligand-affinity conformations is achieved by binding an adaptor protein, such as vinculin, or by MT1-MMP-mediated proteolytic cleavage during integrin maturation (Baciu, 2003; Deryugina et al., 2000; Tadokoro et al., 2003; Takino et al., 2006). Direct downstream signalling targets of integrins are focal adhesion kinase (FAK), Src-family of kinases, glycogen synthase-kinase-3 β and protein kinase B (AKT/PKB). These downstream targets have implications for cell proliferation, survival, migration and invasion.

In both migration and invasion programs integrin clustering results in the formation of nascent adhesions and F-actin assembly, which usually occurs in the lamellipodium, immediately behind the leading front of the cell membrane. Nascent adhesions have been described to mature into dot-like adhesions (± 1 µm in diameter) known as focal complexes at the lamellipodium-lamellum interface (transition zone) in fibroblasts (Figure 5.2) (Zimerman et al., 2004). Focal complexes mature into focal adhesions which may typically be 2 µm wide and 3-10 µm long (Zimerman et al., 2004). Focal adhesions of this size are footholds to mechanical force, and reside at the ends of stress fibres. These types of adhesions have been reported not to be prominent in rapidly migrating cells (Ridley et al., 2003). Disassembly of FAs occurs at the rear of the cell during movement (Parsons et al., 2010) and is facilitated by MT1-MMP through ECM cleavage and processing of CD44 (Itoh, 2006; Suenaga et al., 2005).

The structural component of FAs, vinculin, has been used in this study and by others as a marker of FA formation (DeMali, 2004). Structurally, vinculin is composed of three major domains, an N-terminal head, flexible neck region, and C-terminal tail. Associations between the head and tail domains impose a conformational strain on vinculin rendering it inactive (Bakolitsa et al., 2004) and located in the cytoplasm (Chen et al., 2005). Once vinculin is recruited to nascent FAs, it is activated by phosphatidylinositol 4,5-bisphosphate (PIP_2) allowing for the maturation of the FA. Active vinculin is switched to an open conformation allowing interactions between talin and α-actinin to the head, Arp2/3 to the neck, and F-actin, PIP_2, and paxillin to the tail (Humphries et al., 2007; Zamir and Geiger, 2001). Previously, vinculin was merely considered to be a structural linker, however, vinculin also regulates integrin clustering, and the vinculin-tail regulates the link to the mechanotransduction force machinery (Humphries et al., 2007).

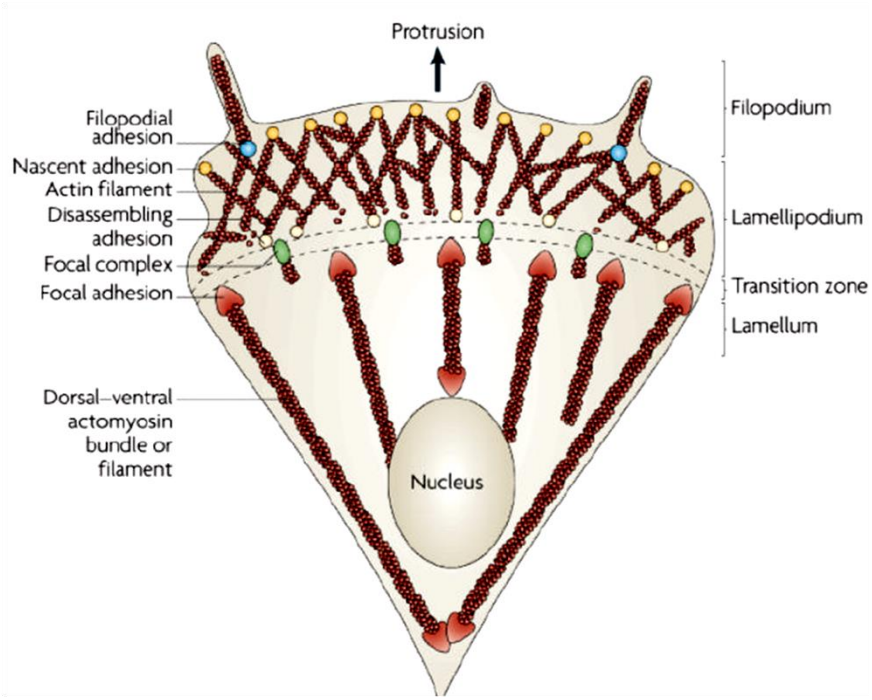

Figure 5.2. Structural elements of a migrating cell.
Protrusion of the leading edge is driven by globular actin assembly into fibrillar actin, depicted in two distinct zones, the lamellipodium (branched F-actin) and the lamellum (parallel stress fibres). Branched actin is depolymerised and reorganised into bundles in the transition zone. Short lived nascent adhesions form in the lamellipodium and may either dissasemble in the transition zone or mature into focal adhesions in the lamellum. In the lamellum, mature focal adhesions faciliate myosin II contractile forces through dorsal-ventral actomyosin filaments [reproduced from Parsons et al. (2010)].

Mechanotransduction is mediated by actin assembly during maturation of FAs into stress fibres and the contraction of these stress fibres by myosin II (Figure 5.2) (Ridley et al., 2003). Myosin II is an ATP dependent molecule that moves anti-parallel actin filaments past each other. Contractile forces are thus generated by the transmission of tension to FAs (Ridley et al., 2003). The tension generated in the rear can open stretch-activated calcium channels (Lee et al., 1999). The influx of calcium may target the calcium activated protease, calpain, capable of cleaving focal adhesion proteins, such as integrins, talin, vinculin and FAK (Figure 5.1), thus resulting in FA disassembly (Glading et al., 2002).

5.2. Migration classes: collective and single cell migration

Hitherto, cell migration within this chapter has been described broadly for normal cells using single cell examples. Cell migration, however, is classified into two classes, collective migration (cell sheets, strands, tube clusters) and single cell migration (amoeboid, mesenchymal movement).

Collective migration defined as the polarised migration of two or more cells, which have retained their cell-cell junctions and move together over or through a substratum. Cell-cell cohesion is mediated by adherens junctions, desmosomes, tight junctions, gap junctions and even integrins (Ilina and Friedl, 2009). During sheet migration, cells retain communication channels to collectively

polarise their movement (Khalil and Friedl, 2010). Cells at the leading border explore the path, generate traction, and remodel the ECM for path generation (Katarina et al., 2007) and, therefore, are described as leader cells for their bipolar nature. Bipolarity is maintained by integrins that adhere at the free pole and E-cadherin junctions engaged with a trailing cell at the rear (Khalil and Friedl, 2010).

Mesenchymal migration of single cells is synonymous with a transitional state between a 'benign' and 'malignant' phenotype as migratory cells become invasive. As already mentioned, MT1-MMP is involved in tumour dissemination through cleavage of cell-cell contacts such as E-cadherin (Covington et al., 2006) and cell-matrix adhesions by shedding CD44 (Marrero-Diaz et al., 2009; Suenaga et al., 2005). Polarised mesenchymal movement in which cells adopt an elongated form and extend protrusions (lamellipodia/filopodia) has been described (Section 5.1). In contrast, non-polarised or random membrane activity leading to additional protrusions, or ectopic sites, may momentarily stabilise and define a new direction of movement. Consequently, this short-lived directional movement becomes random over longer periods allowing the cell to explore its environment or metastasise (Biname et al., 2010).

Metastasis is no longer exclusively considered the result of proteolytic cleavage and movement through matrix barriers. Amoeboid migration is also possible and is the movement or translocation of a single cell without the use of contractile stress fibres or proteolysis (Friedl et al., 1998; Wolf et al., 2003b). In contrast to mesenchymal cell migration that remodels its immediate environment, amoeboid movement allows the cell to circumnavigate matrix barriers by changing shape and squeezing through narrow spaces (Friedl and Wolf, 2003a). Cell matrix interactions are, therefore, weak and short lived (Friedl, 2004). Such movement may also be induced by broad spectrum protease inhibitors as a migratory compensation mechanism (Wolf et al., 2003a).

During non-malignant or controlled migration, MT1-MMP enhances cell-matrix adhesions and aids cell-matrix release through ECM processing (Section 1.4.1) while confined to lamellipodia or invadopodia (Liotta and Kohn, 2001; Takino et al., 2006). The dual effect seems unregulated in uncontrolled migration as MT1-MMP is not confined to micro-invasive structures but rather distributed over the expanse of the plasma membrane (Snyman, 2010). One of the reasons for using 2D migration assays is to test the role of MT1-MMP in migration since 3D assays cannot be used to distinguish between non-proteolytic amoeboid movement and protease-mediated invasion (Friedl and Wolf, 2003a). We explored the role of MT1-MMP in migration using inhibitors of MT1-MMP in cells stimulated to migrate collectively or as single cells on type-I collagen in 2D.

5.3. Collagen type-I influence on MT1-MMP expression levels

In patients with breast cancer, increased levels of stromal collagen type-I have been shown to promote tumour initiation, progression and an increased risk of metastasis (Barkan et al., 2010). Patients diagnosed with invasive ductal carcinoma display dense collagenous stroma increasing their risk of bone and lymph metastasis (Barkan et al., 2010). In addition, collagen type I has been shown to have various effects on *in vitro* cell migration and MMP expression, such as maintaining higher levels of cell surface MT1-MMP by abrogating clathrin internalisation (Lafleur et al., 2006). By providing cells with an excess of a particular substratum, a particular integrin repertoire is inadvertently selected. This activates certain signalling pathways influencing transcription factors, adherence and migration (Zamir and Geiger, 2001).

Collagen type-I is, therefore, implicated in breast cancer progression and invasion *in vivo* and *in vitro*. Synthetic inhibition of MT1-MMP may, therefore, be better observed when cells are stimulated to migrate on collagen type-I substratum. The effect of collagen on MT1-MMP expression in MCF-10A and MCF-10AneoT cells was investigated using a polyclonal chicken (IgY) antibody raised against the recombinantly expressed amino acid sequence Ala^{21}-Ile^{318} (Crouch, 2009; Lichte et al., 1996). This sequence construct includes the pro-domain, catalytic domain and the hinge region of MT1-MMP (Figure 1.5 & 1.6).

5.3.1. Reagents

Polyclonal chicken anti-ProCat IgY.

Antibody raised in chickens inoculated with a synthesised MT1-MMP protein spanning from the hinge region to the pro-domain (anti-ProCat IgY), was a kind gift from Candice Crouch, University of KwaZulu-Natal. Refer to Appendix Table A.1 for further details.

Monoclonal rabbit anti-chicken IgG horseradish peroxidase linked.

Refer to appendix Table A.1 for further details.

Additional reagents required are listed in Sections 2.5, 2.6 and 2.7.

5.3.2. Procedure

As described in Section 2.4 to 2.7.

5.3.3. Results

Anti-ProCat IgY detected a 39 kDa degradative product of MT1-MMP in both cell lines cultured on plastic (untreated) or collagen type I (Figure 5.3-A). Densitometry showed that MT1-MMP levels are

elevated in both cell lines cultured on collagen than those cells cultured on plastic alone (Figure 5.3-B). GAPDH was used as a loading control for standardisation of loading.

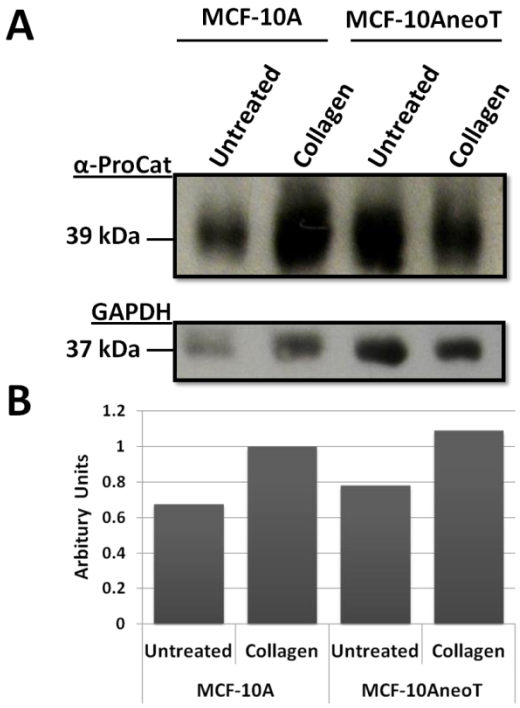

Figure 5.3. Collagen type I increases MT1-MMP expression levels.
(**A**) ECL analysis of MT1-MMP protein from cell lysates of MCF-10A and MCF-10AneoT cells cultured with or without collagen type I substratum using anti-ProCat primary antibody. Cell lysates were prepared as described in Section 2.4. GAPDH served as a loading control and a means to determine expression levels of MT1-MMP. (**B**) Densitometry analysis of MT1-MMP levels in MCF-10AneoT cell lysates with levels normalised against MCF-10A grown on collagen (using arbitrary units of relative intensity).

5.3.4. Discussion

MT1-MMP levels in cells cultured with or without collagen type-I substratum assessed using ECL and GAPDH as a loading control, revealed a 39 kDa band corresponding to the catalytically inactive ectodomain (Rozanov et al., 2005). The hinge region of MT1-MMP is O-linked glycosylated at four sites (Section 1.6) and therefore, may account for the smearing effect observed at 39 kDa. Four glycolipid additions may have been fully, partially or incompletely linked, varying the relative mobility of MT1-MMP during SDS-PAGE electrophoresis (Wu et al., 2004). The 39 kDa degradative product has been observed before (van Lent et al., 2005) with polyclonal antibodies directed against the hinge region detecting 38-42 kDa forms (Rozanov et al., 2005). The polyclonal antibody (pAb 160) used by Toth et al. (2002), directed against the catalytic domain only, does not detect the 39 kDa degradation products as these may contain the prodomain thereby blocking binding to the catalytic site. We deduce that possibly, the 39 kDa band observed and used to compare MT1-MMP levels was non-autocatalytically processed and contains half of the hemopexin domain, the hinge region, the catalytic domain and the prodomain. This is important as all processed forms may be potentially detected by the antibody used in this study as shown in Figure 5.4, with the exception of a ~25 kDa

product of non-autocatalytic shedding. The 39 kDa band, however, was the most prominent form detected and was, therefore, used to assess comparable levels of MT1-MMP when cells are grown with or without collagen type-I. Given all the documented processed forms by Osenkowski et al. (2004), it is tempting to conclude that the 39 kDa band detected in this study corresponds with the 32 kDa non-autocatalytic product depicted in Figure 5.4, but containing the prodomain (7 kDa). Densitometric analysis showed that cells grown on collagen type-I appear to have increased levels of MT1-MMP. Due to this favorable result, cell culture on collagen type-I was employed since it may allow for enhanced effects of MT1-MMP inhibition.

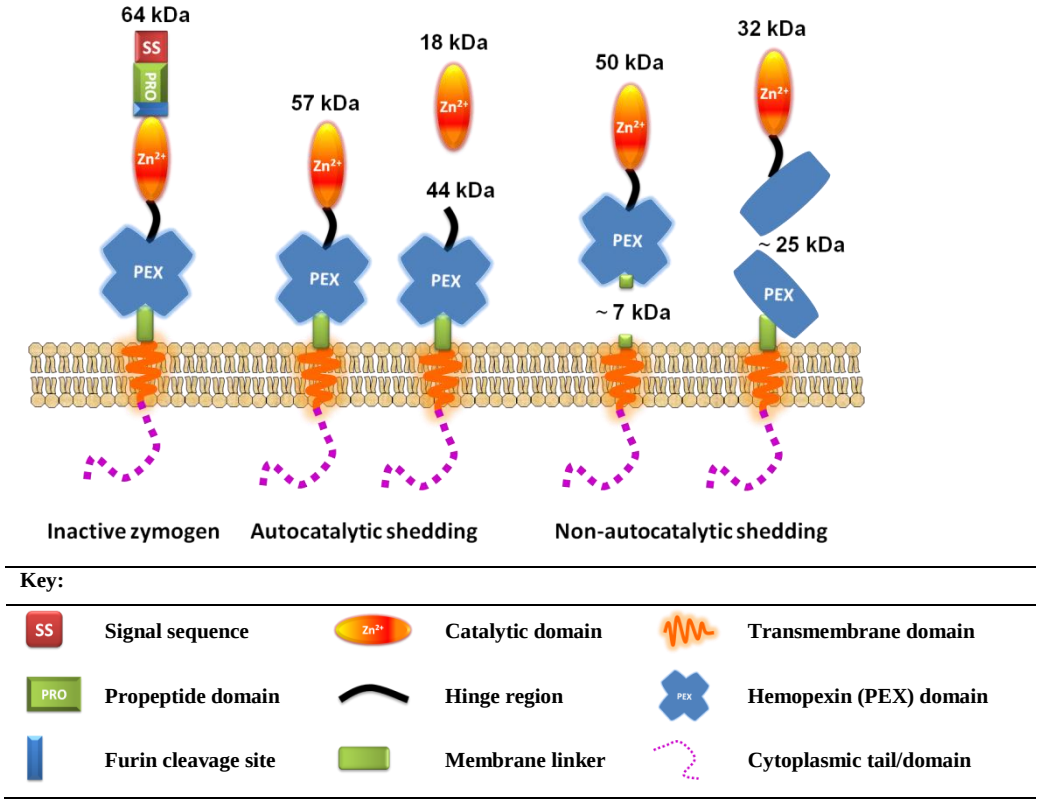

Figure 5.4. Processing forms of MT1-MMP.
MT1-MMP is synthesised as an inactive zymogen of 64 kDa. Furin cleavage or a two-step bait region cleavage in the prodomain with subsequent autocatalytic cleavage results in the active 57 kDa form. Autocatalytic cleavage at the beginning of the hinge region followed by cleavage in the structurally conserved Met-turn (mentioned in Section 3.3) generates the inactive 18 kDa species and the 44 kDa membrane bound species. Non-autocatalytic shedding produces an active 50 kDa soluble form or a 32 kDa species likely mediated by ADAM proteases (Toth et al., 2006) resulting in the remaining 7 kDa and 25 kDa species, respectively [redrawn from Osenkowski et al. (2004)].

ECL and densitometry analysis was only performed once and requires more replicates to attain a standard deviation of data and statistical significance. The MCF-10A cell line has been shown to upregulate MT1-MMP mRNA and protein expression when grown on collagen type-I (Barkan et al., 2010; Gilles et al., 1997b), however, this has not been previously assessed in MCF-10AneoT cells. These preliminary findings provided evidence to suggest that collagen type-I is a suitable substratum to assess MT1-MMP mediated migration.

5.4. Scratch-wound assay.

The scratch-wound assay is a simple, cost effective and rapid assay for the analysis of cell migration *in vitro*. In a scratch assay, a confluent epithelium is scratched with a tool such as a pipette cone to mechanically remove a strip of cells from the monolayer into which cells are free to migrate (Liang et al., 2007). During scratching, some cells may be destroyed, releasing their intracellular contents into the media and leaving adherent cell debris behind. Newly formed boundary cells may become permeable as a result of tearing off adhesive junctions from their previously neighbouring cells. The resulting momentary influx of extracellular medium may trigger migration (Poujade et al., 2007).

5.4.1. Reagents

Cell culture reagents.

As described in Section 2.2.

Inhibitors.

As described in Section 2.8.

Collagen type I.

As described in Section 2.9.

5.4.2. Procedure

Plates were coated with collagen type I as described in Section 2.9. The protocol used for this assay was described by Goetsch and Niesler (2011). Briefly, 2 x 10^4 cells were seeded into 24-well plates untreated or treated with collagen type I, allowed to adhere (24 h) and form monolayers. Confluent monolayers were scratched using a loading tip and washed with HBSS to remove non-adherent cells. Cells were subsequently incubated in freshly prepared treatment mediums with or without inhibitors (24 h) (Section 2.8). Images were captured at 0, 2, 4 and 6 hours post-wounding with a 3 mega pixel Moticam 2300 camera mounted to an Olympus CKX-41. Images were analysed with Motic version 2 software using the free-hand drawing tool to trace the wounded area (µm^2). The percentage wound closure was determined using the following calculation:

$$\%\ \text{Wound closure} = \frac{[\text{Wound area } (0\ h) - \text{Wound area } (x\ h)]}{\text{Wound area } (0\ h)} \times 100$$

Wound area (0 *h*), means the area of initial wounding (µm^2) and wound area (*x h*), means the interim or final wounding area at 2, 4 and 6 hours (µm^2). Assays were repeated 5 times in duplicate.

Rate of migration was calculated by plotting the percentage wound closure over 6 hours on a scatter plot and inserting a trend line to determine the gradient of the straight line graph.

$$\frac{\Delta y}{\Delta x} = Slope(m) \text{ (Derived from trendline; } y = mx + c)$$

The data produced by scratch assays was checked for a normal distribution using the Shapiro-Wilk test for normality. The Shapiro-Wilk test, also known as the W-test for normality, returns a W statistic with its probability value under the assumption that data are normal. Thus, a low probability indicates that the data are unlikely to be from a normal distribution. All data sets were checked and achieved high probabilities. The paired Students t-test, which assumes a normal/Gaussian distribution, was employed to determine statistical significance ($p < 0.05$). All statistical operations were carried out using GenStat 12th edition, and graphical representations were prepared in Microsoft Excel 2007.

Statistical analysis for the rate of migration was performed using analysis of variance (ANOVA) from a split plot design where significance was $p < 0.05$. Posthoc comparison of the least significant difference (LSD) against the difference of means between controls and treatments was carried out. A normalised data distribution was satisfied and confirmed with residuals plotted onto a histogram where results formed a bell shaped curve, and a normal plot where residuals were plotted against the expected normal quantiles, showing a linear distribution (data not shown), further confirming a normal distribution.

5.4.3. Results

In trial experiments of the scratch-wound assay using MCF-10AneoT cells, it was found that these cells did not allow for measurement of reductions in wound area, as these cells did not form confluent monolayers. Wounding did not produce a scratch with a distinctive boundary (Figure 5.5-B). Instead, MCF-10AneoT cells migrated into the wound individually, making wound closure difficult to measure. For this reason, we performed analyses of the effect of inhibitors on the scratch-wound assay on the MCF-10A cells, only (Figure 5.5-A not B).

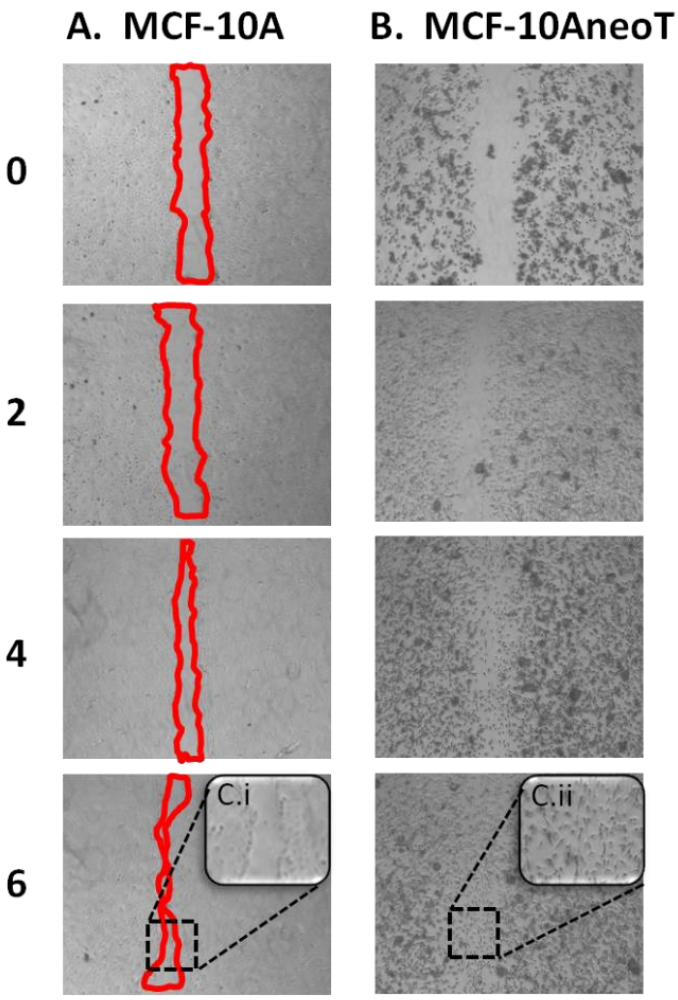

Figure 5.5. Scratch assay methodology.
(**A**) MCF-10A cells and (**B**) MCF-10AneoT cells grown on culture plastic, scratched, and captured at 0, 2, 4,and 6 hours. (**C.i**) MCF-10A cells show defined cell-borders (red line) and partial wound closure by 6 hours. (**C.ii**) MCF-10AneoT show complete migration into wound site without definite cell-borders.

When grown on tissue culture plastic and scratched, both untreated and DMSO-treated MCF-10A cells migrated into the wound area and closed up to 80% of the wound in 6 hours (Figure 5.6-A). Treated with TF 22d (300 µM), MCF-10A cells closed up to 72% of the wound surface area in 6 hours (i.e. 90% of possible closure or a 10% reduction in closure). TF 17-2 inhibited cell migration to a greater extent, the MCF-10A cells closing 51% of the wound within the same timeframe (i.e. 63% of possible closure or a 37% reduction in closure). This suggests that during a 6 hour period, TF 17-2 is approximately 27% more inhibitory of MCF-10A wound closure than the TF 22d when cells are grown as a monolayer on plastic, though both inhibitors significantly inhibited migration on tissue culture plastic compared to the control.

In contrast, when plates were coated with type-I collagen, both compounds significantly inhibited migration of MCF-10A cells to a similar extent, when judged against the DSMO control. The TF 17-2 and TF 22d inhibitors both allowed about 47% wound closure (i.e. to 58% of possible closure or

42% decrease in closure) (Figure 5.6-B). Paradoxically, the overall rate of migration is significantly faster on plastic than on collagen (Figure 5.6-C) possibly due to stronger adhesion to the collagen type-I or the greater reliance on MT1-MMP-mediated proteolysis on such a substratum.

The slower migration of MCF-10A cells on collagen may have obscured any differences in wound closure velocity on collagen relative to plastic for both drugs (Figure 5.6-B), the slower migration rates and lower relative values of controls possibly masking apparent differences in inhibition. Both drugs, however, inhibit migration significantly when compared to their respective DMSO control groups, regardless of the culture surface (Figure 5.6-C $^{(\text{ANOVA})}$). Interestingly, the TF 22d inhibitor showed a significant difference in inhibition (approximately a 36% difference) on different culture surfaces, whereas, the TF 17-2 inhibitor varied much less (between 7-9% per hour difference). This suggests that in the absence or presence of collagen type-I, TF 17-2 has a similar inhibitory effect on wound closure in MCF-10A cells (Figure 5.6).

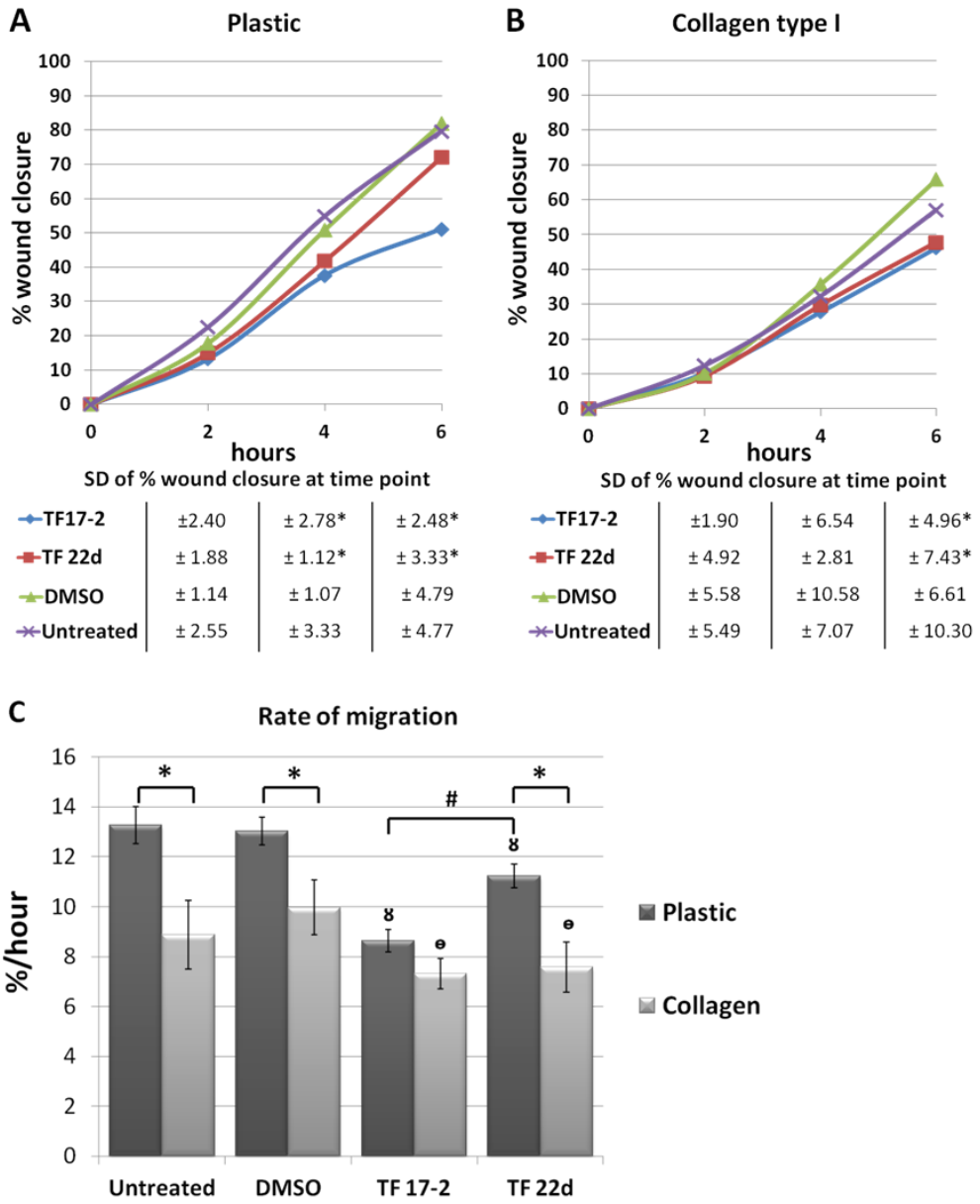

Figure 5.6. Inhibition of MCF-10A wound closure on plastic and collagen type I coated plastic.
Percentage wound closure was recorded as described in Section 5.4. **(A)** Percentage wound closure on plastic showed TF 17-2 (300 µM) inhibited migration by 21% more than TF 22d (300 µM) at 6 hours. **(B)** Percentage wound closure on collagen matrix showed no difference in migration inhibition-potency between the two inhibitors. Wound closure time point's standard deviations of 5 separate experiments (n=5) in duplicate are listed in table form below panels A and B. Significance (*) is compared to DMSO controls determined by paired Students t-test for percentage wound closure where $p < 0.05$. **(C)** Rate of MCF-10A migration was determined from the average of gradients produced by trendline overlays. There is a significant (*) overall decrease in migration rate when cells are cultured on collagen, compared to plastic alone. Compared to their respective DMSO control groups, the inhibitors significantly (plastic ϑ or collagen ᵠ) decreased the rate of migration. Also noted was a significant difference (#) between TF 17-2 and TF 22d when applied to MCF-10A cells grown on tissue culture plastic. Statistical analysis of the rate-of-migration was performed using an ANOVA with post-hoc LSD comparisons. Bars represent mean values of 5 separate experiments performed in duplicate, with error bars representing SEM.

5.4.4. Discussion

MT1-MMP has been cited as a key enzyme in cellular migration (Anilkumar et al., 2005; Kajita et al., 2001; Koshikawa et al., 2000). Here scratch assays were performed to determine the extent of MT1-

MMP and possibly MMP-2 inhibition in normal cell migration. As previously mentioned, TF 17-2 and TF 22d target MT1-MMP (K*i* = 0.2 µM) with 100-fold higher affinity than MMP-2 (K*i* = 28 µM and 14.7 µM, respectively) (Table 3.2).

Over the course of the 48 hour time period of the scratch assay, MCF-10A cells should have secreted their own ECM components onto the plastic, prior to scratching. These components would include fibronectin, collagen type-IV and laminin (Debnath et al., 2003; Koshikawa et al., 2000) and would facilitate attachment to plastic and influence cell migration and hence wound healing (Gilles et al., 2001; Koshikawa et al., 2000). Both inhibitors significantly reduced the migration/wound healing rate and the percentage wound closure in MCF-10A cells cultured on plastic, though wound closure was compromised most by the TF 17-2. This is an interesting observation since the inhibitors have similar affinities for MT1-MMP (K*i* 0.2 and 0.22 for TF 22d and TF 17-2, respectively) but minor differences in affinity for various MMPs. These include a difference in affinity for MMP-2 (13.3 µM difference, Table 3.2, TF 17-2 K*i* = 28 and TF 22d K*i* = 14.7).

Differences in cell migration/wound healing rates observed for TF 17-2- over TF 22d-treated MCF-10A cells on plastic, therefore, could also possibly be attributed to other MMP species such as MMP-7, for which the inhibitors show a higher affinity (Table 3.2, TF 17-2 K*i* = 0.05 and TF 22d K*i* = 0.71) or less likely to MMP-8 and MMP-13 (TF 17-2 K*i* = 4.0 and 2.5, and TF 22d 0.2 0 and 09, respectively). MMP-7 is expressed in MCF-10A cells (Gordon et al., 2003), but MMP-8 and MMP-13 do not seem to be expressed (unpublished data). MMP-7 has not been implicated in migration, though it is active against collagen type IV and fibronectin and is another protease, besides MT1-MMP, that may activate proMMP-2 (McCawley and Matrisian, 2001).

MMP-2 is an excellent "partner" enzyme for MT1-MMP in facilitating cell migration/wound healing, as their combined proteolytic activity facilitates the digestion of almost all ECM components (Sato and Takino, 2010) (Section 1.7.5 and Table 1.1). The affinity of TF 17-2 for MMP-7 is 10-fold higher than that of TF 22d (Table 3.2). Thus inhibition of MT1-MMP and MMP-7 by TF 17-2 may reduce the amount of active MMP-2 more than TF 22d, and hence, explain the observed results of 2D migration/wound healing assays. Since fairly high levels of inhibitor (300 µM) were used, incidental inhibition of other non-target proteases with K*i* values higher than MT1-MMP may have occurred in a concentration-dependent manner.

The significant differences in wound healing in inhibitor-treated MCF-10A cell monolayers on plastic, was not observed in cells cultured on collagen type I, a predominating matrix and a common target for MT1-MMP and MMP-2. These cells showed that both inhibitors had a similar propensity for inhibiting MT1-MMP and possibly MMP-2-mediated migration/wound-healing on collagen type-

I. Collagen type-I abrogates clathrin-dependent internalisation of MT1-MMP, keeping active MT1-MMP on the plasma membrane (Jiang et al., 2001b; Lafleur et al., 2006). In addition, collagen type-I induces MT1-MMP autocatalytic activation thereby regulating activation of proMT1-MMP (Toth et al., 2002). Inhibition of MT1-MMP using synthetic inhibitors in the presence of a collagenous substratum, therefore, may result in cell surface accumulation of the inhibited 57 kDa active form. When collagen type-I is presented as the primary substratum, inhibitor potencies appeared to be similar possibly as both MT1-MMP and MMP-2 are equally active on this matrix. Results may, however, also be influenced by better cell adherence that affect events such as release from the substratum due to inhibition of proteases usually responsible for such an event. This may give rise to a slower overall migration velocity, obscuring any slight differences in inhibitor effects. Alternatively, a less efficient, non MT1-MMP-related method of migration may be induced, possibly involving a different repertoire of integrins upon MT1-MMP inhibition.

Significant inhibition of wound-healing or the migration velocity of normal cells into the wound is not a desirable result for anti-cancer drugs. Ideally, normal cell behaviour should remain relatively unaffected by therapy. However, due to the lack of comparable data for the pre-malignant MCF-10AneoT cell line, we could not assume that the inhibition of migration seen in the MCF-10A cells would be less than that of the MCF-10AneoT cells. Therefore, further studies were conducted to compare the migration of these two cell lines. We used collagen type-I-coated glass coverslips to perform live cell imaging and investigate migration patterns of the individual cells, rather than a collective effect on wound healing.

5.5. Live cell imaging

Live cell imaging was used to analyse migration of individual cells from both cell lines, under various treatment conditions. The scratch assay technique was employed as stimulation of migration was necessary in order to observe MT1-MMP-mediated migration. Benefits of live cell imaging over a conventional scratch assay assessment include the analysis of the differences in migration type, pattern and cell morphology of a large number of individual cells. In the case of the MCF-10AneoT cells that do not exhibit collective cell migration, analysis on an individual cell basis may give a clearer understanding of the influences of inhibitors on cell motility. In this study, live cell imaging allows comparison of the effects of MT1-MMP inhibitors in two different cell lines, a normal MCF-10A and a premalignant MCF-10AneoT cell line.

5.5.1. Reagents

Cell culture reagents.

As described in Section 2.2.

Inhibitors.

As described in Section 2.8.

Collagen type I.

As described in Section 2.9.

Glycerine.

A drop of glycerine was placed onto the 25x objective of the Zeis 710 confocal microscope before viewing.

5.5.2. Procedure

Glass bottomed dishes (MaTek plates) were coated with collagen type I as described in Section 2.9. MCF-10A and MCF-10AneoT cells were seeded (3×10^4 cells in < 500 µl) onto prepared collagen type-I coated plates covering only the central glass plate. Cells were allowed to adhere (30 min), before topping up with complete medium (2 ml). This seeding technique ensures cells reach confluence rapidly. Cells were cultured (24 h) to confluence, before treating with inhibitors and scratching with a loading tip. Spent treatment medium containing floating clumps of free cells from scratching was replaced with fresh treatment medium to remove these non-adherent cells while maintaining treatment of adherent cells. Cells were viewed in the incubation chamber of the Zeiss 710 confocal microscope (25x objective, 37°C, 5% CO_2). Pictures were captured for 90 cycles every 120 sec, equating to 3 hours. The camera exposure time was set between 0.3-0.8 ms for optimal cell contrast.

Cell migration was assessed for 10 individual cells. The data produced was grouped and averaged for each of the two separate experiments. Images were analysed using ImageJ 1.43j, and ImageJ plugins; 'Manual Tracking', and 'Chemotaxis and Migration Tool 1.01'. The sequences of images were loaded into ImageJ. A cell was selected and automatically assigned a colour and an integer value to distinguish the cell from others. The selected cell was tracked by clicking on the centre of the cell nucleus as ImageJ cycled through the sequence of images. The following migration graphs were generated by the Chemotaxis and Migration Tool: velocity, speed of cellular motility (µm/min); accumulated distance ($d_{i,accum}$), the measured path of the cell; Euclidean distance ($d_{i,Euclid}$), the length of the straight line between cell start and end point; and directionality (D_i, direction persistence), the measurement of direction of cell trajectories. Migration paths of individual cells are plotted from a common point, showing distance and directionality of each cell analysed. In this way distances moved by single cells can be visually distinguished and compared collectively to other treatment

groups, allowing for a visual summary of velocity, directionality, Euclidean and accumulated distances.

$$\mathrm{D}i = \frac{di,Euclid}{di,accum} \qquad \mathrm{D} = \frac{1}{n}\sum_{i=1}^{n} \mathrm{D}i = \frac{1}{n}\sum_{i=1}^{n} \frac{\mathrm{d}i,Eucild}{\mathrm{d}i,accum}$$

Single cell trajectory **Average cell trajectory**

Where *n* is the number of cells.

D → 1: straight motion and

D → 0: non-straight motion.

5.5.3. Results

Live cell tracking allowed the comparison of MCF-10A and MCF-10AneoT cell migration, migration classes and directionality, a parameter used to distinguish between normal and malignant migration classes. Although quantitative data is obtained, the small sample size (10 cells) and number of replicates performed (n=2) was low, due to the sum total time lapse and expense of this experiment (48 h), the data generated, therefore, is considered to be of a qualitative nature. It should also be remembered that the time-course for this assay was only 3 hours compared to 6 hours in the scratch assay.

MCF-10A cells on the boundary of the scratch-wound identified and tracked over the course of the experiment showed a flattened morphology and cells appeared to move via a collective migration strategy (Figure 5.7-A). The MCF-10AneoT cells, on the other hand, exhibited a rounded morphology and a lack of cell-cell contacts during migration (Figure 5.7-B). At the end of 3 hours (finish) collective cell migration in the MCF-10A cell line with cells migrating in a single direction, into the scratch-wound, was observed (Figure 5.7-A). MCF-10AneoT cell migration into the scratch-wound was erratic and influenced by the migration path of other cells (Figure 5.7-B).

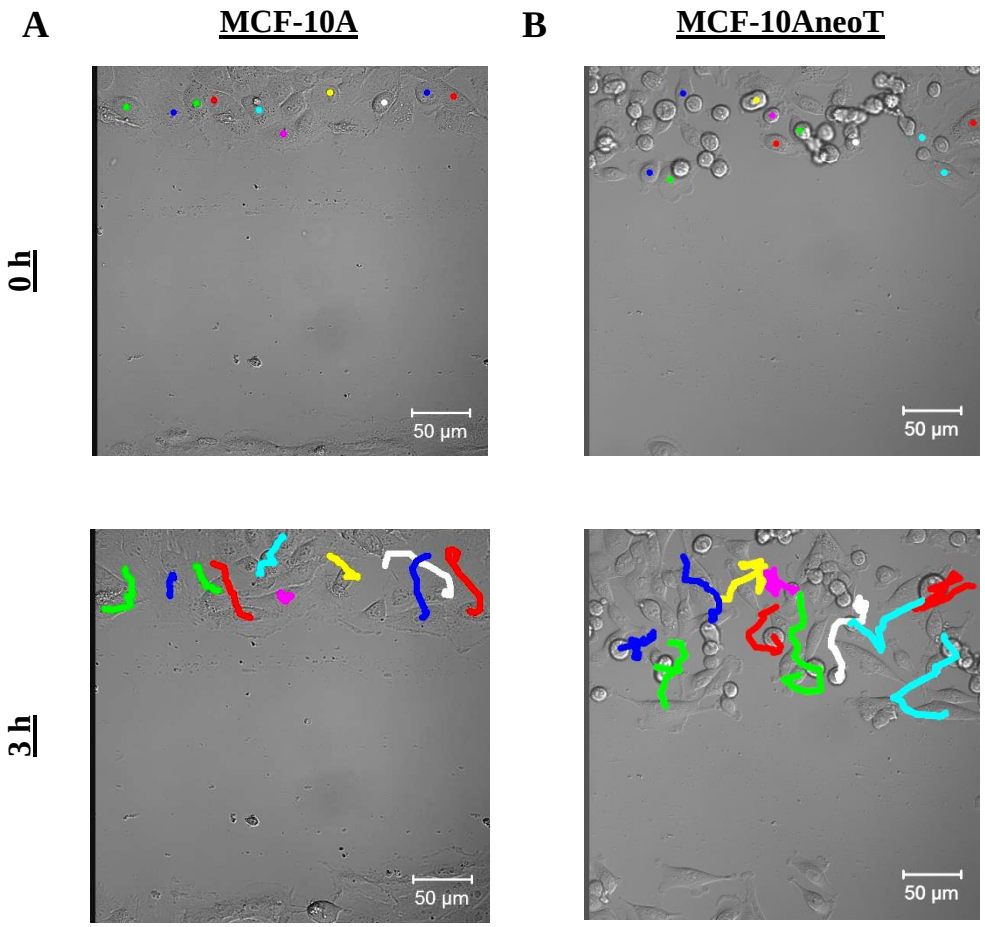

Figure 5.7. Tracking of cells migrating into scratch-wound during live cell imaging.
(**A**) MCF-10A cells and (**B**) MCF-10AneoT cells were tracked using ImageJ 'Manual Tracker' and 'Chemo Taxis Tool' plugins (section 4.5). '0 h' represents migration initiation at hour zero immediately after scratching. Ten cells per frame were analysed over a three hour period, '3 h' (n=2). Coloured lines represent different cells that were tracked representing an individual cell's migration path.

Figure 5.8, panel A, shows migration paths of cells from a single representative video. Migration paths of individual cells plotted from a common point, showed that migration velocity of both cell lines treated with TF 22d, in comparison to DMSO-treated control cells, increased slightly in the MCF-10A (12%) and quite markedly in the MCF-10AneoT cells (47%) (Figure 5.8-A & -C, TF 22d). Although DMSO-treated MCF-10A cells showed increased velocity compared to untreated cells in Figure 5.8, panel A, the overall mean increase in velocity between these two groups was only 0.6% (Figure 5.8-A) showing that DMSO treatment did not affect MCF-10A cell migration.

TF 22d-treated MCF-10AneoT cells, showed a 2.5 µm min^{-1} (16%) increase in average migration compared to the untreated control, and an increase of 8.5 µm min^{-1} (54%) when compared to the DMSO-treated control (Figure 5.8-C). Curiously, between untreated and DMSO-treated MCF-10AneoT cells, the average velocity was reduced from ~13 µm min^{-1} to ~7 µm min^{-1} by DMSO (Figure 5.8-C). This showed that it was essential that all data was assessed against the solvent DMSO control, as solvation of the lipid membrane with DMSO may further exacerbate the premalignant

condition. Even when compensating for DMSO effects, TF 17-2-treatment was seen to decrease the velocity of movement of both cell lines, but especially the MCF-10AneoT cell line (Figure 5.8-C, TF 17-2).

The broad standard deviation observed for velocities in the TF 17-2-treated MCF-10A cell line, also overlaps with the mean of control groups suggesting that TF 17-2 had a variable and possibly even minimal effect on the cell migration velocity of the normal breast epithelial cells. The non-overlapping standard deviation for the TF 17-2 and DMSO-treated MCF-10AneoT cells suggests a marked average inhibition of migration velocity by 36% in TF 17-2 treated MCF-10AneoT cells (Figure 5.8-C). The large standard error between data sets possibly indicates some variation in response by treated cells and may be due to the presence of heterogenous populations of MCF-10A stem cell populations (Bhat-Nakshatri et al., 2010) or differences in cell cycles stages. This seems to be reflected in the migration patterns of the video trace (Figure 5.8-A, TF 17-2, MCF-10AneoT), though seems less evident in the MCF-10A cells.

TF 22d and TF 17-2 overall have opposite effects on the MCF-10AneoT cell line, where TF 22d inhibitor increased the average MCF-10AneoT cell movement velocity (not a desirable effect) and TF 17-2 decreased velocity (a desirable effect) (Figure 5.8-C).

In the MCF-10A cell line, the migration path (direction persistence) of most treatment groups is similar (Figure 5.8-B, 0.85-0.9 units) and appears to splay outwards as time progresses (Figure 5.7, 3 h, and Figure 5.8-A, untreated, DMSO, TF 22d, TF 17-2 and -B). This is most likely due to collective migration, as cells appear to be associated (Figure 5.7). DMSO-treated MCF-10A cells appear to migrate further, compared to untreated cells, according to the overall Euclidian distance recorded (Figure 5.8-A and -D). Treated MCF-10A cells also show greater direction persistence compared to that of untreated MCF-10AneoT cells (Figure 5.8-B, 0.85-0.9 and 0.35-0.5 units, respectively). TF 22d and TF 17-2-treatment appears to have little effect on direction persistence of the MCF-10AneoT cell line, affecting persistence only marginally in both cell lines (Figure 5.8-B, TF 17-2 vs. TF 22d and the DMSO control). In the MCF-10AneoT cell line, similar erratic multidirectional movements are observed in treated and untreated samples (Figure 5.8-A). Euclidean distances are also not easily assessed when path lines overlap and cells migrate in the opposite direction to the scratch-wound. These paths are depicted by black lines in the migration graphs and were mainly seen in the untreated and DMSO-treated MCF-10AneoT cells (Figure 5.8-A, untreated and DMSO-treated cells, black lines). Visual inspection of video traces of the movement away from the scratch-wound in untreated and DMSO-treated cells, however, seem to show that such movements were moderated by treatment with both inhibitors (Figure 5.8-A. Compare untreated and DMSO-treated cells with migration patterns of TF 22d and TF 17-2-treated cells), where black lines disappear post treatment.

On average untreated MCF-10A cells move a greater Euclidean distance overall compared to the MCF-10AneoT cells (Figure 5.8-D). This may be due to the inherent directional migration of MCF-10A cells, confirming the known principle that accumulated distance in a single direction results in greater Euclidean distances in comparison to distance due to random migration (Figure 5.8-D & E).

Comparison and measure of inhibitor-effects are perhaps best interpreted against the solvent control, as this should largely eliminate solvent effects (Figure 5.8-D). The MCF-10AneoT cell line treated with TF 17-2 migrated to a mean Euclidean distance of 75 µm compared to the 128 µm achieved by the DMSO control, representing a 60% decrease in distance (Figure 5.8-D). A similar proportional decrease in Euclidean distance (64%) was also observed between the MCF-10A DMSO control and the TF 17-2 treated MCF-10A cells (Figure 5.8-D). Treated and untreated MCF-10A cells covered a much greater overall Euclidean distance than the MCF-10AneoT cells. TF 17-2-treated MCF-10A cells, however, migrated a shorter mean Euclidean distance (36% less than the DMSO control and 22% less than the TF 22d-treated cells) but similar Euclidean distances to untreated controls. In comparison, the TF 22d-treated MCF-10A cells moved a Euclidean distance of 15% less than the DMSO control (Figure 5.8-D).

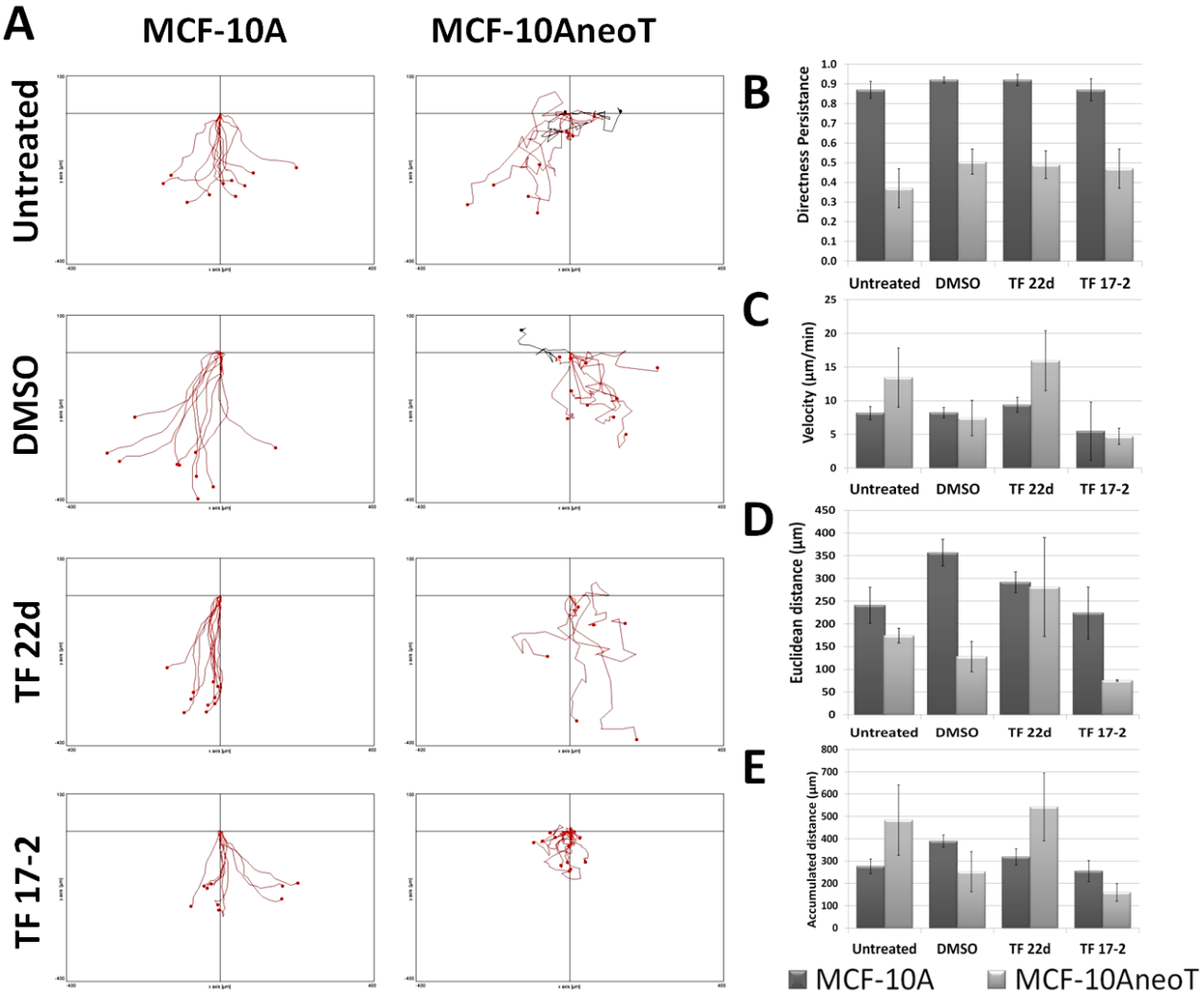

Figure 5.8. Live cell imaging of migrating MCF-10A and MCF-10AneoT cells cultured on collagen type I. Live cell imaging was carried out as described in Section 5.5.2. (**A**) Migration graphs depicting differences between MCF-10A and MCF-10AneoT cell migration from a common point. The common point is 0 µm and both axes terminate at 400 µm. MCF-10A show similar migration paths, while MCF-10AneoT shows random migration in the general direction of least resistance. (**B**) Direction persistence was quantified as described in Section 5.5.2. No increase in directionality was observed for the MCF-10AneoT cell line treated with inhibitors. (**C**) Velocity graph shows increased velocity in MCF-10AneoT cells treated with TF 22d, whereas TF 17-2 inhibited migration in both cell lines. (**D**) Euclidean distances covered by MCF-10AneoT cells were inhibited when treated with TF 17-2, and TF 22d to a lesser extent. (**E**) Accumulated distance reveals the total distance moved by a cell within treatment groups.

TF 22d-treated MCF-10AneoT cells, however, showed an increase in mean Euclidean distance of 153 µm above that of the DMSO control, an approximately 157% increase compared to the 15% decrease induced in MCF-10A cells (Figure 5.8-D). The equivalent accumulated distance migrated would be a 200% increase. This curious result also showed that an average 15 µm min^{-1} velocity (Figure 5.8-C) markedly increased the Euclidean distance covered by MCF-10AneoT (Figure 5.8D). The large standard deviations observed in the MCF-10AneoT cells may have been due to a few cells becoming rounded in morphology (possibly with less cell-matrix adhesions) and moving with higher velocities. This migration pattern may be via a non-amoeboid, "semi-detached mechanism", rounded-up shape of migration as no detachment was seen following treatment with the inhibitors mainly targeting MT1-

MMP, as was previously suggested to be possible by Friedl and Wolf, 2003b (Figure 1.4). Movement was possibly facilitated by adherence via integrins other than those processed by MT1-MMP, i.e. integrins activated via processing by MMPs other than MT1-MMP (Defilles et al., 2011).

5.5.4. Discussion

According to the scratch assay performed on plastic, using light microscopy and discontinuous imaging of the MCF-10A cells, the TF 22d inhibitor had a statistically significant effect, albeit, to a lesser extent than TF 17-2. The TF 17-2 inhibitor seemed to have a significant inhibitory effect on normal cell line wound healing, reducing motility/wound healing by approximately 30% in both cases. High resolution images captured using confocal microscopy, rather than low resolution light microscopy, however, afford a more accurate and informative picture. This allowed analysis of an individual normal and abnormal cell's migratory behaviour under both treated and untreated conditions and confirms the greater inhibitory activity of the TF 17-2 inhibitor on the migration of the premalignant cell line, compared to the normal cell line, over a 3 hour period. Confocal microscopy of live cells showed a mean decrease in Euclidean distance of 60% (Figure 5.8-D), and an accumulated decrease of at least 40% (Figure 5.8-E).

Live cell imaging on collagen gave a similar result to the light microscopy scratch wound healing assay when TF 17-2-treated MCF-10A cells migrated a shorter mean Euclidean distance (36% less than the DMSO control) compared to TF 22d-treated MCF-10A cells (15% less). These results correlate well with the 6 hour time points in the light microscopy scratch assay (30% less than the DMSO control) and hence seem to validate the confocal live cell analyses that was performed for half the time (at least for the MCF-10A cells, as the MCF-10AneoT cells were not analysed).

Since the MCF-10AneoT cell line, treated with TF 17-2, migrated a distance decreased by 60%, this seems to indicate that the TF 17-2 inhibitor may offer some selectivity, as judged in 2D in this preliminary investigation. All MCF-10AneoT cell migration patterns exhibit large standard deviations, possibly due to the erratic migration characteristics of the MCF-10AneoT cell line. Such data shows that live cell analysis of individual cell migration patterns yields information that reflects complicated variations in cell migration. Single hourly images of scratch assay wound closures, on the other hand, reveal only the cumulative wound closure patterns, with no revelation of the random pattern of migration captured during live cell imaging.

An overall analysis of the live cell migration results show that MCF-10A cells achieved Euclidean distances that are similar to their accumulated distances. This correlates with the high directional persistence values obtained for this cell line. Interestingly, TF 17-2 seems to have the most adverse

effect on normal cell migration, reducing distances and velocity more than TF 22d. However, both inhibitors in this context have only minor inhibitory effects on normal cell migration compared to effects on the premalignant cells.

In summary, TF 17-2 reduces the MCF-10AneoT cell lines ability to migrate (reducing velocity and Euclidean migration distances migrated by 42% and 36%, respectively), while the TF 22d inhibitor increased migration velocity (by 213% compared to the DMSO control) and Euclidean migration distances (by 157% compared to the DMSO control), possibly by either inducing or prolonging, rounded cell migration. This would seem to represent a third mechanism of movement, neither the normal MT1-MMP-mediated nor amoeboid, but possibly involving adherence integrins other than those processed by MT1-MMP or different signalling pathways. Baciu *et al*. (2003) showed that MT1-MMP deficient cells were unable to bind collagen type-I effectively due to trans-dominant inhibition of $\alpha_2\beta_1$ collagen binding integrin by integrin pro-α_v, suggesting that inhibition of MT1-MMP would have a similar effect. Confocal live cell imaging of the MCF-10A and MCF-10AneoT cells over a 3 hour period also revealed that several classes of migration were used by both cell lines. The MCF-10A cell line exhibited collective cell migration, where leader cells explored their environment with lamellipodia, while the MCF-10AneoT cells displayed single cell migration. Graphs of migration patterns show that the collective migration of untreated and treated MCF-10A have better directional persistence than single cell migration of MCF-10AneoT cells but direction persistence was not markedly affected by inhibitor treatments.

Data also potentially reveals how results may be complicated by assay conditions. In some cases, for example, cell debris left behind after scratching may create a barrier that could influence the path of migration, or decrease the velocity of migration. Only one such event was observed, where boundary cells retracted before moving into the scratch-wound site. This underscored the importance of repeating experiments. Such events may have influenced Euclidean results in particular. Another phenomenon which is generally evident in the MCF-10A cell line was the tendency to splay outwards during migration. This outward splay of boundary cells, depicted in migration graphs, appears to be due to the availability of extra space presented by the scratch-wound. Leading-edge cells are able to spread out, whereas trailing cells in the monolayer remain restricted by intercellular contacts.

Video analysis proved that the MCF-10AneoT cell line can change its morphology several times in a 3 h period. These morphologies may be substratum anchorage-independent, where rounded cells 'hitch a ride' on other migratory cells. In some cases these loosely adherent, rounded cells may spread revealing the classical mesenchymal (fibroblast-like) morphology. In normal cells, mesenchymal morphology is usually short lived as new ectopic sites (ruffling borders) emerge (Biname et al., 2010). A common morphology observed in the MCF-10AneoT cell line is the spindle

shape. This is generated during rapid extension and release of thin lamellipodia-like extensions. Sometimes, disassembly of the cell tail/rear is not complete causing the release of the cell from this appendage, leaving behind a cellular bleb. This blebbing has been observed before in fibroblasts and is a result of tension forces physically breaking the link between actin and the actin cytoskeleton (Lauffenburger and Horwitz, 1996).

Direction persistence is regarded as an indicator of polarised or a transient migratory phenotype (Chen and Parks, 2009; Ewald et al., 2012). The MCF-10AneoT cell line has previously undergone a partial reversion in phenotype (Li et al., 2008), which lead us to hypothesise that inhibition of MT1-MMP may elicit a similar partial reversion. This hypothesis is based on the fact that MT1-MMP processes a broad spectrum of substrates (Table 1.1) (Sato et al., 2005; Somerville et al., 2003), inhibition may allow the re-establishment of E-cadherin junctions, while collagen type I provides an abundant matrix on which FA's may adhere. In essence, we are interested in the possibility that MT1-MMP inhibition may facilitate normal signalling and re-establish polarised or direction-persistent migration, overriding constitutive signaling by H-Ras(V^{12}) that seems to cause random migration. Unfortunately the directionality value generated by the program of 0.5 does not seem to be sensitive enough to tell if directionality was induced. The value generated for the MCF-10AneoT cells of 0.5 does suggest a partial directionality of movement existed and this is maintained with treatment with both drugs (Figure 5.8-B). This, however, may also be the result of the scratch-wound providing a path of least resistance by offering a clearing into which cells can migrate, distorting the migration path (Théry 2010). The video trace and the Euclidean and accumulated values were far more informative and responsive to changes induced and differences in migration pattern, than the final directionality value.

The MCF-10AneoT cell line exhibited random migration that was often associated with cells with a rounded morphology and these showed an increased migration velocity compared to other cells of a more flattened phenotype. TF 22d treatment of MCF-10AneoT cells seemed to increase migration velocity perhaps due to the observed increase in number of rounded cell phenotypes and associated capacity for higher migration velocities, resulting in an overall faster measured velocity for this cell line.

In order to ascertain whether cell adherence and migration velocity were affected by MMP inhibitors, the number and size of FAs were probed by labelling for vinculin and actin.

5.6. Immunofluorescent labeling of vinculin and actin

During cell migration both MT1-MMP and integrins are located at the tips of filopodia or lamellipodia (Gonzalo et al., 2010) (Figure 5.2). Once recruited to FAs, MT1-MMP proteolytic

activity can expose cryptic sites on the ECM for integrin-mediated interactions. At the rear of the cell, MT1-MMP may have an impact on FA turnover by processing the ECM that in turn facilitates cellular detachment (Gonzalo et al., 2010; Takino et al., 2006). We hypothesised, therefore, that FA formation and processing may be negatively affected by treatment with inhibitors of MT1-MMP and speculated that this may result in changes in the size of FAs, compared to control groups, and that inhibition of MT1-MMP may adversely affect migration velocity.

Vinculin was chosen as a marker for cell matrix adhesion sites as it is a common component of FAs. In addition to FAs, vinculin is also a component of adherens junctions which facilitate cell-cell cohesion (DeMali, 2004). Previously, vinculin was regarded solely as a structural link between adhesion receptors and the actin cytoskeleton. Now, studies have shown that vinculin may play a regulatory role in cell migration (DeMali, 2004). First, vinculin may couple cell adhesions with membrane protrusion by facilitating actin assembly to localized sites of integrin clustering (DeMali and Burridge, 2003). Second, cell migration and survival may be controlled through the recruitment of paxillin to FAs, a process dependent on vinculin (Subauste et al., 2004). Third, cell-cell adhesions through E-cadherin are regulated by vinculin interations with β-catenin (Peng et al., 2010). Therefore, vinculin serves as a molecular indicator of FA formation which may provide qualitative data reflecting possible differences in modes of migration in normal and Ras(V^{12})-transfected cells. As E-cadherin and collagen type I are substrates of MT1-MMP, the aim of this experiment was to visually compare differences in cell adhesions or adhesion size of untreated and inhibitor treated cells in order to provide insight into the possible effects and mode of action of inhibitors.

To achieve high resolution images from within the FA plane of the specimen, we used confocal microscopy. Laser scanning confocal microscopy is a technique used to obtain quantitative and qualitative data from fluorescently labelled subcellular molecules within thin sections of a sample/specimen. Confocal microscopy allows optical sectioning of samples. Focused lasers are used to excite fluorophores which emit light at set wavelengths. Scattered light or out-of-focus light is excluded from detection by restricting the light through a narrow aperture, known as a pinhole. The smaller the pinhole the thinner the optical slice visualised and hence the greater the resolution achieved. Only fluorescent light from this thin focal plane within a sample is detected. A wide-open pinhole results in imaging of a thicker optical slice and the capture of a fluorescent image of multiple optical planes of the specimen accompanied by a reduction in resolution. When the pinhole aperture is set to 1 Airy unit this refers to the width of diffraction pattern of light that produces an optimal confocal image. Signals that pass through the pinhole are detected by photo multiplier detectors (PMTs) which convert the signal into voltages and finally, a digital output. For this study, vinculin and actin antigens were used as markers for adherence and migration.

As described earlier in Section 5.1, the FA structures (indicated by vinculin labelling associated with the formation of nascent adhesions and F-actin assembly in lamellipodia, immediately behind the leading front) in both migrating and invading cells, would be anticipated to be associated with integrin clustering. These would be anticipated to mature into dot-like nascent adhesions (± 1 µm in diameter) known as FA complexes at the lamellipodium-lamellum interface (transition zone) as seen in fibroblasts (Figure 5.2) (Zimerman et al., 2004) and, later, mature into FAs of typically of 2 µm wide and 3-10 µm long (Zimerman et al., 2004).

5.6.1. Reagents

Collagen type I.

As described in Section 2.9.

Paraformaldehyde (PFA) stock solution (16% (m/v))

PFA (160 g) was dissolved in 900 ml dH_2O with heating (60-65°C). The solution was removed from the heat, cleared with 1 M NaOH, made up to 1 l and allowed to cool (RT). The solution was filtered through Whatman No. 1 filter paper, and aliquoted out (50 ml). Stock solutions were stored at -20°C.

PFA in PBS (3.7% (m/v)), pH 7.4 (PFA fixative).

PFA stock solution (16%, 1 ml) was added to PBS, pH 7.4 (3 ml). The solution was made up just before use.

Phosphate buffered saline (PBS) [8.06 mM Na_2HPO_4, 1.47 mM KH_2PO_4, 136.89 mM NaCl, 2.68 mM KCl, 1 mM $CaCl_2$, 0.5 mM $MgCl_2.6H_2O$, pH 7.4].

Na_2HPO_4 (1.145 g) and KH_2PO_4 (0.2 g) were dissolved in dH_2O (900 ml). NaCl (7.99 g), KCl (0.199 g), $CaCl_2$ (0.147 g) and $MgCl_2.6H_2O$ (0.1015 g) were added. The pH was adjusted to 7.4 before making the remaining volume up to 1 l.

Blocking solution (BSA-PBS).

Bovine serum albumin (BSA, 1% (m/v)) was dissolved in PBS. Where necessary the pH was readjusted to 7.4.

Hank's balanced salt solution (HBSS).

As described in Section 2.2.1.

Monoclonal mouse anti-vinculin.

As described in Appendix Table A.1.

Hoechst 33342

As described in Appendix Table A.1.

Phalloidin-TRITC (1 mg/ml).

As described in Appendix Table A.1.

Moviol (10% (m/v)) and 23 M glycerol in Tris (0.1 M, pH 8.5).

Moviol (2.4 g) was dissolved in 0.2 M Tris (12 ml) in a closed container, wrapped in foil and stirred overnight. Glycerol (6 g) and dH_2O (6 ml) was added and stirred overnight. The solution was centrifuged (500 x *g*, 15 min) (Ono et al., 2001) and 100 µl aliquots were stored in microfuge tubes at -20°C.

Glycerol 'immersion oil'.

A drop of immersion oil was placed on the coverslip before inverting and placing onto the 40x objective of the confocal microscope.

5.6.2. Procedure

Cells were cultured as described in Section 2.2 and seeded onto collagen type I coated glass coverslips (Section 2.9). Cells were allowed to adhere (24 h) before the addition of inhibitors dissolved in complete medium (500 µl) as described in Section 2.8. Immunolabelling was carried out as described by Sloane et al. (1994). Briefly, coverslips were washed with warm HBSS (400 µl, x 3) to remove serum proteins and unbound inhibitor. Cells were fixed with PFA (3.7% (v/v), 400 µl, 10 min) and washed with HBSS (400 µl, x 3) before incubating in blocking solution (400 µl, 45 min). Coverslips were incubated in mouse anti-vinculin [1:1000] diluted in BSA-PBS (250 µl, 1 h), before washing with PBS (400 µl, x3). Coverslips were incubated in anti-mouse-DyLite-488 [1:800] secondary antibody and phalloidin-TRITC [1:10000] (400 µl, 1 h). The DNA stain, Hoechst [1: 5000] was added during the last 10 min of the secondary antibody incubation step. The excess Hoechst and unbound secondary antibody were thoroughly washed out with PBS (400 µl, x 6). Coverslips were subsequently fixed with PFA (3.7% (v/v), 400 µl, 10 min), before washing with PBS (400 µl, x 3), rinsing in dH_2O and mounting onto a glass slide with Moviol (2 µl). Slides were either viewed immediately or stored at -20°C o/n.

5.6.3. Results

The confocal images produced from ICC of migrating cells, treated or untreated with inhibitors and labelled for vinculin and actin, showing representative figures from four independent experiments performed in duplicate, is given below (Figures 5.9 and 5.10).

Effect of MMPIs on vinculin positive adhesions in MCF-10A cells

Collective cell migration in the untreated and DMSO-treated MCF-10A cell line seemed to result in increased accumulation of vinculin and adhesions only along the boundary of the scratch-wound (Figure 5.9, all figures in columns "vinculin and actin"). These leader cells form small nascent vinculin-positive FAs at the tips of lamellipodia (seemingly in a cluster). In addition, vinculin co-localisation with actin (yellow) seemed to occur at cell-cell contacts only at the edges of leading-edge lamellipodia where actin branching appeared to be organised (Figure 5.9, vinculin and actin). No other cell-cell contacts were observed in cells behind the leader cells, suggesting vinculin is not involved in maintaining cell-cell contacts during collective migration in MCF-10A cells. Occasionally, TF 17-2 and TF 22d treatments showed some cells situated 2-4 tiers behind leader cells labelling heavily for cytosolic vinculin (Figure 5.9, TF 17-2 and TF 22d). No cell-cell contacts seemed apparent but small FAs seemed to form at the base of these cells (Figure 5.9, TF 17-2 and TF 22d).

In untreated and DMSO treated MCF-10A cells (Figure 5.9, untreated and DMSO), vinculin positive nascent FAs (approximately 1 μm in length) in the lamellipodia were common only in cells in the leading edge. These had large vinculin-positive FA sites in the lamellae, with actin-rich lamellipodia extended into the scratch-wound (Figure 5.9, untreated and DMSO). This was especially true in DMSO-treated cells where FAs were longer (approximately 1 - 3μm in length) and seemed more mature (longer) (Figure 5.9, DMSO). FA formation elsewhere in the associated cell monolayer was not seen (Figure 5.9, DMSO). Also noted was the low level of actin staining in most untreated and DMSO-treated cells, with the exception of leading-edge cells (Figure 5.9, untreated and DMSO).

In TF 17-2-treated MCF-10A cells, vinculin and actin staining appeared to be more diffuse throughout the cell than in the control groups and the TF 22d-treated cells (Figure 5.9, TF 17-2, DMSO and TF 22d). In addition, vinculin was sparsely distributed throughout the TF 17-2-treated cells, as well as being associated with sparse, small (less than 1 μm in length) nascent FAs adhesions in the lamellipodia (Figure 5.9, TF 17-2). These nascent adhesions, however, did not cluster as markedly to form adhesions with a size similar to those observed in DMSO, TF 22d and untreated MCF-10A cells (Figure 5.9, TF 17-2 vs. untreated, TF 22d and DMSO). The smallest FA structure formation by TF 17-2-treated cells, correlated with the greatest inhibition of migration rate (though slight) (Figure 5.8, C).

In TF 22d-treated MCF-10A cells, mature FAs (1 -3 μm) are apparent with similar well-formed, large elongated adhesions appearing in the lamellipodia, slightly larger than those seen in DMSO-treated MCF-10A cells (Figure 5.9, TF 22d, DMSO and untreated) and correlated with a slightly greater

migration rate (Figure 5.8 C). F-actin staining was generally more prominent in all TF 22d-treated cells (even more than in TF 17-2-treated cells) showing ruffled cell borders, with extensively branched actin in the lamellipodia. In addition, TF 22d-treated MCF-10A cells exhibited well-defined cell-cell contacts at lamellipodia where F-actin was branched (Figure 5.9, TF 22d), suggesting more intercellular contacts and a more marked cell-cell contact during collective migration than in all other untreated and treated groups. This correlated with marginally greater migration velocity (Figure 5.8, C) than all other treated and untreated samples (Figure 5.8 C).

Distribution of vinculin and F-actin in MCF-10AneoT cells treated with MMPIs.

Vinculin and actin localisation and labelling intensity varied according to the cellular morphology observed in the MCF-10AneoT cell line (Figure 5.10). Generally, malformed FAs were observed in untreated or DMSO-treated spindle-shaped MCF-10AneoT cells (Figure 5.10 untreated [overview & insert] and DMSO [overview]) with sparse labelling for vinculin. Small and almost non-existent FAs were observed in rounded-adherent cells (Figure 5.10, DMSO-insert). Untreated cells with a mesenchymal morphology (i.e. individual cells with an elongated morphology, often had a leading edge made obvious by increased actin assembly at the leading edge and thinner trailing tail, as seen in the untreated labelling-method control labelled only for phalloidin (Figure 5.10, untreated and control). These showed abnormal FA-like structures of indeterminate size (possibly greater than 3 μm in length) with vinculin localised along the basal plane, mainly at the leading edge of the cell (established by optical sectioning through the cell to the base, Figure 5.10, untreated). The greater size of FAs in the untreated control relative to the smaller, almost non-existent FAs in the DMSO control correlated with the higher migration rate for the untreated cells relative to the DMSO-treated control (Figure 5.10, untreated and DMSO, and Figure 5.8 C) i.e. DMSO decreasing migration rates relative to the untreated control (Figure 5.8 C). The largest FAs, seen in the TF 17-2-treated premalignant cells, however, did not correlate with the most rapid movement but the slowest (Figure 5.10, TF 17-2).

Untreated and DMSO-treated MCF-10AneoT cells exhibited similar morphologies and similar vinculin labelling but DMSO-treated cells show less colocalisation with phalloidin-labelled actin than the untreated (Figure 5.10, untreated and DMSO). This and other DMSO-induced phenotype characteristics correlated with a decrease in velocity of movement (Figure 5.8 C). Rounded cell morphologies in these DMSO-treated groups appear to have unorganised actin with no defined branching in lamellipodia, resulting in ruffled borders (Figure 5.10, DMSO, box). In the tips of mesenchymal-like cells (elongated cells), vinculin labelling begins to exhibit the formation of small, sparse nascent FAs (approximately less than 1 μm in length) as integrins begin to cluster along actin ruffled borders, in spite of the low colocalisation of vinculin with phalloidin-labelled actin (Figure

5.10, DMSO, box). When, in some cases, the untreated mesenchymal-like MCF-10AneoT cells become spindle-shaped, the extended morphology seems to place strain on the actin cytoskeleton as the cell forms long filaments that extend from the cell tip to the nucleus (Figure 5.10, DMSO).

TF 17-2-treated MCF-10AneoT cells exhibited a noticeable change in morphology and apparent adherence, post treatment. These cells appeared to spread over the collagen type-I matrix and showed a more normal morphology (i.e. less extended morphology with a tendency to re-associate via cell-cell contact, in a manner intermediate to that seen in DMSO and TF 22d-treated normal MCF-10A cells, Figure 5.10, TF 17-2 vs. Figure 5.9, DMSO and TF 17-2) rather than the untreated and TF 22d-treated MCF-10AneoT cells (Figure 5.10, untreated and TF 22d). TF 17-2-treated cells, moreover, formed more mature FAs (1-2 μm in length) compared to in the MCF-10AneoT DMSO controls (Figure 5.10, TF 17-2 vs. DMSO). They also showed extended actin bundles and vinculin association vaguely similar to that seen in the untreated and DMSO-treated normal MCF-10A cell line post treatment with TF 17-2, where FAs seem less well developed (Figure 5.10, TF 17-2 vs. Figure 5.9 DMSO and untreated). They also exhibited well organised actin branching (Figure 5.10, TF 17-2, enlargement insert) and the greatest reduction in cell migration (Figure 5.8 C, TF17-2).

In contrast, TF 22d-treated MCF-10AneoT cells exhibited the same membrane ruffling as untreated and DMSO treated cells, but a less extended morphology, possibly due to unorganised actin branching (Figure 5.10, untreated, DMSO and TF 22d). In addition, vinculin labelling was relatively sparsely distributed throughout the cells (indication of FA formation) but colocalised to a minor extent with actin at ruffled cell borders (Figure 5.10, TF 22d). Cells which appear to be migrating showed a broad ruffling front (rounded morphology) with a markedly defined actin association (Figure 5.10, TF 22d), and seemed to be associated with the highest migration velocity (Figure 5.8, C). This morphological phenotype with the least well-formed FAs shows the greatest mobility in the MCF-10AneoT cells (Figure 5.10 TF 22d and Figure 5.8 C) in contrast to the finding for the MCF-10As where the larger FAs correlated with the highest migration (Figure 5.9 TF 22d and Figure 5.8 C). From these results, it would seem that TF 17-2 may have caused some reversion of the mutationally activated, mesenchymal-like *ras* phenotype, to a more epithelial, less migratory phenotype.

Generally, however, with the exception of the spindle morphologies, which exhibited distinguishable but malformed FAs at terminal regions (Figure 5.10, untreated and DMSO), MCF-10AneoT cells of the untreated and DMSO control groups did not form normal looking nascent FAs (Figure 5.10, Untreated and DMSO). FAs rather showed sparsely distributed staining of vinculin in all treated cells of different morphology (Figure 5.10). Poorly organised actin and down regulation of vinculin-associated FA formation, is known to occur at ruffled membrane borders under the influence of the constitutively active H-Ras(V^{12}) (Joneson et al., 1996). H-Ras up-regulates MT1-MMP and possibly

influences this phenotype. Whereas MT1-MMP levels are not high in normal cells, the effect of MT1-MMP-directed MMPIs seems to have the greatest effect on the mesenchymal-like MCF-10AneoT cell phenotype.

In summary, the inhibitors did not show a major effect in the MCF-10A cells, though a slight increase in migration rate and larger FA development was seen in these cells with TF 22d treatment and a decrease in FA size and migration rate seen with TF 17-2 treatment. In contrast, in the premalignant cell line, FAs were enlarged with TF 17-2 treatment and migration velocity decreased. FAs were also reduced in size with the TF 22d treatment, and the induced rounded morphology and least developed FAs, correlated with an increase in migration rate/velocity. At this stage, therefore, in the light of single cell migration assays and the above labelling results, it seems that the inhibitors tested have an opposite effect on the normal and premalignant cells. The larger elongated vinculin-labelled FA structures seen in MCF-10A cells correlate with a minor but noticeable increase in velocity of movement whereas the smaller FAs correlate with a major increase in velocity of movement in the premalignant cells.

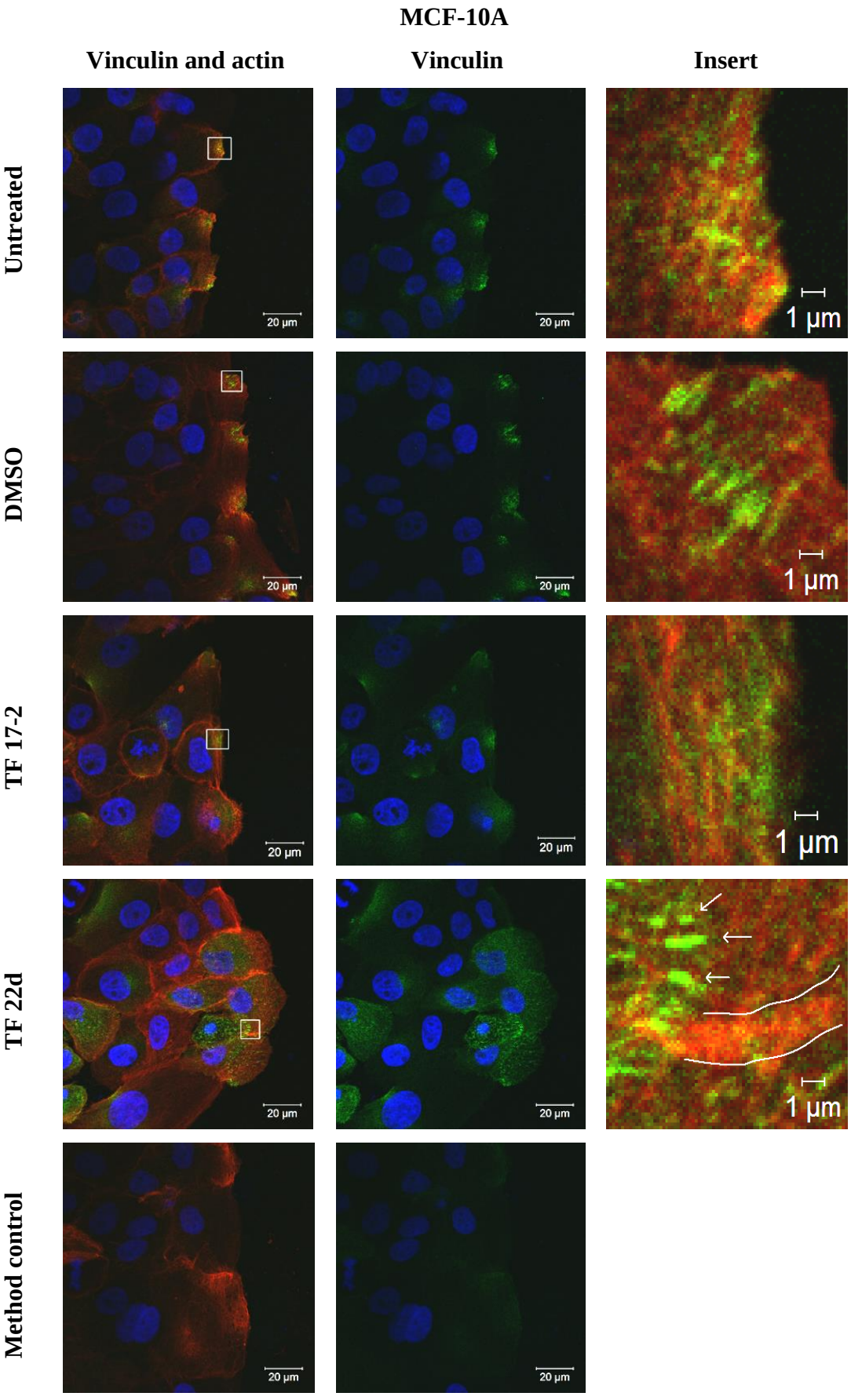
MCF-10A
Vinculin and actin
Vinculin
Insert
Untreated
DMSO
TF 17-2
TF 22d
Method control
20 µm
1 µm

Figure 5.9. Confocal images of migrating MCF-10A cells labelled for F-actin and vinculin.
Immunocytochemistry analysis of MCF-10A cells migrating into a scratch-wound, fixed with 3.7% paraformaldehyde (10 min) 3 hours post wounding and probed as described in Section 6.2. Untreated and DMSO treated cells present with clustered vinculin (green) positive FAs showing elongated nascent FAs in the organised and branched regions of F-actin (red) of the lamellipodia. TF 17-2-treated cells show poor vinculin clustering suggesting small dispersed nascent adhesions in branched F-actin regions of lamellipodia. Generally, actin staining intensity was greater for cells treated with the inhibitors, especially boundary cells. TF 22d-treated cells show mature focal adhesions throughout the lamellae with nascent adhesion in the lamellipodia. Interestingly, these cells also displayed cell-cell contacts between branched F-actin of lamellipodia. Lines indicate cell-cell contact, arrows indicate vinculin positive focal adhesions and boxed areas of interest are reproduced at 20x magnification under 'insert' column. Experiments were performed four times in duplicate viewing two frames per specimen. Vinculin method controls, containing no primary antibody, show no specific labelling of vinculin or other proteins by the secondary antibody.

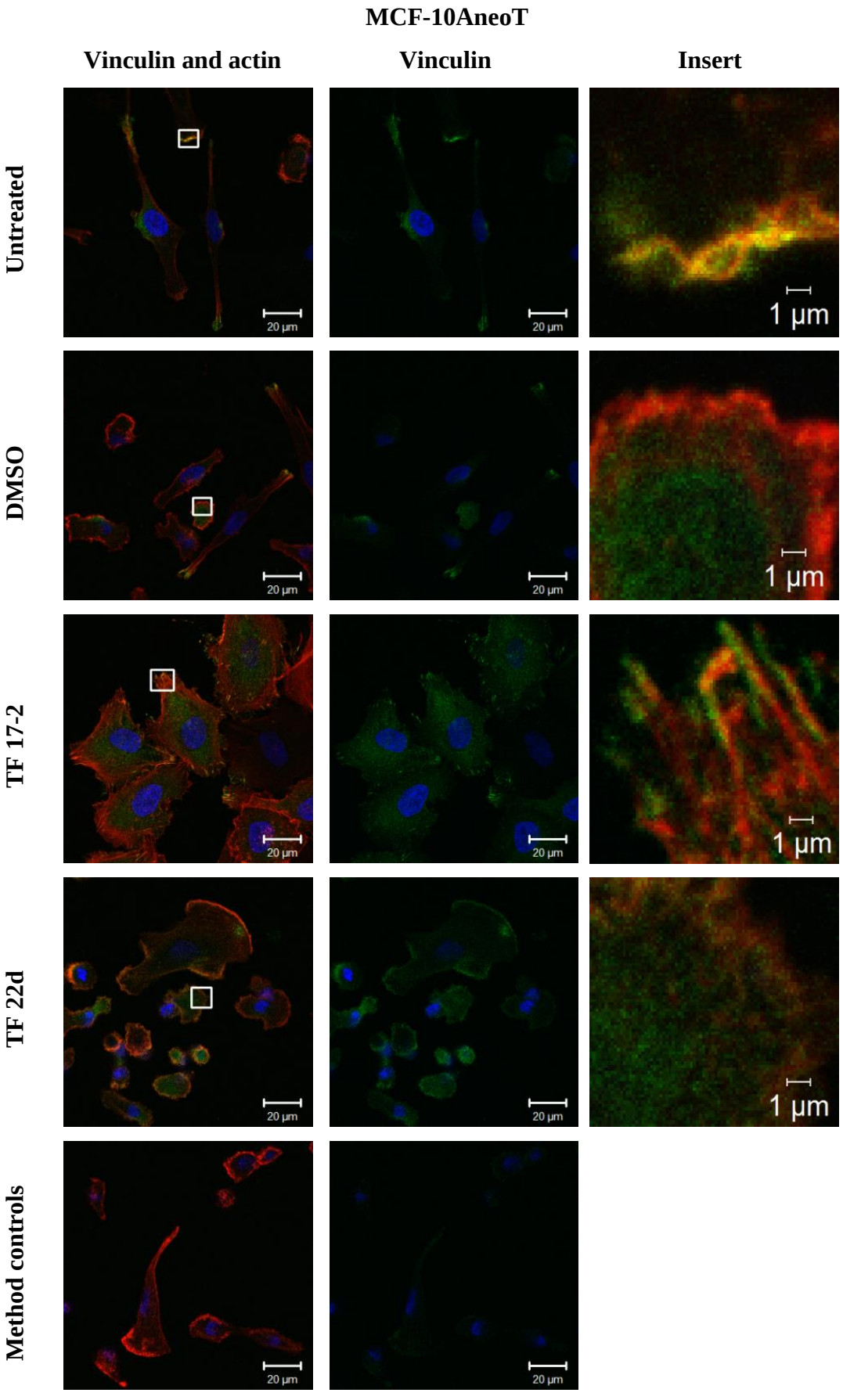
MCF-10AneoT
Vinculin and actin
Vinculin
Insert
Untreated
DMSO
TF 17-2
TF 22d
Method controls
20 µm
1 µm

Figure 5.10. Confocal images of migrating MCF-10AneoT cells labelled for F-actin (red) and vinculin (green).

Immunocytochemistry analysis of MCF-10AneoT cells migrating into a scratch-wound, fixed with 3.7% paraformaldehyde (10 min) 3 hours post wounding and probed as described in Section 6.2. Untreated and DMSO-treated non-spindle shaped cells present with unclustered or sparsely distributed vinculin (green) indicating nascent focal adhesions with little adherence. F-actin (red) staining shows membrane ruffling and unorganised actin branching. TF 17-2-treated cells show excellent integrin clustering resulting in cell spreading also shown by the organised actin cytoskeleton. TF 22d-treated cells show well developed FAs with sparsely distributed vinculin throughout cells. In addition, TF 22d-treated cells exhibited more rounded morphologies and showed less cell spreading with unorganised actin branching. Boxed areas in the left pane are reproduced at 20x magnification. Experiments were performed four times in duplicate viewing two frames per specimen. Vinculin method controls, containing no primary antibody, show no specific labelling of vinculin or other proteins by the secondary antibody.

5.6.4. Discussion

The literature on the relationship of FAs size and rate of migration is still confused, contradictory and counter-intuitive. Large stress fibre formation, associated with large FA formation, is reported to be indicative of a greater contractile force, since myosin-II bundles actin filaments and is responsible for sliding anti-parallel filaments across one another (Parsons et al., 2010). Intuitively, one may assume that a greater contractile force is produced and larger FAs seem to indicate high migration velocity. FAs, however, have reported to function at the ends of stress fibres as footholds for mechanical force but do not seem to be prominent in rapidly migrating cells (Ridley et al., 2003). In contrast, small focal adhesions, associated with small stress fibres, may be assumed to result in lower adherence to the substratum, and, therefore, require less time to disassemble, increasing velocity as has been previously suggested (Volberg et al., 1995; Xu et al., 1998), though it has also been reported that large FAs may also be associated with rapid movement (Defilles et al., 2011). This contradiction, therefore, remains uninvestigated in the context of breast epithelial cells.

In seemed rational to try to establish whether FA size influences migration velocity in breast epithelial cells, as vinculin-actin staining correlated with the migration rates/velocities in the scratch assay and live cell imaging and to use untreated and DMSO-treatment groups as basic controls for evaluating actin/vinculin staining in relation to that in inhibitor-treated breast epithelial cells.

FAs in MCF-10A cells treated with MMPIs

Untreated and DMSO-treated normal MCF-10A cells have large FAs in leading-edge cells migrating into the scratch-wound. If the predictions of Defilles et al. (2011) are accurate, these large FAs indicate rapid movement. The large FAs in the lamellipodia of leader cells on the edge of the wound are likely to be those of the normally fast migrating phenotypically normal, temporarily motile, breast epithelial cells. Such cells normally form an apically and basolaterally polarised cell monolayer, and a polarised phenotype transiently or partially lost here during migration, as cell-cell association is maintained (Debnath et al., 2003; Sharpless and DePinho, 2004). Considering the rate of movement, though this varies little with the various treatments, the size of the FA seems to correlate with velocity and accumulated distance reflected by the program used to analyse velocity.

The slowest migrating TF 17-2-treated MCF-10A cells exhibited sparsely distributed vinculin with localised areas of clustering within the lamellipodia. This was taken as being indicative of abnormal nascent FA formation due to treatment. In the scratch assay, MCF-10A collective cell migration seemed significantly inhibited in comparison to the DMSO and untreated controls. Live cell imaging, however, showed only a marginal reduction in migration velocity. The small size of the FAs within this treatment group may, therefore, be as a result of defective integrin maturation (Ratnikov et al., 2002).

Alternatively, processing of $\alpha_v\beta_3$ integrins has been shown to repress $\alpha_2\beta_1$ integrin-mediated migration of cells on type-I collagen. In the absence of processing or during inhibition of MT1-MMP, a lack of processing of $\alpha_v\beta_3$ integrins in the MCF-10A cells may decrease the functional activity of $\alpha_2\beta_1$ integrins affecting cell adhesion to collagen type-I (Baciu, 2003**)** and migration via a PI3K/Akt-dependent pathway (Defilles et al., 2011). This has been reported to result in activation of a PI3K/Akt independent-dependent pathway and a different form of migration (Defilles et al., 2011), perhaps by inhibiting MT1-MMP-mediated MMP-2 and MMP-7 activation. This may alter maturation of integrins and affect FA attachment to the ECM and FA turnover during ECM release. Concomitant reduction in MMP-2 and MMP-7 activity may further hinder the ECM modification and integrin cross-talk required for MCF-10A migration (Defiles et al., 2012). When correlated with velocity of movement, this would seem to indicate that smaller FAs result in slower movement in the MCF-10A cells. However, it should be remembered that the vinculin labelling and hence FA size measurements are being correlated here, in the case of the normal cell line, are those of cells in normal monolayer (associated with other cells). These are being correlated with the movement of single cells (albeit in a semi monolayer in the live cell imaging experiment) and those of single cells in only the live cell experiment in the case of the MCF-10AneoT cells.

The collective tensile force generated by TF 17-2-treated leading edge cells would be anticipated to be lower due to the small size of the FAs and the formation of less organised actin and vinculin associations compared to those produced in DMSO and untreated cells. This hypothesis correlates well with the scratch assay conducted on MCF-10A cells on plastic, as significant inhibition of migration is observed after 3 hours (Figure 5.6). Such a result suggests that TF 17-2 hinders FA formation and turnover in the MCF-10A cell line, lowering tensile forces, through MMP inhibition, resulting in a slower collective migration rate. This occurs without noticeable differences in individual cell velocities, as shown in live cell imaging during the initial 3 hour period. This tends to validate our approach.

MCF-10A cells treated with TF 22d, however, exhibit large FAs and cell-cell contacts at lamellipodia. Such large FAs may be indicative of strong traction forces and rapid movement of some leader cells in normal cells. Concomitant increases in intercellular cohesion of leader cells between their lamellipodia seem to promote better directional persistence. These intercellular contacts may be tension-bearing sites that mediate mechanical force (le Duc et al., 2010). The collective migration observed in scratch assays showed that TF 22d inhibits collective migration rates less than TF 17-2. We suggest, therefore, that the TF 22d enhances FA maturation and turnover and promotes intercellular contacts at lamellipodia during collective migration, through an as yet, undetermined mechanism that must be different from the MT1-MMP-mediated normal mechanism and possibly via different integrins.

Taken together with vinculin and actin labelling results, these suggest that TF 22d-induces a subtle increase in FA size to better facilitate collective cell migration resulting in a similar migration rate due to similar adherence and FA turnover, compared to control groups in MCF-10A cells on plastic, despite the presence of the inhibitor.

In summary, initially it was thought that, under the influence of MMPIs, ECM or FA processing may become disrupted resulting in impaired migration velocity. If we now examine our results for the MCF-10A cells treated with inhibitors these results do not entirely seem to confirm our hypothesis and show that any disruption in FA formation due to MT1-MMP inhibition, does result in slower collective migration, relative to control groups (except in the case of treatment with the TF 17-2 inhibitor). Relative to the control groups, vinculin staining in both inhibitor-treated groups was generally higher. Previous studies have shown that low vinculin labelling, seen here in all control groups, may indicate an increased migration rate (Volberg et al., 1995; Xu et al., 1998) and thus, the observed high vinculin labelling indicates that we should anticipate decreased migration rates in inhibitor-treated cells, as observed.

FAs in MCF-10AneoT treated with MMPIs

Terminal FA formation by spindle-shaped MCF-10AneoT cells is possibly best explained by considering fibroblast behaviour as these sometimes exhibit similar morphologies. In fibroblasts, the rearmost adhesions often tether the cell strongly to the substratum, resulting in a long tail anchored to the site of adhesion. The tension is sufficient to physically break the linkage between integrins and the actin cytoskeleton. The result is that the integrins are left behind while the rest of the cell moves on (Ridley et al., 2003). Such failed detachment of a cell's trailing end has been observed in the MCF-10AneoT cell line. This may explain FA formation in spindle-shaped MCF-10AneoT cells as reduction in cell volume and an accumulation of actin and its association partners at trailing ends. This produces FAs sites that seem to label for vinculin. Overall, the DMSO and untreated MCF-10AneoT cells appear to stain with low levels of vinculin and this has been associated with defective cell spreading and increased migration (Volberg et al., 1995; Xu et al., 1998).

The slower-migrating TF 17-2 treated MCF-10AneoT cells also exhibited the most notable change in their morphology. These cells spread out assuming a flattened morphology with organised actin branching, possibly as a result, mature FAs along the outer perimeter (Figure 5.10, TF 17-2). Such vinculin positive FA formation may be indicative of clustered integrins that in normal cells, recruit ECM-degrading proteolytic enzymes to perform pericellular ECM remodelling to generate a path for migrating cells (Paňková et al., 2010). In addition, the formation of an organised actin cytoskeleton and mature FAs may indicate enhanced activation of ROCK, found to directly phosphorylate myosin

light chain-2 (MCL2) (Amano et al., 1996), enhancing myosin II ATPase activity allowing myosin II to become engaged in more efficient F-actin interactions (Mierke et al., 2008). (Figure 5.1).

In the MCF-10AneoT cell line, cell-cell contacts were not apparent (Figure 5.10) and, therefore, we cannot suggest a partial reversion from the premalignant to a normal epithelial phenotype. Nevertheless, in conjunction with the live cell imaging results for cell velocities, we propose that the inhibition of migration velocity in the MCF-10A cell line is due to better adherence to the substratum. This suggests, however, that the slight decrease in migration velocity of the MCF-10A cell line upon treatment with TF 17-2 was due to a prevention or delay of integrin maturation, as FAs are smaller than the FAs in the TF 17-2-treated MCF-10AneoT cells, a result opposite to that in the premalignant cell line (Figure 5.9 and 5.10, TF 17-2).

Such contradicting results observed between the normal and premalignant cell lines is possibly explained if we examine the effect H-Ras(V^{12}) transfection has on MT1-MMP trafficking. In normal cells active MT1-MMP plasma membrane levels are controlled and restricted to sites of pericellular proteolysis (Gonzalo et al., 2010). These sites are usually at the tips of lamellipodia, invadopodia, filopodia or podosomes (Frittoli et al., 2011; Lafleur et al., 2009). In cancer cells, active MT1-MMP levels are less stringently controlled, perhaps due to defective trafficking which alters caveolae function (Gálvez et al., 2003). The MCF-10AneoT cell line has been shown to have up-regulated MT1-MMP levels and a lack of directed MT1-MMP trafficking possibly due to an abundance of active and inactive MT1-MMP species occupying the plasma membrane evidently via uncontrolled or mistrafficking of MT1-MMP (Snyman, 2010).

Based on the above information, it would be anticipated that in caveolae, when MT1-MMP, mainly distributed in the front and back of normal MCF-10A migrating cells, is inhibited, FA formation, MT1-MMP-mediated ECM modifications and integrin maturation may be disturbed at localised protrusion sites. In contrast, in MCF-10AneoT cells, inhibition of MT1-MMP that is more generally distributed over the cell membrane may have a "whole cell effect" possibly limiting non-caveolae-associated MT1-MMP-mediated pericellular proteolysis, while inhibiting MT1-MMP in FAs, allowing FAs to form through non-MT1-MMP-mediated maturation and processing of integrins, resulting in actin polymerisation and a normally organised actin cytoskeleton. The observed differences in effect between treated cell lines may be that exposed, aberrantly trafficked, non-caveolae-associated MT1-MMP may be preferentially inhibited due to its more exposed position and less steric hindrance due to its presence in caveolae. This, in turn may create a situation where normal caveolae-associated MT1-MMP could maintain FA maturation without restoring normal migration, possibly due to mistrafficking of other essential, migration-associated molecules.

Thus, in MCF-10A cells, which require low levels of MT1-MMP trafficked to where CD44, and integrins are located in the invasion front-associated caveolae in order to migrate, TF 17-2-treated cells may show FA abnormalities when MT1-MMP is inhibited, compared to control groups. MCF-10AneoT, on the other hand, may demonstrate enhanced FA formation as, MT1-MMP signalling, in caveolae, is restored. This view tends to be upheld by the abnormal appearance of FAs and the actin cytoskeleton in the absence of TF 17-2 treatment of the MCF-10AneoTs.

Other possibilities are that the TF 17-2 inhibitor may be inhibiting other MT1-MMP-mediated processes resulting in depletion of ATP pools (Dang et al., 2009). This may reduce the functional capacity of the ATP-dependent force transducer, myosin-II during migration via a mechanism explained in Chapter 6.

TF 22d-treated MCF-10AneoT cells appeared to assume non-directional rounded morphologies resulting in unorganised actin branching and sparsely distributed vinculin labelling, except in FAs. Low general vinculin labelling may, however, be the best indication of high migration velocities in premalignant cells, as nascent FAs may be transient resulting in low adherence to the substratum (Paňková et al., 2010).

Less well formed or smaller FAs seem to correlate with reduced migration in MCF-10A cells and elevated migration velocities in MCF-10AneoT cells. We propose, therefore, that TF 22d may increase the invasive capability of premalignant MCF-10AneoT cells by inducing non-directional rounded morphologies, through an as yet undetermined mechanism that possibly involves other MMPs besides MT1-MMP. Due to MT1-MMP's ability to process integrin pro-forms, it has been shown that in MT1-MMP-deficient MCF7 cells, αvβ3 integrins suppressed the functional activity of the collagen-binding α2β1 integrin-receptor reducing adhesion to collagen type-I (Baciu et al., 2003). In contrast to TF 17-2, MCF-10A cells treated with TF 22d exhibit enhanced FA formation and cell-cell contacts, whereas the MCF-10AneoT cell line exhibited poor FA formation and maintenance. The mode of action of these inhibitors must, therefore, be different in these two cell lines.

In conclusion, scratch assays and live cell imaging of migration rates correlated well with the ICC images labeling for vinculin and actin. This study revealed that the migratory machinery of normal and premalignant cells is differentially affected by both inhibitors even though the inhibitors target the same MMPs with similar affinities, with the exception of MMP-7. TF 17-2 in both cell lines enhances cell spreading yet reduces FA size in MCF-10A cell and promotes FA formation in MCF-10AneoT cells. TF 22d on the other hand, promotes FA maturation in MCF-10A cells and exacerbates the premalignant state of MCF-10AneoT by inducing a rounded morphology and

increasing migration velocities. The possible influences of MMP-7 on epithelial migration will be further discussed in Chapter 6.

CHAPTER 6.

General discussion

6.1. MT1-MMP and breast cancer

Breast cancer has become the leading cancer diagnosed among women globally (Jemal et al., 2011). High mortality rate, especially in developing countries seem to be the result of late stage initial diagnosis and a lack of access to modern health care facilities (Jemal et al., 2011; Vorobiof et al., 2001). Late stage breast cancer usually spreads to the lymph nodes, brain, bone, lung or spinal cord before the patient is diagnosed, making treatment more difficult (Kang et al., 2003; Minn et al., 2005; Weil et al., 2005). Dissemination from the primary tumour is the first step in metastatic spread (Berx et al., 2007), a process mediated by proteolytic enzymes that facilitate the degradation of matrix barriers and cell-cell contacts (Itoh, 2006).

A number of MMPs have been shown to be highly up-regulated or overexpressed in late stage metastatic breast cancer, indirectly indicating a role in dissemination, invasion and metastasis (Kohrmann et al., 2009). MT1-MMP, together with MMP-2 are of particular interest in this field (Ishigaki et al., 1999) due to their broad substrate specificity especially in relation to the extracellular matrix proteins and cell surface molecules involved in migration and invasion (Table 1.1) (Deryugina et al., 2001; Folgueras et al., 2004; Strongin, 2010). Many studies have implicated MT1-MMP as a primary target. Recent studies using synthetic peptides and antibodies targeting the catalytic domain of MT1-MMP, show a significant reduction in tumour size and migratory ability of cells (Devy et al., 2009; Sela-Passwell et al., 2012; Suojanen et al., 2009) whereas MT1-MMP knockouts show no invasiveness (Sabeh et al., 2004). Many other studies have similarly shown MT1-MMP to be involved, not only in invasion but in many cancer-promoting events like genetic instability and mutation. MT1-MMP also seems intimately associated with the distinctive metabolic phenotype of a cancer cell and largely remains cell-associated, whereas, most other MMPs are secreted, making them poor targets, though they may assist invasion under certain circumstances (Folgueras et al., 2004). Since MT1-MMP remains plasma membrane associated and seems to have a role in malignant progression and invasion, such properties make MT1-MMP a good target for future therapies (Hernandez-Barrantes et al., 2000; Zucker et al., 2002).

6.2. Distinctive metabolic phenotype of a cancer cell and effects of TF 17-2

Cancer cells have a distinctive metabolic feature, their ability to metabolise under anoxic conditions and use glucose largely via glycolysis and not generate energy via the mitochondria, a phenotype facilitated by the hypoxia-induced factor (HIF). Since the primary role of the mitochondria is to

produce ATP molecules via oxidative phosphorylation, the global pool of ATP molecules in cancer cells is reduced resulting in enhanced anaerobic glycolysis to maintain ATP levels. Although oxidative phosphorylation produces 36 ATP molecules per glucose molecule, glycolysis only produces 2 ATP molecules per glucose. Anaerobic glycolysis is an inefficient way of synthesising ATP, but it is the more rapid mechanism for producing ATP (Chiche et al., 2010) and cancer cells have long been recognised to shift their metabolism toward anaerobic glycolysis to meet the energy demands of hyper-proliferation (Dang et al., 2009).

Another protein contributing to the cancer phenotype, is Myc. This has been proposed to regulate the metabolic activity required for G1/S transition and increased metabolic activity and expression of glycolytic enzymes such as lactate dehydrogenase A (LDHA), and several enzymes involved in nucleotide synthesis and ATP production (Shim et al., 1997). Ras(V^{12}) does this in a similar fashion. LDHA reduces pyruvate, derived from glucose during glycolysis, to lactate via an NAD^+/NADH dependent mechanism (Shim et al., 1997). Inhibition of LDHA, reduces the pool of ATP available, resulting in the reduction of cell proliferation (Fantin et al., 2006; Salomon et al., 2000). The LDHA reaction is, therefore, key in regenerating oxidized NAD^+ required to ensure continuous glycolysis and ATP production and cell proliferation.

There is a close association between the induction of MT1-MMP expression during hypoxic conditions, especially facilitated by Myc, a protein similarly associated with increased glycolytic activity. HIF-1 activity has also been shown to be induced through the loss or inactivation of p53, or oncogenic activation such as H-Ras(V^{12}) (Bárdos and Ashcroft, 2004). Thus, hypoxia related mechanisms may also be induced through Ras activation resulting in increased glycolysis and MT1-MMP expression. HIF seems to be linked to MT1-MMP expression as an HIF binding site affecting MT1-MMP transcription has been identified 125 bp from the transcription start site in the proximal promoter region of MT1-MMP (Petrella et al., 2005).

Another protein important in the regulation of glycolysis and is significantly increased in proliferating migratory neoplastic cancer cells with a high glycolytic rate (Chevrollier et al., 2005; Giraud et al., 1998) is the adenine nucleotide translocator 2 (ANT2) (Chevrollier et al., 2005). ANT2 catalyses ADP/ATP exchanges across the mitochondrial inner membrane and links the mitochondrial ATP production with cellular ATP consumption. ANT2 is also present at the cell's plasma membrane in addition to its usual location in the mitochondria plasma membrane (Radichev et al., 2009). Transcriptional silencing of ANT2 has been shown to induce apoptosis in human hormone-dependent breast cancer cells and inhibits tumour growth through a reduction in available intracellular ATP concentrations (Le Bras et al., 2006) likely due to the further destabilisation of the mitochondria (Chevrollier et al., 2005). ANT2 has been shown to associate with MT1-MMP (Radichev et al.,

2009). This association and the influence on metabolism remains to be determined (Loers et al., 2012; Radichev et al., 2009), however, one of the anomalies of the current study was that TF 17-2 seemed to suppress proliferation of MCF-10AneoT cells (evident by decreased cell counts) while increasing their metabolic activity (evident due to increased MTS assay values from significantly lower cell numbers).

Since the effects of the ANT2 association with MT1-MMP remain unknown, we propose that TF 17-2 may negatively or positively affect the association of ANT2 with MT1-MMP (Radichev et al., 2009) thereby disrupting ATP pools, reducing proliferation by encouraging NAD^+/NADH conversion via glycolysis and disrupting mitochondrial stability. Such results correlate well with toxicity assays performed by Kapischke et al. (2008). In the latter study PancTu-1 pancreatic tumours showed no toxic effects when treated with 300 µM TF 17-2, while at 3 mM, DNA-synthesis was reduced by 20% without inducing apoptosis. We propose that similar effects were seen in the current studies on epithelial cells, as the latter cells showed decreased proliferation without induction of apoptosis (as DNA levels are a direct indicator of cell number). The difference in tolerance of epithelial cells to TF 17-2 may, however, be cell type dependent.

Usually, increased or decreased proliferation rates are reflected with proportional increases or decreases in metabolic activity (Chiche et al., 2010). In this study, a decrease in proliferation accompanied by an increase in metabolism is not an anticipated result but may possibly be explained by the oncogenic transformation of MCF-10A by H-Ras(V^{12}), the lack of p16 and p14 (Zientek-Targosz et al., 2008) and subsequent loss of p53 activity, amplification of *MYC* in the MCF-10A cells (Debnath et al., 2003) and MT1-MMP's association with proteins such as ANT2 suggest that MT1-MMP expression may influence metabolism.

Transfection with oncogenic H-Ras(V^{12}) in MCF-10AneoT cells initiates a complex array of signal transduction pathways including the Raf/MAPK (ERK) pathway involved in plasma membrane-to-nucleus signalling independent of normal mitogen-induced cell proliferation (Robinson and Cobb, 1997), and the PI3K/AKT pathway (Section 1.3.2). This is involved in cell survival signalling (Larue and Bellacosa, 2005) while the associated Rac/Rho pathway is involved in cytoskeletal remodelling (Figure 6.1). H-Ras(V^{12}), therefore, may act by enhancing cell survival, proliferation, and cytoskeletal reorganisation facilitating cell migration and Myc activation (Kelekar and Cole, 1987) and accumulation (Sears et al., 2000), which may further contribute to MCF-10AneoT proliferation. With 2-fold higher ERK activation via H-Ras, a reduction in microtubule stability has been reported in the MCF-10AneoT cell line with subsequent increase in proliferation and exocytosis (Harrison and Turley, 2001). Enhancement of exocytosis may be as a result of the concomitant reduction in

cytoskeletal organisation and microtubule stability and may increase the surface presence of MT1-MMP.

Constitutively active H-Ras(V^{12}) promotes EMT, cell migration and invasion by down-regulating E-cadherin and up-regulating MT1-MMP (Figure 6.1), a process resulting in disruption of tight junctions. Epithelial tight junctions and adherens junctions (AJs) are anchored to F-actin and microtubules (Gooding et al., 2004). Irregularities in the AJ complex due to microtubule and actin instability may lead to the release of β-catenin from AJ complexes (Ivanov et al., 2006) and subsequent transcription of c-Myc, cyclin D1 and MT1-MMP (Figure 6.1) (Zucker and Cao, 2009). Therefore, Ras and Myc work collaboratively to stimulate survival, proliferation, migration and EMT pathways (Wang et al., 2011) resulting in MT1-MMP up-regulation and irregular cell surface distribution in cells with compromised microtubule stability and increasing exocytosis, as observed in MCF-10AneoT cells.

We hypothesised, based on results in the literature, that inhibition of MT1-MMP would reduce cancer cell migration. MMP inhibitors, however, have a concentration dependent effect, depending on the K*i* of the inhibitor. The two MMPIs used herein, have 100-fold selectivity for MT1-MMP over MMP-2 and were assessed for their (i): ability to "fit" into the active site of MT1-MMP and MMP-2, (ii): toxicity, over a range of concentrations, and (iii): their ability to hinder breast epithelial cell migration of normal and premalignant cells.

One of the aims of the current study was to compare known K*i* values for MT1-MMP and MMP-2 using computational molecular docking and assess how reliably modelling can predict K*i* values. These predictions of K*i*'s could then be used to substitute for *in vitro* assays to establish K*i*'s so that potential targets for inhibition, such as the related MT2-MMP, may be predicted without the necessity to perform *in vitro* kinetic assay.

6.3. Predictive docking, pharmacokinetics and toxicity

The molecular interactions of our synthetic inhibitors, TF 17-2 and TF 22d, with target proteins, MT1-MMP and MMP-2, assessed using AutoDock Vina (Trott and Olson, 2010) showed that the flexibility of the butanyl group of TF 17-2 imparted a binding efficiency that was not observed in TF 22d.

TF 17-2 was predicted to form monodentate coordination complexes with the Zn(II) of MT1-MMP and MMP-2, while sterically blocking the access of substrates to the S1'-pocket. TF 22d on the other hand, has less torsional flexibility than TF 17-2 and was predicted to form a monodentate co-ordination complex with MT1-MMP and a bidentate co-ordination complex with MMP-2. The *in*

silico affinity constants determined from the free energy of binding values did not correlate with *in vitro* affinity constants performed by Fischer, however (2004). This may be due to a shortage of parameters relating to the zinc ion when using empirical force fields in AutoDock Vina (Tuccinardi et al., 2006). *In silico* studies suggested that inflexible groups within MMPIs are more likely to achieve selectivity and low free energy values whereas flexible MMPIs may allow multiple interactions reducing the incidence of a low free energy of binding when local steric groups influence binding. This means that *in silico* studies using AutoDock Vina and our compounds may have shown a preference for less flexible molecules during LGA ranking and docking scoring. We, therefore, found that it was possibly safer to rely less on predictions and rely more on *in vitro* affinity results (Table 3.2), since predictive docking results did not recapitulate *in vitro* K*i* affinity assays, but rather, showed identical affinity of TF 17-2 and TF 22d for MT1-MMP with 100-fold lower affinity for MMP-2. These results suggest that predictions of inhibitor potency must be interpreted with caution.

Upon further investigation of the experimental conditions used for the *in vitro* K*i* assays performed by Fischer (2004), it was found that the experiments were carried out at suboptimal temperatures (25°C). In addition, the final DMSO concentration in serial dilutions of fluorogenic substrates varied from a final concentration of 0.5-1% (v/v) DMSO (Kapischke et al., 2008). This may be a potential problem as a final concentrations of DMSO of 1-3% (v/v) have been shown to perturb enzyme structure and function by disrupting hydrophobic substrate interactions (Overall, 2002; Xu et al., 2004) and significantly reduce MMP-2 gelatinolytic activity by 64-79% (Murphy et al., 1994). *In vitro* K*i* values also, therefore, may be unreliable predictors in this instance.

The use of 1% (v/v) DMSO as a solvent for MMP substrates was previously common practice in enzyme assays (Polette et al., 1999). The influences of DMSO on all MMP activity urgently requires further investigation to either rule out DMSO as a suitable solvent for enzyme assays or establish a maximum standard DMSO concentration for future enzymatic experiments. *In vitro* affinity results may still prove valid in the context of this study as we used final DMSO concentration of 0.05% (v/v), however, the suboptimal temperature conditions remains a questionable aspect in the context of *in vitro* enzyme-inhibitor affinity assays.

One highly important aspect relating to inhibitor testing for target enzyme inhibition is the test for toxicity in the relevant biological system. To this end inhibitor toxicity was assessed using a metabolic indicator, MTS, and the possible induction of apoptosis or necrosis was assessed using flow cytometry. The metabolic assay revealed TF 22d to be non-toxic overall. TF 17-2, on the other hand, reduced the metabolic activity of MCF-10A cells at 300 µM and appeared to increase the metabolism of MCF-10AneoT cells while suppressing their proliferation. Such results for TF 17-2 satisfied our requirements for a suitable MMPI and further applications to test our hypothesis was conducted. We

performed migration assay to test the hypothesis that the inhibition of MT1-MMP will reduce breast cancer cell migration.

6.4. Inhibition of cell migration

Only TF 17-2 (Kapischke et al., 2008) and not TF 22d has previously been tested in cell migration assays. Since MCF-10A cells have been shown to up-regulate MT1-MMP during migration (Gilles et al., 2001), we tested these MMPIs for their ability to inhibit cell migration using the scratch wound assay. Both MMPIs significantly reduced collective cell migration during wound closure, however, TF 17-2 reduced single cell migration during wound closure in the MCF-10AneoT cells and only very slightly in the MCF-10A cells. TF 17-2 appeared to inhibit wound closure 20% more than TF 22d and we suggest that TF 17-2 slightly hinders FA formation and turnover thereby lowering tensile forces applied to natural ECM deposits on plastic in MCF-10A cells and hence migration. On the other hand, TF 17-2 treated MCF-10AneoT cells showed a subtle enhancement of FA size resulting in a reduction of migration rate compared to control groups, possibly due to the disruption of ATP pools contributing to reduced myosin-II activity. In addition, fluorescence labelling showed that TF 17-2 induced the formation of an organised actin cytoskeleton in MCF-10AneoT cells and mature FAs that resulted in a spread out flattened morphology. TF 22d on the other hand, reduced MCF-10AneoT cellular adherence inducing a rounded morphology resulting in an increase in migration velocity.

The TF inhibitors have not been screened against subfamilies of metzincins with which they may possibly interact as they have a similar catalytic domain (Fisher and Mobashery, 2006; Lopez-Otin and Matrisian, 2007). ADAM proteases are functionally similar to MT-MMPs in their capacity to remodel ECM, affect integrin adherence and cell-cell adhesions (Seals and Courtneidge, 2003; White, 2003). Thus, we are uncertain whether such proteases may have influenced results. TF 17-2 and TF 22d used in this study are two MMPIs that were previously assayed for their inhibitory activity on many MMPs, including MMPs with anti-tumour activity (Table 3.2) (Fischer, 2004). The genetically similar MCF-10A and MCF-10AneoT cell lines, however, do not express MMPs-8, -12, and -13, MMPs also inhibited to some degree (unpublished data).

Table 6.1. Summary of the effects of TF 17-2 and TF 22d on normal and premalignant epithelial breast cells.

	MCF-10A		MCF-10AneoT	
	TF 17-2	TF 22d	TF 17-2	TF 22d
Metabolism	↓	⇔	↑	⇔
Proliferation	⇔	⇔	↓	⇔
Toxicity	None	None	None	None
Wound closure	↓↓	↓	n/a	n/a
Velocity	⇔	⇔	↓	↑↑
FA formation	↓	↑	↑	↓
Actin organisation	↑	↑	↑↑	↓

Increase (↑), decrease (↓), no change (⇔).

Table 6.1 is a summary of the most important findings of this study. We see that, TF 22d appears to be non-toxic and decreases normal cell wound closure but appears to increase migration of premalignant cells *in vitro* when grown in 2D on collagen type-I by reducing adherence and promoting rounded-cell morphology. TF 22d, therefore, does not seem an optimal choice for treatment of premalignant cells, according to the cell model used in this study. TF 17-2 on the other hand, produced results that showed a selective anti-proliferative effect in the premalignant cell line via an as yet unspecified metabolic mechanism, and suppressed oncogenic transformation effects resulting in the treated cells regaining an organised actin cytoskeleton and mature focal adhesions, satisfying criteria for further tests as an ancillary to anticancer drugs.

6.5. Future research and implications of this study

Further experimentation is required to assess the ERK activation levels and possible suppression of genes associated with H-Ras oncogenic transformation, such as *Snail*, *Twist-1*, *E-cadherin*, and *MMP-2* (Batlle et al., 2000; Elloul et al., 2005; Moon et al., 2000; Nairismagi et al., 2012), when treated with TF 17-2. These studies will establish whether this inhibitor and its target can elicit the suppression of the aforementioned transcription factors for phenotype reversion. Through the inhibition of MT1-MMP we may be able to restore cell-cell contacts by reducing MT1-MMP cleavage of E-cadherin and decrease MT1-MMP mediated ERK activation (D'Alessio et al., 2008; Takino et al., 2010), possibly inducing a normal phenotype (Figure 6.1).

The MCF-10AneoT cell line has previously undergone a reversion of phenotype, exhibiting cell-cell contact with a localised distribution of E-cadherin as an indicator of a normal phenotype (Li and Mattingly, 2008). These studies used MCF-10AneoT cells transfected with E-cadherin and incubated with ERK MAPK inhibitor (PD184352) for 3 days to elicit a partial phenotype reversion which is evidence for the pathway outlined in Figure 6.1. In a separate study, H-Ras(V^{12}) of MCF-10AneoT

cells has been shown to produce 2-fold higher ERK activation level than the parental cell line, MCF-10A (Harrison and Turley, 2001). Harrison and Turley (2001) also reported that the microtubules in MCF-10AneoT cell line were unstable due to defective acetylation. Microtubules serve as tracks for cellular transport and regulate cell shape and polarity, all of which are required functions for cell motility (Elbaum et al., 1999). Unstable microtubules are reorganised and form cellular extensions and lamellipodia rapidly during migration or invasion (Gloushankova et al., 1995). Such rapid reorganisation promotes the exocytosis of molecules important for ECM degradation, such as MMPs (Harrison and Turley, 2001) and enhances proliferation as the formation of the mitotic spindle during interphase requires an estimated 20- to 100-fold decrease in microtubule stability (Jordan and Wilson, 1998). In such an instance where constitutive Ras signalling may be overcome resulting in phenotype reversion, we propose that, through the inhibition of MT1-MMP we may be able to restore cell-cell contacts by reducing MT1-MMP cleavage of E-cadherin and decrease MT1-MMP mediated ERK activation (D'Alessio et al., 2008; Takino et al., 2010), possibly inducing a normal phenotype. The biochemical signalling pathway that could be involved in this reversion is outlined in Figure 6.1 and depicts the influence of up-regulated levels of MT1-MMP on cell migration/EMT.

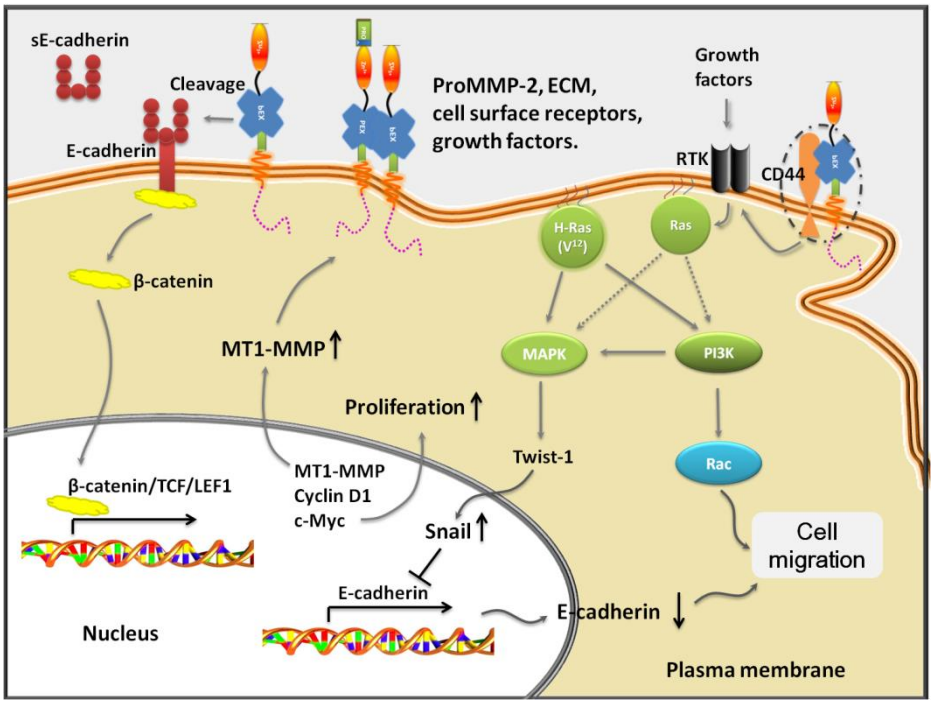

Figure 6.1. Constitutively active H-Ras(V^{12}) promotes EMT, cell migration and invasion by down-regulating E-cadherin and up-regulating MT1-MMP.
MT1-MMP cleavage of E-cadherin-β-catenin complex results in β-catenin translocation into the nucleus where it acts as a transcription factor along with TCF/LEF1 to up-regulate genes responsible for proliferation such as c-Myc and Cyclin D1, and MT1-MMP. MT1-MMP up-regulation increases active MMP-2 levels that contribute to the processing of many ECM constituents, cell surface receptors and growth factors. Heterodimerisation of MT1-MMP with CD44 and growth factors activate receptor tyrosine kinases (RTKs) that in turn activate Ras. Stimulated Ras and/or constitutively active H-Ras(V^{12}) signal through MAPK (ERK), PI3K and Rac promoting cell migration. MAPK signals to the nucleus leading to EMT by enhancing Twist-1 and Snail activation and subsequently decreasing E-cadherin transcription [reconstructed from Zucker and Cao (2009)].

In this study we showed that MMPI mediated inhibition of premalignant cell-migration and reconstitution of stable F-actin assembly is possible. The broader implications of these findings is that inhibition of MT1-MMP may reduce ECM modifications resulting in decreased ERK MAPK activation levels. The resultant decreased ERK promotes the expression of E-cadherin sequestering beta-catenin in cell-cell adhesion junctions reducing transcription of pro-migratory factors. Such a reduction in pro-migratory factors may decrease stimulation of the EMT/migratory phenotype thereby negating effects of constitutive signalling by H-Ras(V^{12}). In addition, inhibition of MT1-MMP may restore cell-cell contacts, by reducing MT1-MMP-mediated cleavage of E-cadherin, and decrease MT1-MMP-mediated ERK activation (D'Alessio et al., 2008; Takino et al., 2010), possibly inducing a normal phenotype.

Future studies using MCF-10AneoT cells in 3D culture grown in the presence of added extracellular constituents may provide an environment that better represents *in vivo* conditions. Such studies can use real time PCR to quantitatively assess transcriptional levels of *Snail*, *Twist-1*, *E-cadherin*, *MT1-MMP* and *MMP-2* when cells are treated with TF 17-2 or TF 22d. To broaden the validity of these future studies, multiple cancer and non-cancer cell lines should be utilised.

6.6. Concluding remarks

MT1-MMP remains an attractive anti-invasive, anti-cancer therapeutic target for late stage invasive breast cancers. Accordingly, Perentes et al. (2011) found that MT1-MMP is more prevalent during blood vessel invasion than lymphatic vessel invasion in 102 breast cancer biopsies. This finding further corroborates the role MT1-MMP plays in metastatic dissemination and vascular survival in late stage cancers.

In the current study, we tested whether the freeware program, AutoDock Vina, could be used as a reliable substitute for assessing the inhibitory constant, K*i*, in situations where *in vitro* kinetic assays are not possible or affordable. *In silico* predictions of TF 17-2 and TF 22d binding to MT1-MMP and MMP-2 showed inconsistencies in binding poses possibly as a result of differences in torsional flexibility between distinguishing R-groups of these MMPIs. We found that *in silico* binding affinity correlated poorly with established *in vitro* kinetic assay results. Such poor correlation was due to a lack of empirical parameters for zinc ions (Tuccinardi et al., 2006) by AutoDock Vina and *in vitro* kinetic assay data that was derived under suboptimal temperature conditions. In addition, we concluded that *in vitro* kinetic studies for MMPs require global standardisation of experimental procedures and reassessment to achieve a reliable comparison between *in vitro* and *in silico* experiments.

We assessed the toxicity of TF 17-2 and TF 22d to ensure a safe maximum concentration for use on epithelial cells of similar concentrations to those established in a previous study (Kapischke et al., 2008). TF 22d was found to be non-toxic to normal and premalignant epithelial cell lines at the concentration range tested. TF 17-2, on the other hand, showed a selective suppression of proliferation in the premalignant cell line with a concomitant increase in metabolic activity, possibly due to a disruption of MT1-MMP associations with ANT2. Incongruously, a significant reduction in metabolic activity that did not affect proliferation in the non-transformed MCF-10A cell line was noted. Such a result for TF 17-2 suggests that this MMPI selectively influences premalignant cells or cells with the H-*ras*(V^{12}) oncogene.

Another aim of this study was to assess whether the inhibition of MT1-MMP would reduce cell migration. TF 17-2 did indeed inhibit cell migration, with treated cells exhibiting enhanced adhesive and cytoskeletal structures suggesting a suppression of the effects induced by H-Ras(V^{12}). TF 22d on the other hand, increased premalignant cell migration and reduced cytoskeletal organisation through an as yet undetermined mechanism. The experimental system used in this study, however, did not provide a multitude of ECM and ECM constituents on which the cells could adhere. In a case where multiple ECM structures and components are available, the observed rounded cell morphology of the MCF-10AneoT cell line may not have occurred due to better cell adherence. Thus, TF 22d warrants further investigation using invasion assays or assays with ECM constituents that recapitulate the *in vivo* environment more effectively.

In conclusion, the preliminary results provided herein revealed that TF 17-2 is a promising anti-cancer drug candidate exhibiting three mechanisms of action. TF 17-2 inhibited MT1-MMP-mediated migration, and possibly invasion since these programs use similar biochemical mechanisms. Such a property may reduce metastatic spread in patients. In addition, TF 17-2 reduces premalignant cell proliferation, suggesting this drug could manage tumour size and symptoms. One very promising mechanism of action of TF 17-2 was the concomitant increase in metabolic activity with suppression of proliferation. Such increased metabolic activity may be capitalised upon by using TF 17-2 in combination with a chemotherapeutic agent that targets highly metabolically active cells. TF 22d appeared to be a less suitable MMP inhibitor, increasing premalignant cell migration velocity and potentially metastasis.

Multiple applications are possible for TF 17-2 or TF 22d if proven successful in future studies. Inhibition of MT1-MMP may reduce mortality of late stage breast cancer patients, and since MT1-MMP is implicated in other degenerative diseases such as Alzheimer's, multiple sclerosis, arthritis, osteoporosis and cardiac remodelling post infarction (Fingleton, 2008; Tam et al., 2002; Yong et al., 2001), these MMPIs may provide additional treatment options.

Appendix

A. Antibodies

Table A.1. Antibodies (Ab) and markers used in ECL and immunocytochemistry (ICC).

Ab/marker	Exp. use	Working dil./conc.	Ext/Em (nm)	Manufacturer
1° Chicken anti-ProCat IgY (raised against human MT1-MMP)	ECL	50 µg/ml	N/A	Produced by our laboratory
2° Rabbit anti-chicken-HRPO IgG (monoclonal)	ECL	1:15000	N/A	Sigma-Aldrich
1° Rabbit anti-GAPDH IgG (raised against human GAPDH)	ECL	0.1 µg/ml	N/A	Santa Cruz Biotechnology, Inc.
2° Goat anti-rabbit-HRPO IgG	ECL	1:12000	N/A	Sigma-Aldrich
1° Mouse anti-vinculin monoclonal (raised against human vinculin)	ICC	1:1000	N/A (1° Ab)	Sigma-Aldrich
2° Rabbit anti-mouse- DyLite 488	ICC	1:800	493/518	Thermo Fisher Scientific
Hoechst 33342	ICC	1:5000	343/483	Thermo Fisher Scientific
Phalloidin-TRITC	ICC	1:10000	547/572	Sigma-Aldrich

B. Flow cytometry

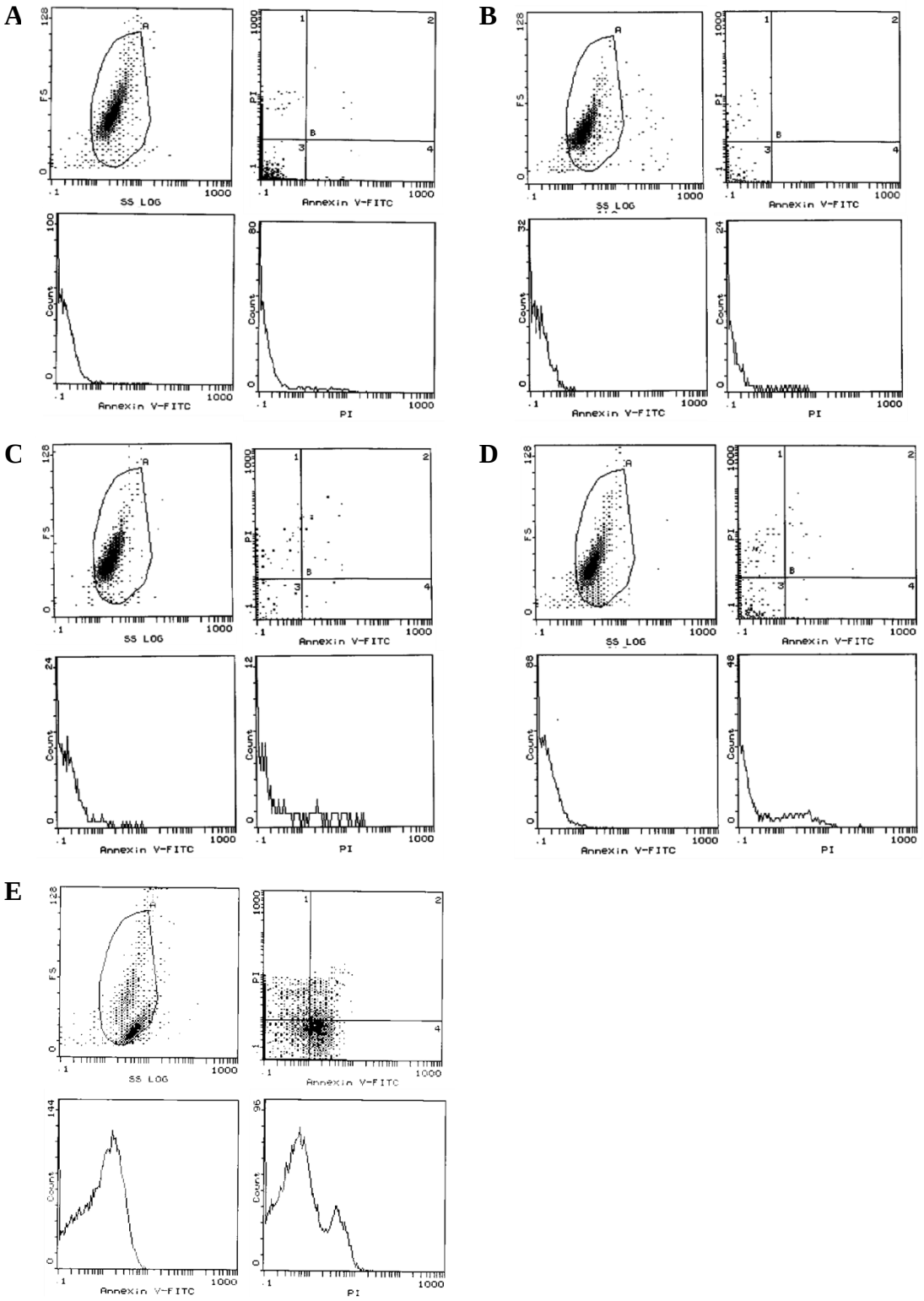

Figure B.1. Sample data generated by the annexin V-FITC/PI apoptosis assay from MCF-10A using flow cytometry.
(**A**) TF 22d (300 µM), 66 084 events. (**B**) TF 17-2 (300 µM), 16 351 events. (**C**) DMSO (0.05% (v/v)), 17 290 events. (**D**) Untreated, 57 201 events. (**E**) Cycloheximide (200 µg/ml) 40 938 events. Cells were treated as described in Section 4.4.4

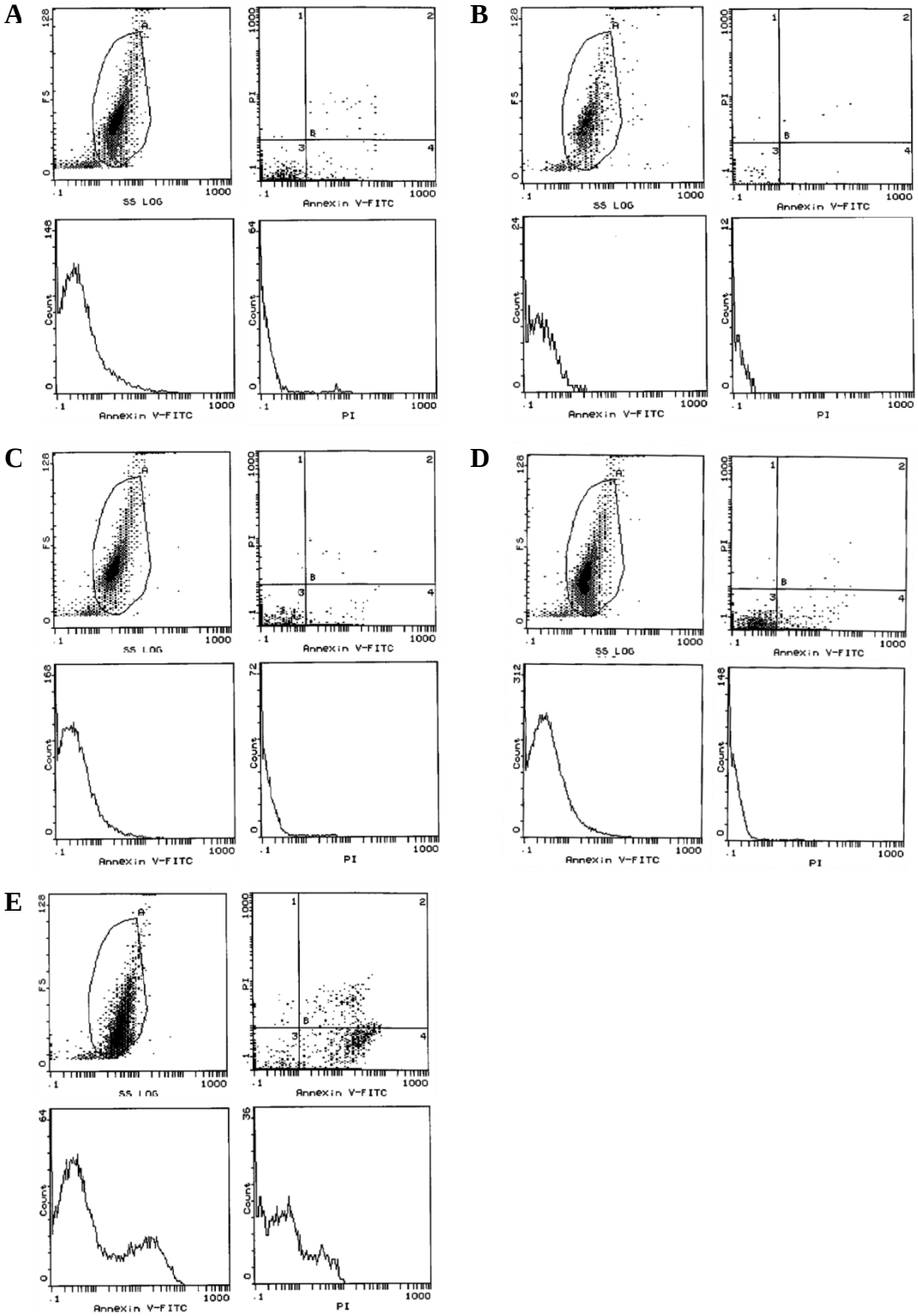

Figure B2. Sample data generated by the annexin V-FITC/PI apoptosis assay from MCF-10AneoT using flow cytometry.

(**A**) TF 22d (300 µM), 50 510 events. (**B**) TF 17-2 (300 µM), 6 518 events. (**C**) DMSO (0.05% (v/v)), 58 418 events. (**D**) Untreated, 41 903 events. (**E**) Cycloheximide (200 µg/ml) 21 616 events. Cells were treated as described in Section 4.4.4.

C. Metabolic stability of TF 17-2.

A major concern of any new drug is its half life *in vivo*. Good bioavailability or a good pharmacokinetic profile means that a drug will maintain functional efficacy *in vivo* long enough to exert its desired effect. Prior to use in animal models, such information is useful for dosing and treatment schemes (Guengerich, 2007). Thus, TF 17-2 metabolic stability was examined prior to injection into SCID/bg mice during the study conducted by Kapischke et al. (2008)

A common initial study is usually 'microsomal stability' to predict if a drug will be eliminated too rapidy. These microsomes contain cytochrome P450s, an essential group of enzymes involved in the metabolism of drugs, and account for ~75% of drug metabolism (Guengerich, 2007). Microsomal stability, therefore, provides a good initial assessment of drug tolerance to metabolic processes.

Figure C.1, shows the high pressure liquid chromatography (HPLC) analysis results of various incubations of TF 17-2 with microsomes. Testosterone was used as a method control and showed changes to its molecular structure a two hour incubation, whereas, TF 17-2 remained unaffected. It was therefore concluded by our collaborators that TF 17-2 exhibited a good pharmacokinetic profile (Fischer, 2004) and significantly reduced PDAC tumour size in SCID/bg mice through MMP inhibition (Kapischke et al., 2008).

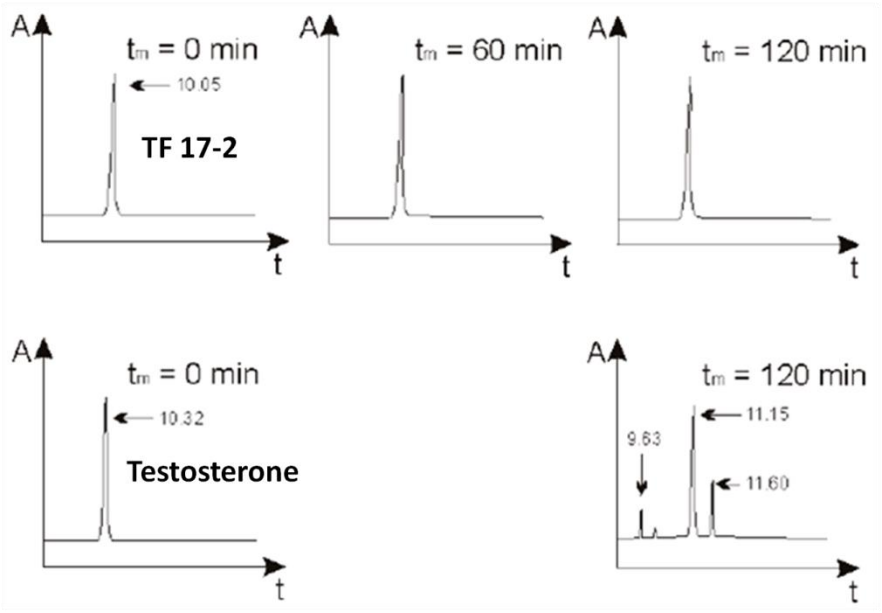

Figure C.1. Metabolic stability of TF 17-2 (Fischer, 2004).
Testosterone was used as a control for the detection of microsomal activity. Selected conditions: sodium phosphate buffer, pH 7.4, 37°C, incubation period: 60, 120 min, analytical column Aquapore OD-300 C_{18}, pore size 7 µm, temperature of column 30°C, λ 221 nm.

References

ACD/ChemSketch (2005). Advanced Chemistry Development. Toronto, ON, Canada *(version 8.17)*, www.acdlabs.com.

Ahn, S.M., Jeong, S.J., Kim, Y.S., Sohn, Y., and Moon, A. (2004). Retroviral delivery of TIMP-2 inhibits H-ras-induced migration and invasion in MCF-10A human breast epithelial cells. Cancer Lett *207*, 49-57.

Al-Ejeh, F., Smart, C.E., Morrison, B.J., Chenevix-Trench, G., López, J.A., Lakhani, S.R., Brown, M.P., and Khanna, K.K. (2011). Breast cancer stem cells: treatment resistance and therapeutic opportunities. Carcinogenesis *32*, 650-658.

Albini, A., Melchiori, A., Santi, L., Liotta, L.A., Brown, P.D., and Stetler-Stevenson, W.G. (1991). Tumor Cell Invasion Inhibited by TIMP-2. Journal of the National Cancer Institute *83*, 775-779.

Amano, M., Ito, M., Kimura, K., Fukata, Y., Chihara, K., Nakano, T., Matsuura, Y., and Kaibuchi, K. (1996). Phosphorylation and Activation of Myosin by Rho-associated Kinase (Rho-kinase). Journal of Biological Chemistry *271*, 20246-20249.

Andarawewa, K.L., Boulay, A., Masson, R., Mathelin, C., Stoll, I., Tomasetto, C., Chenard, M.-P., Gintz, M., Bellocq, J.-P., and Rio, M.-C. (2003). Dual Stromelysin-3 Function during Natural Mouse Mammary Tumor Virus-ras Tumor Progression. Cancer Research *63*, 5844-5849.

Anilkumar, N., Uekita, T., Couchman, J.R., Nagase, H., Seiki, M., and Itoh, Y. (2005). Pamitoylation at Cys574 is essential for MT1-MMP to promote cell migration. The FASEB Journal, express article 10.1096/fj.1004-3651fje.

Aplin, A.E., Howe, A., Alahari, S.K., and Juliano, R.L. (1998). Signal Transduction and Signal Modulation by Cell Adhesion Receptors: The Role of Integrins, Cadherins, Immunoglobulin-Cell Adhesion Molecules, and Selectins. Pharmacol Rev *50*, 197-264.

Bachman, K.E., Argani, P., Samuels, Y., Silliman, N., Ptak, J., Szabo, S., Konishi, H., Karakos, B., Blair, B.G., Lin, C., *et al.* (2004). The *PI3KCA* gene is mutated with high frequency in human breast cancers. Cancer Biology & Therapy *3*, 772-775.

Baciu, P.C., Suleiman, E.A., Deryugina, E.I., and Strongin, A.Y. (2003). Membrane type-1 matrix metalloproteinase (MT1-MMP) processing of pro-α_v integrin regulates cross-talk between $\alpha_v\beta_3$ and $\alpha_2\beta_1$ integrins in breast carcinoma cells. Experimental Cell Research *291*, 167-175.

Bakolitsa, C., Cohen, D.M., Bankston, L.A., Bobkov, A.A., Cadwell, G.W., Jennings, L., Critchley, D.R., Craig, S.W., and Liddington, R.C. (2004). Structural basis for vinculin activation at sites of cell adhesion. Nature *430*, 583-586.

Balbín, M., Fueyo, A., Tester, A.M., Pendás, A.M., Pitiot, A.S., Astudillo, A., Overall, C.M., Shapiro, S.D., and López-Otín, C. (2003). Loss of collagenase-2 confers increased skin tumor susceptibility to male mice. Nature Genetics *35*, 252-256.

Bar-Sagi, D. (2001). A Ras by any other name. Molecular and Cellular Biology *21*, 1441-1443.

Bárdos, J.I., and Ashcroft, M. (2004). Hypoxia-inducible factor-1 and oncogenic signalling. BioEssays *26*, 262-269.

Barkan, D., Green, J.E., and Chambers, A.F. (2010). Extracellular matrix: A gatekeeper in the transition from dormancy to metastatic growth. European Journal of Cancer *46*, 1181-1188.

Barltrop, J.A., Owen, T.C., Cory, A.H., and Cory, J.G. (1991). 5-(3-carboxymethoxyphenyl)-2-(4,5-dimethylthiazolyl)-3-(4-sulfophenyl) tetrazolium, inner salt (MTS) and related analogs of 3-(4,5-

dimethylthiazolyl)-2,5-diphenyltetrazolium bromide (MTT) reducing to purple water-soluble formazans as cell-viability indicators. Bioorg Med Chem Lett *1*, 611-614.

Basolo, F., Elliott, J., Tait, L., Chen, X.Q., Maloney, T., Russo, I.H., Pauley, R., Momiki, S., Caamano, J., Klein-Szanto, A.J.P., *et al.* (1991). Transformation of Human Breast Epithelial Cells by c-Ha-ras Oncogene. Molecular Carcinogenesis *4*, 25-35.

Batlle, E., Sancho, E., Franci, C., Dominguez, D., Monfar, M., Baulida, J., and Garcia de Herreros, A. (2000). The transcription factor Snail is a repressor of E-cadherin gene expression in epithelial tumour cells. Nat Cell Biol *2*, 84-89.

Bearden Jr, J.C. (1978). Quantitation of submicrogram quantities of protein by an improved protein-dye binding assay. Biochimica et Biophysica Acta (BBA) - Protein Structure *533*, 525-529.

Berg, K., Zhai, L., Chen, M., Kharazmi, A., and Owen, T.C. (1994). Thye use of a watersoluble formazan complex to quantitate the cell number and mitochondiral function of Leishmania major promastigotes. Parasitiol Res *80*, 235-239.

Bertram, J.S. (2001). The molecular biology of cancer. Molecular Aspects of Medicine *21*, 167-223.

Berx, G., Raspé, E., Christofori, G., Thiery, J., and Sleeman, J. (2007). Pre-EMTing metastasis? Recapitulation of morphogenetic processes in cancer. Clinical and Experimental Metastasis *24*, 587-597.

Bhat-Nakshatri, P., Appaiah, H., Ballas, C., Pick-Franke, P., Goulet, R., Badve, S., Srour, E., and Nakshatri, H. (2010). SLUG/SNAI2 and Tumor Necrosis Factor Generate Breast Cells With CD44+/CD24- Phenotype. BMC Cancer *10*, 411.

Bigg, H.F., Morrison, C.J., Butler, G.S., Bogoyevitch, M.A., Wang, Z., Soloway, P.D., and Overall, C.M. (2001). Tissue Inhibitor of Metalloproteinases-4 Inhibits But Does Not Support the Activation of Gelatinase A via Efficient Inhibition of Membrane Type 1-Matrix Metalloproteinase. Cancer Research *61*, 3610-3618.

Biname, F., Pawlak, G., Roux, P., and Hibner, U. (2010). What makes cells move: requirements and obstacles for spontaneous cell motility. Molecular BioSystems *6*, 648-661.

Blagg, J.A., Noe, M.C., Wolf-Gouveia, L.A., Reiter, L.A., Laird, E.R., Chang, S.-P.P., Danley, D.E., Downs, J.T., Elliott, N.C., Eskra, J.D., *et al.* (2005). Potent pyrimidinetrione-based inhibitors of MMP-13 with enhanced selectivity over MMP-14. Bioorganic & Medicinal Chemistry Letters *15*, 1807-1810.

Böhm, H.-J. (1994). The development of a simple empirical scoring function to estimate the binding constant for a protein-ligand complex of known three-dimensional structure. Journal of Computer-Aided Molecular Design *8*, 243-256.

Bos, J.L. (1989). *Ras* oncogenes in human cancer: a review. Cancer Research *49*, 4682-4689.

Bourguignon, L.Y.W., Gilad, E., Brightman, A., Diedrich, F., and Singleton, P. (2006). Hyaluronan-CD44 Interaction with Leukemia-associated RhoGEF and Epidermal Growth Factor Receptor Promotes Rho/Ras Co-activation, Phospholipase Cε-Ca^{2}+ Signaling, and Cytoskeleton Modification in Head and Neck Squamous Cell Carcinoma Cells. J Biol Chem *281*, 14026-14040.

Bourguignon, L.Y.W., Gunja-Smith, Z., Iida, N., Zhu, H.B., Young, L.J.T., Muller, W.J., and Cardiff, R.D. (1998). CD44v3,8–10 Is Involved in Cytoskeleton-Mediated Tumor Cell Migration and Matrix Metalloproteinase (MMP-9) Association in Metastatic Breast Cancer Cells. Journal of Cellular Physiology *176*, 206–215.

Bradford, M.M. (1976). A rapid and sensitive method for the quantitation of microgram quantities of protein utilizing the principle of protein-dye binding. Analytical Biochemistry *72*, 248-254.

Brandstetter, H., Grams, F., Glitz, D., Lang, A., Huber, R., Bode, W., Krell, H.-W., and Engh, R.A. (2001). The 1.8-Å Crystal Structure of a Matrix Metalloproteinase 8-Barbiturate Inhibitor Complex Reveals a

Previously Unobserved Mechanism for Collagenase Substrate Recognition. Journal of Biological Chemistry *276*, 17405-17412.

Bravo-Cordero, J.J., Marrero-Diaz, R., Megias, D., Genis, L., Garcia-Grande, A., Garcia, M.A., Arroyo, A.G., and Montoya, M.C. (2007). MT1-MMP proinvasive activity is regulated by a novel Rab8-dependent exocytic pathway. EMBO J *26*, 1499-1510.

Brock, C., Schaefer, M., Reusch, H.P., Czupalla, C., Michalke, M., Spicher, K., Schultz, G., and Nürnberg, B. (2003). Roles of Gβγ in membrane recruitment and activation of p110γ/p101 phosphoinositide 3-kinase γ. The Journal of Cell Biology *160*, 89-99.

Brooks, P.C., Strömblad, S., Sanders, L.C., von Schalscha, T.L., Aimes, R.T., Stetler-Stevenson, W.G., Quigley, J.P., and Cheresh, D.A. (1996). Localization of Matrix Metalloproteinase MMP-2 to the Surface of Invasive Cells by Interaction with Integrin αvβ3. Cell *85*, 683-693.

Bruice, P.Y. (2007). Organic Chemistry, Fifth edn (Santa Barbara, Pearson Education International).

Buttke, T.M., McCubrey, J.A., and Owen, T.C. (1993). Use of an aqeous soluble tetrazolium/formazan assay to measure viability and proliferation of lymphokine-dependent cell lines. Journal of Immunological Methods *157*, 233-240.

Cain, K., Bratton, S.B., Langlais, C., Walker, G., Brown, D.G., Sun, X.M., and Cohen, G.M. (2000). Apaf-1 oligomerizes into biologically active similar to 700-kDa and inactive similar to 1.4-MDa apoptosome complexes. Journal of Biological Chemistry *275*, 6067-6070.

Cano, A., Perez-Moreno, M.A., Rodrigo, I., Locascio, A., Blanco, M.J., del Barrio, M.G., Portillo, F., and Nieto, M.A. (2000). The transcription factor Snail controls epithelial-mesenchymal transitions by repressing E-cadherin expression. Nat Cell Biol *2*, 76-83.

Cantley, L.C. (2002). The Phosphoinositide 3-Kinase Pathway. Science *296*, 1655-1657.

Cao, J., Chiarelli, C., Richman, O., Zarrabi, K., Kozarekar, P., and Zucker, S. (2008). Membrane Type 1 Matrix Metalloproteinase Induces Epithelial-to-Mesenchymal Transition in Prostate Cancer. Journal of Biological Chemistry *283*, 6232-6240.

Cao, J., Sato, H., Takino, T., and Seiki, M. (1995). The C-terminal Region of Membrane Type Matrix Metalloproteinase Is a Functional Transmembrane Domain Required for Pro-gelatinase A Activation. Journal of Biological Chemistry *270*, 801-805.

Case, D.A., Cheatham, T.E., Darden, T., Gohlke, H., Luo, R., Merz, K.M., Onufriev, A., Simmerling, C., Wang, B., and Woods, R.J. (2005). The Amber biomolecular simulation programs. Journal of Computational Chemistry *26*, 1668-1688.

Castellano, E., and Downward, J. (2011). RAS Interaction with PI3K. Genes & Cancer *2*, 261-274.

Chen, H.-C., Appeddu, P.A., Isoda, H., and Guan, J.-L. (1996). Phosphorylation of Tyrosine 397 in Focal Adhesion Kinase Is Required for Binding Phosphatidylinositol 3-Kinase. Journal of Biological Chemistry *271*, 26329-26334.

Chen, H., Cohen, D.M., Choudhury, D.M., Kioka, N., and Craig, S.W. (2005). Spatial distribution and functional significance of activated vinculin in living cells. The Journal of Cell Biology *169*, 459-470.

Chen, P., and Parks, W.C. (2009). Role of matrix metalloproteinases in epithelial migration. Journal of Cellular Biochemistry *108*, 1233-1243.

Chevrollier, A., Loiseau, D., Chabi, B., Renier, G., Douay, O., Malthièry, Y., and Stepien, G. (2005). ANT2 Isoform Required for Cancer Cell Glycolysis. Journal of Bioenergetics and Biomembranes *37*, 307-317.

Chiche, J., Brahimi-Horn, M.C., and Pouysségur, J. (2010). Tumour hypoxia induces a metabolic shift causing acidosis: a common feature in cancer. Journal of Cellular and Molecular Medicine *14*, 771-794.

Choi, K.Y., Swierczewska, M., Lee, S., and Chen, X. (2012). Protease-activated drug development. Theranostics *2*, 156-178.

Cichy, J., and Puré, E. (2003). The liberation of CD44. The Journal of Cell Biology *161*, 839–843.

Clark, E.S., Whigham, A.S., Yarbrough, W.G., and Weaver, A.M. (2007). Cortactin Is an Essential Regulator of Matrix Metalloproteinase Secretion and Extracellular Matrix Degradation in Invadopodia. Cancer Research *67*, 4227-4235.

Clevers, H. (2011). The cancer stem cell: premises, promises and challenges. Nature Medicine, 313-319.

Cohen, G.M. (1997). Caspases: the executioners of apoptosis. Biochemistry Journal *326*, 1-16.

Collins, J.M. (1984). Pharmacologic rationale for regional drug delivery. Journal of clinical oncology *2*, 498-504.

Comptom, S.J., and Jones, C.G. (1985). Mechanism of dye response and interference in Bradford protein assay. Analytical Biochemistry *151*, 369-374.

Coon, M., Ball, A., Pound, J., Ap, S., Hollenback, D., White, T., Tulinsky, J., Bonham, L., Morrison, D.K., Finney, R., *et al.* (2003). Inhibition of lysophosphatidic acid acyltransferase β disrupts proliferative and survival signals in normal cells and induces apoptosis of tumor cells. Molecular Cancer Therapeutics *2*, 1067-1078.

Cory, A.H., Owen, T.C., Barltrop, J.A., and Cory, J.G. (1991). Use of an aqeuous soluble tetrazolium/formazan assay for cell growth assays in culture. Cancer Commun *3*, 201-212.

Cosconati, S., Forli, S., Perryman, A.L., Harris, R., Goodsell, D.S., and Olson, A.J. (2010). Virtual screening with AutoDock: theory and practice. Expert Opinion on Drug Discovery *5*, 597-607.

Coussens, L.M., Fingleton, B., and Matrisian, L.M. (2002). Matrix Metalloproteinase Inhibitors and Cancer—Trials and Tribulations. Science *295*, 2387-2392.

Coussens, L.M., Tinkle, C.L., Hanahan, D., and Werb, Z. (2000). MMP-9 Supplied by Bone Marrow–Derived Cells Contributes to Skin Carcinogenesis. Cell *103*, 481-490.

Covington, M.D., Burghardt, R.C., and Parrish, A.R. (2006). Ischemia-induced cleavage of cadherins in NRK cells requires MT1-MMP (MMP-14). American Journal of Physiology - Renal Physiology *290*, F43-F51.

Crouch, C.J. (2009). Membrane type-1 matrix metalloproteinase (MT1-MMP) as a targhet in cancer therapy. In School of Biological Sciences, Biochemistry (Pietermaritzburg, University of KwaZulu-Natal), pp. 182.

D'Alessio, S., Ferrari, G., Cinnante, K., Scheerer, W., Galloway, A.C., Roses, D.F., Rozanov, D.V., Remacle, A.G., Oh, E.-S., Shiryaev, S.A., *et al.* (2008). Tissue Inhibitor of Metalloproteinases-2 Binding to Membrane-type 1 Matrix Metalloproteinase Induces MAPK Activation and Cell Growth by a Non-proteolytic Mechanism. Journal of Biological Chemistry *283*, 87-99.

Danen, E.H.J. (2003). Integrins: Regulators of Tissue Function and Cancer Progression. Current Pharmaceutical Design *11*, 881-891.

Danen, E.H.J., and Sonnenberg, A. (2003). Erratum: Integrins in regulation of tissue development and function. J Pathol; 200: 471–480. The Journal of Pathology *201*, 632-641.

Dang, C.V., Le, A., and Gao, P. (2009). MYC-Induced Cancer Cell Energy Metabolism and Therapeutic Opportunities. Clinical Cancer Research *15*, 6479-6483.

Darzynkiewicz, Z., Juan, G., Li, X., Gorczyca, W., Murakami, T., and Traganos, F. (1997). Cytometry in cell necrobiology: analysis of apoptosis and accidental cell death (necrosis). Cytometry *27*, 1-20.

Davis II, J.W., Melendez, K., Salas, V.M., Lauer, F.T., and Burchiel, S.W. (2000). 2,3,7,8-Tetrachlorodibenzo-*p*-dioxin (TCDD) inhibits growth factor withdrawal-induced apoptosis in the mammary epithelial cell line, MCF-10A. Carcinogenesis *21*, 881-886.

Debnam, P.M., and Shearer, G. (1997). Colormimetric assay for substrates of $NADP^+$-dependent dehydrogenases based on reduction of a tretrazolium dye to its soluble formazan. Analytical Biochemistry *250*, 253-255.

Debnath, J., Muthuswamy, S.K., and Brugge, J.S. (2003). Morphogenesis and oncogenesis of MCF-10A mammary epithelial acini grown in three-dimensional basement membrane cultures. Methods *30*, 256-268.

Defilles, C., Montero, M-P., Lissitzky, J-C., Rome, S., Siret, C., Luis, J., Andre, F., and Rigot, V. (2011). α_v integrin processing interferes with the crosstalk between $\alpha_v\beta_5/\beta_6$ and $\alpha_2\beta_1$ integrin. Biology of the cell *103* (11) 519-529.

DeMali, K.A. (2004). Vinculin – a dynamic regulator of cell adhesion. Trends in Biochemical Sciences *29*, 565-567.

DeMali, K.A., and Burridge, K. (2003). Coupling membrane protrusion and cell adhesion. Journal of Cell Science *116*, 2389-2397.

Dennison, C. (2003). A guide to protein isolation, Vol 3, 2 edn (Dordrecht, Kluwer Academic Publishers).

Deryugina, E.I., Bourdon, M.A., Jungwirth, K., Smith, J.W., and Strongin, A.Y. (2000). Functional activation of integrin αvβ3 in tumor cells expressing membrane-type 1 matrix metalloproteinase. International Journal of Cancer *86*, 15-23.

Deryugina, E.I., Ratnikova, B., Monosova, E., Postnovaa, T.I., DiScipiob, R., J.W., S., and Strongina, A.Y. (2001). MT1-MMP Initiates Activation of pro-MMP-2 and Integrin avß3 Promotes Maturation of MMP-2 in Breast Carcinoma Cells. Experimental Cell Research *263*, 209-223.

Devel, L., Czarny, B., Beau, F., Georgiadis, D., Stura, E., and Dive, V. (2010). Third generation of matrix metalloprotease inhibitors: Gain in selectivity by targeting the depth of the S1′ cavity. Biochimie *92*, 1501-1508.

Devy, L., Huang, L., Naa, L., Yanamandra, N., Pieters, H., Frans, N., Chang, E., Tao, Q., Vanhove, M., Lejeune, A., *et al.* (2009). Selective Inhibition of Matrix Metalloproteinase-14 Blocks Tumor Growth, Invasion, and Angiogenesis. Cancer Research *69*, 1517-1526.

Dhanaraj, V., Williams, M.G., Ye, Q.Z., Molina, F., Johnson, L.L., Ortwine, D.F., Pavlovsky, A., Rubin, J.R., Skeean, R.W., White, A.D., *et al.* (1999). X-ray structure of gelatinase A catalytic domain complexed with a hydroxamate inhibitor. Croatica Chemica Acta *72*, 575-591.

Dukes, K.A., and Sullivan, L.M. (2008). A review of basic biostatistics. In evaluating techniques in biochemical research, D Zuk, ed (Cambridge, MA:Cell Press), 50-56.

Eisenach, P.A., Corrêa de Sampaio, P., Murphy, G., and Roghi, C. (2012). Membrane-type 1 matrix metalloproteinase (MT1-MMP) ubiquitination at K581 increases cellular invasion through type-I collagen. Journal of Biological Chemistry.

Elbaum, M., Chausovsky, A., Levy, E.T., Shtutman, M., and Bershadsky, A.D. (1999). Microtubule involvement in regulating cell contractility and adhesion-dependent signalling: a possible mechanism for polarization of cell motility. Biochemical Society symposium *65*, 147-172.

Eldridge, M.D., Murray, C.W., Auton, T.R., Paolini, G.V., and Mee, R.P. (1997). Empirical scoring functions: I. The development of a fast empirical scoring function to estimate the binding affinity of ligands in receptor complexes. Journal of Computer-Aided Molecular Design *11*, 425-445.

Ellerbroek, S.M., and Stack, M.S. (1999). Membrane associated matrix metalloproteinases in metastasis. BioEssays *21*, 940-949.

Elloul, S., Bukholt Elstrand, M., Nesland, J.M., Tropé, C.G., Kvalheim, G., Goldberg, I., Reich, R., and Davidson, B. (2005). Snail, Slug, and Smad-interacting protein 1 as novel parameters of disease aggressiveness in metastatic ovarian and breast carcinoma. Cancer *103*, 1631-1643.

Elmore, S. (2007). Apoptosis: a review of programmed cell death. Toxicology Pathology *35*, 495-516.

Endo, K., Takino, T., Miyamori, H., Kinsen, H., Yoshizaki, T., Furukawa, M., and Sato, H. (2003). Cleavage of Syndecan-1 by Membrane Type Matrix Metalloproteinase-1 Stimulates Cell Migration. Journal of Biological Chemistry *278*, 40764-40770.

English, W.R., Holtz, B., Vogt, G., Knäuper, V., and Murphy, G. (2001). Characterization of the Role of the "MT-loop". Journal of Biological Chemistry *276*, 42018-42026.

Ewald, A.J., Huebner, R.J., Palsdottir, H., Lee, J.K., Perez, M.J., Jorgens, D.M., Tauscher, A.N., Cheung, K.J., Werb, Z., and Auer, M. (2012). Mammary collective cell migration involves transient loss of epithelial features and individual cell migration within the epithelium. Journal of Cell Science.

Fantin, V.R., St-Pierre, J., and Leder, P. (2006). Attenuation of LDH-A expression uncovers a link between glycolysis, mitochondrial physiology, and tumor maintenance. Cancer Cell *9*, 425-434.

Federici, G., Espina, V., Liotta, L., and H., E.K. (2011). Breast Cancer Stem Cells: A New Target for Therapy. Oncology *25*.

Fernandez-Catalan, C., Bode, W., Huber, R., Turk, D., Calvete, J.J., Lichte, A., Tschesche, H., and Maskos, K. (1998). Crystal structure of the complex formed by the membrane type 1-matrix metalloproteinase with the tissue inhibitor of metalloproteinases-2, the soluble progelatinase A receptor. EMBO J *17*, 5238-5248.

Fingleton, B. (2008). MMPs as therapeutic targets—Still a viable option? Seminars in Cell & Developmental Biology *19*, 61-68.

Fischer, T. (2004). Design und Synthese von Matrix Metalloproteinase Inhibitoren mit 1,2,4-Triazin-Grundgerüst. In Fakultät für Chemie (Bielefeld, Universität Bielefeld).

Fisher, J., and Mobashery, S. (2006). Recent advances in MMP inhibitor design. Cancer and Metastasis Reviews *25*, 115-136.

Folgueras, A.F., Pendas, A.M., Sanchez, L.M., and Lopez-Otin, C. (2004). Matrix metalloproteinases in cancer: from new functions to improved inhibition strategies. International Journal of Developmental Biology *48*, 411-424.

Freshney, R.I. (2005). Quantitation. In Culture of Animal Cells (John Wiley & Sons, Inc.).

Friedl, P. (2004). Prespecification and plasticity: shifting mechanisms of cell migration. Current Opinion in Cell Biology *16*, 14-23.

Friedl, P., Entschladen, F., Conrad, C., Niggemann, B., and Zänker, K.S. (1998). CD4+ T lymphocytes migrating in three-dimensional collagen lattices lack focal adhesions and utilize β1 integrin-independent strategies for polarization, interaction with collagen fibers and locomotion. European Journal of Immunology *28*, 2331-2343.

Friedl, P., and Wolf, K. (2003a). Proteolytic and non-proteolytic migration of tumour cells and leucocytes. In Proteases and the Regulation of Biological Processes, J.N.H.S.G. Saklatvala, ed., pp. 277-285.

Friedl, P., and Wolf, K. (2003b). Tumour-cell invasion and migration: diversity and escape mechanisms. Nat Rev Cancer *3*, 362-374.

Frittoli, E., Palamidessi, A., Disanza, A., and Scita, G. (2011). Secretory and endo/exocytic trafficking in invadopodia formation: The MT1-MMP paradigm. European Journal of Cell Biology *90*, 108-114.

Froufe, H.J.C., Abreu, R.M.V., and Ferreira, I.C.F.R. (2011). Using molecular docking to investigate the anti-breast cancer activity of low molecular weight compounds present on wild mushrooms. SAR & QSAR in Environmental Research *22*, 315-328.

Fulda, S., and Debatin, K.-M. (2006). Extrinsic versus intrinsic apoptosis pathways in anticancer chemotherapy. Oncogene *25*, 4798-4811.

Galluzzi, L., Maiuri, M.C., Vitale, I., Zischka, H., Castedo, M., Zitvogel, L., and Kroemer, G. (2007). Cell death modalities: classifications and pathophysiological implications. Cell Death and Differentiation *14*, 1237-1243.

Gálvez, B.G., Matías-Román, S., Yáñez-Mó, M., Vincente-Manzanares, M., Sánchez-Madrid, F., and Arroyo, A.G. (2003). Caveolae are a novel pathway for membrane-type 1 matrix metalloproteinase traffic in human endothelial cells. Molecular Biology of the Cell *15*, 678-687.

Gatti, R., Belletti, S., Orlandini, G., Bussolati, O., Dall'Asta, V., and Gazzola, G.C. (1998). Comparison of annexin V and calcein-AM as early vital markers of apoptosis in adherent cell by confocal laser microscopy. The Journal of Histochemistry and Cytochemistry *46*, 895-900.

Gharaibeh, B., Lu, A., Tebbets, J., Zheng, B., Feduska, J., Crisan, M., Peault, B., Cummins, J., and Huard, J. (2008). Isolation of a slowly adhering cell fraction containing stem cells from murine skeletal muscle by the preplate technique. Nat Protocols *3*, 1501-1509.

Gialeli, C., Theocharis, A.D., and Karamanos, N.K. (2011). Roles of matrix metalloproteinases in cancer progression and their pharmacological targeting. FEBS Journal *278*, 16-27.

Gilles, C., Polette, M., Birembaut, P., Brünner, N., and Thompson, E.W. (1997a). Expression of c-ets-1 mRNA is associated with an invasive, EMT-derived phenotype in breast carcinoma cell lines. Clinical and Experimental Metastasis *15*, 519-526.

Gilles, C., Polette, M., Coraux, C., Tournier, J.-M., Meneguzzi, G., Munaut, C., Volders, L., Rousselle, P., Birembaut, P., and Foidart, J.-M. (2001). Contribution of MT1-MMP and of human laminin-5 γ2 chain degradation to mammary epithelial cell migration. Journal of Cell Science *114*, 2967-2976.

Gilles, C., Polette, M., Seiki, M., Birembaut, P., and Thompson, E.W. (1997b). Implication of collagen type I-induced membrane-type 1-matrix metalloproteinase expression and matrix metalloproteinase-2 activation in the metastatic progression of breast carcinoma. Laboratory investigation; a journal of technical methods and pathology *76*, 651-660.

Gingras, D., and Béliveau, R. (2010). Emerging concepts in the regulation of membrane-type 1 matrix metalloproteinase activity. Biochimica et Biophysica Acta (BBA) - Molecular Cell Research *1803*, 142-150.

Gingras, D., Bousquet-Gagnon, N., Langlois, S., Lachambre, M.-P., Annabi, B., and Béliveau, R. (2001). Activation of the extracellular signal-regulated protein kinase (ERK) cascade by membrane-type-1 matrix metalloproteinase (MT1-MMP). FEBS Letters *507*, 231-236.

Giraud, S., Bonod-Bidaud, C., Wesolowski-Louvel, M., and Stepien, G. (1998). Expression of human ANT2 gene in highly proliferative cells: GRBOX, a new transcriptional element, is involved in the regulation of glycolytic ATP import into mitochondria. Journal of Molecular Biology *281*, 409-418.

Givan, A.L. (2004). Flow cytometry protocols, Vol 263, 2 edn (Totowa, NJ, Humana Press Inc.).

Glading, A., Lauffenburger, D.A., and Wells, A. (2002). Cutting to the chase: calpain proteases in cell motility. Trends in Cell Biology *12*, 46-54.

Gloushankova, N.A., Krendel, M.F., Sirotkin, V.A., Bonder, E.M., Feder, H.H., Vasiliev, J.M., and Gelfand, I.M. (1995). Dynamics of active lamellae in cultured epithelial cells: effects of expression of exogenous N-ras oncogene. Proceedings of the National Academy of Sciences *92*, 5322-5325.

Goetsch, K.P., and Niesler, C.U. (2011). Optimization of the scratch assay for in vitro skeletal muscle wound healing analysis. Analytical Biochemistry *411*, 158-160.

Golubkov, V.S., Boyd, S., Savinov, A.Y., Chekanov, A.V., Osterman, A.L., Remacle, A., Rozanov, D.V., Doxsey, S.J., and Strongin, A.Y. (2005). Membrane Type-1 Matrix Metalloproteinase (MT1-MMP) Exhibits an Important Intracellular Cleavage Function and Causes Chromosome Instability. Journal of Biological Chemistry *280*, 25079-25086.

Golubkov, V.S., Chekanov, A.V., Savinov, A.Y., Rozanov, D.V., Golubkova, N.V., and Strongin, A.Y. (2006). Membrane Type-1 Matrix Metalloproteinase Confers Aneuploidy and Tumorigenicity on Mammary Epithelial Cells. Cancer Research *66*, 10460-10465.

Golubkov, V.S., Chekanov, A.V., Shiryaev, S.A., Aleshin, A.E., Ratnikov, B.I., Gawlik, K., Radichev, I., Motamedchaboki, K., Smith, J.W., and Strongin, A.Y. (2007). Proteolysis of the Membrane Type-1 Matrix Metalloproteinase Prodomain. Journal of Biological Chemistry *282*, 36283-36291.

Golubkov, V.S., Cieplak, P., Chekanov, A.V., Ratnikov, B.I., Aleshin, A.E., Golubkova, N.V., Postnova, T.I., Radichev, I.A., Rozanov, D.V., Zhu, W., *et al.* (2010). Internal Cleavages of the Autoinhibitory Prodomain Are Required for Membrane Type 1 Matrix Metalloproteinase Activation, although Furin Cleavage Alone Generates Inactive Proteinase. Journal of Biological Chemistry *285*, 27726-27736.

Gomis-Rüth, F.X. (2009). Catalytic Domain Architecture of Metzincin Metalloproteases. Journal of Biological Chemistry *284*, 15353-15357.

Gonzalo, P., Moreno, V., Gálvez, B.G., and Arroyo, A.G. (2010). MT1-MMP and integrins: Hand-to-hand in cell communication. BioFactors *36*, 248-254.

Gooding, J.M., Yap, K.L., and Ikura, M. (2004). The cadherin–catenin complex as a focal point of cell adhesion and signalling: new insights from three-dimensional structures. BioEssays *26*, 497-511.

Goodwin, C.J., Holt, S.J., Downes, S., and Marshall, N.J. (1995). Microculture tetrazolium assays: a comparison between two new tetrazolium salts XTT and MTS. Journal of Immunological Methods *179*, 95-103.

Gordon, L.A., Mulligan, K.T., Maxwell-Jones, H., Adams, M., Walker, R.A., and Jones, J.L. (2003). Breast cell invasive potential relates to the myoepithelial phenotype. International Journal of Cancer *106*, 8-16.

Gorrin-Rivas, M.J., Arii, S., Furutani, M., Mizumoto, M., Mori, A., Hanaki, K., Maeda, M., Furuyama, H., Kondo, Y., and Imamura, M. (2000a). Mouse Macrophage Metalloelastase Gene Transfer into a Murine Melanoma Suppresses Primary Tumor Growth by Halting Angiogenesis. Clinical Cancer Research *6*, 1647-1654.

Gorrin-Rivas, M.J., Arii, S., Mori, A., Takeda, Y., Mizumoto, M., Furutani, M., and Imamura, M. (2000b). Implications of human macrophage metalloelastase and vascular endothelial growth factor gene expression in angiogenesis of hepatocellular carcinoma. Annals of Surgery *231*, 67-73.

Grille, S.J., Bellacosa, A., Upson, J., Klein-Szanto, A.J., van Roy, F., Lee-Kwon, W., Donowitz, M., Tsichlis, P.N., and Larue, L. (2003). The Protein Kinase Akt Induces Epithelial Mesenchymal Transition and Promotes Enhanced Motility and Invasiveness of Squamous Cell Carcinoma Lines. Cancer Research *63*, 2172-2178.

Guengerich, F.P. (2007). Cytochrome P450 and Chemical Toxicology. Chemical Research in Toxicology *21*, 70-83.

Guex, N., Peitsch, M., Schwede, T., and Diemand, A. (1997). SWISS-MODEL and the Swiss-PdbViewer:An environment for comparative protein modelling. Electrophoresis *18*, 2714-2723.

Guo, H., Li, R., Zucker, S., and Toole, B.P. (2000). EMMPRIN (CD147), an Inducer of Matrix Metalloproteinase Synthesis, Also Binds Interstitial Collagenase to the Tumor Cell Surface. Cancer Research *60*, 888-891.

Gupta, P.B., Chaffer, C.L., and Weinberg, R.A. (2009). Cancer stem cells: mirage or reality? Nat Med *15*, 1010-1012.

Haga, H., Irahara, C., Kobayashi, R., Nakagaki, T., and Kawabata, K. (2005). Collective Movement of Epithelial Cells on a Collagen Gel Substrate. Biophys J *88*, 2250-2256.

Hamilton, S.R., Fard, S.F., Paiwand, F.F., Tolg, C., Veiseh, M., Wang, C., McCarthy, J.B., Bissell, M.J., Koropatnick, J., and Turley, E.A. (2007). The Hyaluronan Receptors CD44 and Rhamm (CD168) Form Complexes with ERK1,2 That Sustain High Basal Motility in Breast Cancer Cells. The Journal of Biological Chemistry *282*, 16667–16680.

Hangai, M., Kitaya, N., Xu, J., Chan, C.K., Kim, J.J., Werb, Z., Ryan, S.J., and Brooks, P.C. (2002). Matrix Metalloproteinase-9-Dependent Exposure of a Cryptic Migratory Control Site in Collagen is Required before Retinal Angiogenesis. The American Journal of Pathology *161*, 1429-1437.

Hardie, D.G. (2011). Why Starving Cells Eat Themselves. Science *331*, 410-411.

Harrison, R.E., and Turley, E.A. (2001). Active ERK regulates microtubule stability in H-ras-transformed cells. Neoplasia *3*, 385-394.

Hashimoto, H., Takeuchi, T., Komatsu, K., Miyazaki, K., Sato, M., and Higashi, S. (2011). Structural Basis for Matrix Metalloproteinase-2 (MMP-2)-selective Inhibitory Action of beta-Amyloid Precursor Protein-derived Inhibitor. Journal of Biological Chemistry *286*, 33236-33243.

Hawley, T.S., and Hawley, R.G. (2004). Flow cytometry protocols, Vol 263, 2 edn (Totowa, NJ, Humana Press Inc.).

Hayes, A.J., and Markovic, B. (2002). Toxicity of Australian essential oil *Backhousia citriodora* (Lemon myrtle). Part1. Antimicrobial activity and in vitro cytotoxicity. Food and Chemical Toxicology *40*, 535-543.

Hernandez-Barrantes, S., Toth, M., Bernardo, M.M., Yurkova, M., Gervasi, D.C., Raz, Y., Sang, Q.A., and Fridman, R. (2000). Binding of Active (57 kDa) Membrane Type 1-Matrix Metalloproteinase (MT1-MMP) to Tissue Inhibitor of Metalloproteinase (TIMP)-2 Regulates MT1-MMP Processing and Pro-MMP-2 Activation. Journal of Biological Chemistry *275*, 12080-12089.

Hsu, S., Yu, F.X.X., Huang, Q., Lewis, J., Singh, B., Dickinson, D., Borke, J., Sharawy, M., Wataha, J., Yamamoto, T., *et al.* (2003). A mechanism-based in vitro anticancer drug screening approach for phenolic phytochemicals. Assay and Drug Development Technologies *1*, 611-618.

Huey, R., and Morris, G.M. (2008). Using AutoDock 4 with AutoDockTools: a tutorial. In http://autodockscrippsedu/faqs-help/tutorial/using-autodock-4-with-autodocktools, M.G.L. The Scripps Research Institute, ed. (California).

Huey, R., Morris, G.M., Olson, A.J., and Goodsell, D.S. (2007). A semiempirical free energy force field with charge-based desolvation. Journal of Computational Chemistry *28*, 1145-1152.

Humphries, J.D., Wang, P., Streuli, C., Geiger, B., Humphries, M.J., and Ballestrem, C. (2007). Vinculin controls focal adhesion formation by direct interactions with talin and actin. The Journal of Cell Biology *179*, 1043-1057.

Ilina, O., and Friedl, P. (2009). Mechanisms of collective cell migration at a glance. Journal of Cell Science *122*, 3203-3208.

Imbalzano, K.M., Tatarkova, I., Imbalzano, A.N., and Nickerson, J.A. (2009). Increasingly transformed MCF-10A cells have a progressively tumor-like phenotype in three-dimensional basement membrane culture. Cancer Cell International *9*.

Inki, P., and Jalkanen, M. (1996). The Role of Syndecan-1 in Malignancies. Annals of Medicine *28*, 63-67.

Iozzo, R.V. (1999). The Biology of the Small Leucine-rich Proteoglycans. Journal of Biological Chemistry *274*, 18843-18846.

Ishigaki, S., Toi, M., Ueno, T., Matsumoto, H., Muta, M., Koike, M., and Seiki, M. (1999). Significance of Membrane Type 1 Matrix Metalloproteinase Expression in Breast Cancer. Cancer Science *90*, 516-522.

Itoh, Y. (2006). MT1-MMP: A key regulator of cell migration in tissue. IUBMB Life *58*, 589-596.

Itoh, Y., Ito, N., Nagase, H., and Seiki, M. (2008). The Second Dimer Interface of MT1-MMP, the Transmembrane Domain, Is Essential for ProMMP-2 Activation on the Cell Surface. The Journal of Biological Chemistry *283*, 13053–13062.

Ivanov, A.I., McCall, I.C., Babbin, B., Samarin, S.N., Nusrat, A., and Parkos, C.A. (2006). Microtubulies regulate dissasembly of epithelial apical junctions. BMC Cell Biology *7*.

Jacobsen, J.A., Major Jourden, J.L., Miller, M.T., and Cohen, S.M. (2010). To bind zinc or not to bind zinc: An examination of innovative approaches to improved metalloproteinase inhibition. Biochimica et Biophysica Acta (BBA) - Molecular Cell Research *1803*, 72-94.

Jemal, A., Bray, F., Center, M.M., Ferlay, J., Ward, E., and Forman, D. (2011). Global cancer statistics. CA: A Cancer Journal for Clinicians *61*, 69-90.

Jemal, A., Center, M.M., DeSantis, C., and Ward, E.M. (2010). Global Patterns of Cancer Incidence and Mortality Rates and Trends. Cancer Epidemiology Biomarkers & Prevention *19*, 1893-1907.

Jiang, A., Lehti, K., Wang, X., Weiss, S.J., Keski-Oja, J., and Pei, D. (2001a). Regulation of membrane-type matrix metalloproteinase 1 activity by dynamin-mediated endocytosis. Proceedings of the National Academy of Sciences *98*, 13693-13698.

Jiang, A., Lehti, K., Wang, X., Weiss, S.J., Keski-Oja, J., and Pei, D. (2001b). Regulation of membrane-type matrix metalloproteinase 1 activity by dynamin-mediated endocytosis. PNAS *98*, 13693–13698.

Joneson, T., White, M.A., Wigler, M.H., and Bar-Sagi, D. (1996). Stimulation of Membrane Ruffling and MAP Kinase Activation by Distinct Effectors of RAS. Science *271*, 810-812.

Jordan, M.A., and Wilson, L. (1998). Microtubules and actin filaments: dynamic targets for cancer chemotherapy. Current Opinion in Cell Biology *10*, 123-130.

Jost, M., Folgueras, A.R., Frérart, F., Pendas, A.M., Blacher, S., Houard, X., Berndt, S., Munaut, C., Cataldo, D., Alvarez, J., *et al.* (2006). Earlier Onset of Tumoral Angiogenesis in Matrix Metalloproteinase-19–Deficient Mice. Cancer Research *66*, 5234-5241.

Kadler, K.E., Holmes, D.F., Trotter, J.A., and Chapman, J.A. (1996). Collagen fibril formation. Biochem J *316*, 1-11.

Kadota, M., Yang, H.H., Gomez, B., Sato, M., Clifford, R.J., Meerzaman, D., Dunn, B.K., Wakefield, L.M., and Lee, M.P. (2010). Delineating Genetic Alterations for Tumor Progression in the MCF-10A Series of Breast Cancer Cell Lines. PLoS ONE *5*, e9201.

Kajita, M., Itoh, Y., Chiba, T., Mori, H., Okada, A., Kinoh, H., and Seiki, M. (2001). Membrane-type 1 Matrix Metalloproteinase Cleaves CD44 and Promotes Cell Migration. The Journal of Cell Biology *153*, 893–904.

Kang, Y., Siegel, P.M., Shu, W., Drobnjak, M., Kakonen, S.M., Cordón-Cardo, C., Guise, T.A., and Massagué, J. (2003). A multigenic program mediating breast cancer metastasis to bone. Cancer Cell *3*, 537-549.

Kapadia, G., Chrambach, A., and Rodbard, D. (1974). Approaches of macromolecular mapping by polyacrylamide gel electrophoresis. (New York, de Gruyter).

Kapischke, M., Fischer, T., Tiessen, K., and Tschesche, H. (2008). Characterisation of a novel matrix metalloproteinase inhibitor on pancreatic adenocarcinoma cells in vitro and in an orthotopic pancreatic cancer model in vivo. International Journal of Oncology *32*, 273-282.

Kasahara, A., Hayashi, N., Mochizuki, K., Oshita, M., Katayama, K., Kato, M., Masuzawa, M., Yoshihara, H., Naito, M., Miyamoto, T., *et al.* (1997). Circulating matrix metalloproteinase-2 and tissue inhibitor of metalloproteinase-1 as serum markers of fibrosis in patients with chronic hepatitis C: Relationship to interferon reponse. Journal of Hepatology *26*, 574-583.

Katarina, W., Wu, Y.I., Yueying, L., Geiger, J., Tam, E., Overall, C., Stack, M.S., and Friedl, P. (2007). Multi-step pericellular proteolysis controls the transition from individual to collective cancer cell invasion. Nature Cell Biology *9*, 893-904.

Kelekar, A., and Cole, M.D. (1987). Immortalization by c-myc, H-ras, and Ela oncogenes induces differential cellular gene expression and growth factor responses. Molecular and Cellular Biology *7*, 3899-3907.

Kerr, J.F., Wyllie, A.H., and Currie, A.R. (1972). Apoptosis: a basic biological phenomenon with wide-ranging implications in tissue kinetics. British Journal of Cancer *26*, 239-257.

Khalil, A.A., and Friedl, P. (2010). Determinants of leader cells in collective cell migration. Integrative Biology *2*, 568-574.

Kim, I.-Y., Jeong, S.-J., Kim, E.-S., Kim, S.H., and Moon, A. (2007). Type I Collagen-induced Pro-MMP-2 Activation is Differentially Regulated by H-Ras and N-Ras in Human Breast Epithelial Cells. Journal of Biochemistry and Molecular Biology *40*, 825-831.

Kim, M.-S., Lee, E.-J., Kim, H.-R.C., and Moon, A. (2003). p38 Kinase Is a Key Signaling Molecule for H-Ras-induced Cell Motility and Invasive Phenotype in Human Breast Epithelial Cells. Cancer Research *63*, 5454-5461.

Kitchen, D.B., Decornez, H., Furr, J.R., and Bajorath, J. (2004). Docking and scoring in virtual screening for drug discovery: methods and applications. Nature Reviews Drug Discovery *3*, 935-949.

Kohrmann, A., Kammerer, U., Kapp, M., Dietl, J., and Anacker, J. (2009). Expression of matrix metalloproteinases (MMPs) in primary human breast cancer and breast cancer cell lines: New findings and review of the literature. BMC Cancer *9*, 188.

Koshikawa, N., Giannelli, G., Cirulli, V., Miyazaki, K., and Quaranta, V. (2000). Role of Cell Surface Metalloprotease MT1-MMP in Epithelial Cell Migration over Laminin-5. The Journal of Cell Biology *148*, 615-624.

Kresge, N., Simoni, R.D., and Hill, R.L. (2006). SDS-PAGE to determine the molecular weight of proteins: the work of Klaus Weber and Mary Osborn. Journal of Biological Chemistry *281*, 19-21.

Kumari, S., Rastogi, R.P., Singh, K.L., Singh, S.P., and Sinha, R.P. (2008). DNA Damage: Detection Strategies. Experimental and clinical Sciences International Journal *7*, 44-62.

Kuo, Y.-C., Su, C.-H., Liu, C.-Y., Chen, T.-H., Chen, C.-P., and Wang, H.-S. (2009). Transforming growth factor-β induces CD44 cleavage that promotes migration of MDA-MB-435s cells through the up-regulation of membrane type 1-matrix metalloproteinase. International Journal of Cancer *124*, 2568-2576.

Kurokawa, K., Nakamura, T., Aoki, K., and Matsuda, M. (2005). Mechanism and role of localized activation of Rho-family GTPases in growth factor-stimulated fibroblasts and neuronal cells. Biochemical Society Transactions *33*, 631-634.

Laemmli, U.K. (1970). Cleavage of structural proteins during the assembly of the head of bacteriophage T4. Nat *277*, 680-685.

Lafleur, M.A., Mercuri, F.A., Ruangpanit, N., Seiki, M., Sato, H., and Thompson, E.W. (2006). Type-1 collagen abrogates the clathrin-mediated internalization of membrane-type-1 matrix metalloproteinase (MT1-MMP) via the MT1-MMP hemepexin domain. The Journal of Biological Chemistry *281*, 6826-6840.

Lafleur, M.A., Xu, D., and Hemler, M.E. (2009). Tetraspanin Proteins Regulate Membrane Type-1 Matrix Metalloproteinase-dependent Pericellular Proteolysis
1149. Mol Biol Cell *20*, 2030-2040.

Lang, R., Braun, M., Sounni, N.E., Noel, A., Frankenne, F., Foidart, J.M., Bode, W., and Maskos, K. (2004). Crystal Structure of the Catalytic Domain of MMP-16/MT3-MMP: Characterization of MT-MMP Specific Features. Journal of Molecular Biology *336*, 213-225.

Larue, L., and Bellacosa, A. (2005). Epithelial-mesenchymal transition in development and cancer: role of phosphatidylinositol 3' kinase/AKT pathways. Oncogene *24*, 7443-7454.

Lauffenburger, D.A., and Horwitz, A.F. (1996). Cell Migration: A Physically Integrated Molecular Process. Cell *84*, 359-369.

Le Bras, M., Borgne-Sanchez, A., Touat, Z., El Dein, O.S., Deniaud, A., Maillier, E., Lecellier, G., Rebouillat, D., Lemaire, C., Kroemer, G., *et al.* (2006). Chemosensitization by Knockdown of Adenine Nucleotide Translocase-2. Cancer Research *66*, 9143-9152.

le Duc, Q., Shi, Q., Blonk, I., Sonnenberg, A., Wang, N., Leckband, D., and de Rooij, J. (2010). Vinculin potentiates E-cadherin mechanosensing and is recruited to actin-anchored sites within adherens junctions in a myosin II–dependent manner. The Journal of Cell Biology *189*, 1107-1115.

Lecoeur, H. (2002). Nuclear apoptosis detection by flow cytometry: influence of endogenous endonucleases. Experimental Cell Research *277*, 1-14.

Lee, H., Overall, C.M., McCulloch, C.A., and Sodek, J. (2006). A critical role for the membrane-type 1 matrix metalloproteinase in collagen phagocytosis. Molecular Biology of the Cell *17*, 4812-4826.

Lee, J., Ishihara, A., Oxford, G., Johnson, B., and Jacobson, K. (1999). Regulation of cell movement is mediated by stretch-activated calcium channels. Nature *400*, 382-386.

Lee, M.C.S., Miller, E.A., Goldberg, J., Orci, L., and Schekman, R. (2004). Bi-directional protein transport between the ER and Golgi. Annual Review of Cell & Developmental Biology *20*, 87-123.

Lehti, K., Lohi, J., Juntunen, M.M., Pei, D., and Keski-Oja, J. (2002). Oligomerization through Hemopexin and Cytoplasmic Domains Regulates the Activity and Turnover of Membrane-type 1 Matrix Metalloproteinase. Journal of Biological Chemistry *277*, 8440-8448.

Lehti, K., Valtanen, H., Wichsrtom, S., Lohi, J., and Keski-Oja, J. (2000). Regulation of membrane-type-1 matrix metalloproteinase activity by its cytoplasmic domain. Journal of Biological Chemistry *275*, 15006-15013.

Lestari, F., Hayes, A.J., Green, A.R., and Markovic, B. (2005). In vitro cytotoxicity of selected chemicals commonly produced during fire combustion using human cell lines. Toxicology in Vitro *19*, 653–663.

Leygue, E., Snell, L., Dotzlaw, H., Troup, S., Hiller-Hitchcock, T., Murphy, L.C., Roughley, P.J., and Watson, P.H. (2000). Lumican and decorin are differentially expressed in human breast carcinoma. The Journal of Pathology *192*, 313-320.

Li, Q., and Mattingly, R.R. (2008). Restoration of E-cadherin Cell-Cell Junctions Requires Both Expression of E-cadherin and Suppression of ERK MAP Kinase Activation in Ras-Transformed Breast Epithelial Cells. Neoplasia *10*, 1444-1458.

Li, Q., Mullins, S.R., Sloane, B.F., and Mattingly, R.R. (2008). p21-Activated Kinase 1 Co-ordinates Aberrant Cell Survival and Pericellular Proteolysis in a Three-Dimensional Culture Model for Premalignant Progression of Human Breast Cancer. Neoplasia *10*, 314-328.

Li, Q., Park, P.W., Wilson, C.L., and Parks, W.C. (2002). Matrilysin Shedding of Syndecan-1 Regulates Chemokine Mobilization and Transepithelial Efflux of Neutrophils in Acute Lung Injury. Cell *111*, 635-646.

Li, Y., Aoki, T., Mori, Y., Ahmad, M., Miyamori, H., Takino, T., and Sato, H. (2004). Cleavage of Lumican by Membrane-Type Matrix Metalloproteinase-1 Abrogates This Proteoglycan-Mediated Suppression of Tumor Cell Colony Formation in Soft Agar. Cancer Research *64*, 7058-7064.

Liang, C.-C., Park, A.Y., and Guan, J.-L. (2007). In vitro scratch assay: a convenient and inexpensive method for analysis of cell migration in vitro. Nat Protocols *2*, 329-333.

Lichte, A., Kolkenbrock, H., and Tschesche, H. (1996). The recombinant catalytic domain of membrane-type matrix metalloproteinase-1 (MT1-MMP) induces activation of progelatinase A and progelatinase A complexed with TIMP-2. FEBS Letters *397*, 277-282.

Lin, F., and Wang, R. (2010). Systematic Derivation of AMBER Force Field Parameters Applicable to Zinc-Containing Systems. Journal of Chemical Theory and Computation *6*, 1852-1870.

Lindeman, G.J., and Visvader, J.E. (2010). Insights into the cell of origin in breast cancer and breast cancer stem cells. Asia-Pacific Journal of Clinical Oncology *6*, 89-97.

Liotta, L.A., and Kohn, E.C. (2001). The microenvironment of the tumour-host interface. Nature *411*, 375-379.

Liu, S., Dontu, G., Mantle, I.D., Patel, S., Ahn, N.-s., Jackson, K.W., Suri, P., and Wicha, M.S. (2006). Hedgehog Signaling and Bmi-1 Regulate Self-renewal of Normal and Malignant Human Mammary Stem Cells. Cancer Research *66*, 6063-6071.

Liu, S., Dontu, G., and Wicha, M. (2005). Mammary stem cells, self-renewal pathways, and carcinogenesis. Breast cancer research *7*, 86 - 95.

Liu, X., Kim, C.N., Yang, J., Jemmerson, R., and Wang, X. (1996). Induction of Apoptotic Program in Cell-Free Extracts: Requirement for dATP and Cytochrome c. Cell *86*, 147-157.

Lock, J.G., Wehrle-Haller, B., and Strömblad, S. (2008). Cell–matrix adhesion complexes: Master control machinery of cell migration. Seminars in Cancer Biology *18*, 65-76.

Loers, G., Makhina, T., Bork, U., Dörner, A., Schachner, M., and Kleene, R. (2012). The Interaction between Cell Adhesion Molecule L1, Matrix Metalloproteinase 14, and Adenine Nucleotide Translocator at the Plasma Membrane Regulates L1-Mediated Neurite Outgrowth of Murine Cerebellar Neurons. The Journal of Neuroscience *32*, 3917-3930.

Lopez-Otin, C., and Matrisian, L.M. (2007). Emerging roles of proteases in tumour suppression. Nat Rev Cancer *7*, 800-808.

Lowry, O.H., Rosebrough, N.J., Farr, A.L., and Randall, R.J. (1951). Protein measurement with the folin phenol reagent. Journal of Biological Chemistry *193*, 265-275.

Lu, C., Li, X.-Y., Hu, Y., Rowe, R.G., and Weiss, S.J. (2010). MT1-MMP controls human mesenchymal stem cell trafficking and differentiation. Blood *115*, 221-229.

Malich, G., Markovic, B., and Winder, C. (1997). The sensitivity and specifity of the MTS tetrazolium assay for detecting the in vitro cytotoxicity of 20 chemicals using human cell lines. Toxicology *124*, 179-192.

Maquoi, E., Sounni, N.E., Devy, L., Olivier, F., Frankenne, F., Krell, H.-W., Grams, F., Foidart, J.-M., and Noël, A. (2004). Anti-Invasive, Antitumoral, and Antiangiogenic Efficacy of a Pyrimidine-2,4,6-trione Derivative, an Orally Active and Selective Matrix Metalloproteinases Inhibitor. Clinical Cancer Research *10*, 4038-4047.

Marrero-Diaz, R., Bravo-Cordero, J.J., Megías, D., García, M.A., Bartolomé, R.A., Teixido, J., and Montoya, M.C. (2009). Polarized MT1-MMP-CD44 interaction and CD44 cleavage during cell retraction reveal an essential role for MT1-MMP in CD44-mediated invasion. Cell Motility and the Cytoskeleton *66*, 48-61.

Maskos, K. (2005). Crystal structures of MMPs in complex with physiological and pharmacological inhibitors. Biochimie *87*, 249-263.

McCawley, L.J., Crawford, H.C., King, L.E., Mudgett, J., and Matrisian, L.M. (2004). A Protective Role for Matrix Metalloproteinase-3 in Squamous Cell Carcinoma. Cancer Research *64*, 6965-6972.

McCawley, L.J., and Matrisian, L.M. (2001). Matrix metalloproteinases: they're not just for matrix anymore! Current Opinion in Cell Biology *13*, 534-540.

Mierke, C.T., Rösel, D., Fabry, B., and Brábek, J. (2008). Contractile forces in tumor cell migration. European Journal of Cell Biology *87*, 669-676.

Miletti, K.E., Saglimbeni, G.N., Chen, S., and Rodriguez-Rodriguez, L. (2004). CD44 up-regulates the expression of matrix metalloproteinases (MMPs) in ovarian and breast carcinoma cells. Proc Amer Assoc Cancer Res *45*, 1823.

Minn, A.J., Gupta, G.P., Siegel, P.M., Bos, P.D., Shu, W., Giri, D.D., Viale, A., Olshen, A.B., Gerald, W.L., and Massague, J. (2005). Genes that mediate breast cancer metastasis to lung. Nature *436*, 518-524.

Moissoglu, K., and Schwartz, M.A. (2006). Integrin signalling in directed cell migration. Biology of the cell *98*, 547-555.

Moon, A., Kim, M.S., Kim, T.G., Kim, S.H., Kim, H.E., Chen, Y.Q., and Kim, H.R.C. (2000). H-ras, but not N-ras, induces an invasive phenotype in human breast epithelial cells: A role for MMP-2 in the H-ras-induced invasive phenotype. International Journal of Cancer *85*, 176-181.

Morel, A.P., Lièvre, M., Thomas, C., Hinkal, G., Ansieau, S., and Puisieux, A. (2008). Generation of breast cancer stem cells through epithelial-mesenchymal transition. PLoS ONE *3*, e2888.

Morgunova, E., Tuuttila, A., Bergmann, U., Isupov, M., Lindqvist, Y., Schneider, G., and Tryggvason, K. (1999). Structure of Human Pro-Matrix Metalloproteinase-2: Activation Mechanism Revealed. Science *284*, 1667-1670.

Morgunova, E., Tuuttila, A., Bergmann, U., and Tryggvason, K. (2002). Structural insight into the complex formation of latent matrix metalloproteinase 2 with tissue inhibitor of metalloproteinase 2. Proceedings of the National Academy of Sciences *99*, 7414-7419.

Mori, H., Tomari, T., Koshikawa, N., Kajita, M., Itoh, Y., Sato, H., Tojo, H., Yana, I., and Seiki, M. (2002). CD44 directs membrane-type 1 matrix metalloproteinase to lamellipodia by associating with its hemopexin-like domain. The EMBO Journal *21*, 3949–3959.

Morris, G.M., Goodsell, D.S., Halliday, R.S., Huey, R., Hart, W.E., Belew, R.K., and Olson, A.J. (1998). Automated docking using a Lamarckian genetic algorithm and an empirical binding free energy function. Journal of Computational Chemistry *19*, 1639-1662.

Morris, G.M., Huey, R., Lindstrom, W., Sanner, M.F., Belew, R.K., Goodsell, D.S., and Olson, A.J. (2009). AutoDock4 and AutoDockTools4: Automated docking with selective receptor flexibility. Journal of Computational Chemistry *30*, 2785-2791.

Morrison, C.J., Butler, G.S., Bigg, H.F., Roberts, C.R., Soloway, P.D., and Overall, C.M. (2001). Cellular Activation of MMP-2 (Gelatinase A) by MT2-MMP Occurs via a TIMP-2-independent Pathway. Journal of Biological Chemistry *276*, 47402-47410.

Moss, N.M., Barbolina, M.V., Liu, Y., Sun, L., Munshi, H.G., and Stack, M.S. (2009a). Ovarian Cancer Cell Detachment and Multicellular Aggregate Formation Are Regulated by Membrane Type 1 Matrix Metalloproteinase: A Potential Role in I.p. Metastatic Dissemination. Cancer Research *69*, 7121-7129.

Moss, N.M., Wu, Y.I., Liu, Y., Munshi, H.G., and Stack, M.S. (2009b). Modulation of the Membrane Type 1 Matrix Metalloproteinase Cytoplasmic Tail Enhances Tumor Cell Invasion and Proliferation in Three-dimensional Collagen Matrices. Journal of Biological Chemistry *284*, 19791-19799.

Murawaki, Y., Ikuta, Y., and Kawasaki, H. (1999). Clinical usefulness of serum tissue inhibitor of metalloproteinases (TIMP)-2 assay in patients with chronic liver disease in comparison with serum TIMP-1. Clinica Chimica Acta *281*, 109-120.

Murphy, G., Nguyen, Q., Cockett, M.I., Atkinson, S.J., Allan, J.A., Knight, C.G., Willenbrock, F., and Docherty, A.J.P. (1994). Assessment of the role of the fibronectin-like domain of gelatinase A by analysis of a deletion mutant. Journal of Biological Chemistry *269*, 6632-6636.

Nairismagi, M.L., Vislovukh, A., Meng, Q., Kratassiouk, G., Beldiman, C., Petretich, M., Groisman, R., Fuchtbauer, E.M., Harel-Bellan, A., and Groisman, I. (2012). Translational control of TWIST1 expression in MCF-10A cell lines recapitulating breast cancer progression. Oncogene.

Nelson, A.R., Fingleton, B., Rothenberg, M.L., and Matrisian, L.M. (2000). Matrix metalloproteinases: Biological activity and clinical implications. Journal of clinical oncology *18*, 1135.

Nemunaitis, J., Poole, C., Primrose, J., Rosemurgy, A., Malfetano, J., Brown, P., Berrington, A., Cornish, A., Lynch, K., Rasmussen, H., *et al.* (1998). Combined analysis of studies of the effects of the matrix metalloproteinase inhibitor marimastat on serum tumor markers in advanced cancer: selection of a biologically active and tolerable dose for longer-term studies. Clinical Cancer Research *4*, 1101-1109.

Nobes, C.D., and Hall, A. (1995). Rho, Rac, and Cdc42 GTPases regulate the assembly of multimolecular focal complexes associated with actin stress fibers, lamellipodia, and filopodia. Cell *81*, 53-62.

Nyalendo, C., Beaulieu, E., Sartelet, H., Michaud, M., Fontaine, N., Gingras, D., and Béliveau, R. (2008). Impaired tyrosine phosphorylation of membrane type 1-matrix metalloproteinase reduces tumor cell proliferation in three-dimensional matrices and abrogates tumor growth in mice. Carcinogenesis *29*, 1655-1664.

Ochieng, J., Basolo, F., Albini, A., Melchiori, A., Watanabe, H., Elliott, J., Raz, A., Parodi, S., and Russo, J. (1991). Increased invasive, chemotactic and locomotive abilities of c-Ha-ras-transformed human breast epithelial cells. Invasion Metastasis *11*, 38-47.

Ohuchi, E., Imai, K., Fujii, Y., Sato, H., Seiki, M., and Okada, Y. (1997). Membrane Type 1 Matrix Metalloproteinase Digests Interstitial Collagens and Other Extracellular Matrix Macromolecules. Journal of Biological Chemistry *272*, 2446-2451.

Okada, Y., Morodomi, T., Enghild, J.J., Suzuki, K., Yasui, A., Nakanishi, I., Salvesen, G., and Nagase, H. (1990). Matrix metalloproteinase 2 from human rheumatoid synovial fibroblasts. Purification and activation of the precursor and enzymic properties. European Journal of Biochemistry *194*, 721-730.

Okamoto, I., Kawano, Y., Murakami, D., Sasayama, T., Araki, N., Miki, T., Wong, A.J., and Saya, H. (2001). Proteolytic release of CD44 intracellular domain and its role in the CD44 signaling pathway. The Journal of Cell Biology *155*, 755–762.

Olson, M.F., and Marais, R. (2000). Ras protein signalling. Semin Immunol *12*, 63-73.

Ono, M., Murakami, T., Kudo, A., Isshiki, M., Sawada, H., and Segawa, A. (2001). Quantitative comparison of anti-fading mounting media for confocal laser scanning microscopy. The Journal of Histochemistry and Cytochemistry *49*, 305-311.

Ornsein, L. (1964). Disc electrophoresis. I. Background and thoery. Ann NY Acad Sci *121*, 321-349.

Osenkowski, P., Toth, M., and Fridman, R. (2004). Processing, shedding, and endocytosis of membrane type 1-matrix metalloproteinase (MT1-MMP). Journal of Cellular Physiology *200*, 2-10.

Ota, I., Li, X.-Y., Hu, Y., and Weiss, S.J. (2009). Induction of a MT1-MMP and MT2-MMP-dependent basement membrane transmigration program in cancer cells by Snail1. Proceedings of the National Academy of Sciences *106*, 20318-20323.

Overall, C. (2002). Molecular determinants of metalloproteinase substrate specificity. Molecular Biotechnology *22*, 51-86.

Paňková, K., Rösel, D., Novotný, M., and Brábek, J. (2010). The molecular mechanisms of transition between mesenchymal and amoeboid invasiveness in tumor cells. Cellular and Molecular Life Sciences *67*, 63-71.

Paoli, M., Anderson, B.F., Baker, H.M., Morgan, W.T., Smith, A., and Baker, E.N. (1999). Crystal structure of hemopexin reveals a novel high-affinity heme site formed between two [beta]-propeller domains. Nat Struct Mol Biol *6*, 926-931.

Parkin, G. (2004). Synthetic Analogues Relevant to the Structure and Function of Zinc Enzymes. Chemical Reviews *104*, 699-768.

Parsons, J.T., Horwitz, A.R., and Schwartz, M.A. (2010). Cell adhesion: integrating cytoskeletal dynamics and cellular tension. Nat Rev Mol Cell Biol *11*, 633-643.

Peng, X., Cuff, L.E., Lawton, C.D., and DeMali, K.A. (2010). Vinculin regulates cell-surface E-cadherin expression by binding to β-catenin. Journal of Cell Science *123*, 567-577.

Perentes, J.Y., Kirkpatrick, N.D., Nagano, S., Smith, E.Y., Shaver, C.M., Sgroi, D., Garkavtsev, I., Munn, L.L., Jain, R.K., and Boucher, Y. (2011). Cancer Cell–Associated MT1-MMP Promotes Blood Vessel Invasion and Distant Metastasis in Triple-Negative Mammary Tumors. Cancer Research *71*, 4527-4538.

Peters, M.B., Yang, Y., Wang, B., Füsti-Molnár, L.s., Weaver, M.N., and Merz, K.M. (2010). Structural Survey of Zinc-Containing Proteins and Development of the Zinc AMBER Force Field (ZAFF). Journal of Chemical Theory and Computation *6*, 2935-2947.

Petrella, B.L., Lohi, J., and Brinckerhoff, C.E. (2005). Identification of membrane type-1 matrix metalloproteinase as a target of hypoxia-inducible factor-2 alpha in von Hippel-Lindau renal cell carcinoma. Oncogene *24*, 1043-1052.

Piccard, H., Van den Steen, P.E., and Opdenakker, G. (2007). Hemopexin domains as multifunctional liganding modules in matrix metalloproteinases and other proteins. Journal of Leukocyte Biology *81*, 870–892.

Pike, R.N. (1990). A study of the proteinase, cathepsin L, in the context of tumour invasion. In Biochemistry (Pietermaritzburg, University of Natal).

Pinkel, D., and Stovel, R. (1985). Flow chambers and sample handling. (London, Academic Press).

Poincloux, R., Lizárraga, F., and Chavrier, P. (2009). Matrix invasion by tumour cells: a focus on MT1-MMP trafficking to invadopodia. Journal of Cell Science *122*, 3015-3024.

Polette, M., Huet, E., Birembaut, P., Maquart, F.X., Hornebeck, W., and Emonard, H. (1999). Influence of oleic acid on the expression, activation and activity of gelatinase a produced by oncogene-transformed human bronchial epithelial cells. International Journal of Cancer *80*, 751-755.

Pols, M.S., and Klumperman, J. (2009). Trafficking and function of the tetraspanin CD63. Experimental Cell Research *315*, 1584-1592.

Pommier, Y., Sordet, O., Antony, S., Hayward, R.L., and Kohn, K.W. (2004). Apoptosis defects and chemotherapy resistance: molecular interaction maps and networks. Oncogene *23*, 2934-2949.

Porter, P. (2008). "Westernizing" Women's Risks? Breast Cancer in Lower-Income Countries. New England Journal of Medicine *358*, 213-216.

Poujade, M., Grasland-Mongrain, E., Hertzog, A., Jouanneau, J., Chavrier, P., Ladoux, B., Buguin, A., and Silberzan, P. (2007). Collective migration of an epithelial monolayer in response to a model wound. Proceedings of the National Academy of Sciences *104*, 15988-15993.

Pozzi, A., LeVine, W.F., and Gardner, H.A. (2002). Low plasma levels of matrix metalloproteinase 9 permit increased tumor angiogenesis. Oncogene *21*, 272-281.

Prat, A., and Perou, C.M. (2011). Deconstructing the molecular portraits of breast cancer. Molecular Oncology *5*, 5-23.

Primrose, J.N., Bleiberg, H., Daniel, F., Van Belle, S., Mansi, J.L., Seymour, M., Johnson, P.W., Neoptolemos, J.P., Baillet, M., Barker, K., *et al.* (1999). Marimastat in recurrent colorectal cancer: exploratory evaluation of biological activity by measurement of carcinoembryonic antigen. British Journal of Cancer *79*, 509-514.

Promega (1996). CellTiter 96^{TM} AQ_{ueous} non-radioactive cell proliferation assay. Technical Bulletin *169*, Madison.

Puklin-Faucher, E., and Sheetz, M.P. (2009). The mechanical integrin cycle. Journal of Cell Science *122*, 179-186.

Radichev, I.A., Remacle, A., G. , Sounni, N.E., Shiryaev, S.A., Rozanov, D.V., Zhu, W., Golubkova, N.V., Postnova, T.I., Golubkov, V.S., and Strongin, A.Y. (2009). Biochemical evidence of the interactions of membrane type-1 matrix metalloproteinase (MT1-MMP) with adenine nucleotide translocator (ANT): potential implications linking proteolysis with energy metabolism in cancer cells. Biochem Journal *420*, 37-47.

Rahman, M. (2006). Introduction to flow cytometry. (Kidlington, UK., Serotec Ltd.).

Rammler, D.H., and Zaffaroni, A. (1967). Biological implications of DMSO based on a review of its chemical properties. Annals of the New York Academy of Sciences *141*, 13-23.

Ratnikov, B.I., Rozanov, D.V., Postnova, T.I., Baciu, P.C., Zhang, H., Discipio, R.G., Chestukhina, G.G., Smith, J.W., Deryugina, E.I., and Strongin, A.Y. (2002). An alternative processing of integrin alpha(v) subunit in tumor cells by membrane type-1 matrix metalloproteinase. Journal of Biological Chemistry *277*, 7377-7385.

Ravanti, L., Heino, J., López-Otín, C., and Kähäri, V.-M. (1999). Induction of Collagenase-3 (MMP-13) Expression in Human Skin Fibroblasts by Three-dimensional Collagen Is Mediated by p38 Mitogen-activated Protein Kinase. Journal of Biological Chemistry *274*, 2446-2455.

Rawlings, N.D., and Barrett, A.J. (1995). Evolutionary families of metallopeptidases. Methods in enzymology *248*, 183-227.

Raymond, S., and Weintraub, L. (1959). Acrylamide gel as a supporting medium for zone electrophoresis. Science *130*, 711.

Read, S.M., and Northcote, D.H. (1981). Minimization of variation in the response to different proteins of the Coomassie blue G dye-binding assay for protein. Analytical Biochemistry *116*, 53-64.

Remacle, A., Murphy, G., and Roghi, C. (2003). Membrane type 1-matrix metalloproteinase (MT1-MMP) is internalised by two different pathways and is recycled to the cell surface. Journal of Cell Science *116*, 3905-3916.

Remacle, A.G., Golubkov, V.S., Shiryaev, S.A., Dahl, R., Stebbins, J.L., Chernov, A.V., Cheltsov, A.V., Pellecchia, M., and Strongin, A.Y. (2012). Novel MT1-MMP small molecule inhibitors based on insights into hemopexin domain function in tumor growth. Cancer Research.

Renart, J., Reiser, J., and Stark, G.R. (1979). Transfer of proteins from gels to diazobenzyloxymethyl-paper and detection with antisera: A method for studying antibody specificity and antigen structure. . Proceedings of the National Academy of Sciences of the United States of America *76*, 3116-3120.

Reynolds, J.A., and Tanford, C. (1970). The gross conformation of protein-sodium dodecyl sulfate complexes. Journal of Biological Chemistry *245*, 5161-5165.

Richards, E.G., and Lecanidou, R. (1974). Polymerization kinetics and properties of polyacrylamide gels. (New York, de Gruyter).

Richards, R.D., and Smith, J.W. (2007). Novel antagonists of the thioesterase domain of human fatty acid synthase. Molecular Cancer Therapeutics *6*, 2120-2126.

Ridley, A.J., Schwartz, M.A., Burridge, K., Firtel, R.A., Ginsberg, M.H., Borisy, G., Parsons, J.T., and Horwitz, A.R. (2003). Cell Migration: Integrating Signals from Front to Back. Science *302*, 1704-1709.

Riss, T.L., and Moravec, R.A. (1992). Comparison of MTT, XTT and a novel tetrazolium compound MTS for in vitro proliferation and chemosensitivity assay. Mol Biol Cell *3*.

Robinson, M.J., and Cobb, M.H. (1997). Mitogen-activated protein kinase pathways. Current Opinion in Cell Biology *9*, 180-186.

Rosemurgy, A., Harris, J., Langleben, A., Casper, E., Goode, S., and Rasmussen, H. (1999). Marimastat in Patients With Advanced Pancreatic Cancer: A Dose-Finding Study. American Journal of Clinical Oncology *22*, 247-252.

Roy, S., Luetterforst, R., Harding, A., Apolloni, A., Etheridge, M., Stang, E., Rolls, B., Hancock, J.F., and Parton, R.G. (1999). Dominant-negative caveolin inhibits H-Ras function by disrupting cholesterol-rich plasma membrane domains. Nature Cell Biology *1*, 98-105.

Rozanov, D.V., Golubkov, V.S., and Strongin, A.Y. (2005). Membrane type-1 matrix metalloproteinase (MT1-MMP) protects malignant cells from tumoricidal activity of re-engineered anthrax lethal toxin. The International Journal of Biochemistry & Cell Biology *37*, 142-154.

Sabeh, F., Ota, I., Holmbeck, K., Birkedal-Hansen, H., Soloway, P., Balbin, M., Lopez-Otin, C., Shapiro, S., Inada, M., Krane, S., *et al.* (2004). Tumor cell traffic through the extracellular matrix is controlled by the membrane-anchored collagenase MT1-MMP. The Journal of Cell Biology *167*, 769-781.

Saelens, X., Festjens, N., Vande Walle, L., van Gurp, M., van Loo, G., and Vandenabeele, P. (2004). Toxic proteins released from mitochondria in cell death. Oncogene *23*, 2861-2874.

Sakamoto, T., and Seiki, M. (2010). A Membrane Protease Regulates Energy Production in Macrophages by Activating Hypoxia-inducible Factor-1 via a Non-proteolytic Mechanism. Journal of Biological Chemistry *285*, 29951-29964.

Salomon, A.R., Voehringer, D.W., Herzenberg, L.A., and Khosla, C. (2000). Understanding and exploiting the mechanistic basis for selectivity of polyketide inhibitors of F0F1-ATPase. Proceedings of the National Academy of Sciences *97*, 14766-14771.

Salzman, G.C., Singham, S.B., Johnston, R.G., and Bohren, C.F. (1990). Light scattering and cytometry, 2nd edn (New York, Wiley-Liss).

Sansone, P., Storci, G., Tavolari, S., Guarnieri, T., Giovannini, C., Taffurelli, M., Ceccarelli, C., Santini, D., Paterini, P., Marcu, K.B., *et al.* (2007). IL6 triggers malignant features in mammospheres from human ductal breast carcinoma and normal mammary gland. Journal of Clinical Investigation *117*, 3988-4002.

Sato, H., Kinoshita, T., Takino, T., Nakayama, K., and Seiki, M. (1996). Activation of a recombinant membrane type 1-matrix metalloproteinase (MT1-MMP) by furin and its interaction with tissue inhibitor of metalloproteinases (TIMP)-2. FEBS Letters *393*, 101-104.

Sato, H., and Takino, T. (2010). Co-ordinate action of membrane-type matrix metalloproteinase-1 (MT1-MMP) and MMP-2 enhances pericellular proteolysis and invasion. Cancer Science *101*, 843-847.

Sato, H., Takino, T., and Miyamori, H. (2005). Roles of membrane-type matrix metalloproteinase-1 in tumor invasion and metastasis. Cancer Science *96*, 212-217.

Sato, H., Takino, T., Okada, Y., Cao, J., Shinagawa, A., TYamamoto, E., and Seiki, M. (1994). A matrix metalloproteinase expressed on the surface of invasive tumour cells. Nature *370*, 61-65.

Savinov, A.Y., Remacle, A.G., Golubkov, V.S., Krajewska, M., Kennedy, S., Duffy, M.J., Rozanov, D.V., Krajewski, S., and Strongin, A.Y. (2006). Matrix Metalloproteinase 26 Proteolysis of the NH2-Terminal Domain of the Estrogen Receptor β Correlates with the Survival of Breast Cancer Patients. Cancer Research *66*, 2716-2724.

Schenk, S., and Quaranta, V. (2003). Tales from the crypt[ic] sites of the extracellular matrix. Trends in Cell Biology *13*, 366-375.

Schnute, M.E., O'Brien, P.M., Nahra, J., Morris, M., Howard Roark, W., Hanau, C.E., Ruminski, P.G., Scholten, J.A., Fletcher, T.R., Hamper, B.C., *et al.* (2010). Discovery of (pyridin-4-yl)-2H-tetrazole as a novel scaffold to identify highly selective matrix metalloproteinase-13 inhibitors for the treatment of osteoarthritis. Bioorganic & Medicinal Chemistry Letters *20*, 576-580.

Seals, D.F., and Courtneidge, S.A. (2003). The ADAMs family of metalloproteases: multidomain proteins with multiple functions. Genes & Development *17*, 7-30.

Sears, R., Nuckolls, F., Haura, E., Taya, Y., Tamai, K., and Nevins, J.R. (2000). Multiple Ras-dependent phosphorylation pathways regulate Myc protein stability. Genes & Development *14*, 2501-2514.

Seiki, M. (2003). Membrane-type 1 matrix metalloproteinase: a key enzyme for tumor invasion. Cancer Letters *194*, 1-11.

Sela-Passwell, N., Kikkeri, R., Dym, O., Rozenberg, H., Margalit, R., Arad-Yellin, R., Eisenstein, M., Brenner, O., Shoham, T., Danon, T., *et al.* (2012). Antibodies targeting the catalytic zinc complex of activated matrix metalloproteinases show therapeutic potential. Nat Med *18*, 143-147.

Shackleton, M., Quintana, E., Fearon, E.R., and Morrison, S.J. (2009). Heterogeneity in Cancer: Cancer Stem Cells versus Clonal Evolution. Cell *138*, 822-829.

Shapiro, A.L., Vinuela, E., and Maizel, J.V.J. (1967). Molecular weight estimation of polypeptide chains by electrophoresis in SDS-polyacrylamide gels. Biochem Biophys Res Commun *28*, 815-820.

Shapiro, S.D. (1998). Matrix metalloproteinase degradation of extracellular matrix: biological consequences. Current opinion in cell biology *10*, 602-608.

Sharpless, N.E., and DePinho, R.A. (2004). Telomeres, stem cells, senescence, and cancer. Journal of Clinical Investigation *113*, 160–168.

Sheridan, C., Kishimoto, H., Fuchs, R.K., Mehrotra, S., Bhat-Nakshatri, P., Turner, C.H., Goulet Jr., R., Badve, S., and Nakshatri, H. (2006). CD44+/CD24- breast cancer cells exhibit enhanced invasive properties: an early step necessary for metastasis. Breast cancer research *8*.

Sherr, C.J. (2006). Divorcing ARF and p53: an unsettled case. Nature Reviews Cancer *9*, 663-673.

Shim, H., Dolde, C., Lewis, B.C., Wu, C.-S., Dang, G., Jungmann, R.A., Dalla-Favera, R., and Dang, C.V. (1997). c-Myc transactivation of LDH-A: Implications for tumor metabolism and growth. Proceedings of the National Academy of Sciences *94*, 6658-6663.

Shin, I.-C., and Moon, A. (2002). Involvement of Phosphatidylinositol 3-kinase (PI3K) pathway in invasion and motility H-ras-transformed MCF-10A cells. Journal of Korean Association of Cancer Prevention *7*, 6-12.

Sloane, B.F., Moin, K., Sameni, M., Tait, L.R., Rozhin, J., and Ziegler, G. (1994). Membrane association of cathepsin B can be induced by transfection of human breast epithelial cells with c-Ha-ras oncogene. Journal of Cell Science *107*, 373-384.

Small, J.V., Stradal, T., Vignal, E., and Rottner, K. (2002). The lamellipodium: where motility begins. Trends in Cell Biology *12*, 112-120.

Snyman, C. (2010). Effect of c-Ha-Ras(V12) on protease trafficking in invasive breast cancer cells. In School of Biochemistry (Pietermaritzburg, The University of KwaZulu-Natal).

Snyman, C., and Elliott, E. (2011). An optimized protocol for handling and processing fragile acini cultured with the hanging drop technique. Analytical Biochemistry *419*, 348-350.

Somerville, R., Oblander, S., and Apte, S. (2003). Matrix metalloproteinases: old dogs with new tricks. Genome Biology *4*, 216.

Soule, H.D., Maloney, T.M., Wolman, S.R., Peterson, W.D., Brenz, R., McGrath, C.M., Russo, J., Pauley, R.J., Jones, R.F., and Brooks, S.C. (1990). Isolation and charaterisation of a spontaneously immortalized human breast epithelial cell line, MCF10. Cancer Research *50*, 6075-6086.

Soussi, T., and Lozano, G. (2005). p53 mutation heterogeneity in cancer. Biochemical and Biophysical Research Communications *331*, 834-842.

Stephens, L., Eguinoa, A., Corey, S., Jackson, T., and Hawkins, P.T. (1993). Receptor stimulated accumulation of phosphatidylinositol (3,4,5)-trisphosphate by G-protein mediated pathways in human myeloid derived cells. The EMBO Journal *12*, 2265-2273.

Strewler, G.J. (2006). The stem cell niche and bone metastasis. IBMS BoneKEy *3*, 19-29.

Strongin, A.Y. (2010). Proteolytic and non-proteolytic roles of membrane type-1 matrix metalloproteinase in malignancy. Biochimica et Biophysica Acta *1803*, 133-141.

Strongin, A.Y., Collier, I., Bannikov, G., Marmer, B.L., Grant, G.A., and Goldberg, G.I. (1995). Mechanism Of Cell Surface Activation Of 72-kDa Type IV Collagenase. Journal of Biological Chemistry *270*, 5331-5338.

Subauste, M.C., Pertz, O., Adamson, E.D., Turner, C.E., Junger, S., and Hahn, K.M. (2004). Vinculin modulation of paxillin–FAK interactions regulates ERK to control survival and motility. The Journal of Cell Biology *165*, 371-381.

Suenaga, N., Mori, H., Itoh, Y., and Seiki, M. (2005). CD44 binding through the hemopexin-like domain is critical for its shedding by membrane-type 1 matrix metalloproteinase. Oncogene *24*, 859-868.

Suojanen, J., Salo, T., Koivunen, E., Sorsa, T., and Pirila, E. (2009). A novel and selective membrane type-I matrix metalloproteinse (MT1-MMP) inhibitor reduces cancer cell motility and tumour growth. Cancer Biology Therapy *24*, 2362-2370.

Szabova, L., Chrysovergis, K., Yamada, S.S., and Holmbeck, K. (2007). MT1-MMP is required for efficient tumor dissemination in experimental metastatic disease. Oncogene *27*, 3274-3281.

Taatjes, D.J., Sobel, B.E., and Budd, R.C. (2008). Morphological and cytochemical determination of cell death by apoptosis. Histochemistry and Cell Biology *129*, 33-43.

Tadokoro, S., Shattil, S.J., Eto, K., Tai, V., Liddington, R.C., de Pereda, J.M., Ginsberg, M.H., and Calderwood, D.A. (2003). Talin Binding to Integrin ß Tails: A Final Common Step in Integrin Activation. Science *302*, 103-106.

Tait, L., Soule, H.D., and Russo, J. (1990). Ultrastructural and immunocytochemical characterisation of an immortalized human breast epithelial cell line, MCF10 Cancer Research *50*, 6087-6094.

Takeha, S., Fujiyama, Y., Bamba, T., Sorsa, T., Nagura, H., and Ohtani, H. (1997). Stromal Expression of MMP-9 and Urokinase Receptor Is Inversely Associated with Liver Metastasis and with Infiltrating Growth in Human Colorectal Cancer: A Novel Approach from Immune/Inflammatory Aspect. Cancer Science *88*, 72-81.

Takino, T., Miyamori, H., Kawaguchi, N., Uekita, T., Seiki, M., and Sato, H. (2003). Tetraspanin CD63 promotes targeting and lysosomal proteolysis of membrane-type 1 matrix metalloproteinase. Biochemical and Biophysical Research Communications *304*, 160-166.

Takino, T., Miyamori, H., Watanabe, Y., Yoshioka, K., and Sato, H. (2004). Membrane type-1 matrix metalloproteinase regulates collagen-dependent mitogen-activated protein/extracellular signal-related kinase activation and cell migration. Cancer research *64*, 1044-1049.

Takino, T., Tsuge, H., Ozawa, T., and Sato, H. (2010). MT1-MMP promotes cell growth and ERK activation through c-Src and paxillin in three-dimensional collagen matrix. Biochemical and Biophysical Research Communications *396*, 1042-1047.

Takino, T., Watanabe, Y., Matsui, M., Miyamori, H., Kudo, T., Seiki, M., and Sato, H. (2006). Membrane-type 1 matrix metalloproteinase modulates focal adhesion stability and cell migration. Experimental Cell Research *312*, 1381-1389.

Tallant, C., Marrero, A., and Gomis-Rüth, F.X. (2010). Matrix metalloproteinases: Fold and function of their catalytic domains. Biochimica et Biophysica Acta (BBA) - Molecular Cell Research *1803*, 20-28.

Tam, E.M., Moore, T.R., Butler, G.S., and Overall, C.M. (2004). Characterization of the Distinct Collagen Binding, Helicase and Cleavage Mechanisms of Matrix Metalloproteinase 2 and 14 (Gelatinase A and MT1-MMP). Journal of Biological Chemistry *279*, 43336-43344.

Tam, E.M., Wu, Y.I., Butler, G.S., Stack, M.S., and Overall, C.M. (2002). Collagen Binding Properties of the Membrane Type-1 Matrix Metalloproteinase (MT1-MMP) Hemopexin C Domain. The Ectodomain of the 44-kDa Autocatalytic Product of MT1-MMP Inhibits Cell Invasion by Disrupting Native Type I Collagen Cleavage. The Journal of Biological Chemistry *277*, 39005–39014.

Théry, M. (2010). Micropatterning as a tool to decipher cell morphogenesis and functions. Journel of Cell science 123, 4201-4213.

Thullberg, M., Bartkova, J., Khan, S., Hansen, K., Ronnstrand, L., Lukas, J., Strauss, M., and Bartek, J. (2000). Distinct versus redundant properties among members of the INK4 family of cyclin-dependent kinase inhibitors. FEBS Letters *470*, 161-166.

Toth, M., Hernandez-Barrantes, S., Osenkowski, P., Bernardo, M.M., Gervasi, D.C., Shimura, Y., Meroueh, O., Kotra, L.P., Galvez, B.G., Arroyo, A.G., *et al.* (2002). Complex pattern of membrane type 1 matrix metalloproteinase shedding. The Journal of Biological Chemistry *277*, 26340-26350.

Toth, M., Sohail, A., Mobashery, S., and Fridman, R. (2006). MT1-MMP shedding involves an ADAM and is independent of its localization in lipid rafts. Biochemical and Biophysical Research Communications *350*, 377-384.

Towbin, H., Staehelin, T., and Gordon, J. (1979). Electrophoretic transfer of proteins from polyacrylamide gels to nitrocellulose sheets: procedure and some applications. Proceedings of the National Academy of Sciences of the United States of America *79*, 4350-4354.

Trott, O., and Olson, A.J. (2010). Software News and Update AutoDock Vina: Improving the Speed and Accuracy of Docking with a New Scoring Function, Efficient Optimization, and Multithreading. Journal of Computational Chemistry *31*, 455-461.

Tuccinardi, T., Martinelli, A., Nuti, E., Carelli, P., Balzano, F., Uccello-Barretta, G., Murphy, G., and Rossello, A. (2006). Amber force field implementation, molecular modelling study, synthesis and MMP-1/MMP-2 inhibition profile of (R)- and (S)-N-hydroxy-2-(N-isopropoxybiphenyl-4-ylsulfonamido)-3-methylbutanamides. Bioorganic & Medicinal Chemistry *14*, 4260-4276.

Ueda, J., Kajita, M., Suenaga, N., Fujii, K., and Seiki, M. (2003). Sequence-specific silencing of MT1-MMP expression suppresses tumor cell migration and invasion: importance of MT1-MMP as a therapeutic target for invasive tumors. Oncogene *22*, 8716–8722.

Uekita, T., Itoh, Y., Yana, I., Ohno, H., and Seiki, M. (2001). Cytoplasmic tail-dependent internalization of membrane-type 1 matrix metalloproteinase is important for its invasion-promoting activity. The Journal of Cell Biology *155*, 1345-1356.

Ulrich, D., Lichtenegger, F., Eblenkamp, M., Repper, D., and Pallua, N. (2004). Matrix Metalloproteinases, Tissue Inhibitors of Metalloproteinases, Aminoterminal Propeptide of Procollagen Type III, and Hyaluronan in Sera and Tissue of Patients with Capsular Contracture after Augmentation with Trilucent Breast Implants. Plastic and Reconstructive Surgery *114*, 229-236.

van Engeland, M., Nieland, L.J.W., Ramaekers, F.C.S., Schutte, B., and Reutelingsperger, C.P.M. (1997). Annexin V-Affinity Assay: A Review on an Apoptosis Detection System Based on Phosphatidylserine Exposure. Cytometry *31*, 1-9.

van Lent, P.L.E.M., Span, P.N., Sloetjes, A.W., Radstake, T.R.D.J., van Lieshout, A.W.T., Heuvel, J.J.T.M., Sweep, C.G.J., and van den Berg, W.B. (2005). Expression and localisation of the new metalloproteinase inhibitor RECK (reversion inducing cysteine-rich protein with Kazal motifs) in inflamed synovial membranes of patients with rheumatoid arthritis. Annals of the Rheumatic Diseases *64*, 368-374.

van Rooyen, D.M. (2009). Membrane type-1 matrix metalloproteinase (MT1-MMP) in c-ha-ras-induced breast cancer cell invasion. In Biochemistry (Pietermaritzburg, University of KwaZulu-Natal).

Vance, J.E. (2008). Phosphatidylserine and phophatidylethanolamine in mammalian cells: two metabolically related aminophopholipids. Journal of lipid research *49*, 1377-1387.

Velcich, A., Klampfer, L., Meriadason, J., Smartt, H., Guilmeau, S., Maier, S., Yang, W., Christman, J., Heerdt, B., and Augenlicht, L. (2006). Genetics and epigenetics in cancer biology Second edn (Los Angeles, Elsevier).

Vermes, I., Haanen, C., Steffens-Nakken, H., and Reutelingsperger, C. (1994). A novel assay for apoptosis Flow cytometric detection of phosphatidylserine expression on early apoptotic cells using fluorescein labelled Annexin V. Journal of Immunological Methods *184*, 39-51.

Visse, R., and Nagase, H. (2003). Matrix metalloproteinases and tissue inhibitors of metalloproteinases: structure, function and biochemistry. Circulation Research *92*, 825-839.

Vitale, I., Galluzzi, L., Castedo, M., and Kroemer, G. (2011). Mitotic catastrophe: a mechanism for avoiding genomic instability. Nat Rev Mol Cell Biol *12*, 385-392.

Voet, D., and Voet, J.D. (2004). Biochemistry, 3rd edn (Wiley International).

Voice, J.K., Klemke, R.L., Le, A., and Jackson, J.H. (1999). Four Human Ras Homologs Differ in Their Abilities to Activate Raf-1, Induce Transformation, and Stimulate Cell Motility. Journal of Biological Chemistry *274*, 17164-17170.

Volberg, T., Geiger, B., Kam, Z., Pankov, R., Simcha, I., Sabanay, H., Coll, J.L., Adamson, E., and Ben-Ze'ev, A. (1995). Focal adhesion formation by F9 embryonal carcinoma cells after vinculin gene disruption. Journal of Cell Science *108*, 2253-2260.

Vorobiof, D.A., Sitas, F., and Vorobiof, G. (2001). Breast cancer incidence in South Africa. Journal of clinical oncology *19*, 125-127.

Walker, A.R.P., Adam, F.I., and Walker, B.F. (2004). Breast cancer in black African women: a changing situation. The Journal of the Royal Society for the Promotion of Health *124*, 81-85.

Wang, C., Lisanti, M.P., and Liao, D.J. (2011). Reviewing once more the c-myc and Ras collaboration: Converging at the cyclin D1-CDK4 complex and challenging basic concepts of cancer biology. Cell Cycle *10*, 57-67.

Wang, X., Ma, D., Keski-Oja, J., and Pei, D. (2004). Co-recycling of MT1-MMP and MT3-MMP through the Trans-Golgi Network. Journal of Biological Chemistry *279*, 9331-9336.

Wang, Z., Juttermann, R., and Soloway, P.D. (2000). TIMP-2 Is Required for Efficient Activation of proMMP-2 in Vivo. Journal of Biological Chemistry *275*, 26411-26415.

Wanga, H.-S., Hunga, Y., Sub, C.-H., Penga, S.-T., Guoa, Y.-J., Laia, M.-C., Liua, C.-Y., and Hsuc, Y.-W. (2005). CD44 Cross-linking induces integrin-mediated adhesion and transendothelial migration in breast cancer cell line by up-regulation of LFA-1 (aLh2) and VLA-4 (a4h1). Experimental Cell Research *304*, 116– 126.

Waybright, T.J., Britt, J.R., and McCloud, T.G. (2009). Overcoming Problems of Compound Storage in DMSO: Solvent and Process Alternatives. Journal of Biomolecular Screening *14*, 708-715.

Weber, K., and Osborn, M. (1969). The reliability of molecular wieght determinations by dodecyl sulfate-polyacrylimide gel electrophoresis. The Journal of Biological Chemistry *244*, 4406-4412.

Weil, R.J., Palmieri, D.C., Bronder, J.L., Stark, A.M., and Steeg, P.S. (2005). Breast cancer metastasis to the central nervous system. American Journal of Pathology *167*, 913-920.

Weinberg, R.A. (1995). The retinoblastoma protein and cell cycle control. Cell *81*, 323-330.

Westermarck, J., and Kahari, V.-M. (1999). Regulation of matrix metalloproteinase expression in tumor invasion. The FASEB Journal *13*, 781-792.

White, J.M. (2003). ADAMs: modulators of cell–cell and cell–matrix interactions. Current Opinion in Cell Biology *15*, 598-606.

Will, H., Atkinson, S.J., Butler, G.S., Smith, B., and Murphy, G. (1996). The Soluble Catalytic Domain of Membrane Type 1 Matrix Metalloproteinase Cleaves the Propeptide of Progelatinase A and Initiates Autoproteolytic Activation. Journal of Biological Chemistry *271*, 17119-17123.

Willingham, M.C. (1999). Cyochemical Methods for the Detection of Apoptosis. The Journal of Histochemistry and Cytochemistry *47*, 1101-1109.

Willumsen, B.M., Norris, K., Papageorge, A.G., Hubbert, N.I., and Lowy, D.R. (1984). Harvey murine sarcoma virus p21 ras protein: biological and biochemical significance of the cysteine nearest the carboxy terminus. EMBO J *3*, 2581-2585.

Witty, J.P., Lempka, T., Coffey, R.J., and Matrisian, L.M. (1995). Decreased Tumor Formation in 7,12-Dimethylbenzanthracene-treated Stromelysin-1 Transgenic Mice Is Associated with Alterations in Mammary Epithelial Cell Apoptosis. Cancer Research *55*, 1401-1406.

Wolf, K., Mazo, I., Leung, H., Engelke, K., von Andrian, U.H., Deryugina, E.I., Strongin, A.Y., Bröcker, E.-B., and Friedl, P. (2003a). Compensation mechanism in tumor cell migration: mesenchymal-amoeboid transition after blocking of pericellular proteolysis. The Journal of Cell Biology *160*, 267-277.

Wolf, K., Müller, R., Borgmann, S., Bröcker, E.-B., and Friedl, P. (2003b). Amoeboid shape change and contact guidance: T-lymphocyte crawling through fibrillar collagen is independent of matrix remodeling by MMPs and other proteases. Blood *102*, 3262-3269.

Woodward, W.A., Chen, M.S., Behbod, F., Alfaro, M.P., Buchholz, T.A., and Rosen, J.M. (2007). WNT/beta-catenin mediates radiation resistance of mouse mammary progenitor cells. Proceedings of the National Academy of Sciences *104*, 618-623.

Wu, Y.I., Munshi, H.G., Sen, R., Snipas, S.J., Salvesen, G.S., Fridman, R., and Stack, M.S. (2004). Glycosylation Broadens the Substrate Profile of Membrane Type 1 Matrix Metalloproteinase. Journal of Biological Chemistry *279*, 8278-8289.

Wyllie, A.H., Kerr, J.F.R., and Currie, A.R. (1980). Cell death: the significance of apoptosis. International Review of Cytology *68*, 251-306.

Xu, J., Rodriguez, D., Petitclerc, E., Kim, J.J., Hangai, M., Yuen, S.M., Davis, G.E., and Brooks, P.C. (2001). Proteolytic exposure of a cryptic site within collagen type IV is required for angiogenesis and tumor growth in vivo. The Journal of Cell Biology *154*, 1069-1080.

Xu, W., Coll, J.L., and Adamson, E.D. (1998). Rescue of the mutant phenotype by reexpression of full-length vinculin in null F9 cells; effects on cell locomotion by domain deleted vinculin. Journal of Cell Science *111*, 1535-1544.

Xu, X., Wang, Y., Lauer-Fields, J.L., Fields, G.B., and Steffensen, B. (2004). Contributions of the MMP-2 collagen binding domain to gelatin cleavage: Substrate binding via the collagen binding domain is required for hydrolysis of gelatin but not short peptides. Matrix Biology *23*, 171-181.

Yamazaki, D., Kurisu, S., and Takenawa, T. (2005). Regulation of cancer cell motility through actin reorganization. Cancer Science *96*, 379-386.

Yang, E., Zha, J., Jockel, J., Boise, L.H., Thompson, C.B., and Korsmeyer, S.J. (1995). Bad, a heterodimeric partner for Bcl-xL and Bcl-2, displaces bax and promotes cell death. Cell *80*, 285-291.

Yilmaz, M., and Christofori, G. (2009). EMT, the cytoskeleton, and cancer cell invasion. Cancer and Metastasis Reviews *28*, 15-33.

Yong, V.W., Power, C., Forsyth, P., and Edwards, D.R. (2001). Metalloproteinases in biology and pathology of the nervous system. Nature Reviews Neuroscience *2*, 502-511.

Yoshikawa, T., Yanoma, S., Tsuburaya, A., Kobayashi, O., Sairenji, M., Motohashi, H., Miyagi, Y., Morinaga, S., Noguchi, Y., and Yamamoto, Y. (2006). Expression of MMP-7 and MT1-MMP in peritoneal dissemination of gastric cancer. Hepatogastroenterology *53*, 964-967.

Youle, R.J., and Strasser, A. (2008). The BCL-2 protein family: opposing activities that mediate cell death. Nature Reviews Molecular Cell Biology *9*, 47-59.

Yu, W.-H., Woessner, J.F., McNeish, J.D., and Stamenkovic, I. (2002). CD44 anchors the assembly of matrilysin/MMP-7 with heparin-binding epidermal growth factor precursor and ErbB4 and regulates female reproductive organ remodeling. Genes & Development *16*, 307-323.

Zamir, E., and Geiger, B. (2001). Molecular complexity and dynamics of cell-matrix adhesions. Journal of Cell Science *114*, 3583-3590.

Zientek-Targosz, H., Kunnev, D., Hawthorn, L., Venkov, M., Matsui, S.-I., Cheney, R., and Ionov, Y. (2008). Transformation of MCF-10A cells by random mutagenesis with frameshift mutagen ICR191: A model for identifying candidate breast-tumor suppressors. Molecular Cancer *7*, 51.

Zimerman, B., Volberg, T., and Geiger, B. (2004). Early molecular events in the assembly of the focal adhesion-stress fiber complex during fibroblast spreading. Cell Motility and the Cytoskeleton *58*, 143-159.

Zucker, S., and Cao, J. (2009). Selective matrix metalloproteinse (MMP) inhibitors in cancer therapy: Ready for prime time? Cancer Biology & Therapy *8*, 2371-2373.

Zucker, S., Hymowitz, M., Conner, C.E., DiYanni, E.A., and Cao, J. (2002). Rapid Trafficking of Membrane Type 1-Matrix Metalloproteinase to the Cell Surface Regulates Progelatinase A Activation. Lab Invest *82*, 1673-1684.

Zuo, S.S., and Lundahl, P. (2000). A micro-Bradford membrane protein assay. Anal Biochem *284*, 162-164.